Titre: Title:	Numerical and Experimental Investigation of Liquid and Gas/Liquid Flows in Stirred Tank Reactors
Auteur: Author:	Hamed Bashiri
Date:	2015
Type:	Mémoire ou thèse / Dissertation or Thesis
Référence: Citation:	Bashiri, H. (2015). Numerical and Experimental Investigation of Liquid and Gas/Liquid Flows in Stirred Tank Reactors [Thèse de doctorat, École Polytechnique de Montréal]. PolyPublie. https://publications.polymtl.ca/1886/

UNIVERSITÉ DE MONTRÉAL

NUMERICAL AND EXPERIMENTAL INVESTIGATION OF LIQUID AND GAS/LIQUID FLOWS IN STIRRED TANK REACTORS

HAMED BASHIRI
DÉPARTEMENT DE GÉNIE CHIMIQUE
ÉCOLE POLYTECHNIQUE DE MONTRÉAL

THÉSE PRÉSENTÉE EN VUE DE L'OBTENTION
DU DIPLÔME DE PHILOSOPHIÆ DOCTOR
(GÉNIE CHIMIQUE)
AÔUT 2015

UNIVERSITÉ DE MONTRÉAL

ÉCOLE POLYTECHNIQUE DE MONTRÉAL

Cette thése intitulée :

NUMERICAL AND EXPERIMENTAL INVESTIGATION OF LIQUID AND GAS/LIQUID FLOWS IN STIRRED TANK REACTORS

présentée par : BASHIRI Hamed

en vue de l'obtention du diplôme de : Philosophiæ Doctor

a été dûment acceptée par le jury d'examen constitué de :

M. CICOIRA, Fabio, Ph.D., président

M. CHAOUKI, Jamal, Ph.D., membre et directeur de recherche

M. BERTRAND, François, Ph.D., membre et codirecteur de recherche

M. FRADETTE, Louis, Ph.D., membre

M. GALINDO, Enrique, Ph.D., membre

DEDICATION

I would like to dedicate this work to my lovely parents, my sister and brothers who taught me never to give up. I would like to thank them for their everlasting and unconditional love, endless support, their generosity and enormous patience. Without them this work would not be possible.

ACKNOWLEDGMENTS

This work was completed with support from the Natural Sciences and Engineering Research Council of Canada (NSERC) at the École Polytechnique. The financial support of the NSERC is gratefully acknowledged.

There are many wonderful people whom I would like to thank for their guidance and support over the period of my PhD study. They range from good friends who have been around through the best and worst times to the various important people who showed their support at critical moments and kept things rolling. To name all individually would miss the point and would not do justice to their immense contributions. In particular, I would like to thank the following people :

First of all, I would like to extend my great appreciation to my supervisors Professor Jamal Chaouki and Professor François Bertrand for all their support, guidance and inspiration through my PhD journey, and for their dedication and patience in reviewing my work. They gave me a lot of freedom in my work, and were always present to help me see things in perspective. Working with them allowed me to build up my professional skills, and their generosity enabled me to attend several conferences across the world and gave me the privilege to interact with their industrial partners and key people in this field. We built a friendship, in addition to the student-supervisor relationship.

I would like to thank Prof. Enrique Galindo, Prof. Louis Fradette, Prof. Fabio Cicoira and Prof. Steven Dufour as the members of my PhD committee for accepting to review my thesis and be part of this event.

During these years I have had a privilege of working in two outstanding research groups. Special thoughts go out to all students and employees at the URPEI group and professor Chaouki's team for all their support, particularly to :

Dr. Ebrahim Alizadeh for his close collaboration in conducting the experiments, plus his friendship and support ; Dr. Mourad Heniche, who was with us at the beginning of this

work, for all the valuable discussions we had about CFD ; Dr. David Vidal for his kindness in providing me with all the French translations in my thesis, for his great input and constructive comments on my work, and also for taking the time to discuss everything from MATLAB programming to the history of Europe ; Dr. Olivier Dubé and Mr. Bruno Blais for all fruitful discussions we had concerning my PhD topic ; Dr. Babak Esmaeili and Dr. Rouzbeh Jafari for their advices and generousity ; Dr. Laurent Spreutels, Dr. Majid Rasouli and Dr. Amin Esmaeili for their friendship and sharing their thoughts in the many discussions we had ; and to all other friends who shared many great moments with me during all these years.

I also would like to extend my thanks to everyone in the chemical engineering department. Special thanks go to Mr. Yazid Belkeri, Mr. Robert Delisle, Mr. Gino Robin, and Ms. Evelyne Rousseau.

I would also like to thank Dr. Shaffiq Jaffer for the fruitful discussions regarding my research and for inviting me to participate and present some parts of my work at the TOTAL-sponsored students meeting. I would also like to thank Dr. Jocelyn Doucet for all valuable discussions we had regarding mixing and the commercialization of chemical processes.

I would like to acknowledge my managers and colleagues at CanmetENERGY, especially Dr. Sophie Hosatte, Dr. Marzouk Benali and Ms. Chantal Leroy for their thoughtfulness and kind understating of the special situation I had in the final months of my PhD, and who kindly let me handle my work while I was finalizing my thesis ; and Dr. José A. Candanedo for his kindness in reviewing some chapters of my thesis.

Last but not least, special thanks go to Dr. Shabnam Sanaei for being by my side during both the tough and happy moments, and for keeping hope alive every single day of this PhD journey ; however, this will never fully reflect my feeling of appreciation about her perpetual kindness. Her endless support has had a great impact on my success.

RÉSUMÉ

Les réacteurs à cuve agitée (STR) sont couramment utilisés dans les industries pétrolières, chimiques, biochimiques, pétrochimiques, minières et métallurgiques. De nos jours, ralenties par des facteurs et des barrières tant économiques qu'environnementaux, ces industries sont ardemment à la recherche de procédés efficaces et fiables permettant de minimiser le gaspillage d'énergie et de matières premières ainsi que la production de sous-produits indésirables et nocifs. De fait, la recherche de lignes directrices pour la mise à l'échelle de tels procédés, du laboratoire à l'échelle industrielle, est devenue une tâche indispensable pour les ingénieurs des procédés. Les procédures classiques de conception et de mise à l'échelle des STR supposent que les paramètres hydrodynamiques sont constants à travers le réacteur (hypothèse du "mélange parfait"). Cette hypothèse est assez simpliste et sans doute abusive, particulièrement pour les STR de grands volumes. Il est reconnu que la conception et la mise à l'échelle d'équipements de procédé peuvent difficilement être couronnées de succès sans la prise en compte de l'hydrodynamique locale. Une compréhension de l'hydrodynamique et du mélange est donc essentielle pour la conception et la mise à l'échelle précises des STR. L'objectif général de cette étude a par conséquent été d'améliorer la compréhension de l'hydrodynamique à l'intérieur des STR et d'aider la conception et la mise à l'échelle de tels systèmes. Pour atteindre cet objectif, une combinaison judicieuse de divers outils de conception incluant la modélisation compartimentale (CM), la mécanique des fluides numérique (CFD) et la mécanique des fluides expérimentale (EFD) a été utilisée. Comme le taux de dissipation de l'énergie cinétique de turbulence (ε) affecte de façon importante la performance des STR, la première partie de cette thèse a été consacrée aux effets des conditions opératoires et de la mise à l'échelle sur la distribution de ε dans les STR. Les résultats de simulations CFD monophasiques par la méthode des volumes finis sur des STR équipés d'une turbine Rushton (RT) ont été utilisés pour déterminer les paramètres d'un modèle à deux zones compartimentales qui y décrit l'inhomogénéité de la turbulence. Une méthode améliorée a été proposée pour trouver

la frontière entre deux régions caractéristiques. A l'aide de cette méthode, les effets de divers critères classiques de mise à échelle ont été étudiés. Il a été observé que la distribution de ε et, en conséquence, les paramètres du modèle compartimental changent considérablement lorsque les critères classiques de mise à l'échelle ont été suivis.

Par la suite, la méthode non-intrusive dite du suivi de particules radioactives (RPT) a été utilisée pour une analyse exhaustive de l'écoulement parfaitement turbulent du fluide dans un STR de laboratoire équipé d'une turbine RT ou d'une turbine à pales inclinées (PBT). Cette étude couvre les descriptions eulérienne et lagrangienne du mouvement du fluide. Les mesures RPT du champ d'écoulement turbulent dans un STR agité par une turbine RT ont été comparées à des mesures laser et à des résultats de simulations CFD de modèles de turbulence basés sur une méthode de RANS (Reynolds-averaged Navier-Stokes). Un bon accord a été trouvé entre toutes les méthodes pour les profils de vitesse moyenne tridimensionnelle prédits et mesurés en tous points du STR. La technique RPT a été utilisée pour la première fois pour mesurer le champ d'écoulement turbulent dans une cuve agitée par une turbine PBT. Deux indices de mélange, un basé sur le concept d'indépendance stochastique et l'autre sur le concept statistique de perte de mémoire dans les procédés de mélange, ont été utilisés pour mesurer le temps de mélange à l'aide des données RPT. Cette étude montre que la technique RPT s'avère très prometteuse pour étudier les écoulements turbulents et les caractéristiques du mélange dans les STR, ainsi que pour évaluer la validité des modèles numériques. La RPT a aussi été utilisée pour valider un modèle CFD simulant les écoulements turbulents monophasiques. Les résultats de ce modèle ont été utilisés comme une condition initiale pour des simulations CFD plus complexes d'écoulement turbulent gaz-liquide dans des STR qui présentées dans la dernière partie de la thèse.

Finalement, la troisième partie de la thèse présente le développement d'un modèle multi-échelle d'écoulement gaz-liquide comme outil pour la conception et la mise à l'échelle de STR. Le modèle est basé sur la compartimentalisation du STR en zones et l'utilisation de simulations simplifiées d'écoulement gaz-liquide moins coûteuses en temps calcul. Ce modèle

a prédit la valeur moyenne du coefficient volumique de transfert de matière (k_La) dans chaque zone à l'aide de paramètres hydrodynamique locaux y figurant (c.-à-d. rétention de gaz et le taux de dissipation de l'énergie cinétique de turbulence du liquide). La validité du modèle à chaque étape a été scrupuleusement évaluée à l'aide de données de la littérature. Le modèle proposé a été capable de prédire le coefficient volumique global de transfert de matière à l'intérieur du STR avec une bonne précision. À l'aide de ce modèle, il est apparu que les contributions de chaque zone au transfert de matière global à l'intérieur du STR peuvent changer considérablement en modifiant les conditions opératoires et la mise à l'échelle. Il a été estimé que, en accroissant le volume du STR, le k_La global avait diminué d'au moins 20% suite à une mise à l'échelle classique.

L'originalité scientifique du présent travail repose sur (a) l'introduction d'une nouvelle méthode pour trouver la localisation de la frontière entre deux zones compartimentales caractéristiques des STR qui y décrivent l'inhomogénéité de la turbulence, (b) l'investigation systématique des effets des conditions opératoires et des différentes approches de mise à l'échelle sur le degré d'inhomogénéité de la turbulence dans les STR équipés de turbine RT, (c) les études expérimentales exhaustives sur les écoulements turbulents dans des STR à l'aide de la technique RPT pour les turbines RT et PBT, (d) l'introduction d'une nouvelle méthode pour la mesure non-invasive du temps de mélange dans les STR basée sur le concept statistique de perte de mémoire, (e) le développement d'un modèle multi-échelle pour les écoulements gaz-liquide comme outil de conception et de mise à l'échelle du STR, et (f) l'examen attentif de l'impact des conditions opératoires et de la mise à l'échelle sur les valeurs du coefficient volumique local de transfert de matière. Les découvertes de cette étude ont permis de mettre en lumière les paramètres hydrodynamiques importants pour la conception et la mise à l'échelle des STR. À cet égard, il est permis de croire que des améliorations significatives dans leur conception pourront être réalisées à l'aide du modéle multi-échelle proposé étant donné qu'il considère à la fois le champ d'écoulement effectif et des paramètres hydrodynamiques locaux.

ABSTRACT

Stirred tank reactors (STRs) are widely used in the petroleum, chemical, biochemical, petrochemical, mineral and metallurgical industries. Nowadays, submerged by both economic and environmental drivers and barriers, industries urge for efficient and reliable processes in order to minimize the waste of energy and raw materials, as well as the production of undesirable and harmful by-products. As a result, finding adequate rules for scaling up such processes from the laboratory to an industrial scale has become a crucial task for process engineers. The conventional procedures for design and scale-up of STRs assume that the values of hydrodynamic parameters are constant in the entire reactor ("well-mixed" assumption). This assumption is quite rudimentary and may even be far-fetched, particularly for large-scale STRs. It is well known that the design and scale-up of process equipment can barely be successful without taking local hydrodynamics into account. An understanding of the hydrodynamics and mixing is thus essential for the precise design and scale-up of STRs. The overall objective of this study was to gain insight into the hydrodynamics prevailing in STRs, and help improve the design and scale-up of such systems. To meet this objective, strategic combinations of various design tools, including compartmental modeling (CM), computational fluid dynamics (CFD) and experimental fluid dynamics (EFD), were used.

As the turbulent energy dissipation rate (ε) significantly affects the performance of STRs, the first part of this thesis presents the effects of operating conditions and the scale-up on the distribution of ε in STRs. The results of single-phase finite-volume CFD simulations of STRs equipped with a Rushton turbine (RT) were used to determine the parameters of a two-compartment model that describes the turbulent non-homogeneities therein. An improved method was proposed to find the boundary between the two characteristic regions. Using this method, the effects of various conventional scale-up criteria were investigated. It was observed that the distribution of ε and, as a result, the compartmental model parameters

change considerably when conventional scale-up rules were followed.

Next, so-called radioactive particle tracking (RPT) as a non-intrusive measurement technique was used for the comprehensive analysis of the fully turbulent fluid flow in a laboratory-scale STR equipped with an RT or a pitched blade turbine (PBT). This study covers the Eulerian and Lagrangian descriptions of fluid motions. The RPT measurement of the turbulent flow field in an STR agitated by an RT was benchmarked with CFD simulations of RANS-based turbulence models and laser-based measurements. A good agreement was found between all the methods for the measured and predicted 3D mean velocity profiles at all locations in the STR. The RPT technique was used to measure the turbulent flow field in a tank agitated by a PBT for the first time. Two mixing indices, one based on the concept of stochastic independence and the other on the statistical concept of memory loss in mixing processes, were used to measure mixing times using RPT data. This study shows that the RPT technique holds great promise for investigating turbulent flows and the mixing characteristics of STRs, and for assessing the adequacy of numerical models. RPT also was used to validate a CFD model for simulating single-phase turbulent flow. The results of this model were used as an initial condition for more complex CFD simulations of gas/liquid turbulent flow in the STRs presented in the last part of the thesis.

Finally, the third part of this thesis presents the development of a multiscale gas/liquid flow model as a tool for the design and scale-up of STRs. The model was based on the compartmentalization of the STR into zones and the use of simplified less computationally intensive gas/liquid flow simulations. It predicted the mean value of the local volumetric mass transfer coefficient ($k_L a$) in each compartment based on the local hydrodynamic parameters therein (i.e., gas hold-up and liquid turbulent energy dissipation rate). The adequacy of the model at each step was carefully assessed using experimental data drawn from the literature. The proposed model was able to predict the overall volumetric mass transfer coefficient in the STR with good adequacy. Using this model, it was shown that the contributions of each compartment to the overall mass transfer inside the STR could be changed considerably by

altering the operating conditions and scale-up. It was also estimated that by increasing the STR size the overall volumetric mass transfer coefficient decreased by at least 20% following a conventional scale-up rule.

The scientific novelty of the current work lies in: (a) the introduction of a new method for finding the location of the boundary between the two characteristic compartments of STRs that describes the turbulent non-homogeneities therein, (b) the systematic investigation of the effects of operating conditions and different scale-up approaches on the extent of turbulent non-homogeneities in STRs equipped with an RT, (c) the comprehensive experimental investigations of the turbulent fluid flows in STRs using RPT for both RT and PBT impellers, (d) the introduction of a novel method for the non-invasive measurement of mixing time in STRs based on the statistical concept of memory loss, (e) the development of a multiscale gas/liquid flow model to serve as a tool for the design and scale-up of STRs, and (f) the scrutinization of operating conditions and scale-up impacts on the local volumetric mass transfer coefficient values. The findings of this study have shed light on the hydrodynamic parameters that are important for the design and scale-up of STRs. In this regard, it is also believed that significant design improvements can be achieved by using the proposed multiscale model as it considers the actual flow field and local hydrodynamic parameters.

TABLE OF CONTENTS

LIST OF TABLES

LIST OF FIGURES

LIST OF ABBREVIATIONS

BND	Bubble Number Density
CFD	Computational Fluid Dynamics
CM	Compartment Model
CSP	Capillary Suction Probe
DO	Dissolved Oxygen
EE	Eulerian-Eulerian
EFD	Experimental Fluid Dynamics
EL	Eulerian-Lagrangian
ERT	Electrical Resistance Tomography
IBC	Impeller Boundary Condition
LES	Large Eddy Simulation
LDA	Laser Doppler Anemometry
MRF	Multiple Reference Frame
OUR	Oxygen Uptake Rate
PBM	Population Balance Model
PBT	Pitch Blade Turbine
PDA	Phase Doppler Anemometry
PEPT	Positron Emission Particle Tracking
PIV	Particle Image Velocimetry
RANS	Reynolds Average Navier-Stokes
RPD	Relative Power Demand
RPT	Radioactive Particle Tracking
RT	Rushton Turbine
RTD	Residence Time Distribution

SM	Sliding Mesh
ST	Stirred Tank
STR	Stirred Tank Reactor
TM	Torque Meter
VO	Visual Observation

CHAPTER 1

INTRODUCTION

Stirred tank reactors (STRs) are widely used in many chemical processes such as aerobic fermentation, hydrogenation, neutralization, chlorination, organic oxidation, polymerization, and gold cyanidation. The wide range of applications shows the inherent flexibility of STRs to carry out various process objectives. STRs can provide a high level of effective mixing for both low-viscosity fluids in which the flow is often turbulent and very high-viscosity and non-Newtonian fluids where the flow is often laminar. They are also very effective in providing good contact between phases in many processes where mixing and phase dispersion are required. It has been estimated that approximately 50% of all chemical production processes worldwide by value, worth some US $1,290 billion a year, use STRs (Butcher and Eagles, 2002).

Over the last few decades, the increasing volumes of products manufactured in industrial processes have led to the use of larger and larger reactors. Nowadays, submerged by both economic and environmental drivers and barriers, industries urge for efficient and reliable processes in order to minimize the waste of energy and raw materials, as well as the production of undesirable and harmful by-products. As a result, finding adequate rules for scaling up such processes from the laboratory to an industrial scale has become a crucial task for process engineers (Noorman, 2011).

The design and scale-up of STRs is not straightforward, mainly because chemical reactions are generally related to mass and momentum transfer mechanisms in a complex manner. The current state of the art regarding the scale-up and design of large STRs is based on empirical correlations, best practices (know-how routines), and rules of thumb, even with existing research tools and advances in engineering design. The economic downfall of scale-up issues is important since the quality of products is directly linked to their market. It is

shown that unsuccessful scale-up leads to inefficient large-scale mixing and, possibly, to poor product quality. The cost of improper scale-up and, consequently, poor mixing was estimated at between 1$ and 10$ billion in the U.S. chemical industry alone in 1989 (Paul et al., 2004).

Scale-up procedures are usually based on geometric similarity and keeping mixing characteristics (*e.g.* the tip speed or the power consumption per volume) constant in order to replicate a bench scale (Paul et al., 2004). In these common engineering practices, all spatial variations of properties within each unit operation are generally ignored ("well-mixed" tank assumption). Figure 1.1 illustrates the huge difference in size from a bench-scale to industrial-scale STR used for water treatment and mineral processing. Due to these dramatic changes in the size of STRs during scale-up, the "well-mixed" assumption becomes quite rudimentary and may even be far-fetched, particularly for large-scale STRs.

Another principal difficulty of the scale-up is the fact that it is impossible to maintain all of the mixing characteristics of an STR constant as its size increases. STRs are often characterized in terms of dimensionless groups such as the Reynolds number (Re), the Froude number (Fr), and the gas flow or aeration number (Fl_g). Often, all the complex governing phenomena inside the vessel cannot be described by a single dimensionless numbers, which makes the scale-up of such a system even more complicated. These dimensionless groups are related differently to the vessel dimensions, and thus scaling based on keeping any of them

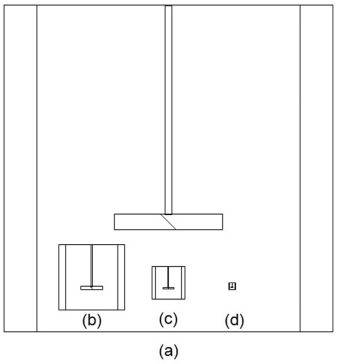

Figure 1.1: Scales of STRs in : (a) the mineral processing and water treatment industries ($T = 15\ m$), (b) the fine chemical ($T = 3\ m$), (c) the pilot scale ($T = 1.5\ m$) and (d) the bench scale ($T = 0.3\ m$) (Machado et al., 2013). T is the tank diameter.

constant leads to changes in the values of other groups.

In order to ensure an adequate design and scale-up as well as the sustainable development, an alternate design approach is thus required that reduces negative environmental impacts and increases the profitability of a given process (improving yield). Such an alternative approach should also provide a better understanding of the fluid dynamics in STRs, including information about internal flow structures (Sommerfeld and Decker, 2004) and local hydrodynamics in STRs that can only be achieved by analyzing the multi-scale fluid dynamics.

The effects of imperfect mixing on the performance of reactors have been well characterized by the concept of residence time distribution (RTD), based on the pioneering work of Danckwerts (1953). Models based on combinations of well-mixed reactors (compartments) are often used to simulate observed RTD data (Kiared et al., 1997; Ranade, 2002; Utgikar, 2009). Relating reactor design, scale, and operating conditions to performance requires many experiments to fit the parameters of the models. Moreover, some concerns still need to be addressed, including the cost of the experimental methods and their scale limitations. Many processes involve high temperatures, high pressures, and hazardous conditions, which makes the acquisition of detailed experimental data impractical (Bashiri et al., 2015).

In recent years computational fluid dynamics (CFD) and the understanding of the physics of multiphase flows have advanced significantly, thanks to the availability of powerful computers and sophisticated experimental validation techniques such as radioactive particle tracking (RPT) and optical probes. This has allowed process engineers to use CFD as a design tool to explore the 3D and transient characteristics of multiphase flows inside process equipment (Ranade, 2002). Significant improvements can be achieved in the design of STRs using a CFD model that considers the actual flow field and local hydrodynamic parameters.

The productivity of many processes is limited by the mass transfer between phases, especially in the case of low soluble species in the gas phase transferring to the liquid phase. This includes many bioprocesses such as the production of expensive specialty chemicals, including proteins, and bulk chemicals such as biofuels, lactic acid, and citric acid, where

oxygen transfer is vital for the success of the process (Garcia-Ochoa et al., 2010). Understanding gas/liquid mass transfer is thus essential for the adequate design of mixing systems. The mass transfer rate can be quantitatively defined as the product of the volumetric mass transfer coefficient (k_La) and the driving force, which is the difference between the saturation concentration of gas and its actual concentration in the liquid phase ($C^* - C(t)$). Accordingly, k_La can affect operations by limiting productivity in various ways, such as changing the reaction rate and, possibly, the selectivity. Numerous correlations have been proposed in the literature that express k_La as a function of the operating conditions of the STR. While these correlations are important to characterize the performance of gas/liquid STRs, they do not provide any information on the local values of this parameter that can bring the concept of imperfect mixing into play. Moreover, as these correlations are often obtained based on experiments in laboratory-scale STRs, their application is limited for the design of large-scale STRs. In fact, no evidence has yet been published regarding their applicability in large STRs.

Since it is important to take the local volumetric mass transfer coefficient into account (Lara et al., 2006), in recent years there has been growing interest in the use of a coupled CFD and a population balance model (PBM) to describe the spatial and temporal evolution of the volumetric mass transfer coefficient inside STRs. Full multiphase CFD simulations that take the evolution of bubble sizes and turbulent eddies into account can help to shed light on the mechanisms governing gas/liquid mixing operations. However, they suffer from various shortcomings, including the enormous computational requirements and the limited understanding of breakage and coalescence processes. To mitigate the computational time issue, the concept of multiscale modeling can be used, in which the hydrodynamic data obtained by simplified and less computationally intensive CFD simulations can pass along to a meso-scale PBM. However, the limited understanding of breakage and coalescence phenomena makes the use of PBM a formidable challenge for design purposes and has given rise to many on-going research endeavours. It is thus crucial to introduce a new approach that combines local hydrodynamics, the concepts of multiscale modeling, mass transfer, and turbulence

theories to predict the local values of the volumetric mass transfer coefficient in an STR. This approach can then be used as a tool for the design and scale-up of STRs.

Motivation and objective

As discussed above, scale-up failures can be attributed to the incomplete understanding of local prevailing hydrodynamic phenomena. A better understanding of the hydrodynamics is thus vital for the successful design and scale-up of STRs. This can be obtained by using available research and engineering tools such as CFD and experimental fluid dynamics (EFD), leading to more efficient design and operation. It can also be used for replacing "know-how" scale-up approaches with "know-why"-based models. In the long run, this will pave the way to better products with less waste, in other words, more "sustainable" processes. Indeed, the overall objective of this study is to gain insight into the hydrodynamics prevailing in STRs and help improve the design and scale-up of such processes.

1.1 References

Bashiri, H., Alizadeh, E., Chaouki, J., and Bertrand, F. (2015). Investigation of turbulent fluid flows in stirred tanks using a non-intrusive particle tracking technique. *Manuscript submitted for publication.*

Butcher, M. and Eagles, W. (2002). Fluid mixing re-engineered. *Chemical engineer*, (733) :28–29.

Danckwerts, P. (1953). Continuous flow systems : distribution of residence times. *Chemical Engineering Science*, 2(1) :1–13.

Garcia-Ochoa, F., Gomez, E., Santos, V. E., and Merchuk, J. C. (2010). Oxygen uptake rate in microbial processes : an overview. *Biochemical Engineering Journal*, 49(3) :289–307.

Kiared, K., Larachi, F., Guy, C., and Chaouki, J. (1997). Trajectory length and residence-time distributions of the solids in three-phase fluidized beds. *Chemical engineering science*, 52(21) :3931–3939.

Lara, A. R., Galindo, E., Ramírez, O. T., and Palomares, L. A. (2006). Living with heterogeneities in bioreactors. *Molecular biotechnology*, 34(3) :355–381.

Machado, M. B., Bittorf, K. J., Roussinova, V. T., and Kresta, S. M. (2013). Transition from turbulent to transitional flow in the top half of a stirred tank. *Chemical Engineering Science*, 98 :218–230.

Noorman, H. (2011). An industrial perspective on bioreactor scale-down : What we can learn from combined large-scale bioprocess and model fluid studies. *Biotechnology journal*, 6(8) :934–943.

Paul, E. L., Atiemo-Obeng, V., and Kresta, S. M. (2004). *Handbook of industrial mixing : science and practice*. John Wiley & Sons.

Ranade, V. V. (2002). *Computational flow modeling for chemical reactor engineering*. Process systems engineering series. Academic Press, San Diego.

Sommerfeld, M. and Decker, S. (2004). State of the art and future trends in CFD simulation of stirred vessel hydrodynamics. *Chemical engineering & technology*, 27(3) :215–224.

Utgikar, V. P. (2009). Modeling in multiphase reactor design : Solid phase residence time distribution in three-phase sparged reactors. *Industrial & Engineering Chemistry Research*, 48(17) :7910–7914.

CHAPTER 2

LITERATURE REVIEW

As mentioned in Chapter 1, the overall objective of this study is to gain insight into the hydrodynamics prevailing in STRs and help improve their design and scale-up. In this chapter, the principal aspects of design, scale-up, and the hydrodynamics of the turbulent liquid and gas/liquid STRs is first introduced. Afterwards, the experimental and numerical tools that have been used to investigate the hydrodynamics of such systems are reviewed, and the most significant relevant findings are discussed. Finally, the knowledge gaps that are addressed in this study are introduced.

2.1 Early history of STRs

The first use of the STRs in the process industry was published in 1556 in the book *De Re Metallica* (nature of metals in Latin) by Georg Bauer (Agricola) explaining the art of mining and extraction of metals (Nienow, 2014; Stankiewicz and Moulijn, 2000; Stitt, 2002). Figure 2.1 shows an engraving of a gold processing plant, including the series of STRs those almost match modern units. The motors were driven by harnessing hydro-power directly instead of using electricity and employing paddle impellers with six flat blades made from wood instead of metal to provide energy to achieve mixing (Nienow, 2014).

In recent years, the understanding of mixing in STRs has significantly progressed, turning the art of stirring into an engineering science that has resulted in considerable improvements to the design of impellers and mixing equipment. The first attempt to bring engineering into the mixing art was done by James Thompson in 1855 (Nienow, 2014). He measured the power required to rotate a disc in water and found a relation that is still used to predict the power consumption of STRs.

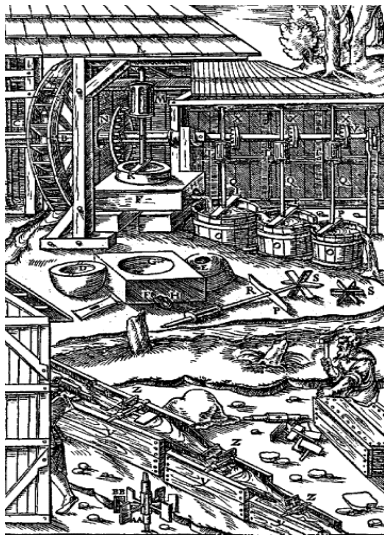

Figure 2.1: A wood cut of a gold processing plant from *De Re Metallica* by Agricola (Stitt, 2002).

STRs are often chosen among other types of reactors (*e.g.* bubble column, airlift or packed bed rectors) to carry out a process when the following conditions exist or should be met (Paul et al., 2004) :

- Highly viscous liquid phase ;
- Large gas flow compared to liquid flow ;
- Good contact between phases ;
- Good heat transfer (*e.g.* isothermal operation, exothermic reactions) ;
- Solid suspension ;
- High level of backmixing in the liquid phase.

The most significant difficulty in the construction of the STRs compared to the other types of reactors is the presence of moving parts, which often need to be well sealed in industrial units.

2.2 Design of STRs

As the other types of reactors, three flow regimes can occur in STRs : laminar, transitional and turbulent. Turbulent flow is usually desirable for many industrial processes due to its

efficient mixing characteristics and to accomplish various process objectives including but not limited to chemical reaction, solid suspension and gas dispersion (Kresta, 1998). STRs are in the fully turbulent regime when the impeller Reynolds number (Re) is over 20000 since beyond this value the power number becomes constant (Machado et al., 2013). The impeller Reynolds number is defined by :

$$Re = \frac{\rho_l N D^2}{\mu_l} \tag{2.1}$$

where ρ_l, N, D and μ_l are the liquid density, impeller rotational speed, impeller diameter and liquid dynamic viscosity, respectively.

There is not a single optimal design of STRs, and the design can change depending on process requirements. However, a so-called standard design is usually followed for turbulent mixing with low viscosity fluids (Oldshue, 1983; Paul et al., 2004; Tatterson, 1991) as illustrated in Figure 2.2. The tank diameter (T), liquid height (H), impeller diameter (D), impeller blade width (W), impeller off-bottom clearance (C), and baffle width (B) are characteristic lengths that determine the flow pattern. Four baffles placed 90^o apart are often employed in standard design to break the solid body rotation of the liquid and the central surface vortex (Tatterson, 1991).

In gas/liquid STRs the gas usually injected into the tank through a ring sparger, which is often placed below the impeller. For some processes such as fermentation, in order to increase the gas residence time, tanks with a higher aspect ratio (H/T) are used (Cabaret et al., 2008). For such a tall vessel, multiple impellers are needed to achieve adequate levels of gas dispersion and liquid mixing.

There are various types of commercially available impellers designed for particular purposes, including gas dispersion, solid suspension and dispersion, and the homogenization of viscous and non-viscous media. Generally, impellers are classified based on their discharge flow directions into radial (*e.g.* Rushton turbine), axial (*e.g.* marine propeller or hydrofoils) and mixed (*e.g.* pitched blade turbine) flow impellers. Radial flow impellers generate a swirling flow that moves towards the vessel walls where the vertical baffles deflect the flow into

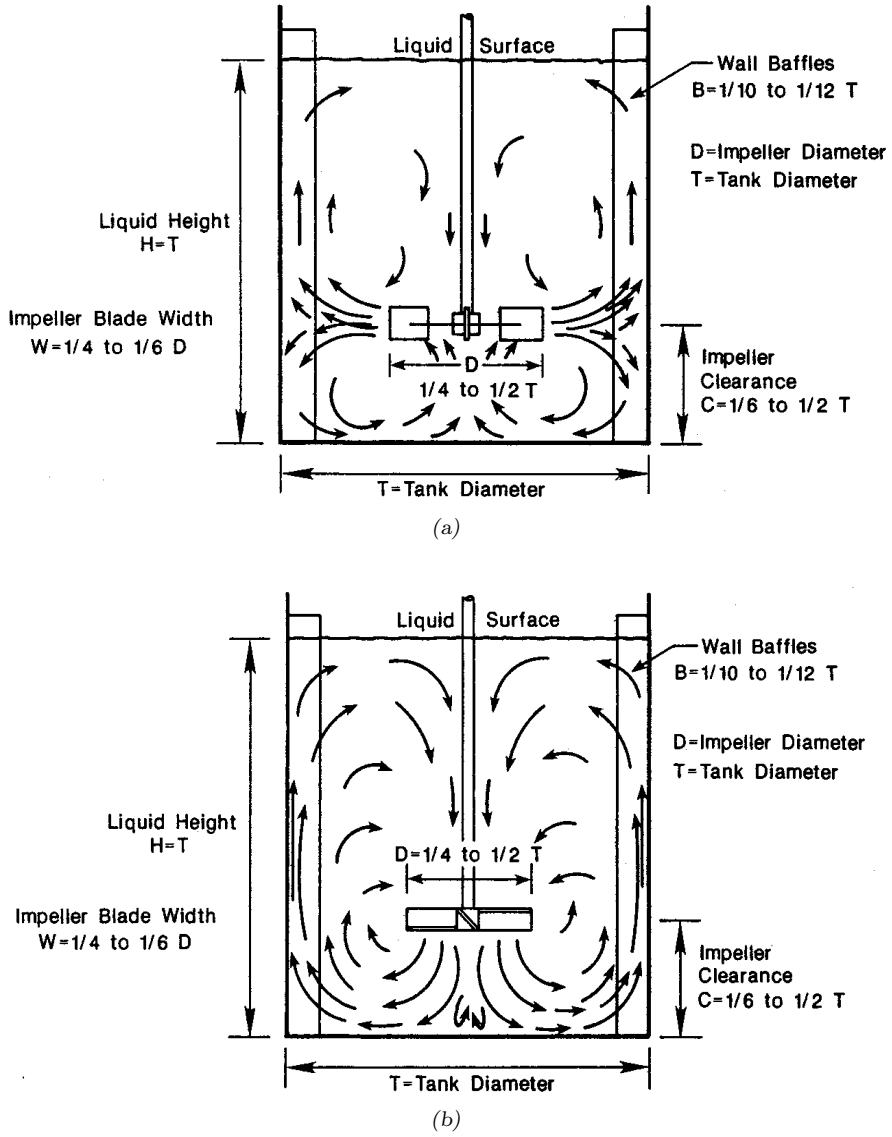

Figure 2.2: Turbulent flow patterns of STRs with the standard tank geometry equipped with (a) a radial impeller, and (b) an axial impeller (Tatterson, 1991).

upwards and a downwards separated flows, creating two loops, as shown in Figure 2.2a (Schäfer et al., 1997). If the impeller off-bottom clearance is reduced ($C/T < 0.2$), the downwards loop may disappear, generating a large loop above the impeller (Montante et al., 1999).

Axial flow impellers only generate one principal single loop, as illustrated in Figure 2.2b. The generated flow by an axial down-pumping impeller goes towards the bottom of the STR and the fluid flow is deflected towards the tank walls. The fluid flow then goes upward along

the baffles to the surface and towards the center of the tank in order to complete the loop back to the impeller. Since they generate intense axial flow towards the bottom of the vessel, they are suitable for solids suspension purposes (Jaworski et al., 1996; Mishra et al., 1998).

The blades of the so-called mixed-flow impellers or pitch blade turbines (PBTs) are angled with respect to the horizontal axis, typically between 30^o and 60^o, and can generate both axial and radial flows. The extent of the radial and axial flows depends on the angle of the blades. Their flow pattern can also be significantly affected by the impeller off-bottom clearance (Kresta and Wood, 1993b). Similar to the axial flow impeller, they can generate a single loop flow pattern and they can also be used for both down- or up-pumping configurations (Jaworski et al., 2001). All the aforementioned impellers can generate wall jets, which are important features of turbulent flow in STRs, particularly for solid/liquid mixing applications (Bittorf and Kresta, 2000; Jaworski and Zakrzewska, 2002). The upward wall jets are influenced by the baffles, and they can decay as the STR height is increased (Bittorf and Kresta, 2001). A detailed comparison of flows generated by different impeller geometries, including average velocity, turbulent kinetic energy, maximum energy dissipation rate, average shear rate and turbulent normal stress variables, can be found in the study by Kumaresan and Joshi (2006).

2.3 Important dimensionless numbers and correlations for the design of STRs

One of the most important dimensionless numbers for mechanical design of STRs and comparing the performance of different impellers is the power number, N_p, given by :

$$N_p = \frac{P}{\rho_l N^3 D^5} \tag{2.2}$$

where P is the impeller power consumption. Each impeller has its own power consumption characteristic that can be illustrated by plotting N_p versus the Reynolds number (Figure 2.3). As can be seen in this figure when the flow is laminar (Region (a) in Figure 2.3 ; $Re <\sim 10$ *to* 50), $N_p \propto Re^{-1}$. The impeller power consumption is thus independent of liquid

density and dependent on liquid viscosity (μ_l). However, in the turbulent flow regime (Region (b) in Figure 2.3 ; $Re >\sim 10^4$), as N_p is constant, the impeller power consumption becomes independent of liquid viscosity and dependent of liquid density. When the Re is between these two regions ((a) and (b) in Figure 2.3), the flow is in transitional regime ($10 < Re < 10^4$). It should be noted that the value of the power number can be influenced by the ratio of impeller thickness to impeller diameter (Bujalski et al., 1987; Rutherford et al., 1996b). Impeller power consumption can be measured using a torque meter (TM) fixed on the shaft. The net torque, proportional to the impeller power, should be calculated as the difference between the torque, measured under specific operating conditions (Γ_{tot}), and the torque resulting from friction in the gearbox and any bearings (Γ_{loss}), measured in the empty vessel (Linek et al., 2012; Moucha et al., 2012). The following equation can be used to calculate the power consumption of an impeller :

$$P = 2\pi N(\Gamma_{tot} - \Gamma_{loss}) \tag{2.3}$$

Another important dimensionless number that can characterize the performance of impellers is the flow number or pumping capacity (Tatterson, 1991), which is defined as follows :

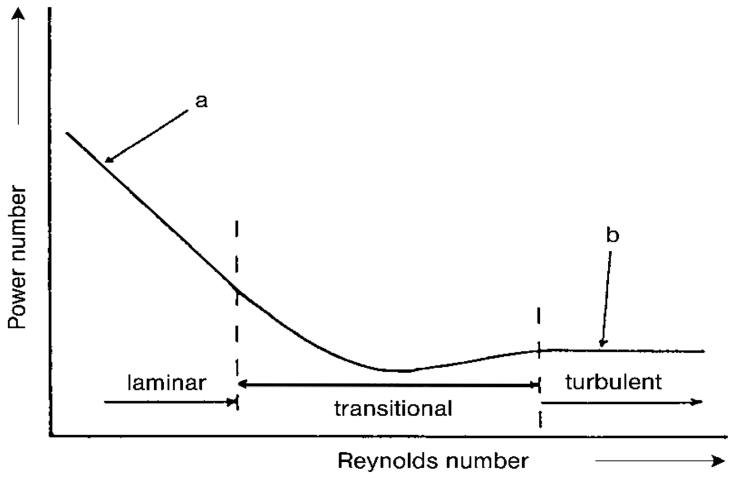

Figure 2.3: Plot of power number versus Reynolds number for a Rushton turbine (Nienow, 2010).

$$N_Q = \frac{Q}{ND^3} \tag{2.4}$$

where Q is the liquid flow rate produced by the impeller rotation. For instance, the following equation can be used to compute Q of radial flow impellers,

$$Q = R \int_{z_1}^{z_2} \int_{0}^{2\pi} v_r d\theta dz \tag{2.5}$$

In this equation R, v_r, z_1 and z_2 denote the radius of the impeller, the radial velocity, and the lower and upper heights of the impeller blades , respectively. By integrating the total outflow through this surface, the flow rate and subsequently the flow number can be determined. The radial velocity can be obtained by experimental measurements or numerical simulations. The value of N_Q under turbulent condition is known to be 0.72 for a Rushton turbine (Paul et al., 2004).

Measuring the mixing quality in STRs is critical in assessing the effectiveness of impellers. Process industries are always on the lookout for ways to improve mixing operations, either by switching to more efficient impellers or by fine-tuning operating conditions. Therefore, quantitative approaches are needed in order to measure the mixing characteristics of impellers (Nienow, 1997). Mixedness can be assessed by measuring the concentration of a colored (Cabaret et al., 2007; Melton et al., 2002), fluorescence (Distelhoff et al., 1997; Guillard et al., 2000) or conductivity (Rewatkar and Joshi, 1991; Zhang et al., 2009) tracer at various locations in the tank, to determine how fast the variance of the tracer concentrations decreases to an expected value over time. The mixing time (θ_m) in STRs is often correlated to the tank to impeller diameter ratio, power number, and impeller rotational speed. The following correlation was proposed by Ruszkowski (1994) and Grenville et al. (1995) to determine the mixing time of STRs operating in a turbulent flow regime :

$$\theta_m = 5.3(T/D)^2 N_p^{-1/3} N^{-1} \tag{2.6}$$

The adequate design and scale-up of gas/liquid STRs requires knowledge of the gas/liquid operating regimes. These flow regimes are often characterized by gas flow number or aeration number, Fl_g, and the Froude number, Fr. They are given by :

$$Fl_g = \frac{Q_g}{ND^3} \tag{2.7}$$

$$Fr = \frac{N^2 D}{g} \tag{2.8}$$

Where Q_g and g are volumetric gas flow rate and gravitational acceleration. Various possible gas/liquid flow regimes that occur in STRs are illustrated in Figure 2.4. Below the established minimum impeller rotational speed ($Fr < 0.045$), the impeller has an ineffectual operation. Above this limit, and when the impeller rotational speed is low or gas flow rate is high, the gas mainly passes through the center of the tank and it moves upward in a limited region around the impeller and shaft without dispersion (regime (a) in Figure 2.4). The liquid flow out of this region is not affected by the gas flow. In this situation the impeller is said to be flooded ; this is undesirable situation and the minimum impeller rotational speed is required to avoid flooding (N_f). Warmoeskerken and Smith (1985) showed that the flooding for a Rushton turbine occurs if :

$$Fl_g > 30Fr(\frac{D}{T})^{3.5} \tag{2.9}$$

By increasing the impeller speed ($N > N_f$), the gas phase is dispersed in the upper part of the tank (regime (b) in Figure 2.4) and in this regime, the STR acts like a bubble column, while the lower section is not in contact with the gas. In the transition regime (regime (c) in figure 2.4), the recirculation of the gas in the STR just begins to form. Further increase in the impeller rotational speed leads to the recirculation of gas in the upper section, and it starts to be dispersed in the lower region (regime (d) in Figure 2.4). This regime is also known as the complete dispersion. Nienow et al. (1977) has proposed the following correlation to obtain the minimum impeller speed required for complete dispersion of the gas for an STR

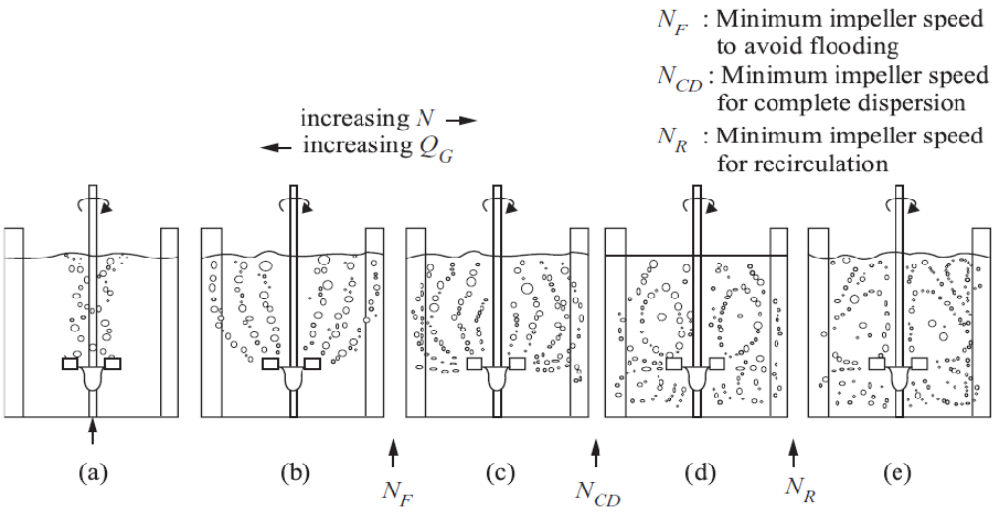

Figure 2.4: Illustration of gas/liquid flow regimes in STRs : (a) flooded, (b) loaded, (c) transition, (d) complete dispersion, (e) complete dispersion with recirculation (Ranade, 2001).

equipped with the Rushton turbine :

$$N_{cd} = \frac{4(Q_g)^{0.5}(T)^{0.25}}{D^2} \tag{2.10}$$

Complete dispersion is an optimal condition for gas/liquid mass transfer and mixing processes. An increase in the impeller rotational speed results in the gross recirculation of the gas, and a high level of turbulence at the surface promotes gas entrainment (surface aeration) (regime (e) in Figure 2.4). Nienow et al. (1977) developed a correlation to find the transition to the recirculation regime for a Rushton turbine, as follows :

$$Fl_g = 13Fr^2(\frac{D}{T})^5 \tag{2.11}$$

Three stable cavity groups can be formed behind the blades of a Rushton turbine : vortex, clinging, and large cavities (Nienow et al., 1997; Paul et al., 2004). The schematics of these cavities are shown in Figure 2.5. The vortex cavities are two rolling vortices of gas at the top and bottom of the impeller blades that form at low gas flow rates. With an increase in gas flow rate clinging cavities are formed that are larger than vortex cavities, and they cling to

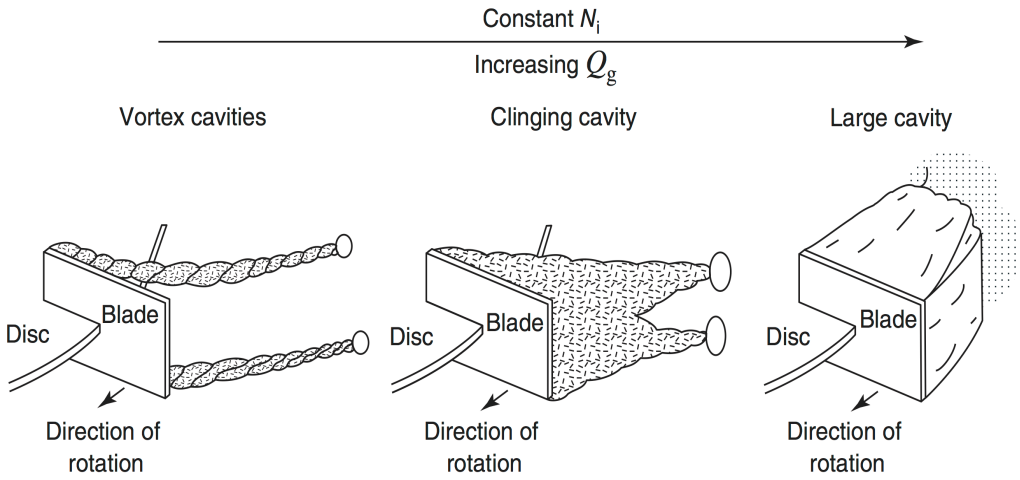

Figure 2.5: Illustration of cavity types for a Rushton impeller (Kadic and Heindel, 2014).

the backside of the blades and produce vortices at the gas tail. The large cavities form at a high gas flow rate, and they can cause a significant reduction in the power number of the impeller and consequently affect its performance. The flow map of a single Rushton turbine can be built based on the correlations (2.9) to (2.11) shown in Figure 2.6.

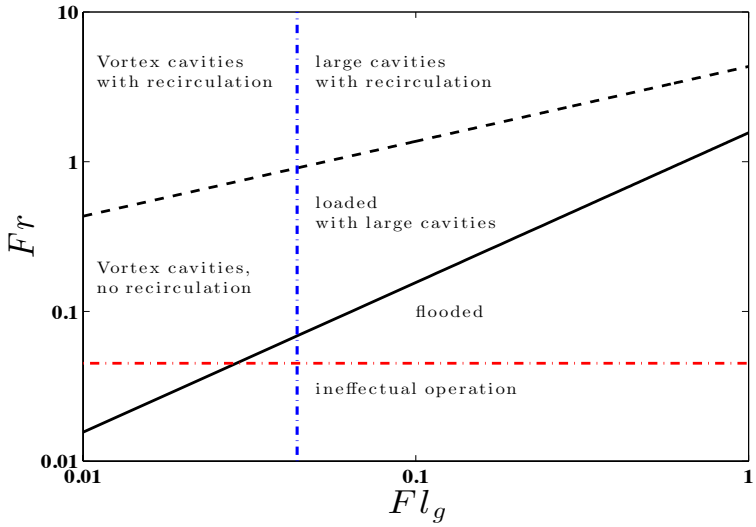

Figure 2.6: Flow map for a Rushton turbine ($D/T = 1/3$).

For the same impeller rotational speed, the power consumption of gas/liquid STRs is lower than that of single-phase STRs, due to the formation of gas cavities behind the impeller

blades. This can affect the impeller performance for mixing, mass transfer and gas dispersion. Cavity formation can be reduced significantly by lowering the pressure difference in front and behind the impeller blades. Recent gas dispersion impellers such as the Chemineer concave disc (CD-6) have been designed to decrease this pressure difference and accordingly to reduce the power consumption for the single phase flow (N_p for CD-6 is 3.2), as well as the relative power demand (RPD) (P_g/P). The RPD or gassing factor depends on the gas flow rate, as well as the impeller shape, diameter, and rotational speed. It generally decreases as the gas flow number increases. Published correlations for RPD and gassed power draw (P_g) are summarized in Table 2.1.

Table 2.1: Empirical correlations for RPD and P_g.

Reference	RPD or P_g	Remark
Michel and Miller (1962) [a]	$P_g = 0.783\left(\frac{N_p N T^3}{Q_g^{0.56}}\right)^{0.459}$	-
Hassan and Robinson (1977)	$RPD = C_p F l_g^{-0.38} We_i^{-0.25}$	$We_i = \frac{N^3 D^3 \rho_c}{\sigma}$
Hughmark (1980)	$RPD = 0.1\left(\frac{Q_g}{NV}\right)^{-0.25}\left(\frac{N^2 D^4}{g D V^{2/3}}\right)^{-0.2}$	-
Midoux and Charpentier (1984)	$P_g = 0.34\sqrt{N_p}\left(\frac{P_g N D}{Q_g^{0.56}}\right)^{0.45}$	-
Cui et al. (1996)	$1 - RPD = 9.9\left(\frac{Q_g N^{0.25}}{D^2}\right)$	for $\frac{Q_g N^{0.25}}{D^2} \leq 0.055$
	$1 - RPD = 0.52 + 0.62\left(\frac{Q_g N^{0.25}}{D^2}\right)$	for $\frac{Q_g N^{0.25}}{D^2} > 0.055$
Middleton and Smith (2004)	$RPD = 0.18 F l_g^{-0.2} Fr^{-0.25}$	for D/T=0.4

a. is cited in Garcia-Ochoa and Gomez (2004).

2.4 Scale-up of STRs

Garcia-Ochoa and Gomez (2009) have divided scale-up approaches in four categories : fundamental methods ; semi-fundamental methods ; dimensional analysis ; and rules of thumb. Fundamental methods use CFD to solve the microscopic balance of momentum and mass transfer in order to predict the behaviour of STRs in larger scales (Gimbun et al., 2009). Many simplified assumptions should be used in order to apply this method due to its intensive computational requirement. The semi-fundamental methods use simplified flow models that are less computationally intensive to predict the performance of industrial-scale STRs (Zahradnık et al., 2001). These models are able to describe the local hydrodynamics of the system, and they can be a helpful design tool for the successful scale-up and optimizing of operating conditions at the production scale (Vlaev et al., 2000). However, even by employing a large number of compartments, fluxes between them are often defined based on global quantities. Consequently, the flow complexity in a stirred tank is oversimplified and may fail to accurately predict the mixing behaviour. In dimensional analysis, the relevant dimensionless numbers for mechanisms involved in the process are first identified and kept constant during the scale-up. However, it is impossible to keep all the important dimensionless numbers constant during the scale-up. The conventional methods of scale-up are the rule of thumb methods that use different criteria such as constant power input per volume, P/V, constant volumetric mass transfer coefficient, k_La, constant impeller tip speed, V_{tip}, while maintaining geometrical similarity depends on the process requirements (Junker, 2004). However, as shown in Table 2.2, it is impossible to keep all these criteria constant during the scale-up.

2.5 Volumetric mass transfer coefficient

The productivity of many processes involving gas/liquid flows is limited by mass transfer between phases, especially in the case of low soluble species in the gas phase that transfer to the liquid phase. This includes many bioprocesses such as the production of expensive specialty chemicals, including proteins, and bulk chemicals such as biofuels, lactic acid, and

Table 2.2: Effects of different scale-up criteria for a linear scale-up factor of 10 (Amanullah et al., 2004).

Scale-up Criteria						
Large Scale/ Small Scale values	Equal P/V	Equal N	Equal U_T	Equal Re	Equal k_La and vvm	Equal k_La Equal and v_s
$P \propto N^3D^5$	1000	10^5	100	0.1	829	1000
$P/V \propto N^3D^2$	1	100	0.1	10^{-4}	0.8	1
$T_c \propto N^{-1}$	4.55	1	10	100	9.4	4.55
$V_{tip} \propto ND$	2.2	10	1	0.1	2.7	2.2
$Re \propto ND^2$	22	100	10	1	27.2	22
$Q \propto ND^3$	220	1000	100	10	272	220
$Fr \propto N^2D$	0.48	10	0.1	10^{-3}	0.5	0.48
k_La at equal vvm	1.59	39.8	0.32	2.5×10^{-5}	1	-
k_La at equal v_s	1	25.1	0.20	1.6×10^{-3}	-	1

citric acid, where oxygen transfer is vital for the success of the process (Garcia-Ochoa et al., 2010; Lara et al., 2006). Understanding gas/liquid mass transfer is thus essential for the adequate design of mixing systems. The mass transfer rate can be quantitatively defined as the product of the volumetric mass transfer coefficient (k_La) and the driving force, which is the difference between the saturation concentration of gas and its actual concentration in the liquid phase ($C^* - C(t)$). Accordingly, k_La can affect operations by limiting productivity in various ways, such as by changing the reaction rate and, possibly, the selectivity.

Experimental methods for measuring k_La can be generally divided into chemical and physical methods. In chemical methods, dissolved oxygen reacts with species in the liquid phase. Therefore, by measuring the concentration of this species versus time k_La can be calculated (Liu et al., 2006). On the other hand, physical methods are based on the measurement of dissolved oxygen concentrations in the liquid during the physical absorption or desorption of oxygen. Nowadays physical methods are the most commonly used methods for k_La measurement (Cabaret et al., 2008). Chemical methods have some limitations compared to physical methods. As chemicals are added to the system, the physicochemical properties of the liquid phase and, as a result, the fluid dynamics can be altered. They can also promote or limit the

coalescence of gas bubbles which affects the specific interfacial area. Moreover, since the absorption rate may be enhanced by fast chemical reactions in the liquid phase, these methods can serve higher values of k_La than the actual value, especially if the experimental conditions are not kept within certain limits. More details regarding these measurement methods and their advantages and limitations can be found in the reviews by Van't Riet (1979), Gaddis (1999), and Garcia-Ochoa et al. (2010).

For several decades, many research endeavours have been dedicated to correlate measured k_La to the operating conditions of the stirred tanks, providing a single average value for this parameter. Correlations based on dimensionless numbers are often in the form of $k_La = f(Fr, Fl_g, D/T, etc.)$; however, the dimensional ones are often in the form of $k_La = f(P_g/V_l, v_{sg})$, where P_g/V_l and v_{sg} are the energy input per liquid volume and the gas superficial velocity, respectively. These correlations for stirred tanks were recently summarized by Yawalkar et al. (2002), Garcia-Ochoa et al. (2010) and Kadic and Heindel (2014). The differences in the values of the exponents proposed by the various authors can be attributed to differences in the geometries of the systems, the range of operating conditions, and the measurement techniques used. Xie et al. (2014) showed that predictions of these correlations can vary, with standard deviations ranging from 10 to 55%, even without a large difference in the scale of the STR. This indicates that these correlations are scale-dependent and that their application would be limited for the design of large-scale reactors (Gabelle et al., 2011; Smith, 2006).

Understanding gas/liquid flow behaviour in terms of operating regimes is vital and should be taken into account for successful STR scale-ups. Yawalkar et al. (2002) used experimental k_La values drawn from the literature for different sizes of STRs (T = 0.39 to 2.7 m) to take the effect of the flow regime into account, and proposed the following correlation for k_La as a function of relative dispersion (N/N_{cd}) (with ±22% accuracy) :

$$k_La = 3.35(N/N_{cd})^{1.464}(v_{sg}) \tag{2.12}$$

Kapic and Heindel (2006) used the same approach and developed the following correlation to predict the k_La of STRs :

$$k_La = 1.59(N/N_{cd})^{1.342}(v_{sg})^{0.93}(T/D)^{0.415} \tag{2.13}$$

While these correlations may provide a better prediction for the k_La, at least up to the pilot-scale STRs, they do not provide any information on the local values of this parameter, which can bring the concept of imperfect mixing into play.

The mass transfer coefficient is enormously affected by hydrodynamics in the reactor. Figure 2.7 is an schematic view of the various factors affecting k_La. Some effort has gone into developing theoretical predictions of k_La by tailoring the operating conditions to mass transfer theories. These methods successfully predict the values of the overall k_La for bubble columns (Kawase et al., 1987, 1992; Sánchez Mirón et al., 2000), airlifts (Sánchez Mirón et al., 2000; Tobajas et al., 1999), and STRs (Garcia-Ochoa and Gomez, 2004; Kawase et al., 1992) of different sizes and under various operating conditions. For instance, Garcia-Ochoa and Gomez (2004) used Higbie's penetration theory of mass transfer (Higbie, 1935) and Kolmogorov's theory of turbulence to predict k_L. Impeller power consumption was used to estimate the average value of the turbulent energy dissipation rate inside the system to consequently predict the average value for k_L. The values of the global interfacial areas were calculated from a theoretical equation for gas hold-up and the mean size of gas bubbles. While the predictions of the model were in reasonable agreement with experimental data and other empirical correlations for both Newtonian and non-Newtonian fluids, they were limited to the overall value of k_La in STRs and could not provide any information regarding local values.

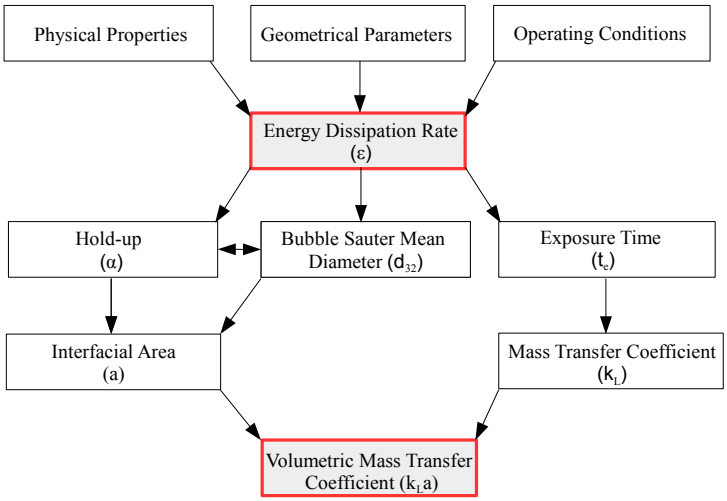

Figure 2.7: Relationship between volumetric mass transfer coefficient and hydrodynamic parameters. Adapted from Garcia-Ochoa et al. (2010).

2.6 Experimental techniques for the characterization of flow in STRs

In order to investigate the hydrodynamics of liquid and gas/liquid STRs and to validate the predictions of modelling tools, experimental measurements of flows are vital. Many techniques have been developed in recent years to measure fluid flows in different process tanks and devices, including STRs (Boyer et al., 2002; Chaouki et al., 1997; Mavros, 2001). Fluid flow measurement techniques can be divided into two general categories : invasive and non-invasive. In the first category, a measurement probe is inserted into the reactor that alters the flow around it, while in the latter measurement probes or devices are positioned close to the reactor without any interaction with the flow therein. Figure 2.8 depicts the available measurement techniques for multiphase flows.

2.6.1 Invasive techniques

Two examples of invasive measurement techniques used for measuring flows in STRs are pitot tube (Wolf and Manning, 1966) and hot-wire anemometry (Cooper and Wolf, 1968). The latter can also be used to measure the local hold-up of gas in gas/liquid STRs (Lu and Ju, 1987). Hot-wire anemometry has no limitations regarding gas hold-up. However, as its

sensors are fragile, employing this technique for solid/liquid flows is not recommended (Boyer et al., 2002). Another invasive technique for the measuring gas hold-up is to use electrical conductivity probes. This technique relies on the difference in conductivity between the liquid and gas (Bouaifi et al., 2001; Cents et al., 2005). In this technique, the liquid phase must be conductive, otherwise an additive (*e.g.* salts) must be added to the system ; this can affect the hydrodynamics of the STR.

In recent years, optical probes have been used to measure gas hold-up and bubble dynamics (velocity, chord lengths, and interfacial area) in gas/liquid (Lee and Dudukovic, 2014; Mueller and Dudukovic, 2010; Wang et al., 2006) and solid hold-up in liquid/solid STRs (Jafari et al., 2012). This technique is based on the difference of refractive indices between gas, liquid and solid phases. For instance, light refracts and reflects from the probe tip surrounded by a liquid and gas, respectively. Mueller (2009) used a four-point optical probe for the estimation of bubble size and bubble velocity distributions in a gas/liquid STR operating at various flow regimes.

Another invasive technique that has been used to measure bubble size distribution and hold-up in gas/liquid STRs is capillary suction probe (CSP) (Alves et al., 2002b; Barigou and Greaves, 1991, 1992; Greaves and Kobbacy, 1984; Laakkonen et al., 2005). In this technique a sample of gas/liquid dispersion is sucked by a pump and sent to a capillary probe where the bubble transfer to gas slugs and their lengths and velocities are measured by light-sensitive sensors (Laakkonen et al., 2005). The main limitations of this technique are the possible flow pattern disturbance by the probe, the inability to determine the size of very large and very small bubbles (depending on the diameter of the capillary), and difficulties in the isokinetic sampling of the bubbles.

Polarographic probes are often used to measure the volumetric mass transfer coefficient (k_La) in gas/liquid STRs (Laakkonen et al., 2007b) employing the dynamic method. This method is based on the measurement of dissolved oxygen (DO) concentration in the liquid phase through the absorption/desorption of oxygen. More precisely, oxygen in the liquid phase

is desorbed by passing nitrogen through the STR. After this step, the gas feed is switched to air, and DO concentration versus time is measured with the probe until a new equilibrium state is reached (Van't Riet, 1979). Then, by solving the dissolved oxygen mass balance, the following equation can be obtained :

$$ln(\frac{C - C^*}{C_0 - C^*}) = -k_L a.t \tag{2.14}$$

Where C, C^* and C_0 are concentrations of oxygen at time t at equilibrium and at $t = 0$, respectively. The assumptions to obtain the above equation are : (1) the oxygen uptake rate (OUR) in the liquid phase is zero ; (2) both gas and liquid are "well-mixed" ; (3) the mass transfer is controlled by resistance in the liquid film ; and (4) the pressure variation inside the tank is negligible. The volumetric mass transfer coefficient is determined from the slope of the natural logarithm of the measured DO concentrations versus time, by employing the least square method (Kapic and Heindel, 2006; Linek et al., 1987; Van't Riet, 1979; Zhu et al., 2001). The probe response time is an important parameter for accurately determining oxygen concentration and should be considered in order to obtain a precise value for $k_L a$ from the dissolved oxygen concentration measurement profiles (Deckwer et al., 1974; Gourich et al., 2008). It should be noted that the measured values for $k_L a$ can also be dependent on the position of the probe in the STR.

2.6.2 Non-Invasive techniques

Many non-invasive techniques have been used to elucidate flow phenomena, including liquid velocity, bubble size, and bubble or particle velocity in multiphase STRs. These techniques involve particle image velocimetry (PIV) (Aubin et al., 2004; Baldi and Yianneskis, 2003, 2004; Deen et al., 2002; Delafosse et al., 2011; Escudie and Line, 2003; Fontaine et al., 2012; Gabriele et al., 2009; Ranade et al., 2001; Roy et al., 2010; Sharp and Adrian, 2001; Sheng et al., 2000), laser doppler anemometry (LDA) (Ducci and Yianneskis, 2005; Kresta and Wood, 1993a; Lee and Yianneskis, 1998; Morud and Hjertager, 1996; Murthy and Jo-

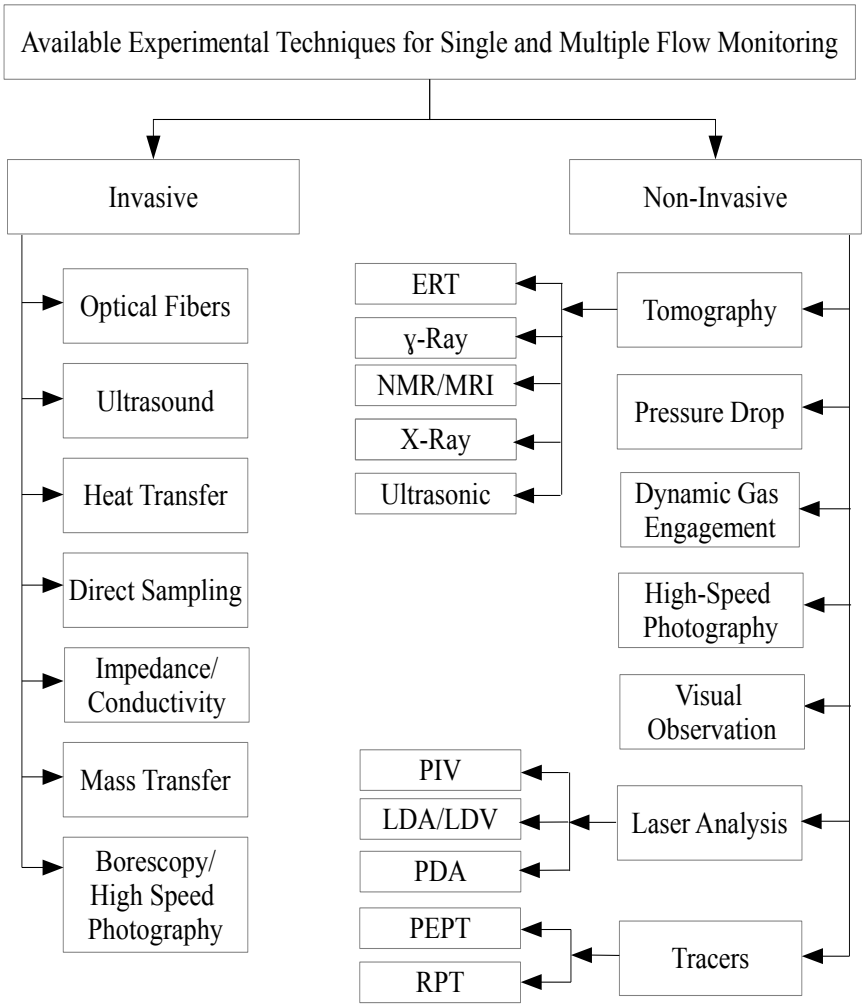

Figure 2.8: Measurement techniques for multiphase flow. Adapted from Mueller (2009).

shi, 2008; Rutherford et al., 1996a; Wu and Patterson, 1989; Zhou and Kresta, 1996), phase doppler anemometry (PDA) (Laakkonen et al., 2005), and high-speed photography techniques (Bouaifi et al., 2001; Córdova-Aguilar et al., 2008; Corkidi et al., 2008; Galindo et al., 2005; Guevara-López et al., 2008; Laakkonen et al., 2005; Takahashi et al., 1992; Takahashi and Nienow, 1993). However, their use is restricted to transparent flows and transparent STR walls, due to the inherent use of a laser or light. Furthermore, the optical velocimetry techniques (PIV, LDA and PDA) only provide Eulerian data, while mixing is intuitively a Lagrangian process. To determine the Lagrangian motion of a fluid parcel, post-processing,

with its intrinsic uncertainties, is required (Heniche and Tanguy, 2006).

Radioactive particle tracking (RPT) and positron emission particle tracking (PEPT) are also non-invasive techniques that measure the velocity of the solid or liquid phase in an opaque system. While PEPT has been used to study fluid flows in SRTs (Fishwick et al., 2005; Pianko-Oprych et al., 2009), it is limited to tanks that are small enough to be placed in the PEPT camera. Furthermore, Chiti et al. (2011) have reported that the time resolution of the PEPT technique is relatively low (typically 40-60 ms). PEPT is also not very efficient for reconstructing tracer particle positions close to the edge of the system (Guida et al., 2012). RPT has been used extensively to characterize solid and liquid flows in different unit operations since it was first introduced by Lin et al. (1985). These units included fluidized beds (Bashiri et al., 2010; Kiared et al., 1999; Mostoufi and Chaouki, 2001, 2004), spouted beds (Cassanello et al., 1999; Djeridane et al., 1998; Roy et al., 1994), cylindrical tumblers (Alizadeh et al., 2013), a V-blender (Doucet et al., 2008), bubble columns (Chen et al., 1999; Devanathan et al., 1990; Xu et al., 2005), and STRs (Guha et al., 2007; Khopkar et al., 2005; Rammohan et al., 2001a,b). The RPT tracks the motion of a single radioactive particle that emits γ-rays, using an array of Sodium Iodide (NaI) scintillation detectors (Figure 2.9). A high-speed data acquisition system counts the number of γ-rays detected by each detector. Then the position of the tracer in time can be reconstructed using a phenomenological relation between the number of photons received and effectively counted by a detector and the position of the emitting source (Beam et al., 1978; Tsoulfanidis and Landsberger, 2011). Details on the calibration of the system, the inverse reconstruction strategy for determining the position of the tracer particle, and the errors associated with the measurement technique are provided by Chaouki et al. (1997) and Doucet et al. (2008).

Several tomographic techniques, such as X-ray (Ford et al., 2008), γ-ray (Khopkar et al., 2005) and electrical resistance tomography (ERT) (Mann et al., 1997; Montante and Paglianti, 2015; Wang et al., 2000), have been developed to measure the local gas hold-up in gas/liquid STRs. While X-ray tomography can provide a very high spatial resolution (Ford et al.,

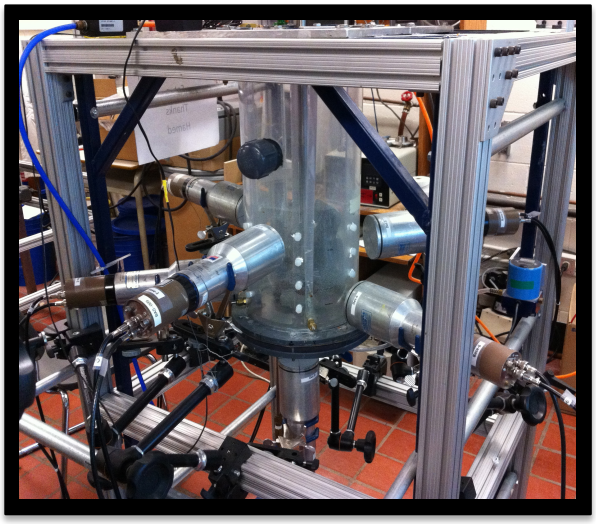

Figure 2.9: Typical positions of Sodium iodide (NaI) scintillation detectors around an STR.

2008), due to the low energy level of X-ray, its use is limited for small STRs that contain low attenuating materials. The γ-rays tomography can be employed for larger tanks due to its higher energy level ; however, it has a lower spatial resolution than X-ray (Kumar et al., 1995). While ERT is an inexpensive choice, it can apply to STRs that involve liquid fluids with dielectric properties. This technique also has low spatial resolution (Mann et al., 1997). Global (or total) gas hold-up ($\overline{\alpha_g}$) can be easily determined visually by measuring the increase in liquid height due to gas sparging inside the STR :

$$\overline{\alpha_g} = \frac{H_D - H}{H_D} \tag{2.15}$$

where H and H_D are the heights of the liquid with no gas sparging and with gas sparging inside the STR, respectively. This method is subjective due to fluctuations of the liquid surface. To reduce measurement subjectivity, visual observations should be repeated for different locations. For instance, H_D can be measured at two diametrically opposite locations on the mid-planes between two adjacent baffles (Saravanan and Joshi, 1996). Meng et al. (2002) proposed an alternative method for cases in which visual determination of an increase in the liquid height is difficult due to low global hold-up or a large amount of turbulence induced by

an impeller. In this method, the global gas hold-up is measured using an inclined tube attached to the outside of the vessel wall at liquid height equal to H. These authors verified the results of this technique by comparing them with the measured values by γ-ray densitometry.

2.7 Numerical modelling of STRs

The design and scale-up of STRs traditionally relies on experimental efforts and empirical correlations. This common approach has faced several difficulties. Usually the empirical correlations are based on vessel average values in the stirred tank. However, this assumption is a main issue in the scale-up of STRs, so that considering local conditions in stirred tanks is crucial, especially in a system where the mixing performance is dictated by physical phenomena whose time scale is shorter than the vessel mixing time. As already reviewed in the previous section, several experimental methods have been developed to find local hydrodynamic parameters (Chaouki et al., 1997; Mavros, 2001). Nevertheless, some concerns still need to be addressed, such as the cost of the experimental method used and its scale limitations. Many processes involve high temperature, high pressure, and hazardous conditions for which detailed experimental data acquisition is not practical. Thanks to the availability of increasingly powerful computers, numerical models are becoming gradually used as a practical tool for understanding fluid dynamics and eventually designing more efficient processes. It is believed that significant improvements can be achieved in the design of STRs using a numerical model that considers the actual flow field and local hydrodynamic parameters. The numerical modelling of STRs can be generally divided into three main approaches : (1) compartment models (CM), also called multi-zone or network-of-zone models ; (2) Computational Fluid Dynamics (CFD) ; (3) CFD-based compartment models, also known as multiscale models. These models are reviewed in the following subsections.

2.7.1 Compartment models (CMs)

CMs divide the STR into a limited number of interconnected volumes. Fluxes between these volumes are defined based on global quantities, such as the flow number. In these volumes, flow properties such as turbulence and concentration are assumed constant. Vasconcelos et al. (1995) studied liquid mixing in multiple-turbine aerated stirred tanks (0.3-0.5 m diameter) in the loading regime by employing a compartments-in-series model. Impeller rotational speed, aeration rate, gas hold-up, power input and reactor geometry were used to obtain the values of the model parameters. The average relative error between calculated and measured (by conductivity probe) values of mixing times were ± 4 %. Vrabel et al. (1999) followed the same approach to describe mixing in a large scale fermenter (30 m^3) equipped with four Rushton turbines. The adequacy of model was verified by comparison between the predicted mixing time and experimental data obtained by fluorescence pulse-response. Vrabel et al. (2000) used a CM model to study the effect of impeller type on the mixing time of large STRs (12 m^3 and 30 m^3) equipped with multiple impellers. It was shown that a considerable reduction in mixing time can be achieved by replacing the upper radial impellers with axial ones at the same power consumption.

Vlaev et al. (2000) studied the performance of a 3 m^3 triple-impeller gas/liquid stirred bioreactor using CM, comprising 600 two-dimensional zones. The gas/liquid flows were calculated by assuming that bubbles move independently at their rise velocity without any effect on the generated liquid flow by the impellers. Assuming single mean bubble size and solving the continuity equation for gas phase, the gas hold-up distribution was predicted inside the system. Mass transfer and bioreactions then combined with gas-liquid flow to predict the spatial distribution of dissolved oxygen and liquid nutrient concentrations. It was shown that while the concentration of oxygen in the gas phase was almost uniform throughout the stirred tank, there was about a forty-fold variation in the dissolved oxygen levels in the liquid phase. Zahradnık et al. (2001) extended this model in order to take the different bubble sizes into account ; however, no information regarding the spatial variations of the specific interfacial

area was provided. The model was used to predict the performance of three different industrial fermenters (3 and 31 m^3 triple-impeller stirred tank reactors, and 236 m^3 bubble column reactor). The predicated spatial variation of gas hold-up showed no difference compared to the one predicted based on single size bubble diameter (d_b =5 mm) (Vlaev et al., 2000). The comparison of the predicted values of local conditions inside these three reactors revealed that the gas hold-up was not distributed uniformly, mass transfer coefficients varied by a factor of 100, oxygen fluxes varied by a factor of 1000, dissolved oxygen varied from 3 to 98% saturation. They mentioned that these variations could affect micro-organism viability and may change metabolic pathways. This method is further extended to a three-dimensional structure comprising 36,000 compartments in order to model local hydrodynamic of gas/liquid flow in a 3 m^3 triple-impeller industrial pilot-plant bioreactor (Hristov et al., 2004, 2001).

Alves et al. (2002a) developed a compartment model that takes the combined effect of bubble coalescence and breakage into account to model the gas dispersion and local bubble size distributions throughout a gas/liquid STR equipped with two Rushton turbines. The liquid and gas flow rates between compartments were determined based on the impeller pumping capacity and the steady-state continuity equation, respectively. The proposed model involved two adjustable parameters that were dependent on the physiochemical properties of the liquid, but independent of operating conditions. It was shown that the model can reasonably predict the local gas hold-up and mean bubble size compared to the experimental values obtained using CSP. Based on the model prediction and experimental measurement, it was observed that bubble coalescence prevails over breakage. The intense coalescence was observed in the turbines discharge streams and near the tank wall. This phenomenon was attributed to the larger collision frequency due to higher turbulence in these regions of the STR.

As compartment models are computationally much less demanding than CFD, they are good choices to couple chemical reactions with fluid dynamics. However, even by employing a large number of compartments, fluxes between them are often defined based on global

quantities. Consequently, flow complexity in a stirred tank is oversimplified and may fail to accurately predict mixing behaviour. Moreover, the single value for bubble size and liquid-side mass transfer coefficient (k_L) were used to define the value of the volumetric mass transfer coefficient inside gas/liquid systems. These simplified assumptions can significantly affect the predicted performance of the system.

2.7.2 Computational fluid dynamics (CFD) modelling of STRs

The use of CFD to study the hydrodynamics of STRs began in the late 1970s (Harris et al., 1996). Most early published works regarding the CFD modelling of STRs involved simulations of single-phase liquid flows (Ranade, 2002; Sommerfeld and Decker, 2004) and were reviewed by Harris et al. (1996) and Brucato et al. (1998). In these studies the predicted results of alternative methods for the simulation of impeller rotation were presented and discussed. These methods included impeller boundary condition (IBC), sliding mesh (SM) and multiple reference frames (MRF). In the first method, the impeller is not explicitly simulated and its effects are modelled by imposing an experimentally determined velocity profile as the impeller boundary condition. In the second and third methods, the tank volume is divided into two parts. With SM, the inner zone rotates with the impeller and the outer zone is stationary. However, in the MRF method, the flow field in the inner region that contains the impeller, is simulated in the rotating reference frame while the stationary reference frame is used for the outer region. As the IBC method can be used only if reliable experimental data are available for the flow near the impeller, it is not a predictive tool. The other two methods can both provide satisfactory results while requiring no experimental information. However, the transient SM technique is much more computationally intensive than MRF.

In the early studies, k-ε is used in order to model turbulent flow in STRs. In recent years, growing attention has been devoted to assessing the performance of different turbulent models, including Reynolds averaged Navier-Stokes (RANS) models, and the large eddy simulation (LES), in predictions of turbulent flow field in STRs (Aubin et al., 2004; Bashiri

et al., 2014; Delafosse et al., 2008, 2009; Gimbun et al., 2012; Murthy and Joshi, 2008). It has been shown that all these models can predict reasonably well the mean velocity profiles in an STR, both quantitatively and qualitatively. LES is better at predicting local turbulent properties (turbulent kinetic energy and its dissipation rate), especially close to the impeller, albeit with an excessive demand on computational resources. In spite of intrinsic limitations of the RANS models, such as the removal of turbulence unsteadiness, it can provide realistic predictions of turbulent flow with affordable computational resources. The prediction uncertainties in RANS models are often only attributed to its inherent limitations, and numerical errors are disregarded. There are few studies in the literature regarding the dependency of RANS results on the numerical strategy (Aubin et al., 2004; Deglon and Meyer, 2006). They show that predictions of the turbulent properties inside STRs can be significantly improved upon by utilizing finer grids and higher-order discretization scheme. These results were recently further justified by Coroneo et al. (2011) and Singh et al. (2011), who used up to 6.6 million cells. An extensive review on CFD simulations of STRs was recently presented by Joshi et al. (2011a) and Joshi et al. (2011b). The quantitative assessments of the accuracy of CFD analyses of STRs repose mainly on a comparison of the flows close to the impeller, which is about 30% of the tank volume. While the flow characteristics are important in the regions near the walls, baffles, and bulk of the tank, little attention has been paid to assess the accuracy of CFD predictions therein. Therefore, a comprehensive experimental measurement study is needed to provide data about these regions for a rigorous quantitative comparison with the predictions of CFD simulations.

Many industrial processes involve gas/liquid dispersion in STRs. Recently, several studies have focused on simulations of gas/liquid flows in STRs. There are mainly two modelling approaches for simulating such flows : Eulerian-Eulerian (EE) and Eulerian-Lagrangian (EL). In EL, a Eulerian framework is used for the continuous phase while the dispersed phases are tracked in a Lagrangian framework ; in EE, Eulerian framework is used for both phases as interpenetrating continua identified by their local average volume fraction (Ranade, 2002).

The EL approach is suitable for simulating dispersed multiphase flows containing low volume fractions of dispersed phases since computational requirements are very large for higher values of volume fractions. Due to this limitation, the EE approach is usually selected for CFD simulations of turbulent gas/liquid flows in STRs. In the EE approach, the mass and momentum balance equations are solved for each phase separately. The momentum equations of the phases interact with each other through the inter-phase momentum exchange. In addition to the modelling of impeller rotation and turbulence, interactions between the phases need to be considered, which makes simulations of turbulent gas/liquid flow in STRs even more complicated.

Deen et al. (2002) used a three-dimensional grid to model gas dispersion in an STR agitated by a Rushton turbine. A single bubble size was used in the simulations, and only drag force was considered for simulations. The bubble drag coefficient was determined from standard correlations for a distorted (Ishii and Zuber, 1979) or spherical shaped bubble (Schiller and Naumann (1933) (Clift et al., 2005). Turbulence was modelled by the standard k-ε model, with an additional turbulent viscosity term to account for bubble-induced turbulence, according to the Sato model (Sato and Sekoguchi, 1975). Impeller rotation was modelled by the SM method, and only 20 impeller revolutions were considered to complete the simulation. Despite using uniform bubble size for the simulations, they were able to observe the formation of gas cavities on each of the blades. The predicted gas and liquid velocities were compared to their experimental values obtained by PIV. While reasonable agreement was found for the liquid and gas radial velocity component values, the axial velocity component of the gas phase was considerably over-predicted by CFD simulations. No values were reported on local or overall gas hold-ups.

Wang et al. (2006) modelled gas/liquid flows in STRs operating at various flow regimes. They compared the predicted local values of gas hold-up with the measured values by a fiber optic probe. While the local gas hold-up was under-predicted in all flow regimes in the impeller discharge stream, reasonable agreement was obtained in the bulk flow region. No comparison

for the overall gas hold-up was reported. Khopkar and Ranade (2006) studied a gas/liquid STR operating at vortex and large cavity flow regimes. It was shown that the drag model proposed by Brucato et al. (1998) with modified constant can lead to a better prediction of gas hold-up distribution compared to the drag model proposed by Bakker and Akker (1994) and Lane et al. (2005). The predicted gassed impeller power consumption, impeller pumping number, and overall gas hold-up was in good agreement with the experimental values. It was also shown that grid size has a significant effect on the prediction of the gas hold-up, although the effect of considering the virtual mass force is negligible.

Scargiali et al. (2007) studied the influence of grid refinement, bubble size, turbulent dispersion, and virtual mass forces on the predictions of the gas hold-up in an STR. The effect of the lift and virtual mass forces on the distribution of gas hold-up was found to be insignificant. It was revealed that the prescribed bubble (2 or 4 mm) and grid sizes (70k and 282k cells) used in the simulations have minimal impact on the prediction of the local and overall gas hold-ups. It was also concluded that the gas/liquid flow patterns in STRs are essentially dominated by the drag force.

Recently, Zhang et al. (2013) showed that the predicted gas/liquid flow patterns and gas hold-up distributions obtained by CFD simulations were similar with or without the incorporation of lift and virtual mass forces into the momentum equations compared to the experimental data obtained by Lu and Ju (1987). It was also shown that the magnitude of the virtual mass and lift forces were much smaller than the drag force in the whole tank. Overall, these studies enlightened the success of gas/liquid CFD simulations that used a uniform bubble size, in the prediction of gas hold-up distribution and its overall values in STRs.

Th prediction of bubble sizes in the vessel is important for finding the mass transfer area inside gas/liquid STRs. In recent years, several studies have tried to predict bubble size distributions by modelling bubble number density (BND) (Bakker and Akker, 1994; Lane et al., 2005) or by using a population balance model (PBM) (Gelves et al., 2014; Gimbun et al.,

2009; Kerdouss et al., 2006, 2008; Laakkonen et al., 2006b; Moilanen et al., 2008; Petitti et al., 2013; Ranganathan and Sivaraman, 2011; Venneker et al., 2002) coupled with CFD simulations. The enormous computational requirements for multiphase models coupled with population balance models (PBMs) makes it difficult to use meshes that are fine enough for simulations. This limitation generally leads to an under-prediction of the turbulent energy dissipation rate (Coroneo et al., 2011; Deglon and Meyer, 2006). Since bubble breakage and coalescence kernels are functions of the liquid turbulent energy dissipation rate (Sajjadi et al., 2012), the accuracy of the predicted bubble size distributions and their mean values are significantly reduced by under-predictions of this parameter (Laborde-Boutet et al., 2009). The parameters of the models for bubble coalescence and breakage were tuned to fit the experimental measurements. This limits the applicability of the model for different configurations, operating conditions and scales of STRs. CFD complexities imply that the final results depend on a considerable number of parameters. Montante et al. (2008) showed that using these models without adjusting their parameters can lead to severe under-predictions of bubble size distributions inside STRs. Considering these issues, further work based on this approach must be undertaken to better understand the relationship between the flow field and the parameters of these models (Ramkrishna and Singh, 2014).

2.7.3 CFD-based compartment models (multiscale models)

CFD can be used as a useful tool to gain insight into the hydrodynamics prevailing in STRs. In principle, it is possible to simulate a whole range of phenomena, including reaction kinetics, bubble-bubble interaction, and gas/liquid mass transfer by adding conservation equations. However, this approach may not be practical, as many equations (mass, momentum, turbulence, energy, reaction kinetics, and population balance) have to be solved simultaneously, which is too demanding for current computational resources. Furthermore, numerical algorithms for solving these coupled equations involving various time and length scales may suffer from a lack of flexibility (Bezzo et al., 2004).

To address theses issues, CFD-based compartment models have been introduced for various process purposes in a series of papers. As was mentioned in subsection 2.7.1, compartmental representation is a well-established mean for describing mixing non-homogeneities in a system by dividing it into a network of interconnected zones, where an idealized mixing pattern is assumed in each individual zone. In CFD-based compartment models, the flow characteristics of each compartment and the flows between them are obtained using CFD simulation data. Then chemical reactions and other phenomena are solved in a network of fully mixed compartments.

One of the earliest use of this approach was applied by Bauer and Eigenberger (2001) to study the behaviour of a gas/liquid bubble column involving a non-isothermal parallel-consecutive reaction. In this study the bubble column comprises two parallel vertical compartments. The flows between adjacent compartments are computed by a multiphase CFD model. Mass, energy and bubble number density equations are then formulated and solved using the simplified compartment model. The local information, including the mean bubble size required by the CFD model, is then determined by this model. Rigopoulos and Jones (2003) followed this approach, though they used the constant bubble size (5 mm) to describe the interfacial area between phases, as well as twenty and ten compartments to model the riser and downcomer, respectively.

A two-compartment population balance model was developed by Maggioris et al. (2000) to predict the droplet size distribution in a polymerization reactor, as a function of operating conditions, by taking the large spatial variations of the turbulent kinetic energy into account. In this work, the volume of the tank was divided into two regions. The first region, near the impeller, was characterized by a high turbulent energy dissipation rate, whereas the second showed a low value of this parameter in the circulating zone. The volume ratio of the impeller and circulating regions, as well as the ratio of turbulent dissipation rates and exchange flow rates in the two compartments, which are compartmental model parameters, were estimated by CFD for different agitation rates and continuous phase viscosities.

Alexopoulos et al. (2002) followed the same methodology to study the effect of the agitation rate, impeller diameter, fluid viscosity, and vessel size on the compartmental model parameters in an STR equipped with a relatively large two-blade flat impeller. Two-compartment formulations of the population balance equation were used to assess the impacts of turbulent non-homogeneities in the STR on the droplet size distribution (DSD) of liquid/liquid dispersions. Agreement was reported between the numerical results and experimental data for drop size distributions.

Bezzo et al. (2003) modelled the dynamic behaviour of a bioreactor containing a highly non-Newtonian fluid. Their compartment model takes biokinetics and mass transfer into account, while the CFD model predicts the flow rates between the compartments and the effective viscosity within each compartment as a function of the shear stress. The volumetric mass transfer coefficient was resorted to a vessel-averaged value obtained by an empirical correlation.

Guha et al. (2006) developed a CFD-based compartmental model to predict the effect of mixing on the performance of STRs for reactive systems. They showed that the effect of the feed location on the product yield and selectivity can be reasonably captured for multiple reaction systems using their proposed model.

Vakili and Esfahany (2009) considered three compartments in a baffled STR equipped with a two-blade turbine. In addition to zones near the impeller and in the bulk of the tank, they considered a third zone with a relatively high turbulent energy dissipation rate in the vicinity of the baffles and tank wall. In this study, the impeller and the tank wall had considerable interaction. The effects of agitation rate, impeller diameter and clearance, and baffle width on the model parameters were investigated. It was shown that the model parameters changed by altering both the agitation rate and geometrical design.

A systematic zoning approach was also proposed by Alopaeus et al. (2009) whereby the tank was divided into two separate regions. The turbulence and fluid flow characteristics of STRs were analysed based on a two-zone model. The effects of the impeller type, liquid

viscosity, and turbulent model were investigated. They developed a so-called zoning curve for better visualization of the turbulent mixing in the tank. However, the zones were not determined based on the distribution of turbulent energy dissipation rate, making their results quite different from those obtained by others (for example, (Alexopoulos et al., 2002), (Vakili and Esfahany, 2009), and (Maggioris et al., 2000)). They showed that a gradual increase of the inner zone volume, from the impeller-swept area towards the tank wall, yields continuous curves for the turbulent energy dissipation rate and the pumping number between the two zones, with respect to their sizes.

Laakkonen et al. (2006a, 2007a,b) developed a multiscale model to predict the local gas hold-up, bubble size distribution, and mass transfer coefficient of two STRs. In their model, the tanks were divided into a limited number of ideally mixed compartments or zones that were connected to each other. The liquid flow rates between the compartments and the average values of the liquid turbulent dissipation rates inside each compartment were passed along to a meso-scale PBM. These quantities were obtained by single-phase CFD simulations and, when the gas flow rates were high, they were further modified to take the change in flow fields due to presence of the gas phase into account (Laakkonen et al., 2007b). However, several parameters of the bubble coalescence and breakage models were tuned to fit the experimental measurements. Moreover, different sets of parameters were used for various ranges of operating conditions (Laakkonen et al., 2006a, 2007a).

Pohn et al. (2011) developed a framework to aid the scale-up of high solid content latex production and processing. In their work, CFD is used to generate flow fields inside a series of reactors, and this information was used by multi-compartment population balance model to assess the impact of non-homogeneous mixing on the evolution of the latex particle size distribution (PSD). The flow field was in turn updated if significant changes in the rheological properties of the latex were detected in any of those compartments. It was shown that the non-homogeneity inside the STR has an effect on the final latex PSD.

Delafosse et al. (2014) developed a CFD-based compartment model to predict the mixing

time of an STR equipped with two four-blade disk turbines. The tank was divided into networks of compartments. The mean and turbulent exchange flow rates between these compartments were calculated based on the results of CFD simulations. These data were then used by the compartment model, which comprised 9,216 compartments. They showed that the proposed model can accurately predict the mixing time of the STR compared with the experimental values measured using the conductivity technique.

Delafosse et al. (2015) coupled a CFD-based compartment model and a stochastic model based on a continuous-time Markov chain (CTMC) to describe spatial heterogeneities, residence and circulation time distributions inside the STR equipped with an axial Mixel TT impeller. A comparison with the experimental data obtained by PIV showed that the CFD-based compartment model can accurately reproduce the spatial heterogeneities inside the STR. It was shown that residence and circulation time distributions in three predefined zones inside the STR can be accurately predicted by the coupled CFD-based compartment and CTMC model compared to experimental results obtained by the optical trajectography technique.

2.8 Problem identification

As mentioned in chapter 1, local hydrodynamics need to be considered during the scale-up. These data can be achieved using computational models and experimental techniques. According to the literature review, the following gaps in the body of knowledge were identified, which will be addressed in this thesis :

– As mentioned in section 2.5, the turbulent energy dissipation rate plays an important role in the prediction of local volumetric mass transfer coefficients (Figure 2.7). In all the investigations discussed above, in order to study turbulent non-homogeneities, compartmentalization of the tank based on the turbulent energy dissipation rate was applied to mixing systems provided with simple impellers (two-blade paddle impeller). This type of impeller has limited application in gas/liquid mixing systems. In addition, the impacts

of common scale-up approaches on the extent of turbulent non-homogeneities and the value of compartmental model parameters have not been addressed in the literature ;

– It can be concluded from the literature that quantitative assessments of the accuracy of CFD analyses rely mainly on a comparison of the flows close to the impeller. Very little attention has been paid to the accuracy of predictions near the reactor walls, baffles, or in the bulk of the vessel. The accurate prediction of flow characteristics in these regions is essential for predicting the mixing characteristics of an STR. A comprehensive study thus needs to be undertaken to experimentally measure the mean velocity field in the regions mentioned above and compare it with the predictions of CFD models ;

– The main methodologies that have been developed to predict the local mass transfer coefficient are based on coupling a population balance model with the Eulerian multi-fluid approach to describe the spatial and temporal evolution of this parameter. Two limitations of this methodology are : (1) it increases the computational demands by many fold, and (2) the inherent complexities associated with this approach imply that the final results depend on a considerable number of parameters that should be tuned to fit the experimental measurements. This limits the applicability of the model for different operating conditions. The first issue was addressed in a few studies employing the modelling method described in section 2.7.3. However, the second issue is still a formidable challenge, due to the present state of understanding of breakage and coalescence phenomena, as well as the lack of extensive experimental data that covers various operating conditions and design configurations.

2.9 References

Alexopoulos, A., Maggioris, D., and Kiparissides, C. (2002). CFD analysis of turbulence non-homogeneity in mixing vessels : a two-compartment model. *Chemical Engineering Science*, 57(10) :1735–1752.

Alizadeh, E., Dubé, O., Bertrand, F., and Chaouki, J. (2013). Characterization of mixing and size segregation in a rotating drum by a particle tracking method. *AIChE Journal*.

Alopaeus, V., Moilanen, P., and Laakkonen, M. (2009). Analysis of stirred tanks with two-zone models. *AIChE journal*, 55(10) :2545–2552.

Alves, S., Maia, C., and Vasconcelos, J. (2002a). Experimental and modelling study of gas dispersion in a double turbine stirred tank. *Chemical Engineering Science*, 57(3) :487–496.

Alves, S., Maia, C., Vasconcelos, J., and Serralheiro, A. (2002b). Bubble size in aerated stirred tanks. *Chemical Engineering Journal*, 89(1) :109–117.

Amanullah, A., Buckland, B. C., and Nienow, A. W. (2004). Mixing in the fermentation and cell culture industries. *Handbook of Industrial Mixing : Science and Practice*, pages 1071–1170.

Aubin, J., Le Sauze, N., Bertrand, J., Fletcher, D. F., and Xuereb, C. (2004). PIV measurements of flow in an aerated tank stirred by a down-and an up-pumping axial flow impeller. *Experimental Thermal and Fluid Science*, 28(5) :447–456.

Bakker, A. and Akker, H. A. (1994). A computational model for the gas-liquid flow in stirred reactors. *Chemical Engineering Research and Design*, 72 :594–606.

Baldi, S. and Yianneskis, M. (2003). On the direct measurement of turbulence energy dissipation in stirred vessels with PIV. *Industrial & engineering chemistry research*, 42(26) :7006–7016.

Baldi, S. and Yianneskis, M. (2004). On the quantification of energy dissipation in the impeller stream of a stirred vessel from fluctuating velocity gradient measurements. *Chemical engineering science*, 59(13) :2659–2671.

Barigou, M. and Greaves, M. (1991). A capillary suction probe for bubble size measurement. *Measurement Science and Technology*, 2(4) :318.

Barigou, M. and Greaves, M. (1992). Bubble-size distributions in a mechanically agitated gas-liquid contactor. *Chemical Engineering Science*, 47(8) :2009–2025.

Bashiri, H., Heniche, M., Bertrand, F., and Chaouki, J. (2014). Compartmental modelling of turbulent fluid flow for the scale-up of stirred tanks. *The Canadian Journal of Chemical Engineering*, 92(6) :1070–1081.

Bashiri, H., Mostoufi, N., Radmanesh, R., Sotudeh-Gharebagh, R., and Chaouki, J. (2010). Effect of bed diameter on the hydrodynamics of gas-solid fluidized beds. *Iran. J. Chem. Chem. Eng. Vol*, 29(3).

Bauer, M. and Eigenberger, G. (2001). Multiscale modeling of hydrodynamics, mass transfer and reaction in bubble column reactors. *Chemical engineering science*, 56(3) :1067–1074.

Beam, G., Wielopolski, L., Gardner, R., and Verghese, K. (1978). Monte carlo calculation of efficiencies of right-circular cylindrical NaI detectors for arbitrarily located point sources. *Nuclear Instruments and methods*, 154(3) :501–508.

Bezzo, F., Macchietto, S., and Pantelides, C. (2003). General hybrid multizonal/CFD approach for bioreactor modeling. *AIChE Journal*, 49(8) :2133–2148.

Bezzo, F., Macchietto, S., and Pantelides, C. C. (2004). A general methodology for hybrid multizonal/CFD models : Part I. theoretical framework. *Computers & chemical engineering*, 28(4) :501–511.

Bittorf, K. J. and Kresta, S. M. (2000). Active volume of mean circulation for stirred tanks agitated with axial impellers. *Chemical engineering science*, 55(7) :1325–1335.

Bittorf, K. J. and Kresta, S. M. (2001). Three-dimensional wall jets : Axial flow in a stirred tank. *AIChE journal*, 47(6) :1277–1284.

Bouaifi, M., Hebrard, G., Bastoul, D., and Roustan, M. (2001). A comparative study of gas hold-up, bubble size, interfacial area and mass transfer coefficients in stirred gas–liquid

reactors and bubble columns. *Chemical Engineering and Processing : Process Intensification*, 40(2) :97–111.

Boyer, C., Duquenne, A.-M., and Wild, G. (2002). Measuring techniques in gas-liquid and gas-liquid-solid reactors. *Chemical Engineering Science*, 57(16) :3185 – 3215.

Brucato, A., Grisafi, F., and Montante, G. (1998). Particle drag coefficients in turbulent fluids. *Chemical Engineering Science*, 53(18) :3295–3314.

Bujalski, W., Nienow, A., Chatwin, S., and Cooke, M. (1987). The dependency on scale of power numbers of Rushton disc turbines. *Chemical Engineering Science*, 42(2) :317–326.

Cabaret, F., Bonnot, S., Fradette, L., and Tanguy, P. A. (2007). Mixing time analysis using colorimetric methods and image processing. *Industrial & engineering chemistry research*, 46(14) :5032–5042.

Cabaret, F., Fradette, L., and Tanguy, P. (2008). Gas–liquid mass transfer in unbaffled dual-impeller mixers. *Chemical Engineering Science*, 63(6) :1636–1647.

Cassanello, M., Larachi, F., Legros, R., and Chaouki, J. (1999). Solids dynamics from experimental trajectory time-series of a single particle motion in gas-spouted beds. *Chemical engineering science*, 54(13) :2545–2554.

Cents, A., Brilman, D., and Versteeg, G. (2005). Ultrasonic investigation of hydrodynamics and mass transfer in a gas-liquid (-liquid) stirred vessel. *International Journal of Chemical Reactor Engineering*, 3(1).

Chaouki, J., Larachi, F., and Dudukovic, M. P. (1997). *Non-invasive monitoring of multiphase flows*. Access Online via Elsevier.

Chen, J., Kemoun, A., Al-Dahhan, M. H., Duduković, M. P., Lee, D., and Fan, L.-S. (1999). Comparative hydrodynamics study in a bubble column using computer-automated radioactive particle tracking (CARPT)/computed tomography (CT) and particle image velocimetry (PIV). *Chemical engineering science*, 54(13) :2199–2207.

Chiti, F., Bakalis, S., Bujalski, W., Barigou, M., Eaglesham, A., and Nienow, A. W. (2011). Using positron emission particle tracking (PEPT) to study the turbulent flow in a baffled vessel agitated by a Rushton turbine : Improving data treatment and validation. *Chemical Engineering Research and Design*, 89(10) :1947–1960.

Clift, R., Grace, J. R., and Weber, M. E. (2005). *Bubbles, drops, and particles*. Courier Dover Publications.

Cooper, R. G. and Wolf, D. (1968). Velocity profiles and pumping capacities for turbine type impellers. *The Canadian Journal of Chemical Engineering*, 46(2) :94–100.

Córdova-Aguilar, M., Díaz-Uribe, R., Escobar, O., Corkidi, G., and Galindo, E. (2008). An optical approach for identifying the nature and the relative 3D spatial position of components of complex structures formed in multiphase dispersion systems. *Chemical Engineering Science*, 63(11) :3047–3056.

Corkidi, G., Voinson, T., Taboada, B., Córdova, M., and Galindo, E. (2008). Accurate determination of embedded particles within dispersed elements in multiphase dispersions, using a 3D micro-stereoscopic vision system. *Chemical Engineering Science*, 63(2) :317–329.

Coroneo, M., Montante, G., Paglianti, A., and Magelli, F. (2011). CFD prediction of fluid flow and mixing in stirred tanks : Numerical issues about the RANS simulations. *Computers & Chemical Engineering*, 35(10) :1959–1968.

Cui, Y., Van der Lans, R., and Luyben, K. C. A. (1996). Local power uptake in gas-liquid systems with single and multiple Rushton turbines. *Chemical engineering science*, 51(11) :2631–2636.

Deckwer, W.-D., Burckhart, R., and Zoll, G. (1974). Mixing and mass transfer in tall bubble columns. *Chemical Engineering Science*, 29(11) :2177–2188.

Deen, N. G., Solberg, T., and Hjertager, B. H. (2002). Flow generated by an aerated Rushton impeller : Two-phase PIV experiments and numerical simulations. *The Canadian Journal of Chemical Engineering*, 80(4) :1–15.

Deglon, D. and Meyer, C. (2006). CFD modelling of stirred tanks : Numerical considerations. *Minerals Engineering*, 19(10) :1059–1068.

Delafosse, A., Calvo, S., Collignon, M.-L., Delvigne, F., Crine, M., and Toye, D. (2015). Euler–Lagrange approach to model heterogeneities in stirred tank bioreactors–Comparison to experimental flow characterization and particle tracking. *Chemical Engineering Science*, 134 :457–466.

Delafosse, A., Collignon, M.-L., Calvo, S., Delvigne, F., Crine, M., Thonart, P., and Toye, D. (2014). CFD-based compartment model for description of mixing in bioreactors. *Chemical Engineering Science*, 106 :76–85.

Delafosse, A., Collignon, M.-L., Crine, M., and Toye, D. (2011). Estimation of the turbulent kinetic energy dissipation rate from 2D-PIV measurements in a vessel stirred by an axial mixel ttp impeller. *Chemical Engineering Science*, 66(8) :1728–1737.

Delafosse, A., Line, A., Morchain, J., and Guiraud, P. (2008). LES and URANS simulations of hydrodynamics in mixing tank : comparison to PIV experiments. *Chemical Engineering Research and Design*, 86(12) :1322–1330.

Delafosse, A., Morchain, J., Guiraud, P., and Liné, A. (2009). Trailing vortices generated by a Rushton turbine : Assessment of URANS and large eddy simulations. *Chemical Engineering Research and Design*, 87(4) :401–411.

Devanathan, N., Moslemian, D., and Dudukovic, M. (1990). Flow mapping in bubble columns using CARPT. *Chemical Engineering Science*, 45(8) :2285–2291.

Distelhoff, M., Marquis, A., Nouri, J., and Whitelaw, J. (1997). Scalar mixing measurements in batch operated stirred tanks. *The Canadian Journal of Chemical Engineering*, 75(4) :641–652.

Djeridane, T., Larachi, F., Roy, D., Chaovki, J., and Legros, R. (1998). Investigation of the mean and turbulent particle velocity fields in a spouted bed using radioactive particle tracking. *The Canadian Journal of Chemical Engineering*, 76(2) :190–195.

Doucet, J., Bertrand, F., and Chaouki, J. (2008). An extended radioactive particle tracking method for systems with irregular moving boundaries. *Powder Technology*, 181(2) :195–204.

Ducci, A. and Yianneskis, M. (2005). Direct determination of energy dissipation in stirred vessels with two-point LDA. *AIChE journal*, 51(8) :2133–2149.

Escudie, R. and Line, A. (2003). Experimental analysis of hydrodynamics in a radially agitated tank. *AIChE journal*, 49(3) :585–603.

Fishwick, R., Winterbottom, M., Parker, D., Fan, X., and Stitt, H. (2005). The use of positron emission particle tracking in the study of multiphase stirred tank reactor hydrodynamics. *The Canadian Journal of Chemical Engineering*, 83(1) :97–103.

Fontaine, A., Guntzburger, Y., Bertrand, F., Fradette, L., and Heuzey, M.-C. (2012). Experimental investigation of the flow dynamics of rheologically complex fluids in a maxblend impeller system using PIV. *Chemical Engineering Research and Design*.

Ford, J. J., Heindel, T. J., Jensen, T. C., and Drake, J. B. (2008). X-ray computed tomography of a gas-sparged stirred-tank reactor. *Chemical Engineering Science*, 63(8) :2075–2085.

Gabelle, J.-C., Augier, F., Carvalho, A., Rousset, R., and Morchain, J. (2011). Effect of tank size on k_La and mixing time in aerated stirred reactors with non-newtonian fluids. *The Canadian Journal of Chemical Engineering*, 89(5) :1139–1153.

Gabriele, A., Nienow, A., and Simmons, M. (2009). Use of angle resolved PIV to estimate local specific energy dissipation rates for up-and down-pumping pitched blade agitators in a stirred tank. *Chemical Engineering Science*, 64(1) :126–143.

Gaddis, E. (1999). Mass transfer in gas–liquid contactors. *Chemical Engineering and Processing : Process Intensification*, 38(4) :503–510.

Galindo, E., Larralde-Corona, C. P., Brito, T., Córdova-Aguilar, M. S., Taboada, B., Vega-Alvarado, L., and Corkidi, G. (2005). Development of advanced image analysis techniques for the in situ characterization of multiphase dispersions occurring in bioreactors. *Journal of biotechnology*, 116(3) :261–270.

Garcia-Ochoa, F. and Gomez, E. (2004). Theoretical prediction of gas–liquid mass transfer coefficient, specific area and hold-up in sparged stirred tanks. *Chemical Engineering Science*, 59(12) :2489–2501.

Garcia-Ochoa, F. and Gomez, E. (2009). Bioreactor scale-up and oxygen transfer rate in microbial processes : an overview. *Biotechnology advances*, 27(2) :153–176.

Garcia-Ochoa, F., Gomez, E., Santos, V. E., and Merchuk, J. C. (2010). Oxygen uptake rate in microbial processes : an overview. *Biochemical Engineering Journal*, 49(3) :289–307.

Gelves, R., Dietrich, A., and Takors, R. (2014). Modeling of gas–liquid mass transfer in a stirred tank bioreactor agitated by a Rushton turbine or a new pitched blade impeller. *Bioprocess and biosystems engineering*, 37(3) :365–375.

Gimbun, J., Rielly, C. D., and Nagy, Z. K. (2009). Modelling of mass transfer in gas–liquid stirred tanks agitated by Rushton turbine and CD-6 impeller : a scale-up study. *Chemical Engineering Research and Design*, 87(4) :437–451.

Gimbun, J., Rielly, C. D., Nagy, Z. K., and Derksen, J. (2012). Detached eddy simulation on the turbulent flow in a stirred tank. *AIChE Journal*, 58(10) :3224–3241.

Gourich, B., Vial, C., El Azher, N., Soulami, M. B., and Ziyad, M. (2008). Influence of hydrodynamics and probe response on oxygen mass transfer measurements in a high aspect ratio bubble column reactor : Effect of the coalescence behaviour of the liquid phase. *Biochemical Engineering Journal*, 39(1) :1–14.

Greaves, M. and Kobbacy, K. (1984). Measurement of bubble size distribution in turbulent gas-liquid dispersions. *Chemical engineering research and design*, 62(1) :3–12.

Grenville, R., Ruszkowski, S., and Garred, E. (1995). Blending of miscible liquids in the turbulent and transitional regimes. In *15th NAMF mixing conference*.

Guevara-López, E., Sanjuan-Galindo, R., Córdova-Aguilar, M. S., Corkidi, G., Ascanio, G., and Galindo, E. (2008). High-speed visualization of multiphase dispersions in a mixing tank. *Chemical Engineering Research and Design*, 86(12) :1382–1387.

Guha, D., Dudukovic, M., Ramachandran, P., Mehta, S., and Alvare, J. (2006). CFD-based compartmental modeling of single phase stirred-tank reactors. *AIChE journal*, 52(5) :1836–1846.

Guha, D., Ramachandran, P., and Dudukovic, M. (2007). Flow field of suspended solids in a stirred tank reactor by lagrangian tracking. *Chemical Engineering Science*, 62(22) :6143–6154.

Guida, A., Nienow, A. W., and Barigou, M. (2012). Lagrangian tools for the analysis of mixing in single-phase and multiphase flow systems. *AIChE Journal*, 58(1) :31–45.

Guillard, F., Trägårdh, C., and Fuchs, L. (2000). A study on the instability of coherent mixing structures in a continuously stirred tank. *Chemical Engineering Science*, 55(23) :5657–5670.

Harris, C., Roekaerts, D., Rosendal, F., Buitendijk, F., Daskopoulos, P., Vreenegoor, A., and Wang, H. (1996). Computational fluid dynamics for chemical reactor engineering. *Chemical Engineering Science*, 51(10) :1569–1594.

Hassan, I. and Robinson, C. W. (1977). Stirred-tank mechanical power requirement and gas holdup in aerated aqueous phases. *AIChE Journal*, 23(1) :48–56.

Heniche, M. and Tanguy, P. A. (2006). A new element-by-element method for trajectory calculations with tetrahedral finite element meshes. *International journal for numerical methods in engineering*, 67(9) :1290–1317.

Higbie, R. (1935). *The rate of absorption of a pure gas into still liquid during short periods of exposure.*

Hristov, H., Mann, R., Lossev, V., and Vlaev, S. (2004). A simplified CFD for three-dimensional analysis of fluid mixing, mass transfer and bioreaction in a fermenter equipped with triple novel geometry impellers. *Food and bioproducts processing*, 82(1) :21–34.

Hristov, H., Mann, R., Lossev, V., Vlaev, S., and Seichter, P. (2001). A 3-D analysis of gas-liquid mixing, mass transfer and bioreaction in a stirred bio-reactor. *Food and bioproducts processing*, 79(4) :232–241.

Hughmark, G. A. (1980). Power requirements and interfacial area in gas-liquid turbine agitated systems. *Industrial & Engineering Chemistry Process Design and Development*, 19(4) :638–641.

Ishii, M. and Zuber, N. (1979). Drag coefficient and relative velocity in bubbly, droplet or particulate flows. *AIChE Journal*, 25(5) :843–855.

Jafari, R., Tanguy, P. A., and Chaouki, J. (2012). Experimental investigation on solid dispersion, power consumption and scale-up in moderate to dense solid–liquid suspensions. *Chemical Engineering Research and Design*, 90(2) :201–212.

Jaworski, Z., Dyster, K., and Nienow, A. (2001). The effect of size, location and pumping direction of pitched blade turbine impellers on flow patterns : LDA measurements and CFD predictions. *Chemical Engineering Research and Design*, 79(8) :887–894.

Jaworski, Z., Nienow, A., and Dyster, K. (1996). An LDA study of the turbulent flow field in a baffled vessel agitated by an axial, down-pumping hydrofoil impeller. *The Canadian Journal of Chemical Engineering*, 74(1) :3–15.

Jaworski, Z. and Zakrzewska, B. (2002). Modelling of the turbulent wall jet generated by a pitched blade turbine impeller : the effect of turbulence model. *Chemical Engineering Research and Design*, 80(8) :846–854.

Joshi, J. B., Nere, N. K., Rane, C. V., Murthy, B., Mathpati, C. S., Patwardhan, A. W., and Ranade, V. V. (2011a). CFD simulation of stirred tanks : Comparison of turbulence models. part I : Radial flow impellers. *The Canadian Journal of Chemical Engineering*, 89(1) :23–82.

Joshi, J. B., Nere, N. K., Rane, C. V., Murthy, B., Mathpati, C. S., Patwardhan, A. W., and Ranade, V. V. (2011b). CFD simulation of stirred tanks : Comparison of turbulence

models (part II : Axial flow impellers, multiple impellers and multiphase dispersions). *The Canadian Journal of Chemical Engineering*, 89(4) :754–816.

Junker, B. H. (2004). Scale-up methodologies for escherichia coli and yeast fermentation processes. *Journal of bioscience and bioengineering*, 97(6) :347–364.

Kadic, E. and Heindel, T. J. (2014). Stirred-tank bioreactors. *An Introduction to Bioreactor Hydrodynamics and Gas-Liquid Mass Transfer*, pages 69–123.

Kapic, A. and Heindel, T. (2006). Correlating gas-liquid mass transfer in a stirred-tank reactor. *Chemical Engineering Research and Design*, 84(3) :239–245.

Kawase, Y., Halard, B., and Moo-Young, M. (1987). Theoretical prediction of volumetric mass transfer coefficients in bubble columns for newtonian and non-newtonian fluids. *chemical Engineering science*, 42(7) :1609–1617.

Kawase, Y., Halard, B., and Moo-Young, M. (1992). Liquid-phase mass transfer coefficients in bioreactors. *Biotechnology and bioengineering*, 39(11) :1133–1140.

Kerdouss, F., Bannari, A., and Proulx, P. (2006). CFD modeling of gas dispersion and bubble size in a double turbine stirred tank. *Chemical Engineering Science*, 61(10) :3313–3322.

Kerdouss, F., Bannari, A., Proulx, P., Bannari, R., Skrga, M., and Labrecque, Y. (2008). Two-phase mass transfer coefficient prediction in stirred vessel with a CFD model. *Computers & Chemical Engineering*, 32(8) :1943–1955.

Khopkar, A., Rammohan, A., Ranade, V., and Dudukovic, M. (2005). Gas–liquid flow generated by a Rushton turbine in stirred vessel : CARPT/CT measurements and CFD simulations. *Chemical Engineering Science*, 60(8) :2215–2229.

Khopkar, A. R. and Ranade, V. V. (2006). CFD simulation of gas–liquid stirred vessel : VC, S33, and L33 flow regimes. *AIChE journal*, 52(5) :1654–1672.

Kiared, K., Larachi, F., Chaouki, J., and Guy, C. (1999). Mean and turbulent particle velocity in the fully developed region of a three-phase fluidized bed. *Chemical engineering & technology*, 22(8) :683–689.

Kresta, S. (1998). Turbulence in stirred tanks : anisotropic, approximate, and applied. *The Canadian Journal of Chemical Engineering*, 76(3) :563–576.

Kresta, S. M. and Wood, P. E. (1993a). The flow field produced by a pitched blade turbine : characterization of the turbulence and estimation of the dissipation rate. *Chemical engineering science*, 48(10) :1761–1774.

Kresta, S. M. and Wood, P. E. (1993b). The mean flow field produced by a 45 pitched blade turbine : changes in the circulation pattern due to off bottom clearance. *The Canadian Journal of Chemical Engineering*, 71(1) :42–53.

Kumar, S. B., Moslemian, D., and Duduković, M. P. (1995). A γ-ray tomographic scanner for imaging voidage distribution in two-phase flow systems. *Flow Measurement and Instrumentation*, 6(1) :61–73.

Kumaresan, T. and Joshi, J. B. (2006). Effect of impeller design on the flow pattern and mixing in stirred tanks. *Chemical engineering journal*, 115(3) :173–193.

Laakkonen, M., Alopaeus, V., and Aittamaa, J. (2006a). Validation of bubble breakage, coalescence and mass transfer models for gas–liquid dispersion in agitated vessel. *Chemical engineering science*, 61(1) :218–228.

Laakkonen, M., Moilanen, P., Alopaeus, V., and Aittamaa, J. (2006b). Dynamic modeling of local reaction conditions in an agitated aerobic fermenter. *AIChE journal*, 52(5) :1673–1689.

Laakkonen, M., Moilanen, P., Alopaeus, V., and Aittamaa, J. (2007a). Modelling local bubble size distributions in agitated vessels. *Chemical Engineering Science*, 62(3) :721–740.

Laakkonen, M., Moilanen, P., Alopaeus, V., and Aittamaa, J. (2007b). Modelling local gas–liquid mass transfer in agitated vessels. *Chemical Engineering Research and Design*, 85(5) :665–675.

Laakkonen, M., Moilanen, P., Miettinen, T., Saari, K., Honkanen, M., Saarenrinne, P., and Aittamaa, J. (2005). Local bubble size distributions in agitated vessel : comparison of three experimental techniques. *Chemical Engineering Research and Design*, 83(1) :50–58.

Laborde-Boutet, C., Larachi, F., Dromard, N., Delsart, O., and Schweich, D. (2009). CFD simulation of bubble column flows : Investigations on turbulence models in RANS approach. *Chemical Engineering Science*, 64(21) :4399–4413.

Lane, G., Schwarz, M., and Evans, G. (2005). Numerical modelling of gas–liquid flow in stirred tanks. *Chemical Engineering Science*, 60(8) :2203–2214.

Lara, A. R., Galindo, E., Ramírez, O. T., and Palomares, L. A. (2006). Living with heterogeneities in bioreactors. *Molecular biotechnology*, 34(3) :355–381.

Lee, B. W. and Dudukovic, M. P. (2014). Determination of flow regime and gas holdup in gas–liquid stirred tanks. *Chemical Engineering Science*, 109 :264–275.

Lee, K. and Yianneskis, M. (1998). Turbulence properties of the impeller stream of a Rushton turbine. *AIChE journal*, 44(1) :13–24.

Lin, J., Chen, M., and Chao, B. (1985). A novel radioactive particle tracking facility for measurement of solids motion in gas fluidized beds. *AIChE Journal*, 31(3) :465–473.

Linek, V., Moucha, T., Rejl, F., Kordač, M., Hovorka, F., Opletal, M., and Haidl, J. (2012). Power and mass transfer correlations for the design of multi-impeller gas–liquid contactors for non-coalescent electrolyte solutions. *Chemical Engineering Journal*, 209 :263–272.

Linek, V., Vacek, V., and Beneš, P. (1987). A critical review and experimental verification of the correct use of the dynamic method for the determination of oxygen transfer in aerated agitated vessels to water, electrolyte solutions and viscous liquids. *The Chemical Engineering Journal*, 34(1) :11–34.

Liu, Y.-S., Wu, J.-Y., and Ho, K.-p. (2006). Characterization of oxygen transfer conditions and their effects on phaffia rhodozyma growth and carotenoid production in shake-flask cultures. *Biochemical engineering journal*, 27(3) :331–335.

Lu, W.-M. and Ju, S.-J. (1987). Local gas holdup, mean liquid velocity and turbulence in an aerated stirred tank using hot-film anemometry. *The Chemical Engineering Journal*, 35(1) :9–17.

Machado, M. B., Bittorf, K. J., Roussinova, V. T., and Kresta, S. M. (2013). Transition from turbulent to transitional flow in the top half of a stirred tank. *Chemical Engineering Science*, 98 :218–230.

Maggioris, D., Goulas, A., Alexopoulos, A., Chatzi, E., and Kiparissides, C. (2000). Prediction of particle size distribution in suspension polymerization reactors : effect of turbulence nonhomogeneity. *Chemical Engineering Science*, 55(20) :4611–4627.

Mann, R., Dickin, F., Wang, M., Dyakowski, T., Williams, R., Edwards, R., Forrest, A., and Holden, P. (1997). Application of electrical resistance tomography to interrogate mixing processes at plant scale. *Chemical engineering science*, 52(13) :2087–2097.

Mavros, P. (2001). Flow visualization in stirred vessels : A review of experimental techniques. *Chemical Engineering Research and Design*, 79(2) :113 – 127.

Melton, L. A., Lipp, C., Spradling, R., and Paulson, K. (2002). DISMT-determination of mixing time through color changes. *Chemical Engineering Communications*, 189(3) :322–338.

Meng, A. X., Hill, G. A., and Dalai, A. K. (2002). Modified volume expansion method for measuring gas holdup. *The Canadian Journal of Chemical Engineering*, 80(2) :194–199.

Michel, B. J. and Miller, S. (1962). Power requirements of gas-liquid agitated systems. *AIChE Journal*, 8(2) :262–266.

Middleton, J. C. and Smith, J. M. (2004). Gas–liquid mixing in turbulent systems. *Handbook of Industrial Mixing : Science and Practice*, pages 585–638.

Midoux, N. u. and Charpentier, J. (1984). Mechanically agitated gas-liquid reactors. part 1. hydrodynamics. *International Chemical Engineering*, 24(2) :249–287.

Mishra, V. P., Dyster, K. N., Nienow, A. W., Mckemmie, J., and Jaworski, Z. (1998). A study of an up-and a down-pumping wide blade hydrofoil impeller : Part I. LDA measurements. *The Canadian Journal of Chemical Engineering*, 76(3) :577–588.

Moilanen, P., Laakkonen, M., Visuri, O., Alopaeus, V., and Aittamaa, J. (2008). Modelling mass transfer in an aerated 0.2 m^3 vessel agitated by Rushton, phasejet and combijet impellers. *Chemical Engineering Journal*, 142(1) :95–108.

Montante, G., Horn, D., and Paglianti, A. (2008). Gas–liquid flow and bubble size distribution in stirred tanks. *Chemical engineering science*, 63(8) :2107–2118.

Montante, G., Lee, K., Brucato, A., and Yianneskis, M. (1999). Double-to single-loop flow pattern transition in stirred vessels. *Can. J. Chem. Eng*, 77 :649–659.

Montante, G. and Paglianti, A. (2015). Gas hold-up distribution and mixing time in gas-liquid stirred tanks. *Chemical Engineering Journal*.

Morud, K. and Hjertager, B. (1996). LDA measurements and CFD modelling of gas-liquid flow in a stirred vessel. *Chemical Engineering Science*, 51(2) :233–249.

Mostoufi, N. and Chaouki, J. (2001). Local solid mixing in gas–solid fluidized beds. *Powder Technology*, 114(1) :23–31.

Mostoufi, N. and Chaouki, J. (2004). Flow structure of the solids in gas–solid fluidized beds. *Chemical Engineering Science*, 59(20) :4217–4227.

Moucha, T., Rejl, F., Kordač, M., and Labík, L. (2012). Mass transfer characteristics of multiple-impeller fermenters for their design and scale-up. *Biochemical Engineering Journal*, 69 :17–27.

Mueller, S. (2009). Optical measurements in gas-liquid stirred tanks.

Mueller, S. G. and Dudukovic, M. P. (2010). Gas holdup in gas-liquid stirred tanks. *Industrial & Engineering Chemistry Research*, 49(21) :10744–10750.

Murthy, B. and Joshi, J. (2008). Assessment of standard k–ε, RSM and LES turbulence models in a baffled stirred vessel agitated by various impeller designs. *Chemical Engineering Science*, 63(22) :5468–5495.

Nienow, A. (1997). On impeller circulation and mixing effectiveness in the turbulent flow regime. *Chemical Engineering Science*, 52(15) :2557–2565.

Nienow, A., Wisdom, D., and Middleton, J. (1977). The effect of scale and geometry on flooding, recirculation and power in gassed stirred vessels. In *Proceedings of the* 2^{nd} *European Conference on Mixing*, page 1.

Nienow, A. W. (2010). Stirred tank reactors. *Ullmann's Encyclopedia of Industrial Chemistry*.

Nienow, A. W. (2014). Stirring and stirred-tank reactors. *Chemie Ingenieur Technik*, 86(12) :2063–2074.

Nienow, A. W., EDWARDS, M. F., and Harnby, N. (1997). *Mixing in the process industries*. Butterworth-Heinemann.

Oldshue, J. Y. (1983). Fluid mixing technology.

Paul, E. L., Atiemo-Obeng, V., and Kresta, S. M. (2004). *Handbook of industrial mixing : science and practice*. John Wiley & Sons.

Petitti, M., Vanni, M., Marchisio, D. L., Buffo, A., and Podenzani, F. (2013). Simulation of coalescence, break-up and mass transfer in a gas–liquid stirred tank with cqmom. *Chemical Engineering Journal*, 228 :1182–1194.

Pianko-Oprych, P., Nienow, A., and Barigou, M. (2009). Positron emission particle tracking (PEPT) compared to particle image velocimetry (PIV) for studying the flow generated by a pitched-blade turbine in single phase and multi-phase systems. *Chemical Engineering Science*, 64(23) :4955–4968.

Pohn, J., Heniche, M., Fradette, L., Cunningham, M., and McKenna, T. (2011). Computational analysis of mixing and scale-up in emulsion polymerization reactors. In *Macromolecular Symposia*, volume 302, pages 133–141. Wiley Online Library.

Ramkrishna, D. and Singh, M. R. (2014). Population balance modeling : Current status and future prospects. *Annual review of chemical and biomolecular engineering*, 5 :123–146.

Rammohan, A., Kemoun, A., Al-Dahhan, M., and Dudukovic, M. (2001a). Characterization of single phase flows in stirred tanks via computer automated radioactive particle tracking (CARPT). *Chemical engineering research and design*, 79(8) :831–844.

Rammohan, A., Kemoun, A., Al-Dahhan, M., and Dudukovic, M. (2001b). A lagrangian description of flows in stirred tanks via computer-automated radioactive particle tracking (CARPT). *Chemical engineering science*, 56(8) :2629–2639.

Ranade, V., Perrard, M., Xuereb, C., Le Sauze, N., and Bertrand, J. (2001). Influence of gas flow rate on the structure of trailing vortices of a Rushton turbine : PIV measurements and CFD simulations. *Chemical Engineering Research and Design*, 79(8) :957–964.

Ranade, V. V. (2001). *Computational flow modeling for chemical reactor engineering*, volume 5. Academic press.

Ranade, V. V. (2002). *Computational flow modeling for chemical reactor engineering*. Process systems engineering series. Academic Press, San Diego.

Ranganathan, P. and Sivaraman, S. (2011). Investigations on hydrodynamics and mass transfer in gas–liquid stirred reactor using computational fluid dynamics. *Chemical Engineering Science*, 66(14) :3108–3124.

Rewatkar, V. and Joshi, J. (1991). Effect of impeller design on liquid phase mixing in mechanically agitated reactors. *Chemical engineering communications*, 102(1) :1–33.

Rigopoulos, S. and Jones, A. (2003). A hybrid CFD-reaction engineering framework for multiphase reactor modelling : basic concept and application to bubble column reactors. *Chemical Engineering Science*, 58(14) :3077–3089.

Roy, D., Larachi, F., Legros, R., and Chaouki, J. (1994). A study of solid behavior in spouted beds using 3-D particle tracking. *The Canadian Journal of Chemical Engineering*, 72(6) :945–952.

Roy, S., Acharya, S., and Cloeter, M. D. (2010). Flow structure and the effect of macro-instabilities in a pitched-blade stirred tank. *Chemical Engineering Science*, 65(10) :3009–3024.

Ruszkowski, S. (1994). A rational method for measuring blending performance, and comparison of different impeller types. In *Institution of chemical engineers symposium series*, volume 136, pages 283–283. Hemsphere publishing corporation.

Rutherford, K., Lee, K., Mahmoudi, S., and Yianneskis, M. (1996a). Hydrodynamic characteristics of dual Rushton impeller stirred vessels. *AIChE Journal*, 42(2) :332–346.

Rutherford, K., Mahmoudi, S., Lee, K., and Yianneskis, M. (1996b). The influence of Rushton impeller blade and disk thickness on the mixing characteristics of stirred vessels. *Chemical engineering research & design*, 74(3) :369–378.

Sajjadi, B., Raman, A., Ibrahim, S., and Shah, R. (2012). Review on gas-liquid mixing analysis in multiscale stirred vessel using CFD. *Reviews in Chemical Engineering*, 28(2-3) :171–189.

Sánchez Mirón, A., Garcia Camacho, F., Contreras Gomez, A., Grima, E. M., and Chisti, Y. (2000). Bubble-column and airlift photobioreactors for algal culture. *AIChE Journal*, 46(9) :1872–1887.

Saravanan, K. and Joshi, J. (1996). Fractional gas hold-up in gas inducing type of mechanically agitated contactors. *The Canadian Journal of Chemical Engineering*, 74(1) :16–30.

Sato, Y. and Sekoguchi, K. (1975). Liquid velocity distribution in two-phase bubble flow. *International Journal of Multiphase Flow*, 2(1) :79–95.

Scargiali, F., Doorazio, A., Grisafi, F., and Brucato, A. (2007). Modelling and simulation of gas–liquid hydrodynamics in mechanically stirred tanks. *Chemical Engineering Research and Design*, 85(5) :637–646.

Schäfer, M., Höfken, M., and Durst, F. (1997). Detailed LDV measurements for visualization of the flow field within a stirred-tank reactor equipped with a Rushton turbine. *Chemical Engineering Research and Design*, 75(8) :729–736.

Sharp, K. and Adrian, R. (2001). PIV study of small-scale flow structure around a Rushton turbine. *AIChE journal*, 47(4) :766–778.

Sheng, J., Meng, H., and Fox, R. (2000). A large eddy PIV method for turbulence dissipation rate estimation. *Chemical Engineering Science*, 55(20) :4423–4434.

Singh, H., Fletcher, D. F., and Nijdam, J. J. (2011). An assessment of different turbulence models for predicting flow in a baffled tank stirred with a Rushton turbine. *Chemical Engineering Science*, 66(23) :5976–5988.

Smith, J. (2006). Large multiphase reactors : some open questions. *Chemical Engineering Research and Design*, 84(4) :265–271.

Sommerfeld, M. and Decker, S. (2004). State of the art and future trends in CFD simulation of stirred vessel hydrodynamics. *Chemical engineering & technology*, 27(3) :215–224.

Stankiewicz, A. I. and Moulijn, J. A. (2000). Process intensification : transforming chemical engineering. *Chemical Engineering Progress*, 96(1) :22–34.

Stitt, E. (2002). Alternative multiphase reactors for fine chemicals : A world beyond stirred tanks ? *Chemical Engineering Journal*, 90(1) :47–60.

Takahashi, K., McManamey, W. J., and Nienow, A. W. (1992). Bubble size distributions in impeller region in a gas-sparged vessel agitated by a Rushton turbine. *Journal of chemical engineering of Japan*, 25(4) :427–432.

Takahashi, K. and Nienow, A. W. (1993). Bubble sizes and coalescence rates in an aerated vessel agitated by a Rushton turbine. *Journal of chemical engineering of Japan*, 26(5) :536–542.

Tatterson, G. B. (1991). *Fluid mixing and gas dispersion in agitated tanks*. McGraw-Hill New York.

Tobajas, M., Garcıa-Calvo, E., Siegel, M., and Apitz, S. (1999). Hydrodynamics and mass transfer prediction in a three-phase airlift reactor for marine sediment biotreatment. *Chemical Engineering Science*, 54(21) :5347–5354.

Tsoulfanidis, N. and Landsberger, S. (2011). *Measurement and detection of radiation*. CRC press.

Vakili, M. and Esfahany, M. N. (2009). CFD analysis of turbulence in a baffled stirred tank, a three-compartment model. *Chemical Engineering Science*, 64(2) :351–362.

Van't Riet, K. (1979). Review of measuring methods and results in nonviscous gas-liquid mass transfer in stirred vessels. *Industrial & Engineering Chemistry Process Design and Development*, 18(3) :357–364.

Vasconcelos, J. M., Alves, S., and Barata, J. M. (1995). Mixing in gas-liquid contactors agitated by multiple turbines. *Chemical engineering science*, 50(14) :2343–2354.

Venneker, B. C., Derksen, J. J., and Van den Akker, H. E. (2002). Population balance modeling of aerated stirred vessels based on CFD. *AIChE Journal*, 48(4) :673–685.

Vlaev, D., Mann, R., Lossev, V., Vlaev, S., Zahradnik, J., and Seichter, P. (2000). Macromixing and streptomyces fradiae : modelling oxygen and nutrient segregation in an industrial bioreactor. *Chemical Engineering Research and Design*, 78(3) :354–362.

Vrabel, P., Van der Lans, R., Cui, Y., and Luyben, K. C. A. (1999). Compartment model approach : Mixing in large scale aerated reactors with multiple impellers. *Chemical Engineering Research and Design*, 77(4) :291–302.

Vrabel, P., van der Lans, R. G., Luyben, K. C. A., Boon, L., and Nienow, A. W. (2000). Mixing in large-scale vessels stirred with multiple radial or radial and axial up-pumping impellers : modelling and measurements. *Chemical Engineering Science*, 55(23) :5881–5896.

Wang, M., Dorward, A., Vlaev, D., and Mann, R. (2000). Measurements of gas–liquid mixing in a stirred vessel using electrical resistance tomography (ERT). *Chemical Engineering Journal*, 77(1) :93–98.

Wang, W., Mao, Z.-S., and Yang, C. (2006). Experimental and numerical investigation on gas holdup and flooding in an aerated stirred tank with Rushton impeller. *Industrial & engineering chemistry research*, 45(3) :1141–1151.

Warmoeskerken, M. and Smith, J. M. (1985). Flooding of disc turbines in gas-liquid dispersions : A new description of the phenomenon. *Chemical engineering science*, 40(11) :2063–2071.

Wolf, D. and Manning, F. (1966). Impact tube measurement of flow patterns, velocity profiles and pumping capacities in mixing vessels. *The Canadian Journal of Chemical Engineering*, 44(3) :137–142.

Wu, H. and Patterson, G. (1989). Laser-doppler measurements of turbulent-flow parameters in a stirred mixer. *Chemical Engineering Science*, 44(10) :2207–2221.

Xie, M., Xia, J., Zhou, Z., Chu, J., Zhuang, Y., and Zhang, S. (2014). Flow pattern, mixing, gas hold-up and mass transfer coefficient of triple-impeller configurations in stirred tank bioreactors. *Industrial & Engineering Chemistry Research*, 53(14) :5941–5953.

Xu, S., Qu, Y., Chaouki, J., and Guy, C. (2005). Characterization of homogeneity of bubble flows in bubble columns using RPT and fibre optics. *International Journal of Chemical Reactor Engineering*, 3(1) :A54.

Yawalkar, A. A., Heesink, A., Versteeg, G. F., and Pangarkar, V. G. (2002). Gas-liquid mass transfer coefficient in stirred tank reactors. *The Canadian Journal of Chemical Engineering*, 80(5) :840–848.

Zahradnık, J., Mann, R., Fialova, M., Vlaev, D., Vlaev, S., Lossev, V., and Seichter, P. (2001). A networks-of-zones analysis of mixing and mass transfer in three industrial bioreactors. *Chemical engineering science*, 56(2) :485–492.

Zhang, Q., Yong, Y., Mao, Z.-S., Yang, C., and Zhao, C. (2009). Experimental determination and numerical simulation of mixing time in a gas–liquid stirred tank. *Chemical Engineering Science*, 64(12) :2926–2933.

Zhang, Y., Bai, Y., and Wang, H. (2013). CFD analysis of inter-phase forces in a bubble stirred vessel. *Chemical Engineering Research and Design*, 91(1) :29–35.

Zhou, G. and Kresta, S. M. (1996). Impact of tank geometry on the maximum turbulence energy dissipation rate for impellers. *AIChE journal*, 42(9) :2476–2490.

Zhu, Y., Bandopadhayay, P. C., and Wu, J. (2001). Measurement of gas-liquid mass transfer in an agitated vessel. a comparison between different impellers. *Journal of chemical engineering of Japan*, 34(5) :579–584.

CHAPTER 3

COHERENCE OF THE ARTICLES

The overall objective of this study was to gain insight into the transport phenomena prevailing in stirred tank reactors, and help improve the design and scale-up of such system. To meet this objective, strategic combinations of compartmental modelling (CM), computational fluid dynamics (CFD) and experimental fluid dynamics (EFD) were employed. According to the literature review and the gaps in the body of knowledge that we discussed in Section 2.8, the specific objectives of this work are as follows :

1. To assess the impact of operating conditions and scale-up criteria on turbulent non-homogeneities in STRs ;
2. To characterize turbulent fluid flows in an STR using radioactive particle tracking (RPT) ;
3. To develop a multiscale model for predicting the local volumetric mass transfer coefficient in gas/liquid STRs.

Chapters 4 to 6 include the main body of this work and corresponding scientific findings. Each chapter consists of an individual scientific article that covers a specific objective. A brief description of each chapter is as follows :

– In chapter 4, the results of single-phase CFD simulations of mixing STRs equipped with a Rushton turbine were used to determine the parameters of a two-compartment model that describes the turbulent non-homogeneities therein. Using this method, the effects of operating condition and various conventional scale-up criteria on the value of the compartmental model parameters were investigated. Chapter 4 covers the first specific objective of this work ;

– Chapter 5 presents a comprehensive analysis of the fully turbulent fluid flow in a

laboratory-scale STR equipped with a radial flow impeller (Rushton turbine ; RT) or an axial flow impeller (pitched blade turbine ; PBT) using the RPT technique. This study covers both Eulerian and Lagrangian descriptions of fluid motions. Chapter 5 covers the second specific objective of this work ;

– In Chapter 6, a multiscale gas/liquid flow model was developed to serve as a tool for the design and scale-up of STRs. The model was based on the compartmentalization of the STR into zones and the use of simplified less computationally intensive gas/liquid flow simulations. It predicted the mean value of the local volumetric mass transfer coefficient (k_La) in each compartment based on the local hydrodynamic parameters therein. This model was used to study the effects of various operating conditions and scale-up on the distribution of k_La in STRs. This chapter covers the third specific objective of this work.

The findings in chapter 4 were used to explain the results of chapter 6 regarding the changes in the predicted local values of k_La during scale-up. The results of the CFD model that was validated by RPT in chapter 5 was used as a basis for gas/liquid simulations used by the developed multiscale model in chapter 6. Moreover, the experimental data obtained in chapter 5 were used to find the residence time distribution (RTD) of the liquid phase that was used to study the effects of scale-up on the overall value of k_La in chapter 6.

Chapter 7 gives a general discussion and a summary of the results and, finally, the conclusion and recommendations for future works are presented in Chapter 8.

CHAPTER 4

ARTICLE 1 : COMPARTMENTAL MODELLING OF TURBULENT FLUID FLOW FOR THE SCALE-UP OF STIRRED TANKS

Hamed Bashiri, Mourad Heniche, François Bertrand, Jamal Chaouki

Department of Chemical Engineering, École Polytechnique de Montŕeal, C.P. 6079 succ. Centre-Ville, Montréal, Québec, Canada, H3C 3A7

(Published in *The Canadian Journal of Chemical Engineering* - DOI : 10.1002/cjce.21955)

Presentation of the article : The results of the single-phase CFD simulations of mixing vessels with four baffles agitated by a Rushton turbine will be used to determine the parameters of a two-compartment model that describes the turbulent non-homogeneities therein. The effects of operating condition and various conventional scale-up criteria on the value of the compartmental model parameters, will be investigated.

Abstract : In this work, the results of single phase CFD simulations of mixing vessels with four baffles agitated by a Rushton turbine are used to determine the parameters of a two-compartment model that describes the turbulent non-homogeneities therein. An improved method is proposed to find the boundary between the two characteristic regions. Using this method, the effects of different conventional scale-up criteria including constant impeller speed, constant impeller tip speed and constant power consumption per liquid volume, on the value of the compartmental model parameters are investigated. It can be observed that the distribution of the turbulent energy dissipation rate and, as a result, the compartmental model parameters change considerably when following conventional scale-up rules. The concept of a general map of compartment energy dissipation rate and volume ratios, which can be used for the scale-up of stirred tanks, is introduced.

Keywords : Rushton turbine, turbulent flow, CFD, compartmental model, scale-up

4.1 Introduction

Stirred Tank Reactors (STRs) are widely used in many chemical processes, such as aerobic fermentation, hydrogenation, neutralisation, chlorination, organic oxidation and gold cyanidation. For instance, the design of STRs significantly affects the mixing quality and properties of gas/liquid systems such as bubble dispersion, bubble size distribution, mass transfer resistance in the liquid film around the bubbles and, consequently, the mass transfer coefficient. The performance at an industrial scale should be comparable with that at the laboratory scale, making the scale-up of STRs a crucial task for process engineers. It is shown that unsuccessful scale-up leads to inefficient large scale mixing and, possibly, to poor product quality. The economic downfall of this issue may be important since the quality of products is directly linked to their market. The cost of improper scale-up and, consequently, poor mixing was estimated between $1 and $10 billion in the U.S. chemical industry alone in 1989 (Paul et al., 2004).

An understanding of flow behaviour is important for precise process design and scale-up, and this can only be achieved by analysing the multi-scale fluid dynamics in process equipment. Design and scale-up of STRs traditionally rely on experimental efforts and empirical correlations. This common approach has faced several difficulties. Usually the empirical correlations are based on vessel average values in the stirred tank. However, this assumption can be considered a main issue in the scale-up of STRs, considering local conditions in stirred tanks are crucial, especially in a system where the mixing performance is dictated by physical phenomena whose time scale is shorter than the vessel mixing time. Several experimental methods have been developed to find local hydrodynamic parameters (Chaouki et al., 1997; Mavros, 2001). Nevertheless, some concerns still need addressing, such as the cost of the experimental method and their scale limitations. Many processes involve high temperature, high pressure, and hazardous conditions for which detailed experimental data acquisition is not practical.

Thanks to the availability of increasingly powerful computers, computational fluid dyna-

mics (CFD) has become gradually used as a practical tool for understanding fluid dynamics and eventually designing efficient processes. CFD is broadly used to study mass, momentum, and heat transfer in chemical process equipment in different flow regimes. It can provide information regarding the velocity, pressure, turbulent kinetic energy and its dissipation with respect to time and space, at a fraction of the cost of the corresponding experiments (Ranade, 2002). It is believed that significant improvement can be achieved in the design of STRs using a CFD model that considers the actual flow field and local hydrodynamic parameters. Numerous numerical studies have been performed to find flow patterns in STRs, which have been reviewed in several articles (Brucato et al., 1994, 1998; Harris et al., 1996; Joshi and Ranade, 2003; Murthy and Joshi, 2008; Sommerfeld and Decker, 2004). Obviously, experimental studies remain crucial for the validation of computational methods used for the simulation of a flow field.

Many industrial processes involve turbulent two-phase flow. Although CFD has been used for such systems, it nonetheless faces uncertainties and difficulties (Joshi and Ranade, 2003; Murthy and Joshi, 2008; Sommerfeld and Decker, 2004) due to a lack of reliable models to describe the interaction between the dispersed phase and the turbulent eddies of the continuous phase as well as droplet, breakage and coalescence. In the case of gas-liquid systems, another issue is the number of physical models needed to describe these phenomena, which makes the numerical simulation of such systems most of the time difficult and complicated. One alternative is to resort to single-phase turbulent flow simulation based on the assumption that the dispersed phase has a weak interaction with the continuous phase. By performing single-phase flow simulation, valuable information about the qualitative behaviour of the flow can be obtained, which can be used as a starting point for more complicated two-phase simulations.

In the common engineering practice of equipment design and scale-up, all spatial variations of properties within each unit operation are generally ignored ("well-mixed tank" assumption). This assumption is quite rudimentary and may be far-fetched, particularly in large-scale

vessels. A conventional way of describing non-ideal mixing within stirred tanks is by means of compartmental modelling. It divides the tank volume into several zones, each of which is considered to be well-mixed and homogeneous with respect to one or more parameters that dictate the performance of the system (Bezzo et al., 2000; Guha et al., 2006). One important property of turbulent flow is the turbulent energy dissipation rate (ε). This parameter affects the heat and mass transfer as well as micro-mixing, which is crucial for reactive flow (Fox and Stiles, 2003). In addition, many characteristic parameters of gas-liquid flow, including gas hold-up, bubble size distribution, and interfacial area are a function of the turbulent energy dissipation rate (Garcia-Ochoa and Gomez, 2009). In fact, throughout the mixing process, a certain amount of energy must be provided by turbulent flow to achieve the process objectives, the break-up and coalescence of drops or bubbles in liquid/liquid and gas/liquid systems, thus making the turbulent energy dissipation rate a critical parameter to assess the mixing efficiency in such systems. In the literature, it has been experimentally and numerically shown that the turbulent energy dissipation rate varies within the mixing vessel (Kresta and Wood, 1991; Micheletti et al., 2004; Ng and Yianneskis, 2000; Wernersson and Trägårdh, 1999). Its value is extremely high near the impeller and low in regions far from it. There is a large body of experimental work that has investigated the occurrence of non-homogeneities in the energy dissipation rate. On the other hand, despite the importance of local energy dissipation rates, available estimations in the literature involve mostly averaged values in the vicinity of the impeller due to experimental difficulties (Ng and Yianneskis, 2000). CFD simulation can then be a good way to provide spatial distributions of this parameter, which can be passed along as input data to a compartmental model.

There are studies that have tried to shed light on the effects of turbulent non-homogeneities on process efficiency. Bałdyga et al. (1995) used a zonal approach in a stirred reactor agitated by a two-bladed flat paddle impeller to evaluate the impact of non-ideal mixing on crystal size distributions by using a population balance model. A two-compartment population balance model was developed by Maggioris et al. (2000) to predict the droplet size distribution in

a polymerisation reactor, as a function of operating conditions, by taking into account the large spatial variations of the turbulent kinetic energy. In their work the volume of the tank was divided into two regions. The first region, near the impeller, was characterised by a high turbulent energy dissipation rate, whereas the second showed a low value of this quantity in the circulating zone. The volume ratio of the impeller and circulating regions, as well as the ratio of turbulent dissipation rates and the exchange flowrates in the two compartments, which are compartmental model parameters, were estimated by CFD for different agitation rates and continuous phase viscosities. Alexopoulos et al. (2002) followed the same methodology to study the effect of the agitation rate, impeller diameter, fluid viscosity and vessel size on the compartmental model parameters. Two-compartment formulations of the population balance equation were used to assess the effect of non-homogeneities in a stirred tank on the droplet size distribution (DSD) of liquid/liquid dispersions. A good agreement was reported between the numerical results and experimental drop size distributions. Vakili and Esfahany (2009) considered three compartments in a baffled agitated tank equipped with a two-blade turbine. In addition to zones near the impeller and in the bulk of the tank, they considered a third zone with a relatively high value of the turbulent energy dissipation rate in the vicinity of the baffles and tank wall. In their study, the impeller and the tank wall had considerable interaction. The effects of the agitation rate, impeller diameter and clearance, and baffle width on the model parameters were investigated. A systematic zoning approach was also proposed by Alopaeus et al. (2009) whereby the tank was divided into two separate regions. Stirred tank turbulence and fluid flow characteristics were analysed based on a two-zone model. The effects of the impeller type, liquid viscosity, and turbulent model were investigated. They developed a so-called zoning curve for better visualisation of the turbulent mixing in the tank. However, the zones were not determined based on the distribution of turbulent energy dissipation rate, making their results quite different from those obtained by others. They showed that a gradual increase of the inner zone volume, from the impeller swept area towards the tank wall, yields continuous curves for the turbulent energy dissipation rate and

the pumping number between the two zones, with respect to their sizes.

In all the investigations discussed above, compartmentalisation of the tank based on the turbulent energy dissipation rate usually has been applied for mixing systems provided with simple impellers. In addition, the impact of common scale-up approaches on the extent of turbulent non-homogeneities and the value of compartmental model parameters has not been addressed in the literature. In the present work, the ability of different turbulent models to predict the flow pattern in STRs agitated by a Rushton turbine is assessed. The CFD-based compartmental modelling strategy described by Alexopoulos et al. (2002) is revisited. A new method is introduced to determine the zone boundaries in the tank in a more straightforward and precise way. Finally, the effect of different scale-up approaches on the extent of turbulent non-homogeneities in STRs and the value of compartmental parameters is investigated systematically.

4.2 Two-compartment model

CFD-based compartmental modelling can be used to determine the distribution of turbulent energy dissipation rate in a stirred tank. The simplest configuration for describing turbulent non-homogeneities in a stirred vessel consists of two compartments, a small one around the impeller and characterized by large energy dissipation rates and turbulence intensities, as well as a larger circulating region, far from the impeller, where the turbulent flow field is nearly homogeneous and the energy dissipation rate is small (Figure 4.1) (Alexopoulos et al., 2002; Maggioris et al., 1998, 2000). This approach can then be viewed as a compromise between full CFD-based multiphase flow models and the use of unrealistic models based on one single constant parameter for the whole system.

As stated previously, CFD simulations can provide local values of the turbulent energy dissipation rate. The information in each cell j of volume v_j can then be post-processed to extract the volume fraction distribution of the turbulent energy dissipation rate to assess the turbulent non-homogeneities in the mixing vessel. If n_j denotes the corresponding fraction of

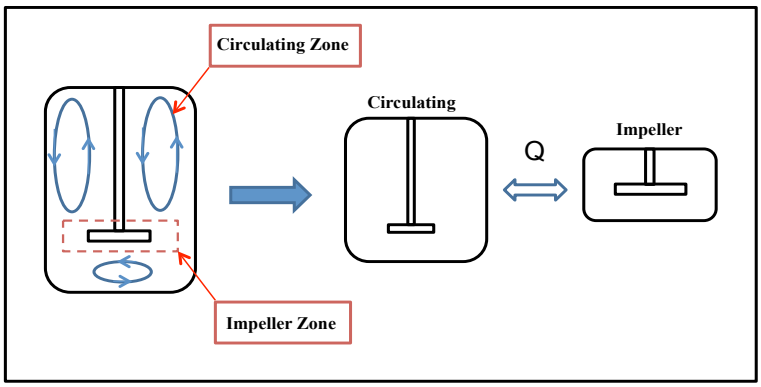

Figure 4.1: Schematic of a two-compartment model of stirred tank.

the vessel volume :

$$n_j = \frac{v_j}{V_{tot}} \tag{4.1}$$

where V_{tot} is the volume of the tank, and ε_i the corresponding turbulent energy dissipation rate, $e_j = \varepsilon_j nj$ therefore represents the weighted amount of energy that is dissipated in this fraction of the vessel volume. The cells being numbered in increasing order with respect to ε, the cumulative weighted sums of energy dissipation rate (E_i) can then be defined over the whole range of energy dissipation rates by varying i in the following expression :

$$E_i = \sum_{j=1}^{i} e_j = \sum_{j=1}^{i} \varepsilon_j n_j \tag{4.2}$$

These expressions can be used to determine the boundary between the impeller and the circulating regions. More precisely, a cut-off energy dissipation rate, ε_{cut}, can serve to identify this boundary so that the cells with a turbulent energy dissipation rate higher than ε_{cut} belong to the impeller region, and the cells with a turbulent energy dissipation rate lower than ε_{cut} belong to the circulating region. The adequacy of these two regions depends on the selection of ε_{cut}. This parameter can be found by determining the break in the cumulative weighted sums of the energy dissipation rate curve. This approach has been used in previous studies (Alexopoulos et al., 2002; Maggioris et al., 1998, 2000; Vakili and Esfahany, 2009). However, finding the exact location of this break is not straightforward and rather subjective. One

contribution of this work is to introduce a more precise method of finding ε_{cut}. Computer programs were written to extract n_j and E_i from CFD simulation results, the details of which are provided in the following sections. Figure 4.2a and 4.2b show respectively typical graphs of the cumulative weighted sums and corresponding volume fractions of the energy dissipation rate obtained from such simulations. Note that the blue region in Figure 4.2b corresponds to one single curve that links, in increasing order, the values of turbulent energy dissipation rate in the corresponding cells. As can be readily seen in Figure 4.2a, choosing ε_{cut} based on the break in the slope of the cumulative weighted sums curve is indeed not easy. On the other hand, as shown in the log-log plot of the volume fractions versus the turbulent energy dissipation rates (Figure 4.2b), the mixing tank can be clearly divided into two regions. A larger fraction of the tank far from the impeller is characterised by a low value of the energy dissipation rate, while a smaller fraction, in the impeller region, is associated with high values of the energy dissipation rate. The boundary between these two regions can be distinguished by means of the shape of the volume fraction curve. More precisely, the fish shape of this curve can be divided into two regions, body and tail. The location where the tail is attached to the body of the fish can serve to set a value for ε_{cut}. The blue region in Figure 4.2b is delimited by two dashed splines. The upper boundary of this curve (top dashed line) is a plateau until it reaches a threshold value of the energy dissipation rate, above which it suddenly goes down in a steep manner. The value of this threshold provides a systematic way to choose ε_{cut}.

The impact of ε_{cut} on the position of the boundary between the two compartments can be assessed by means of the contour plot of the energy dissipation rate. Figure 4.3a shows a top view of the geometry of the system as well as the upper spline delimiting the volume fraction curve of Figure 4.2b. Figure 4.3b, 4.3c and 4.3d show the high energy dissipation rate region for increasing values of ε_{cut} (0.1, 0.35 and 6, respectively). When the value is low (Figure 4.3b), this region includes areas around the baffles, near the walls and in bulk of the vessel. Increasing the value of ε_{cut} to 0.35 (Figure 4.3c) yields a small region around the

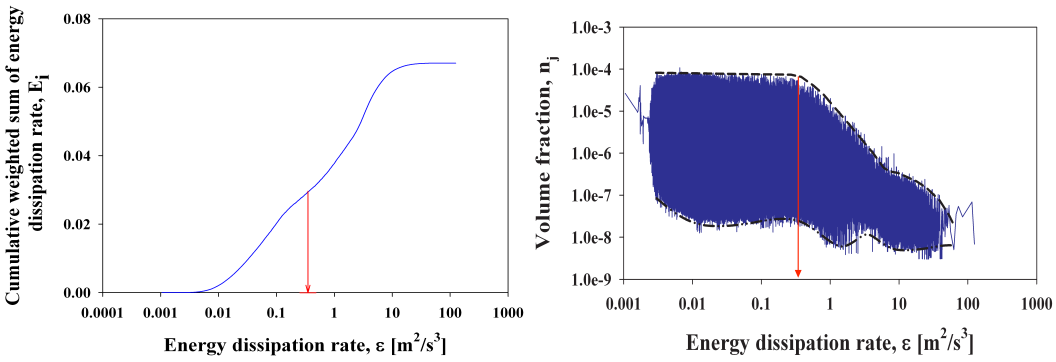

Figure 4.2: Spread of the turbulent energy dissipation rate in the tank. (a) Cumulative weighted sum curve. (b) Volume fraction curve.

impeller. With an additional increase of ε_{cut} to 6, which corresponds to the second change of the slope in the curve, this region restricts itself even more against the impeller, giving birth to a star-like high energy dissipation rate region therein (Figure 4.3d). In this work, the first steep decrease in the volume fraction curves, as illustrated in Figure 4.3c, was used to determine the value of ε_{cut}.

The average energy dissipation rate, $\overline{\varepsilon}$, can be defined as :

$$\overline{\varepsilon} V_{tot} = \overline{\varepsilon}_{imp} V_{imp} + \overline{\varepsilon}_{cir} V_{cir} \tag{4.3}$$

where the total volume is the sum of the impeller and circulating region volumes, V_{imp} and V_{cir}, respectively :

$$V_{tot} = V_{imp} + V_{cir} \tag{4.4}$$

The compartmental model can be defined by two parameters. The first one is the ratio of the energy dissipation rates in each compartment :

$$\lambda = \frac{\overline{\varepsilon}_{imp}}{\overline{\varepsilon}_{cir}} \tag{4.5}$$

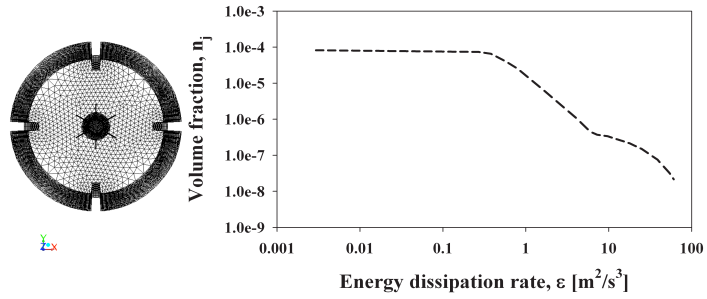

(a)

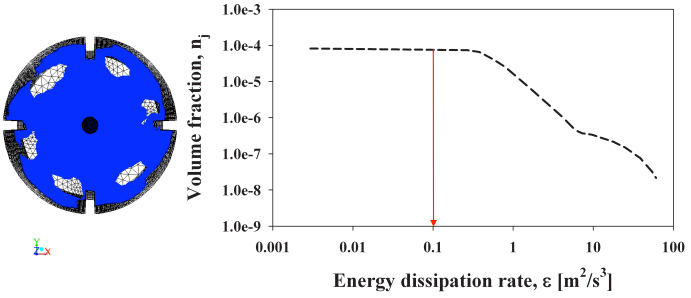

(b)

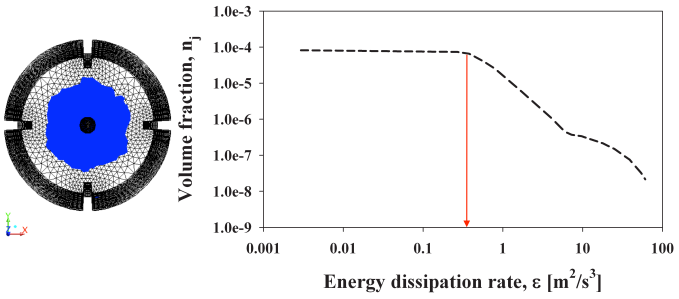

(c)

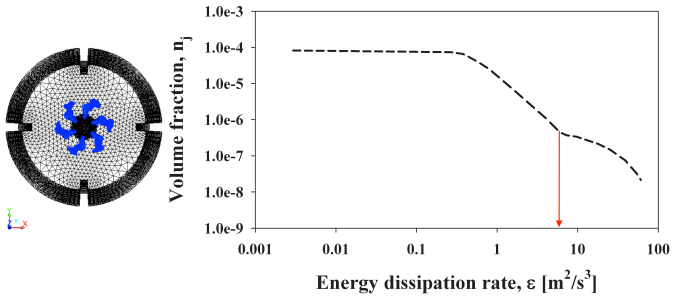

(d)

Figure 4.3: Impeller compartment for different values of the cut-off energy dissipation rate : (a) ε_{cut}=100, (b) ε_{cut}=0.1, (c) ε_{cut}=0.35, (d) ε_{cut}=6.

and the second one is the compartment volume ratio :

$$\beta = \frac{V_{imp}}{V_{cir}} \tag{4.6}$$

For the sake of completeness, note that the values of β corresponding to Figure 4.3b-d are 0.0875, 0.0254 and 0.0007, respectively.

It then comes from (4.4) and (4.6) that :

$$\beta = \frac{V_{imp}}{V_{tot} - V_{imp}} \tag{4.7}$$

The impeller and the circulating compartment volumes and their ratio β can be determined by using the n_j (volume fractions) values and the value of the cut-off turbulent energy dissipation rate, ε_{cut}. More precisely, the impeller compartment volume can be obtained by summing the cell volumes with an energy dissipation rate greater than ε_{cut} :

$$V_{imp} = V_{tot} \sum_{j=1}^{N_{tot}} n_j (H(\varepsilon_j - \varepsilon_{cut})) \tag{4.8}$$

where N_{tot} stands for the total number of the cells and $H(x)$ is the discrete Heaviside step function.

The average turbulent energy dissipation rate can be calculated using the following equation :

$$\bar{\varepsilon} = \sum_{j=1}^{N_{tot}} \varepsilon_j n_j \tag{4.9}$$

Finally, expressions for the average turbulent energy dissipation rate in each region result from (4.7) :

$$\bar{\varepsilon}_{imp} = \sum_{j=1}^{N_{tot}} \frac{V_j \varepsilon_j H(\varepsilon_j - \varepsilon_{cut})}{V_{imp}} \tag{4.10}$$

$$\bar{\varepsilon}_{cir} = \frac{(\bar{\varepsilon} V_{tot} - \bar{\varepsilon}_{imp} V_{imp})}{(V_{tot} - V_{imp})} \tag{4.11}$$

As shown in the next section, these parameters and quantities can describe the mixing performance and represent, in a simple manner, the turbulent energy dissipation rate non-homogeneities in the tank.

4.3 CFD modelling approach

Three-dimensional CFD simulations were conducted in three geometrically similar cylindrical vessels of 7.27, 58.18 and 465.50 L. Four equally spaced baffles were mounted on the tank wall. The tank was agitated by a 6-bladed Rushton turbine. This type of impeller is widely used in the industry and several publications about it have been published over the years. The tank was filled with water as a working fluid up to a height equal to the tank diameter. A schematic of this mixing system is shown in Figure 4.4.

The origin of the coordinate system is the centre of the impeller. The geometry of the vessel and the grids were generated by commercial software package Gambit 2.4. These grids are unstructured and contain different types of cells. Given the complexity of the geometry, unstructured meshes were used to capture the details of the flow field in the entire domain, especially in the discharge area of the impeller and near the baffles. Three computational meshes containing 185, 354 and 462 k cells, and referred to as coarse, medium, and fine, respectively, were used to investigate the sensitivity of the solution to the grid resolution. The meshes were refined around the impeller and baffles where there is significant change in the flow pattern and most of the turbulent energy dissipation is expected to occur. To do so, a size function available in Gambit 2.4 was used to control the size of the meshes in these regions so that the standard wall function (discussed below) can be employed adequately. In this study, commercial code ANSYS Fluent 12.1.4 was used for solving the Reynolds Average Navier-Stokes (RANS) equations with four different turbulent models : the standard, realisable and RNG $k-\varepsilon$ models as well as the RSM model.

More precisely, turbulent fluid flow in the tank is governed by the following continuity

and momentum equations :

$$\frac{\partial \langle u_j \rangle}{\partial x_j} = 0 \tag{4.12}$$

$$-\frac{\partial}{\partial x_j}(\rho \langle u_j \rangle \langle u_i \rangle) - \frac{\partial}{\partial x_j}(\rho \langle u'_j u'_i \rangle) + \frac{\partial}{\partial x_j}\left[\mu\left(\frac{\partial \langle u_i \rangle}{\partial x_j} + \frac{\partial \langle u_j \rangle}{\partial x_i}\right)\right] - \frac{\partial \langle p \rangle}{\partial x_i} + F_i = 0 \tag{4.13}$$

where $i, j = 1, 2, 3$ and $\langle\ \rangle$ stands for the average operator and where F_i corresponds to external body forces. The Reynolds stress term, $-\rho \langle u'_j u'_i \rangle$, must be modelled to close the momentum equation. The Boussinesq hypothesis is used in the (standard, realisable and RNG) k-ε turbulent models to relate the Reynolds stresses to the mean velocity gradient as follows :

$$-\rho \langle u'_j u'_i \rangle = \mu_t \left(\frac{\partial \langle u_i \rangle}{\partial x_j} + \frac{\partial \langle u_j \rangle}{\partial x_i}\right) - \frac{2}{3}\rho k \delta_{ij} \tag{4.14}$$

In these models, two additional transport equations, one for the turbulent kinetic energy, k, and one for the turbulent dissipation rate, ε, must be solved to provide values for the turbulent viscosity, μ_t, which is a function of these two quantities. Alternatively, the Reynolds stress model (RSM) can be used to model the Reynolds stresses, $-\rho \langle u'_j u'_i \rangle$. The RSM solves seven equations for three-dimensional problems : six equations for the symmetric Reynolds stress tensor and another equation for the turbulent energy dissipation rate. The constants inherent to these models were set to the values commonly used in the literature (FLUENT, 2010).

In this work, the simulations were conducted using the steady-state multi reference frames (MRF) approach, whereby the grid was divided into two reference frames to account for the stationary and rotating parts (FLUENT, 2010). Note that it has been shown in the literature that for steady-state simulations of fluid flows in stirred tanks, the MRF technique gives similar results to the much more computationally intensive transient sliding mesh technique (Aubin et al., 2004). Moreover, it has also been observed that the region where the flow is strongly influenced by the blades extends to about one length of $D/2$ away from the impeller tip and 1.5 times the blade height above and below the impeller disc (Lee and

Yianneskis, 1994). This information was used to define the size of the rotating region of the MRF technique. A no-slip boundary condition was imposed at the solid surfaces. In addition, the standard wall function was used to link the viscosity-dominated region between the wall and the fully turbulent region. The adequacy of the standard wall function was verified for all cases. The values of y^+ (non-dimensional wall distance) in the first layer of cells close to the tank walls ($30 < y^+ < 60$) were such that these cells were located within the turbulent layer in all cases. The impeller disk periphery was characterised by values of y^+ that can be smaller in some isolated spots, albeit larger than 11.225, the threshold value above which the standard wall function can be applied.

A zero shear stress was imposed at the tank surface and used as a free surface boundary condition. The SIMPLEC algorithm was used to solve the continuity and the momentum equations. Second order upwind discretisation scheme for the momentum and the k and ε equations was used. The reader is referred to the ANSYS Fluent documentation (FLUENT, 2010) for more details on this topic. In the simulations, convergence was achieved when the residuals on the continuity, velocity, kinetic energy and energy dissipation rate all became

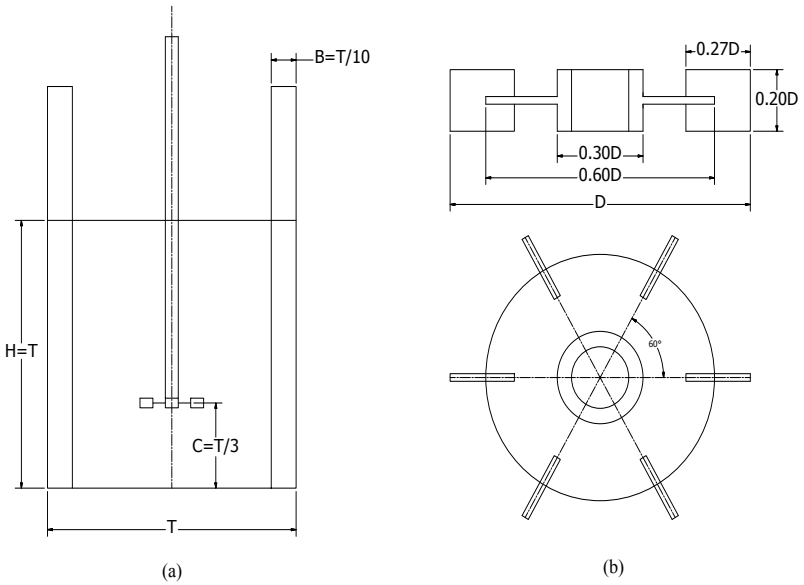

Figure 4.4: Schematic of the mixing systems ; (a) vessel geometry and (b) impeller geometry.

less than 10^{-5}. The accuracy of our simulation results will be discussed in more detail in the following section.

It was shown by Coroneo et al. (2011) that the number of cells has a major effect on the quality of simulation results. Due to the similarity of the medium and fine grid simulation results for all three tank sizes, the medium grid was employed for all vessel sizes. Note that the compartmental method proposed in this work brings into play the ratio of compartment-averaged values of ε, which are significantly less sensitive to the cell size than their local values. Also, it was shown recently by Alopaeus et al. (2009) for a similar mixing system that the ratio of $\varepsilon/\bar{\varepsilon}$ values is grid independent for vessel sizes of 14, 194 and 20,000 dm^3, and $395k$ cells. In addition, the cell size was not uniform in our work. To save on computational time and increase accuracy, the meshes were indeed refined around the impeller and baffles to resolve the large variations of ε in these areas. This refinement strategy led to variations of $\lambda = \bar{\varepsilon}_{imp}/\bar{\varepsilon}_{cir}$ of the order of 5% between the coarse and medium grids, whereas variations smaller than 1% were observed between the medium and the fine grids. One should keep in mind that what matters in this work are not grid independence results per se, but results that are accurate enough for the proposed compartmental model.

The specifications for the 13 simulations that were run are summarized in Table 4.1. Cases 1 through 3 were used for a mesh sensitivity analysis. Cases 2 and 4 through 6 were used to assess the different turbulent models, and cases 2 and 7 through 13 were used for the scale-up study.

4.4 Results and Discussion

In this section, the accuracy of the four turbulent models described in the previous section is assessed. Simulation results obtained with these turbulent models are then compared with data from the literature, followed by an evaluation of the compartmental model parameters based on multi-scale CFD simulations. Finally, the impact of different conventional scale-up approaches on the value of these parameters is discussed.

Table 4.1: Specifications for the simulated cases.

Case	Tank diameter (m)	Mesh size (k)	Type	N (rpm)	V_{tip} (m/s)	P/V (W/m^3)	$Re * 10^{-4}$	Turbulent model	Scale-up rule
1	0.21	185	Mesh Analysis	600	2.05	855	4.28	RNG	-
2	0.21	354	Mesh Analysis	600	2.05	855	4.28	RNG	-
3	0.21	462	Mesh Analysis	600	2.05	855	4.28	RNG	-
4	0.21	354	Turbulent Model	600	2.05	855	4.28	Standard	-
5	0.21	354	Turbulent Model	600	2.05	855	4.28	Realizable	-
6	0.21	354	Turbulent Model	600	2.05	855	4.28	RSM	-
7	0.42	354	Scale-up	600	4.12	3421	17.11	RNG	Rule 1
8	0.42	354	Scale-up	300	2.05	428	8.55	RNG	Rule 2
9	0.42	354	Scale-up	378	2.59	855	10.78	RNG	Rule 3
10	0.42	354	Scale-up	150	1.025	53	4.28	RNG	-
11	0.84	354	Scale-up	600	8.22	13685	68.43	RNG	Rule 1
12	0.84	354	Scale-up	150	2.05	214	7.11	RNG	Rule 2
13	0.84	354	Scale-up	238	3.26	855	27.15	RNG	Rule 3

4.4.1 Assessment of turbulent models

The normalised radial, tangential, and axial velocity profiles obtained with the different turbulence closure models are plotted in Figure 4.5. These profiles are shown at the impeller discharge boundary $r/R = 1.07$, where there are large flow variations. These data are compared with experimental data presented by Wu and Patterson (1989), Zhou and Kresta (1996) and Éscudie and Liné (2003). One can see that all turbulent models can generally predict the trend of the flow pattern in this region. However, the RSM and RNG k-ε models better predict the maximum radial and tangential velocities near the impeller tip (Figure 4.5a and b).

In fact, the standard and realisable k-ε models under-predict the maximum radial velocity by 7% and 10% compared to RSM and RNG k-ε, respectively. A less important under-prediction (3% and 4%, respectively) can be observed for the maximum tangential velocity. These models can likewise better predict the vertical velocity profiles in the axial direction compared to the experimental data (Figure 4.5c).

There are some causes of scatter between the experimental data and between these data and the CFD simulation results. One of the main sources of discrepancy as regards the experimental data is the difference in the performance characteristics of the measurement techniques used, such as the frequency response and the size of the measurement volume. The use of a non-standard experimental set-up can likewise contribute to these differences. For instance, Zhou and Kresta (1996) used a stirred tank in which the impeller diameter and the clearance were half of the tank diameter and, consequently, a significant scatter with other studies can be observed. It was shown by Rutherford et al. (1996) that any change in the ratio of the blade and disc thicknesses to the impeller diameter considerably affects the mean radial velocity : a threefold increase in this ratio was observed to cause a 20% reduction in the mean radial velocity. However, the largest difference was in the impeller tip region with no significant effect in regions far from it. These authors also mentioned that the presence of bolts to fix the blades to the hub and vessel internals can affect the mean flow and the

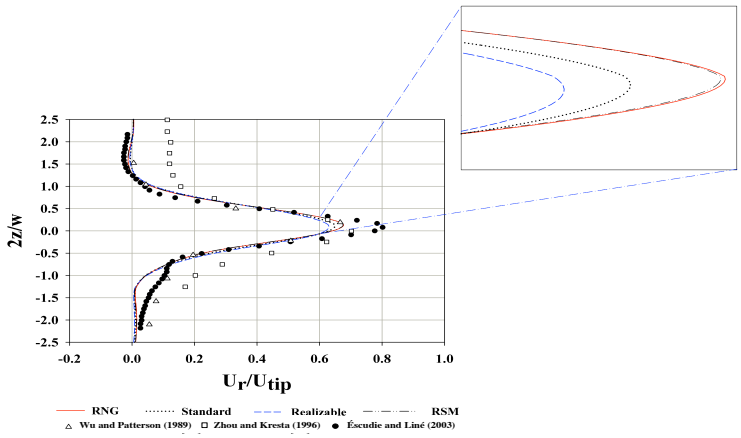

(a)

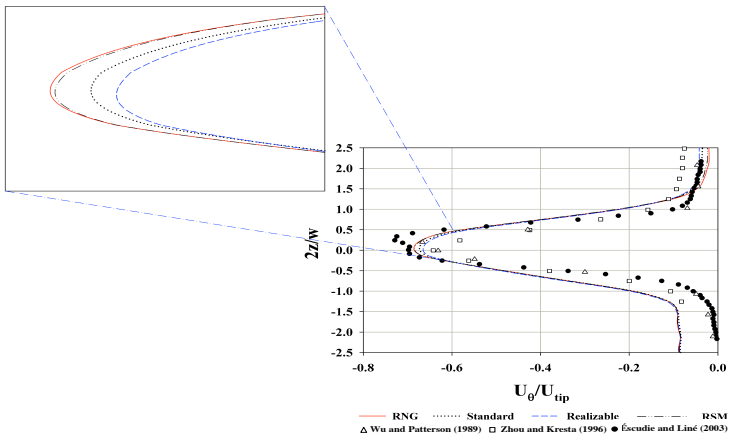

(b)

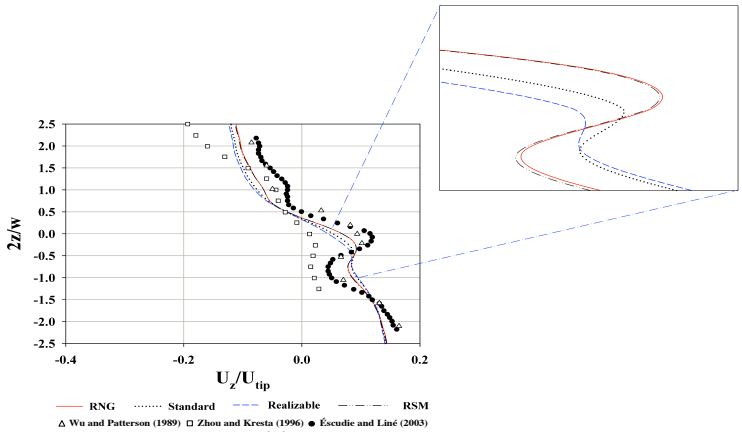

(c)

Figure 4.5: Vertical profiles of the normalized mean velocities $(r/R = 1.07)$; (a) radial velocity, (b) tangential velocity, (c) axial velocity.

trailing vortex structure. Another source of discrepancy between the numerical results and the experimental data is the turbulent model themselves, which are all based on simplifying assumptions (*e.g.* isotropic turbulent eddies). The use of a flat surface at the top of the tank is another source of error.

In Figure 4.5, the flow in the region near the impeller is mainly radial and tangential. It can be noted that the mean radial profile is not symmetrical around the disc of the impeller at z=0 due to the non-symmetrical axial location of the impeller in the tank, as shown in Figure 4.4. The simulation results obtained in this work resemble more those of Wu and Patterson (1989), which is not surprising because the geometries are alike. However, there is in general an under-prediction of the radial and tangential velocities in the impeller jet flow. More particularly, the errors for the predicted maximum radial velocity by the RSM and RNG k-ε models are 8% and 16% compared to the experimental data provided by Wu and Patterson (1989) and Éscudie and Liné (2003), respectively. In the system used by Éscudie and Liné (2003), the blade and disc thicknesses were both 2 mm, whereas the values for the system used in the current study are 1 mm. Based on work of Rutherford et al. (1996), a reduction larger than 10% in the mean radial velocity is then expected. It can also be observed that all the models under-predict the radial velocity in the region under the impeller blade. These discrepancies may be due to differences in the geometrical characteristics of the baffles considered in the current work and the reported investigations. As illustrated in Figure 4.5c, the predicted axial velocity profiles by the RSM and RNG k-ε models are in good agreement with the experimental data, more specifically the ones provided by Wu and Patterson (1989). These two models indeed provide a good prediction of the curvy shape of the axial velocity profile under the impeller. This is further justified in Table 4.2, which gives the coefficient of determination (R^2) corresponding to these predicted velocity profiles when compared to the experimental data of Wu and Patterson (1989).

Evaluating the power number N_p and the radial flow number N_Q is another way of assessing the simulation results. The torque Γ was calculated by integrating the force moments

Table 4.2: Coefficients of determination corresponding to the predicted velocity profiles of Figure 4.5 when compared to the experimental data of Wu and Patterson (1989).

	R^2		
Turbulent model	U_r/U_{tip}	U_θ/U_{tip}	U_z/U_{tip}
RNG	0.940	0.860	0.850
RSM	0.936	0.860	0.850
Standard	0.933	0.859	0.780
Realizable	0.927	0.858	0.730

acting on the shaft and the impeller or, equivalently, on the baffles and the tank wall. The calculated torque is related to the power input P and the power number through the following identities :

$$P = 2\pi N\Gamma \tag{4.15}$$

$$N_p = \frac{P}{\rho N^3 D^5} \tag{4.16}$$

Values of the power numbers obtained from the four turbulent models considered in this work are compared to the value (5.2) reported in the literature (Bujalski et al., 1987; Paul et al., 2004) in Figure 4.6. All models predict the power number with a relative error less than 8%, yet the RSM and RNG k-ε models are more accurate than the standard and realisable turbulent models.

The radial flow number is a measure of the pumping capacity of an impeller and is defined as :

$$N_Q = \frac{Q}{ND^3} \tag{4.17}$$

where Q is the radial flow rate produced by the impeller. To compute Q, a surface needs to be created for the discharge region. This surface corresponds to the side area of a cylinder

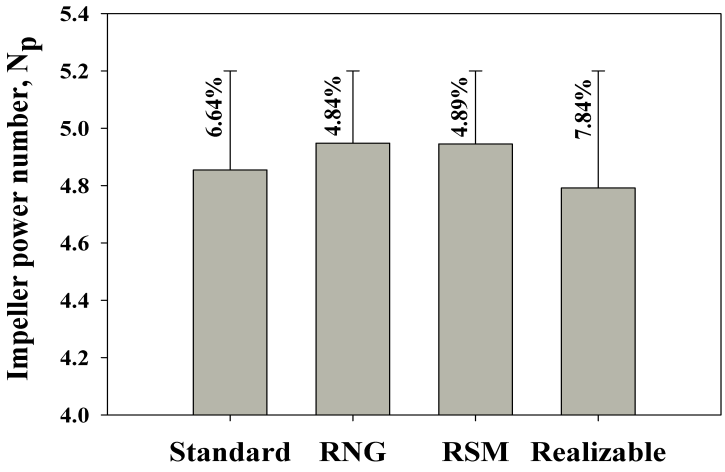

Figure 4.6: Values of the power number obtained with the turbulent models.

surrounding the Rushton turbine. Q can be calculated using the following equation :

$$Q = R \int_{z_1}^{z_2} \int_{0}^{2\pi} v_r d\theta dz \tag{4.18}$$

In this equation R, v_r, z_1 and z_2 denote the radius of the impeller, the radial velocity, and the lower and upper heights of the blades (z_1=6.3 cm and z_2=7.7 cm), respectively. By integrating the total outflow through this surface, the flowrate and, subsequently, the flow number can be obtained. The values of the flow number calculated with the four turbulent models are all within 2% of the value reported for Rushton turbine (Paul et al., 2004). These values are equal to 0.708, 0.707 and 0.717 for the standard, realisable and RNG k-ε models, respectively. This value is equal to 0.710 for the RSM model.

The results obtained in this section indicate that both the RNG k-ε and the RSM turbulent models better predict turbulent flow in a stirred vessel provided with a Rushton turbine. The RNG model was used for all subsequent simulations because it is less computationally intensive and more stable and robust than the RSM model.

4.4.2 Scale-up

Due to the high demand for chemical products, processes must generally be scaled up for industrial production. These processes are usually developed at different scales and the final process optimization is performed at a pilot scale ($50 - 300$ L), where it is assumed that the hydrodynamic and operational conditions are similar to those of the industrial scale. Rule of thumb methods and criteria are commonly used for the scaling-up of a process from laboratory to industrial scales and the setting of operating conditions. The two-compartment method described in Section 4.2 was used to simulate fluid flow for different scales of the Rushton turbine mixing system, in order to stress the differences in hydrodynamics. CFD results were used to evaluate the parameters of the two-compartment model. More precisely, the effect on these parameters of the impeller speed and three conventional scale-up rules were investigated. Note that, based on our modelling results, we observed that around 55% of power input is dissipated in the impeller region, which is consistent with previous work (Alexopoulos et al., 2002; Cutter, 1966; Kresta and Wood, 1991; Ng and Yianneskis, 2000; Podgórska and Bałdyga, 2001; Wu and Patterson, 1989).

Figure 4.7a-d shows the effect of the impeller rotational speed on the compartmental model parameters for two different scales. It can be observed that an increase of this speed leads to an increase of the cut-off energy dissipation rate value, ε_{cut}, for both scales (Figure 4.7a). This is in fact associated with a shift of the energy dissipation rate distributions to higher values with an increase in the impeller speed, hence leading to higher homogeneities in the vessel. Figure 4.7b and c shows that an increase in impeller rotational speed causes a decrease of $\beta = \frac{V_{imp}}{V_{cir}}$ while $\lambda = \frac{\bar{\varepsilon}_{imp}}{\bar{\varepsilon}_{cir}}$ remains almost constant. On the one hand, the values of ε in both regions are increased, which means that they change in the same proportions because λ does not change significantly. On the other hand, the decrease in β , which is less considerable in the larger vessel due to the detrimental effect of the tank wall on the radial jet flow, means that the relative size of the impeller region decreases. In other words, an increase in rotational speed does improve mixing in the impeller region owing to a higher

turbulent energy dissipation rate in a smaller volume. For the circulating region, the increase in volume is compensated by a larger increase in turbulent energy dissipation rate, which explains why mixing is improved in this region as well. The same trend has been observed in the literature (Alexopoulos et al., 2002; Vakili and Esfahany, 2009). Figure 4.7d shows that the exchange flow rate between the two compartments increases with an increase of impeller rotational speed, more importantly in the case of the larger vessel.

In Table 4.1, cases 7-9 and cases 11-13 are scale-ups by factors of 2 and 4 of the tank diameter of case 2, using a constant impeller speed (N) (rule 1), a constant tip speed (V_{tip})

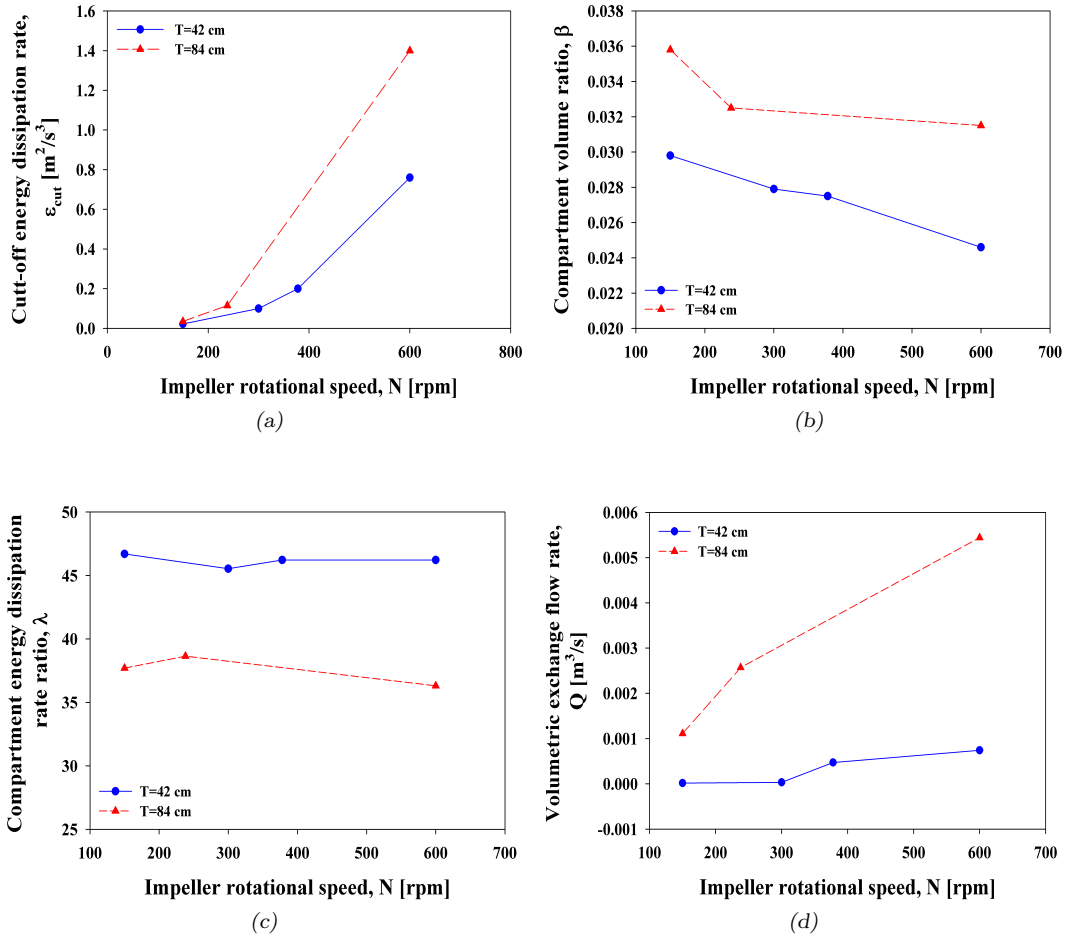

Figure 4.7: Effect of impeller rotational speed on : (a) cut-off energy dissipation rate value, ε_{cut} (b) compartment volume ratio, β (c) compartment energy dissipation rate ratio, λ and (d) volumetric exchange flow rate, Q.

(rule 2) or a constant power consumption per liquid volume (P/V) (rule 3). All of these cases are geometrically similar. The constant tip speed rule is normally used when the material inside the vessel is sensitive to the shear rate, like microorganisms and bacteria in bioprocess reactors. The constant power per liquid volume rule is often used for the scale-up of gas-liquid agitated tanks (Paul et al., 2004). The effects of the three scale-up rules described above on the parameters of the two-compartment model are shown in Figure 4.8a-d. In this figure, the parameter ratios from large (L) to small (S) scales are plotted versus the tank diameter ratios.

The value of the cut-off energy dissipation rate, ε_{cut}, decreases during the scale-up with rules 2 and 3 and increases with rule 1 (Figure 4.8a). It can be seen that the value of the ε_{cut} ratio depends on both the impeller rotational speed and impeller diameter. With rules 2 and 3, the impeller rotational speed is decreased considerably during the scale up, causing a decrease in ε_{cut}. However in the case of rule 1, the increase in the impeller diameter results in an increase of the impeller tip speed and ε_{cut}.

As shown in the Figure 4.8b, the compartment volume ratio increases during the scale-up with all these rules, thus leading to a higher degree of compartmentalisation and more non-homogeneities in the larger tanks. The energy dissipation rate ratio (λ) decreases considerably during the scale-up with all rules (Figure 4.8c). This indicates that the energy dissipation rate distributions change during the scale-up, which can affect the process characteristics. Finally, the ratio of volumetric exchange flow rate between the two compartments increases during the scale-up in all cases, implying that the effect of the impeller diameter on this quantity is greater than that of the impeller rotational speed.

4.4.3 Discussion

As can be inferred from the results of the previous section, the scale-up of stirred tanks based on local hydrodynamic variables is not straightforward. In particular, the scale-up rules affect the value of the compartmental model parameters. In practice, it would be useful

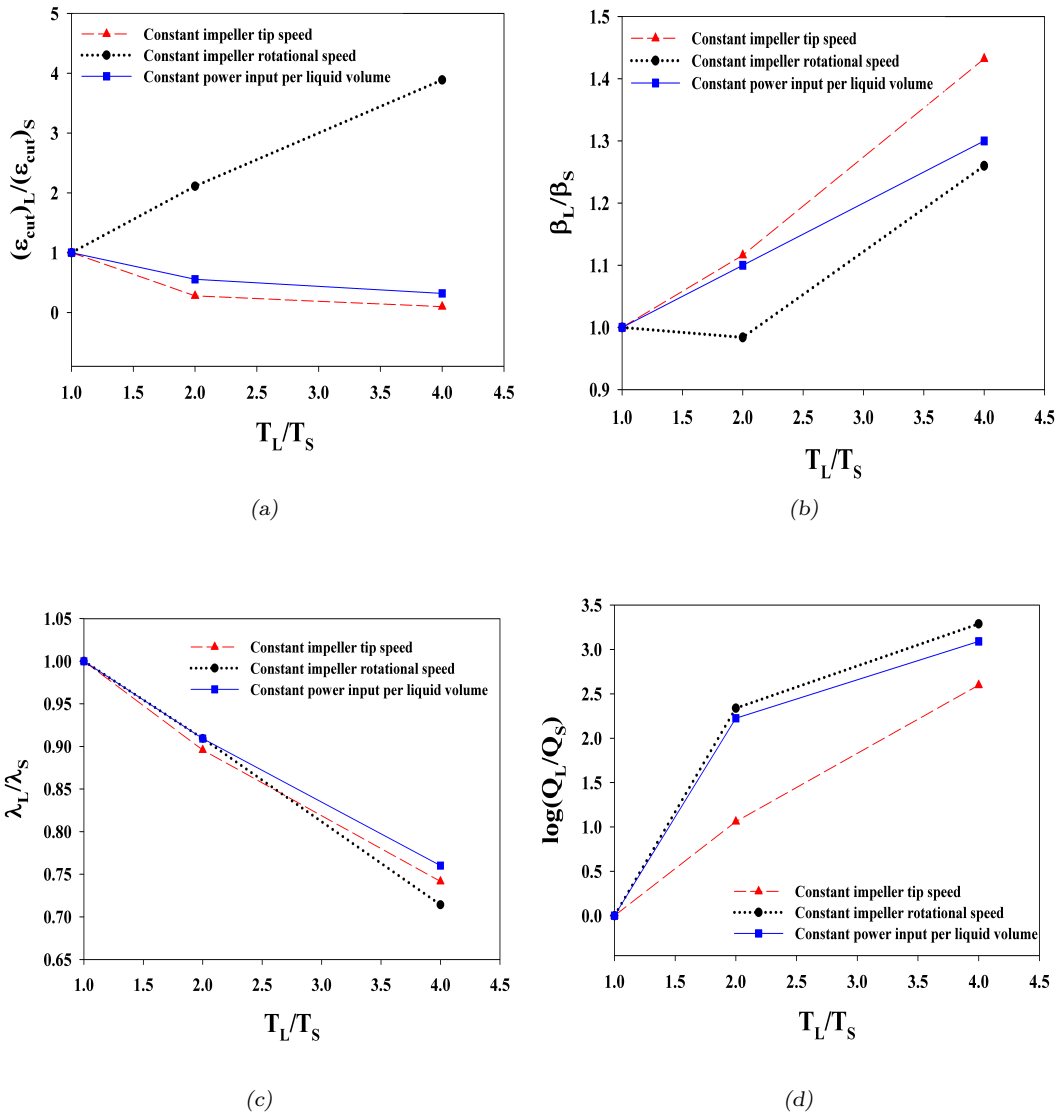

Figure 4.8: Effects of conventional scale-up rules on the compartmental model parameters : (a) cut-off energy dissipation rate ratio, ε_{cut} (b) compartment volume ratio, β (c) energy dissipation rate ratio, λ (d) volumetric exchange flowrate ratio, Q. Indices S and L indicate the small and large tanks, respectively.

to have for instance a general curve that predicts the values of the compartmental model parameters based on a the Reynolds number for each scale-up rule instead of repeating CPU intensive CFD simulations for all desired operating conditions and tank scales. Of course, such maps would need to be generated once for each type of mixing system. These curves could be used to predict the value of compartmental model parameters in larger scale tanks

based on the Reynolds number. Figure 4.9 demonstrates the paths of changes in the volume ratios and the energy dissipation rate ratios for the three scale-up rules. It can be noticed that increasing the Reynolds number leads to an increase of the volume ratio and a decrease of the energy dissipation rate ratio for all these rules.

Compartmental models and the strategy proposed in this work to build them represent a useful tool for the design or improvement of various mixing operations. It was shown in this work that volume fraction curves can be used to identify distinct compartments in tanks agitated by a Rushton turbine. Such curves could likewise be used to investigate the efficiency of chemical reactors on the basis of micro-mixing properties estimated from predicted compartment energy dissipation rates. In gas-liquid mixing, one critical parameter is the bubble size distribution. Population balance models (PBM) are often used to predict these distributions. Parameters of the PBM can be obtained from CFD simulation results or experimental data. Alternatively, the PBM could be combined to the compartmental model proposed in this work to evaluate the bubble size distribution in each compartment of the stirred tank. Such distributions are important since they affect the interfacial mass transfer and quality of product materials (Alexopoulos et al., 2002; Maggioris et al., 1998, 2000;

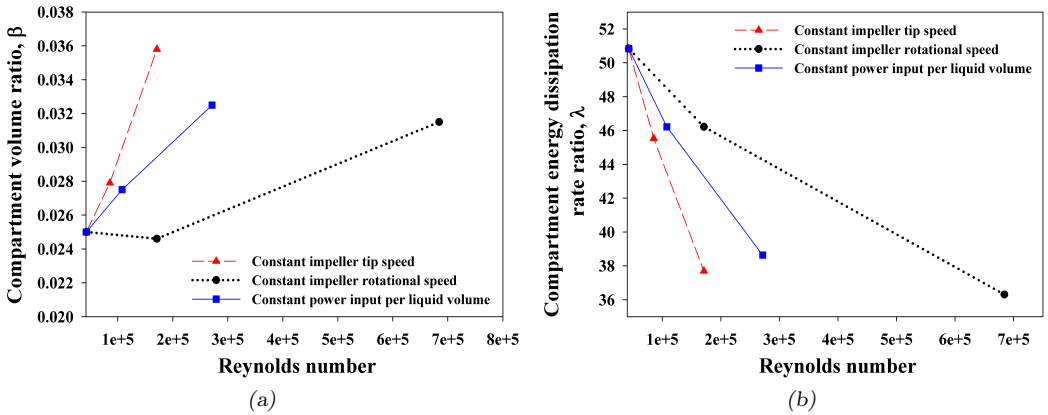

Figure 4.9: Maps of the compartmental model parameters based on different scale-up approaches; (a) compartment volume ratio, β (b) compartment energy dissipation rate ratio, λ .

Podgórska and Bałdyga, 2001; Pohn et al., 2011).

4.5 Conclusion

The objective of this work was to propose a compartmental model, the calibration of which is based on CFD simulation results, to investigate fluid flow in stirred tanks. It was first shown based on experimental observation from the literature and simulation results obtained by us that two compartments can be defined to characterise turbulent flows in tanks equipped with a Rushton turbine : a small region near the impeller with a high value of the average turbulent energy dissipation rate, and a larger zone with a significantly lower value of this quantity. A new method, relying on the use of volume fraction curves, was next introduced for finding the location of the boundary between these compartments, which is more straightforward and precise than other methods from the literature. Volume and energy dissipation rate ratios between these regions were proposed to determine the parameter values of the compartmental model. This model takes into account turbulent non-homogeneities in the tank and can serve to evaluate the performance of various mixing operations. In particular, it was shown that the compartmental model parameters depend on the operating conditions and the vessel size. The effects of three conventional scale-up rules on the parameters of this model were next evaluated for tanks agitated by a Rushton turbine. The concept of general maps for the prediction of the compartmental model parameters was finally discussed. These maps could be used to monitor changes in turbulent non-homogeneities in a mixing tank during scale-up. As mentioned in the introduction, CFD multiphase flow simulations could, in principle, be used for mixing operations involving more than one phase, although they still represent today a formidable challenge due to the lack of reliable models and excessive computational times. The proposed approach can then be viewed as a compromise between full CFD-based multiphase flow models and the use of unrealistic models based on one single constant parameter for the whole system. The idea is to determine the number and location of compartments in a stirred tank, based on the variation of the values of ε, and to pass along

the average value of this parameter in each compartment to a process-scale model (e.g. a population balance model). In this regard, the compartmental model can then be viewed as a multiscale model. In future work, it will be linked to a phenomenological mass transfer model in order to investigate the behaviour and the scale-up of gas-liquid stirred tank reactors.

4.6 References

Alexopoulos, A., Maggioris, D., and Kiparissides, C. (2002). CFD analysis of turbulence non-homogeneity in mixing vessels : a two-compartment model. *Chemical Engineering Science*, 57(10) :1735–1752.

Alopaeus, V., Moilanen, P., and Laakkonen, M. (2009). Analysis of stirred tanks with two-zone models. *AIChE journal*, 55(10) :2545–2552.

Aubin, J., Fletcher, D. F., and Xuereb, C. (2004). Modeling turbulent flow in stirred tanks with CFD : the influence of the modeling approach, turbulence model and numerical scheme. *Experimental thermal and fluid science*, 28(5) :431–445.

Bałdyga, J., Podgorska, W., and Pohorecki, R. (1995). Mixing-precipitation model with application to double feed semibatch precipitation. *Chemical Engineering Science*, 50(8) :1281–1300.

Bezzo, F., Macchietto, S., and Pantelides, C. (2000). A general framework for the integration of computational fluid dynamics and process simulation. *Computers & Chemical Engineering*, 24(2) :653–658.

Brucato, A., Ciofalo, M., Grisafi, F., and Micale, G. (1994). Complete numerical simulation of flow fields in baffled stirred vessels : the inner-outer approach. In 8^{th} *European Conference on Mixing*, number 136, pages 155–162. Institution of Chemical Engineers.

Brucato, A., Ciofalo, M., Grisafi, F., and Micale, G. (1998). Numerical prediction of flow fields in baffled stirred vessels : a comparison of alternative modelling approaches. *Chemical Engineering Science*, 53(21) :3653–3684.

Bujalski, W., Nienow, A., Chatwin, S., and Cooke, M. (1987). The dependency on scale of power numbers of Rushton disc turbines. *Chemical Engineering Science*, 42(2) :317–326.

Chaouki, J., Larachi, F., and Dudukovic, M. P. (1997). *Non-invasive monitoring of multi-phase flows*. Access Online via Elsevier.

Coroneo, M., Montante, G., Paglianti, A., and Magelli, F. (2011). CFD prediction of fluid flow and mixing in stirred tanks : Numerical issues about the RANS simulations. *Computers & Chemical Engineering*, 35(10) :1959–1968.

Cutter, L. A. (1966). Flow and turbulence in a stirred tank. *AIChE Journal*, 12(1) :35–45.

Éscudie, R. and Liné, A. (2003). Experimental analysis of hydrodynamics in a radially agitated tank. *AIChE journal*, 49(3) :585–603.

FLUENT, A. (2010). Ansys-fluent inc. *Fluent 12.1.4. Lebanon, NH*.

Fox, R. O. and Stiles, H. L. (2003). *Computational models for turbulent reacting flows*, volume 419. Cambridge university press Cambridge.

Garcia-Ochoa, F. and Gomez, E. (2009). Bioreactor scale-up and oxygen transfer rate in microbial processes : an overview. *Biotechnology advances*, 27(2) :153–176.

Guha, D., Dudukovic, M., Ramachandran, P., Mehta, S., and Alvare, J. (2006). CFD-based compartmental modeling of single phase stirred-tank reactors. *AIChE journal*, 52(5) :1836–1846.

Harris, C., Roekaerts, D., Rosendal, F., Buitendijk, F., Daskopoulos, P., Vreenegoor, A., and Wang, H. (1996). Computational fluid dynamics for chemical reactor engineering. *Chemical Engineering Science*, 51(10) :1569–1594.

Joshi, J. B. and Ranade, V. V. (2003). Computational fluid dynamics for designing process equipment : expectations, current status, and path forward. *Industrial & engineering chemistry research*, 42(6) :1115–1128.

Kresta, S. M. and Wood, P. E. (1991). Prediction of the three-dimensional turbulent flow in stirred tanks. *AIChE journal*, 37(3) :448–460.

Lee, K. and Yianneskis, M. (1994). The extent of periodicity of the flow in vessels stirred by Rushton impellers. In *AIChE Symposium series*, volume 90, pages 5–18. New York, NY : American Institute of Chemical Engineers, 1971-c2002.

Maggioris, D., Goulas, A., Alexopoulos, A., Chatzi, E., and Kiparissides, C. (1998). Use of CFD in prediction of particle size distribution in suspension polymer reactors. *Computers & chemical engineering*, 22 :S315–S322.

Maggioris, D., Goulas, A., Alexopoulos, A., Chatzi, E., and Kiparissides, C. (2000). Prediction of particle size distribution in suspension polymerization reactors : effect of turbulence nonhomogeneity. *Chemical Engineering Science*, 55(20) :4611–4627.

Mavros, P. (2001). Flow visualization in stirred vessels : A review of experimental techniques. *Chemical Engineering Research and Design*, 79(2) :113 – 127.

Micheletti, M., Baldi, S., Yeoh, S., Ducci, A., Papadakis, G., Lee, K., and Yianneskis, M. (2004). On spatial and temporal variations and estimates of energy dissipation in stirred reactors. *Chemical Engineering Research and Design*, 82(9) :1188–1198.

Murthy, B. and Joshi, J. (2008). Assessment of standard k–ε, RSM and LES turbulence models in a baffled stirred vessel agitated by various impeller designs. *Chemical Engineering Science*, 63(22) :5468–5495.

Ng, K. and Yianneskis, M. (2000). Observations on the distribution of energy dissipation in stirred vessels. *Chemical Engineering Research and Design*, 78(3) :334–341.

Paul, E. L., Atiemo-Obeng, V., and Kresta, S. M. (2004). *Handbook of industrial mixing : science and practice*. John Wiley & Sons.

Podgórska, W. and Bałdyga, J. (2001). Scale-up effects on the drop size distribution of liquid–liquid dispersions in agitated vessels. *Chemical Engineering Science*, 56(3) :741–746.

Pohn, J., Heniche, M., Fradette, L., Cunningham, M., and McKenna, T. (2011). Computational analysis of mixing and scale-up in emulsion polymerization reactors. In *Macromolecular Symposia*, volume 302, pages 133–141. Wiley Online Library.

Ranade, V. V. (2002). *Computational flow modeling for chemical reactor engineering*. Process systems engineering series. Academic Press, San Diego.

Rutherford, K., Mahmoudi, S., Lee, K., and Yianneskis, M. (1996). The influence of Rushton impeller blade and disk thickness on the mixing characteristics of stirred vessels. *Chemical engineering research & design*, 74(3) :369–378.

Sommerfeld, M. and Decker, S. (2004). State of the art and future trends in CFD simulation of stirred vessel hydrodynamics. *Chemical engineering & technology*, 27(3) :215–224.

Vakili, M. and Esfahany, M. N. (2009). CFD analysis of turbulence in a baffled stirred tank, a three-compartment model. *Chemical Engineering Science*, 64(2) :351–362.

Wernersson, E. S. and Trägårdh, C. (1999). Turbulence characteristics in turbine-agitated tanks of different sizes and geometries. *Chemical Engineering Journal*, 72(2) :97–107.

Wu, H. and Patterson, G. (1989). Laser-Doppler measurements of turbulent-flow parameters in a stirred mixer. *Chemical Engineering Science*, 44(10) :2207–2221.

Zhou, G. and Kresta, S. M. (1996). Distribution of energy between convective and turbulent flow for three frequently used impellers. *Chemical engineering research & design*, 74(3) :379–389.

CHAPTER 5

ARTICLE 2 : INVESTIGATION OF TURBULENT FLUID FLOWS IN STIRRED TANKS USING A NON-INTRUSIVE PARTICLE TRACKING TECHNIQUE

Hamed Bashiri, Ebrahim Alizadeh, François Bertrand, Jamal Chaouki

Department of Chemical Engineering, École Polytechnique de Montréal, C.P. 6079 succ. Centre-Ville, Montréal, Québec, Canada, H3C 3A7

(Submitted to *Chemical Engineering Science*.)

Presentation of the article : A comprehensive analysis of fully turbulent fluid flows in a laboratory-scale stirred tank reactor equipped with a radial or an axial flow impeller using radioactive particle tracking (RPT) will be presented.

Abstract : Fully turbulent fluid flows in a laboratory-scale stirred tank (ST) equipped with a radial flow impeller (Rushton turbine ; RT) or an axial flow impeller (pitched blade turbine ; PBT) were analyzed using the radioactive particle tracking (RPT) technique. The present study covered the Eulerian and Lagrangian descriptions of fluid motions. The RPT measurement of the turbulent flow field in a tank agitated by an RT was benchmarked with CFD simulations of RANS-based turbulence models and laser-based measurements. There was good agreement between all the methods for the measured and predicted 3D mean velocity profiles at all locations in the ST. The RPT technique was used to measure the turbulent flow field in a tank agitated by a PBT for the first time. The behavior of the wall jet was investigated. There was close agreement between our results and those of previous studies for both systems. Lagrangian mixing measurements showed that particle trajectories can be used to generate Poincaré maps, which in turn can be used as a tool to visualize the 3D flow structure inside mixing systems. Two mixing indices, one based on the concept of stochastic independence and the other on the statistical concept of memory loss in mixing processes, were used to measure mixing times using RPT results. The present study showed that the RPT technique holds great promise for investigating turbulent flows and the mixing characteristics of STs, and for assessing the adequacy of numerical models.

Keyword : mixing, stirred tank, radioactive particle tracking (RPT), CFD, turbulent flow

5.1 Introduction

Stirred tanks (STs) are widely used for polymerization, oxidation, chlorination, fermentation, waste water treatment, cyanidation and other processes due to their good mixing performance, which ensures efficient contact between phases and a higher mass transfer rate. It has been estimated that approximately 50% of all chemical production processes worldwide by value, worth some US $1,290 billion a year, use STs (Butcher and Eagles, 2002).

Despite being used as a basic unit operation by most chemical processing industries, ST designs are mainly based on global correlations involving for instance the power number, flow number, and Froude number. This can result in a number of uncertainties as such designs cannot provide detailed information on the local flow phenomena that govern the desired process result. Designs based on global correlations cannot take into account the non-uniform and complex 3D flow in an ST. An alternate design approach is thus required to ensure sustainable development, by reducing negative environmental impacts and increasing the process profitability (improving the yield). Such an alternative approach should also provide a better understanding of the fluid dynamics in STs, including information about internal flow structures (Sommerfeld and Decker, 2004).

The availability of increasingly powerful computers has transformed computational fluid dynamics (CFD) into a practical tool for understanding fluid dynamics and, as a result, designing efficient processes (Joshi and Ranade, 2003; Norton and Sun, 2008; Sommerfeld and Decker, 2004). The accuracy of CFD simulations is also improving due to the availability of better physical models, including evolved LES models for the prediction of turbulent flows. However, experimental validation is still required, even for the most accurate CFD models (Boyer et al., 2002). CFD analyses can also complement experimental work by reducing the cost and effort of acquiring experimental results.

CFD is increasingly being used to simulate STs. However, quantitative assessments of the accuracy of CFD analyses repose mainly on a comparison of the flows close to the impeller (Bashiri et al., 2014; Coroneo et al., 2011; Hartmann et al., 2004; Ng et al., 1998), due to

limitations in acquiring whole tank experimental results. Turbulent flow fields in baffled STs are complex and chaotic, and exhibit 3D structures. The velocity fluctuations caused by the periodic passage of the impeller blades make the turbulent structure of the flow fields even more complex, especially in the region close to the impeller. These complexities make flow measurements in STs time consuming and labor intensive.

Many techniques have been developed in recent years to measure fluid flows in different process tanks and devices, including STs (Boyer et al., 2002; Chaouki et al., 1997; Mavros, 2001). Fluid flow measurement techniques can be divided into two general categories : invasive and non-invasive. The pitot tube (Wolf and Manning, 1966) and hot-wire anemometry (Cooper and Wolf, 1968) invasive fluid flow measurement techniques are inefficient due to the intrusive nature of the probe, which may cause local changes in the fluid flow. Laser doppler anemometry (LDA) (Aubin et al., 2001; Ducci and Yianneskis, 2005; Kresta and Wood, 1993a; Lee and Yianneskis, 1998; Murthy and Joshi, 2008; Rutherford et al., 1996a; Wu and Patterson, 1989; Zhou and Kresta, 1996) and particle image velocimetry (PIV) (Aubin et al., 2004b; Baldi and Yianneskis, 2003, 2004; Delafosse et al., 2011; Escudie and Line, 2003; Fontaine et al., 2012; Gabriele et al., 2009; Roy et al., 2010; Sharp and Adrian, 2001; Sheng et al., 2000) are laser-based non-invasive fluid flow measurement techniques that are used to study the velocities, turbulent dissipation rates, and kinetic energies in STs, especially in the vicinity of the impeller. However, their use is restricted to transparent flows and transparent tank walls, due to the inherent use of a laser. In addition, measuring the whole flow fields with these techniques is cumbersome. Furthermore, these optical techniques only provide Eulerian data, while mixing is intuitively a Lagrangian process. To determine the Lagrangian motion of a fluid parcel, post-processing, with its intrinsic uncertainties, is required (Heniche and Tanguy, 2006).

Radioactive particle tracking (RPT) and positron emission particle tracking (PEPT) are also non-invasive techniques. While PEPT has been used to study fluid flows in STs (Fishwick et al., 2005; Pianko-Oprych et al., 2009), it is limited to tanks that are small enough to be

placed in the PEPT camera. Furthermore, Chiti et al. (2011) have reported that the time resolution of the PEPT technique is relatively low (typically 40-60 ms), meaning that the radial velocities measured in the vicinity of the RT impeller are often significantly lower than the values reported in the literature by less than 50%. PEPT is also not very efficient for reconstructing tracer particle positions close to the edge of the system (Guida et al., 2012).

The RPT technique tracks the motion of a single γ-ray-emitting particle using several sodium iodide (NaI) scintillation detectors strategically placed around the system. This method was initially used to study single-phase flows in an ST equipped with an RT (Rammohan et al., 2001a,b). Despite using a relatively large tracer ($\sim$ 2.4 mm) in those studies, they showed the RPT measurement technique can accurately measure the velocity of the flow in STs. While the results indicated that RPT is a promising approach for investigating fluid flows in STs, the authors used a not so high impeller Reynolds number (Re = 12,345) for which the fluid flow could barely be considered to be fully turbulent ($Re \geq 20,000$) (Machado et al., 2013). In addition, comparisons of velocity profiles with previously published results were limited to the region close to the impeller. RPT has also been used to study gas/liquid (Khopkar et al., 2005) and solid/liquid (Guha et al., 2007) flows in RT mixing systems.

Measuring the quality of mixing in STs is just as important as investigating flow patterns. Process industries are always on the lookout for ways to improve mixing operations, either by switching to more efficient impellers or by fine-tuning operating conditions. Therefore, quantitative approaches are needed in order to measure the mixing characteristics of impellers (Nienow, 1997). Mixedness can be assessed by measuring the concentration of a colored (Cabaret et al., 2007; Melton et al., 2002), fluorescence (Distelhoff et al., 1997; Guillard et al., 2000) or conductivity (Rewatkar and Joshi, 1991; Zhang et al., 2009) tracer at various locations in the tank, to determine how fast the variance of the tracer concentrations decreases to an expected value over time. Since some of these methods use probes, their main intuitive drawback is the alteration in fluid flow. While other methods do not use probes, they are of limited use in opaque systems (colorimetric methods, for example). However, techniques

such as RPT, which are based on particle trajectories, do not have these limitations.

We have used RPT extensively to characterize solid flows in fluidized beds (Bashiri et al., 2010; Kiared et al., 1999; Mostoufi and Chaouki, 2001, 2004), spouted beds (Cassanello et al., 1999; Djeridane et al., 1998; Roy et al., 1994), cylindrical tumblers (Alizadeh et al., 2013) and V-blenders (Doucet et al., 2008a). In the present study, we used RPT to study the hydrodynamics of an ST in the fully turbulent flow regime using axial (pitched blade turbine (PBT)) and radial (Rushtone turbine (RT)) impellers. Since these impellers are commonly used in process industries, there is an abundance of published data that can be compared with our experimental results.

Our goal was to assess the capacity of RPT to measure the Lagrangian and Eulerian turbulent fluid flow features of an ST. In Section 5.2, we describe the experimental set-up design and configuration, revisit the basic principles of the RPT technique, and introduce the adopted CFD modeling approach for simulations of mixing systems. In the first part of Section 5.3, we compare the Eulerian fluid flow results of the RPT experiment to those of Murthy and Joshi (2008), which were obtained by LDA and CFD simulations for an RT mixing system. The comparison covers the bulk of the tank. To our knowledge, this is the first time that such a comprehensive comparison has been performed for a turbulent fluid mixing system using the RPT technique. We then present the 3D flow fields generated in the ST by the PBT impeller using RPT. We also describe the ability of RPT to reveal the self-similar behavior of the wall jets generated by the PBT and RT impellers. In the second part of Section 5.3, we present the results of our Lagrangian study of turbulent fluid flows using Poincaré maps as well as the distribution of velocity magnitudes inside the tank. Lastly, we provide a detailed discussion of the results of mixing times obtained with the RPT technique using two mixing indices, one of which is novel.

5.2 Material and methods

5.2.1 Experimental protocol

All experiments were carried out in a flat-base, open-top 6.3-L cylindrical transparent polycarbonate tank of standard design. Four equally spaced ~ 0.1T wide baffles were mounted on the tank wall (T is the tank diameter). The tank was agitated using a 6-bladed RT or a 45° four-bladed PBT (D=T/3 is the impeller diameter). A detailed description of the experiments is presented in Table 5.1.

Table 5.1: Summary of experiments.

Case	Impeller Type	Clearance (C)
1	RT	$1.00D$
2	RT	$0.75D$
3	RT	$1.35D$
4	PBT	$1.00D$
5	PBT	$0.75D$
6	PBT	$1.35D$

Impeller off-bottom clearances (C) were 1.00D for cases 1 and 4, 0.75D for cases 2 and 5, and 1.35D for cases 3 and 6. All the experiments were conducted in the fully turbulent regime ($Re = 2.2 \times 10^4$). The shaft was driven by a 0.2 kW DC motor and could be moved up and down to manually change the impeller off-bottom clearance. The motor speed was automatically controlled. The tank was filled with water as a working fluid up to a height equal to the tank diameter (H=T).

RPT was used as a non-intrusive experimental velocimetry technique (Lin et al., 1985) to investigate the hydrodynamics of the mixing systems. Nine NaI scintillation detectors were strategically placed around the system to track the motion of a tracer particle. A mixture of a tiny amount of scandium oxide powder and epoxy resin was used as a tracer particle ($\sim$ 1 mm in diameter) to follow the movement of the fluid. The tracer particle was activated to 50 μCi in the SLOWPOKE nuclear reactor of École Polytechnique de Montréal. To maximize the accuracy of the RPT results, the detectors were distributed around the mixing system to

meet three conditions : (1) cover the entire volume of the system, (2) be as close as possible to the system without being saturated (their saturation lengths were measured beforehand), and (3) minimize the probability of γ-rays travelling through another detector before reaching a specific detector, to avoid affecting the quality of the recorded signals. It should be noted that a sophisticated technique was recently developed by our research group to optimize detector positioning using a mesh adaptive direct search (MADS) algorithm (Dubé et al., 2014). A high-speed data acquisition system was used to count the number of γ-rays detected by each detector with a 200-Hz data acquisition frequency. Details on the calibration of the system, the inverse reconstruction strategy for determining the position of the tracer particle, and the errors associated with the measurement technique are provided in previous publications (Chaouki et al., 1997; Doucet et al., 2008a).

The trajectory data of the tracer particle and its velocities were converted from the original Cartesian coordinates to cylindrical coordinates because radial profiles of the mean 3D velocities with such coordinates are commonly used in the literature. An in-house code was written to convert the Lagrangian velocities of the particle trajectories to Eulerian flow fields. The code uses a 3D grid consisting of $40\times72\times80$ control volumes that discretizes the system in the r, θ, and z directions, respectively. The grid in the r direction was not uniform in order to generate cells with the same volumes. The reason for using this mesh is explained in Section 5.3. The velocities of the tracer particle in the three directions were averaged for each cell using all of its visits in each of them.

5.2.2 Numerical model

3D CFD simulations were conducted for the RT mixing system. The geometries of the tank and the grids were generated using the commercial software package Gambit 2.4. The computational domain consisted of $\sim$ 400 k structured hexahedral cells. The use of this number of cells for simulating single-phase turbulent flows in STs was extensively examined and explained in our previous study (Bashiri et al., 2014) and is consistent with previous

findings (Deglon and Meyer, 2006). We showed that using more than 350 k cells guarantees the adequacy of the prediction of mean velocities by CFD.

The impeller blades and baffles were assumed to have a zero thickness in order to obtain a better quality mesh. Rutherford et al. (1996b) showed that changes in blade thickness may affect the mean velocity close to the tip of the impeller, but have no significant effect in regions far from it. The mesh was refined close to the impeller and the baffles, taking into account the fact that the radial flow generated by the RT impinges on the tank wall, to better resolve the flow fields in these regions. The Reynolds average Navier-Stokes (RANS) equations for the standard and RNG k-ε turbulence models were solved numerically using the finite volume method with the commercial CFD code ANSYS Fluent 13.1. While LES and DNS can provide much more sophisticated information on anisotropic 3D flows, they are computationally intensive. In the present study, the simulations were conducted using the steady-state multiple reference frames (MRF) approach, where the grid was divided into two reference frames to take the stationary and rotating parts into account. Aubin et al. (2004a) showed that, for steady-state simulations of fluid flows in STs, this technique gives results that are similar to the much more computationally intensive transient sliding mesh technique.

The SIMPLE algorithm was used to couple the continuity and momentum equations. Second-order upwind schemes for the momentum and the k and ε equations were used. A no-slip boundary condition was imposed at the solid surfaces. In addition, the standard wall function was used to link the viscosity-dominated region between the wall and the fully turbulent region. The values of y^+ on the solid walls were checked carefully to verify the adequacy of using the wall function. A zero shear stress was imposed at the liquid surface and was used as a free surface boundary condition. The turbulent fluid flow in the tank was governed by the following continuity and momentum equations :

$$\frac{\partial \langle u_i \rangle}{\partial x_i} = 0 \tag{5.1}$$

$$\rho\langle u_j\rangle\frac{\partial\langle u_i\rangle}{\partial x_j} = -\frac{\partial\langle P\rangle}{\partial x_i} + \frac{\partial}{\partial x_j}(\mu(\frac{\partial\langle u_i\rangle}{\partial x_j} + \frac{\partial\langle u_j\rangle}{\partial x_i}) - \rho\langle u_i' u_j'\rangle) + F_i \tag{5.2}$$

where F_i represents the centrifugal and Coriolis forces applied in the rotating reference frame. Based on the Boussinesq hypothesis, the Reynolds stress terms can be expressed as follows :

$$\rho\langle u_i' u_j'\rangle = -\mu_t(\frac{\partial\langle u_i\rangle}{\partial x_j} + \frac{\partial\langle u_j\rangle}{\partial x_i}) + \frac{2}{3}k\rho\delta_{ij} \tag{5.3}$$

Standard and RNG k-ε models were used to simulate turbulent fluid flows in STs. In these models, the turbulent viscosity (μ_t) is computed by combining the values of the turbulent kinetic energy (k) and the turbulent kinetic energy dissipation rate (ε) :

$$\mu_t = C_\mu\rho\frac{k^2}{\varepsilon} \tag{5.4}$$

This gives rise to two transport equations for k and ε. The inherent constants in these models were set to the values commonly used in the literature (Fluent, 2010). In the simulations, convergence was achieved when the residuals for the continuity, velocities, kinetic energy, and energy dissipation rate all became less than 10^{-4}. In addition, the predicted torques of the shaft and impeller were monitored to ensure that they were stable.

5.3 Results and discussion

The Eulerian measurements of fluid flows were studied by comparing the 3D velocity profiles obtained by RPT to the LDA results of Murthy and Joshi (2008) and the CFD predictions by the two turbulent models described above, in the case of the RT mixing system. The comparisons covered the regions of the tank close to and far away from the impeller. We also measured the PBT velocity profiles at the same spatial locations. To our knowledge, this is the first time that the flow patterns of an axial flow impeller have been measured using the RPT technique. We in particular, studied the ability of RPT to investigate the self-similar

behavior of wall jets. We also discuss the Lagrangian description of fluid dynamics, including Poincaré maps, and the distribution of Lagrangian velocity magnitudes inside the tank for both mixing systems. Lastly, we describe in detail how we measured mixing times using the RPT technique, and discuss the efficiency of the RT and PBT impellers.

5.3.1 Eulerian measurements of turbulent fluid flows

We first performed a mesh dependence analysis using three different grids to determine the adequate number of cells required to compute average velocities using trajectory data obtained by the RPT technique. Details of these grids are presented in Table 5.2, where N_r, N_θ, and N_z refer to the number of cells in the r, θ, and z directions, respectively. We examined the radial profiles of mean velocities at different heights, and present the radial profile of the axial dimensionless velocity at z/H=0.5 for case 1 in Table 5.1. As can be seen in Figure 5.1, the results of meshes II and III (Table 5.2) were similar but slightly different from the results of mesh I. We observed the same trends with the other velocity profiles. As such, we used mesh III in the present study.

Table 5.2: Details of the mesh analysis for the RPT technique.

	N_r	N_θ	N_z
Mesh I	10	36	20
Mesh II	20	36	40
Mesh III	40	72	80

Benchmarking RPT results with CFD and LDA data for the radial flow impeller (RT)

The mean flow pattern and the turbulent characteristics of the flow are both important for the design of a mixing system. The flow pattern depends on a number of factors : impeller geometry, presence and number of baffles, impeller off-bottom clearance, and pumping

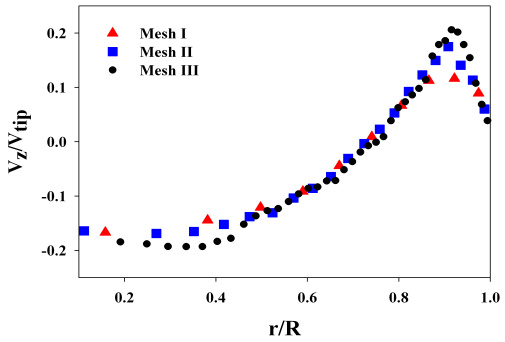

Figure 5.1: Effect of mesh size on the radial profile of the axial dimensionless velocity at z/H=0.5 for the RT impeller (case 1).

direction. In this subsection, the turbulent fluid flow measurements recorded using RPT in the case of the RT mixing system (case 1 of Table 5.1) are compared to the results obtained from our CFD simulations and LDA data reported by Murthy and Joshi (2008) for a similar geometry (Figures 5.2-5.4). The velocities were normalized to the impeller tip speed (V_{tip}) for comparison purposes.

The radial profiles of the mean axial velocities at different heights are shown in Figures 5.2a-h. In general, the RPT technique captured the radial profiles of the mean axial velocities both qualitatively and quantitatively. One can also notice that the predictions of axial velocities for both turbulent models are very similar. As can be seen in Figures 5.2a-h, the wall jet, which is predicted by both turbulent models, had a tendency to attach to the wall of the tank, possibly due to the Coandă effect (Panitz and Wasan, 1972). This effect can also be seen in the study by Brucato et al. (1998), where the axial velocity profiles for an RT impeller system were compared to experimental data. The difference between the radial profiles of mean axial velocities determined by the RPT, LDA and CFD techniques became significant for the location axially near the bottom and radially near the wall of the tank (Figure 5.2b). At this location, the flow structure and, as such, the mean velocity may be affected by the presence of bolts and parts that fix the baffles to the wall of the tank. Bolts used to fix tank internals can affect the mean flow and vortex structure (Rutherford et al.,

1996b).

Figures 5.3a-h show the radial profiles of the mean radial velocities in different axial locations of the tank. As can be seen in Figures 5.3c-e, the radial velocities are relatively high in the immediate impeller discharge zone (Figure 5.3d) as well as in the regions above (Figure 5.3e) and below (Figure 5.3c) it near the wall. The surrounding fluid is entrained by the discharge flow of the impeller in these regions. In particular, it can be seen that the mean radial velocity profile is not symmetrical around the plane where the disc of the impeller is located (Figure 5.3d). More specifically, the mean radial velocity increased more in the plane above this location (Figure 5.3e) than in the plane below it (Figure 5.3c) as the wall is approached. This flow structure formed due to the non-symmetrical axial location of the impeller within the tank and the free surface at the top of it. The radial velocities became quiescent in the rest of the tank, except at the bottom (Figure 5.3a), where the downward flow of the axial wall jet became radial toward the center of the tank. It should be noted that the radial velocity at the impeller plane close to the impeller tip (Figure 5.3d) measured by the RPT technique was lower than the LDA value ($\sim 30\%$). However, the difference was less marked at locations close to the wall of the tank ($< 5\%$). Figure 5.3d shows that the RNG model predicted the same maximum radial velocity at the plane of the impeller disc as that measured by the LDA. However, the standard turbulent model under-predicted this value by $\sim 10\%$. Both of these models over-predicted the radial velocity values compared to those measured by the LDA and RPT techniques away from the impeller towards the wall of the tank.

The radial profiles of the mean tangential velocities for different axial locations are presented in Figures 5.4a-h. In general, the tangential velocity profiles measured by the RPT technique are in good agreement with the LDA results, except for locations below the impeller plane close to the center of the tank (Figures 5.4b and c). The RPT results showed the swirling flow structure that forms just below the impeller (Figure 5.4c) and that dissipates progressively toward the bottom of the tank (Figures 5.4a and b). This flow structure has

been also reported in previous studies (Kemoun et al., 1998; Rammohan et al., 2001b). While this 3D flow structure was captured to some extent by the LDA technique, as can be seen by the shape of the radial profiles of the mean tangential velocities measured by this technique (Figures 5.4b and c), it was not captured by the turbulent models. Note that the characteristics of such a swirling structure can provide valuable information on solid suspension and gas dispersion mechanisms in STs. As can be seen in Figure 5.4d, the mean tangential velocity was over-predicted by both turbulent models compared to values measured by the LDA and RPT techniques ($\sim$ 30-40%) at the impeller plane close to the impeller tip ($0.33 \leq r/R \leq 0.5$). It should be noted here that the mean tangential velocities obtained with the LDA and RPT techniques are in the range of those reported by Lee and Yianneskis (1998) and Yapici et al. (2008) for the RT impeller. As shown in Figures 5.4f-h, the swirling effect was lower in regions far from the impeller towards the surface of the tank.

Figures 5.2-5.4 show that the largest differences between the measured and predicted mean velocities occurred close to the impeller tip, for which there is also a significant discrepancy in the literature. The flow structure in this region is extremely complex due to the rapid acceleration of the fluid caused by steep increases in the radial and tangential velocities when the direction of flow is changed by 90° (from vertically upward and downward to horizontal).

In the work of Murthy and Joshi (2008), the position of the measurement volume for the LDA technique was fixed with respect to the baffles for the velocity measurements. This approach is called 360° ensemble averaging or time resolved data acquisition. It may have an inherent bias toward a higher mean velocity as most of the data come from the region just behind the impeller blade (Kemoun et al., 1998; Rutherford et al., 1996b). Another possibility would be to acquire data for the full range of angles behind the blade (or up to 60° in case of the RT impeller). The data would then have to be averaged to calculate the phase averaged mean. The measured velocity in the impeller region based on these averaging methods can give very different values ($\sim$ 30% difference) (Rutherford et al., 1996b).

Furthermore, when higher velocity flows pass through the measurement volume of the

LDA technique, a larger quantity of fluid containing seeding particles will be swept through it and, as such, a larger number of velocity samples will be recorded. The evaluation of the mean velocities of the flow field using arithmetic averaging thus has an inherent bias toward higher velocity values. More information on this and a bias correction procedure using a time weighting factor, can be found elsewhere (Benedict and Gould, 1999).

Discrepancies between the numerical and experimental results can be attributed to the CFD models themselves. They are all based on simplifying assumptions such as isotropic turbulent eddies, the wall function used, and a flat surface at the top.

The uncertainty in the reconstruction of tracer particle positions due to the statistical nature of the emission and counting processes has been discussed in detail by Chaouki et al. (1997) and Dubé et al. (2014). Given all the sources of uncertainty of the various methods involved here, it can be concluded from Figures 5.2-5.4 that the RPT technique is indeed adequate for the measurement of turbulent flow fields in STs.

RPT results for the axial flow impeller (PBT)

While axial flow impellers such as the PBT are widely used in process industries, investigations of flow patterns reported in the literature have mainly focused on the RT impeller. In the previous subsection, we showed that the RPT technique can provide useful information on the mean velocity profiles in RT mixing systems. The measurement of turbulent flow fields generated by the PBT impeller (case 4 of Table 5.1) using this technique is presented in this subsection.

The radial profiles of the mean axial velocities in different axial locations are shown in Figures 5.5a-h. The downward axial jet generated by the PBT reaches its maximum axial velocity in the $0.2 \leq r/R \leq 0.35$ range (Figures 5.5b and c). The axial jet died down when it reached the bottom of the tank (Figure 5.5a), being transformed into a radial jet toward the side wall of the tank. This was in good agreement with previous investigations using similar mixing systems (Kresta and Wood, 1993b; Kumaresan and Joshi, 2006; Ranade and Joshi,

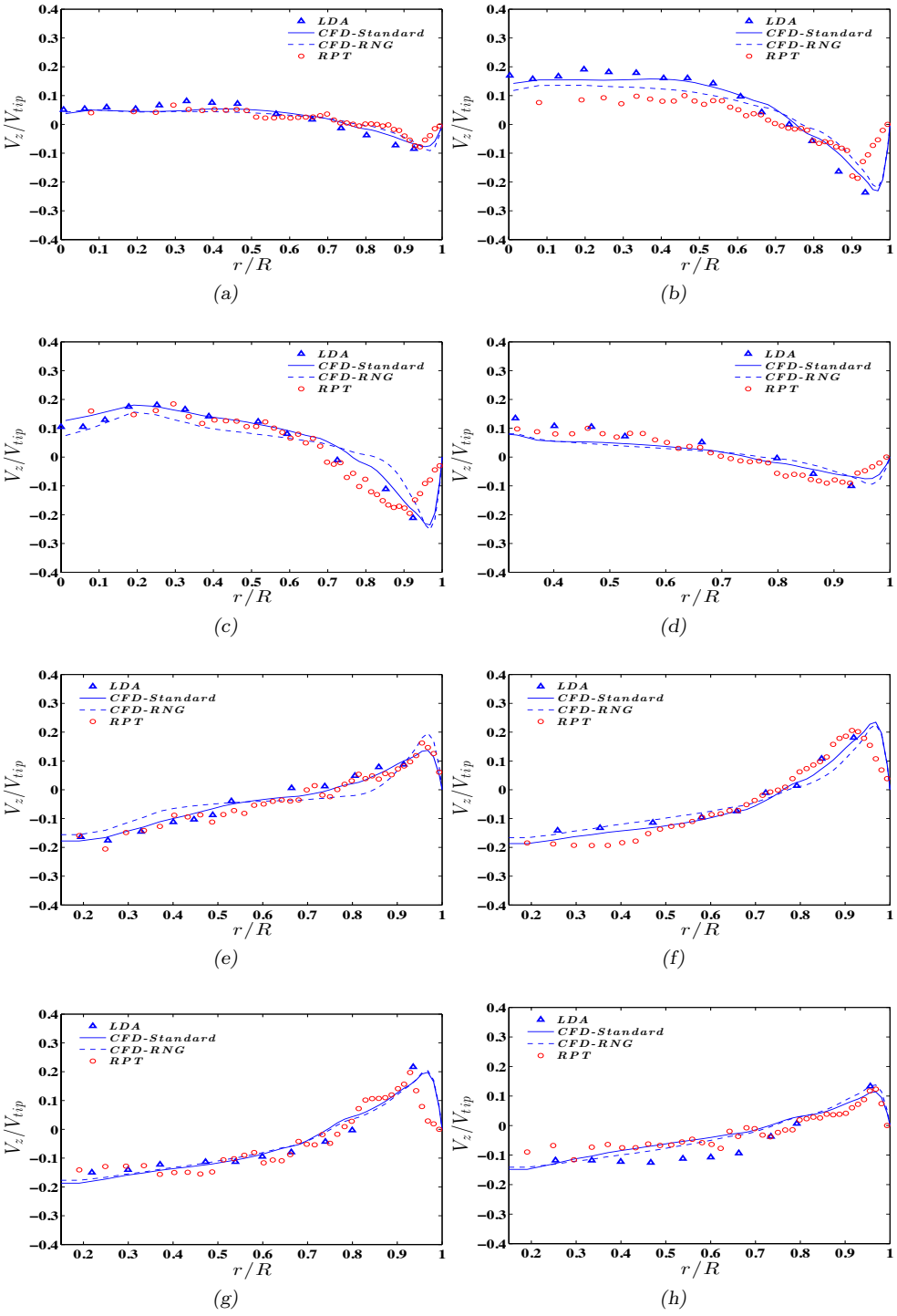

Figure 5.2: Comparison of the simulated and experimental radial profiles of the dimensionless mean axial velocity for the RT impeller (case 1) at various heights : (a) z/H = 0.033, (b) z/H = 0.147, (c) z/H = 0.273, (d) z/H = 0.33, (e) z/H = 0.39, (f) z/H = 0.51, (g) z/H = 0.63, and (h) z/H = 0.81. The LDA data was reported by Murthy and Joshi (2008).

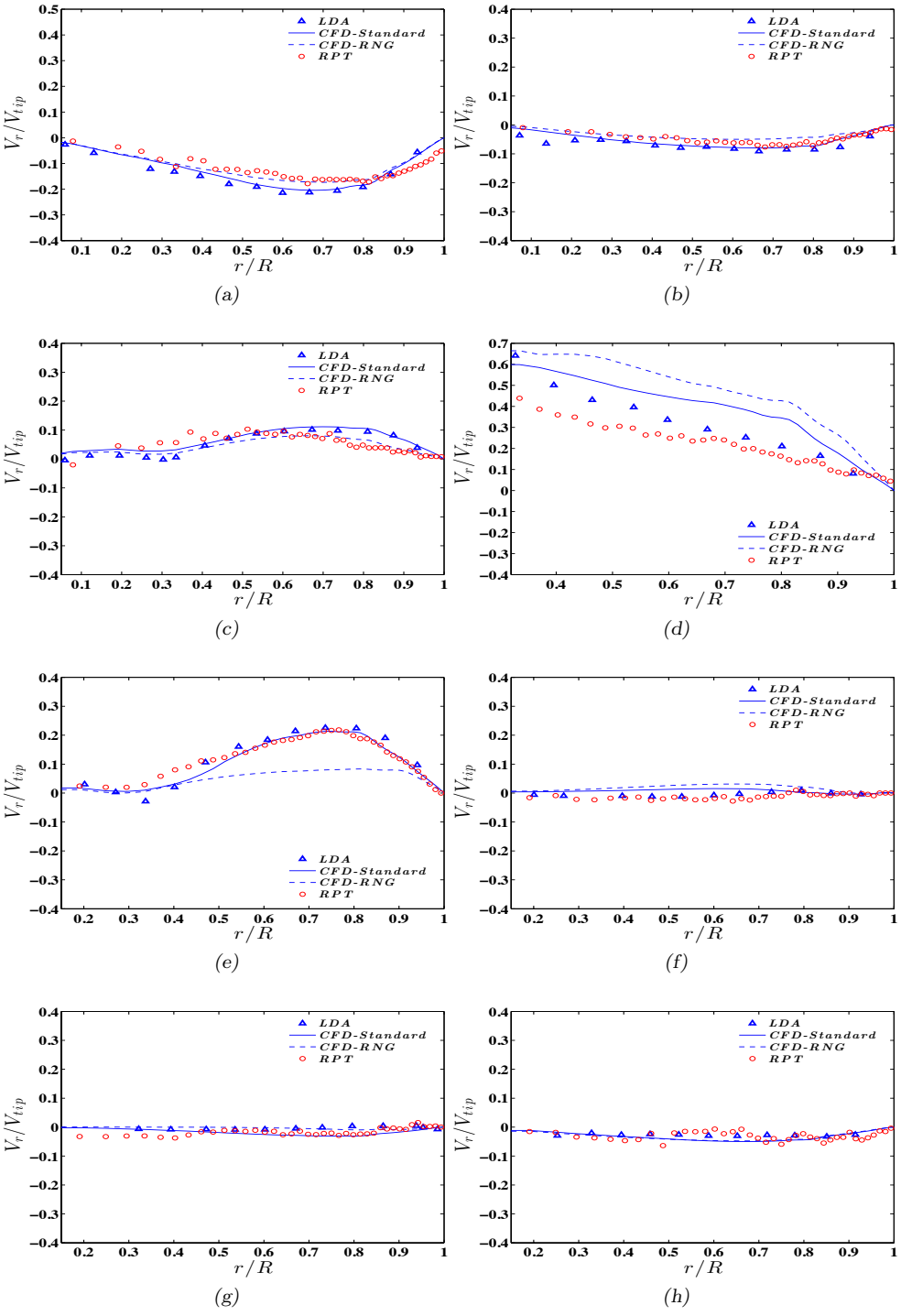

Figure 5.3: Comparison of the simulated and experimental radial profiles of the dimensionless mean radial velocity for the RT impeller (case 1) at various heights : (a) z/H = 0.033, (b) z/H = 0.147, (c) z/H = 0.273, (d) z/H = 0.33, (e) z/H = 0.39, (f) z/H = 0.51, (g) z/H = 0.63, and (h) z/H = 0.81. The LDA data was reported by Murthy and Joshi (2008).

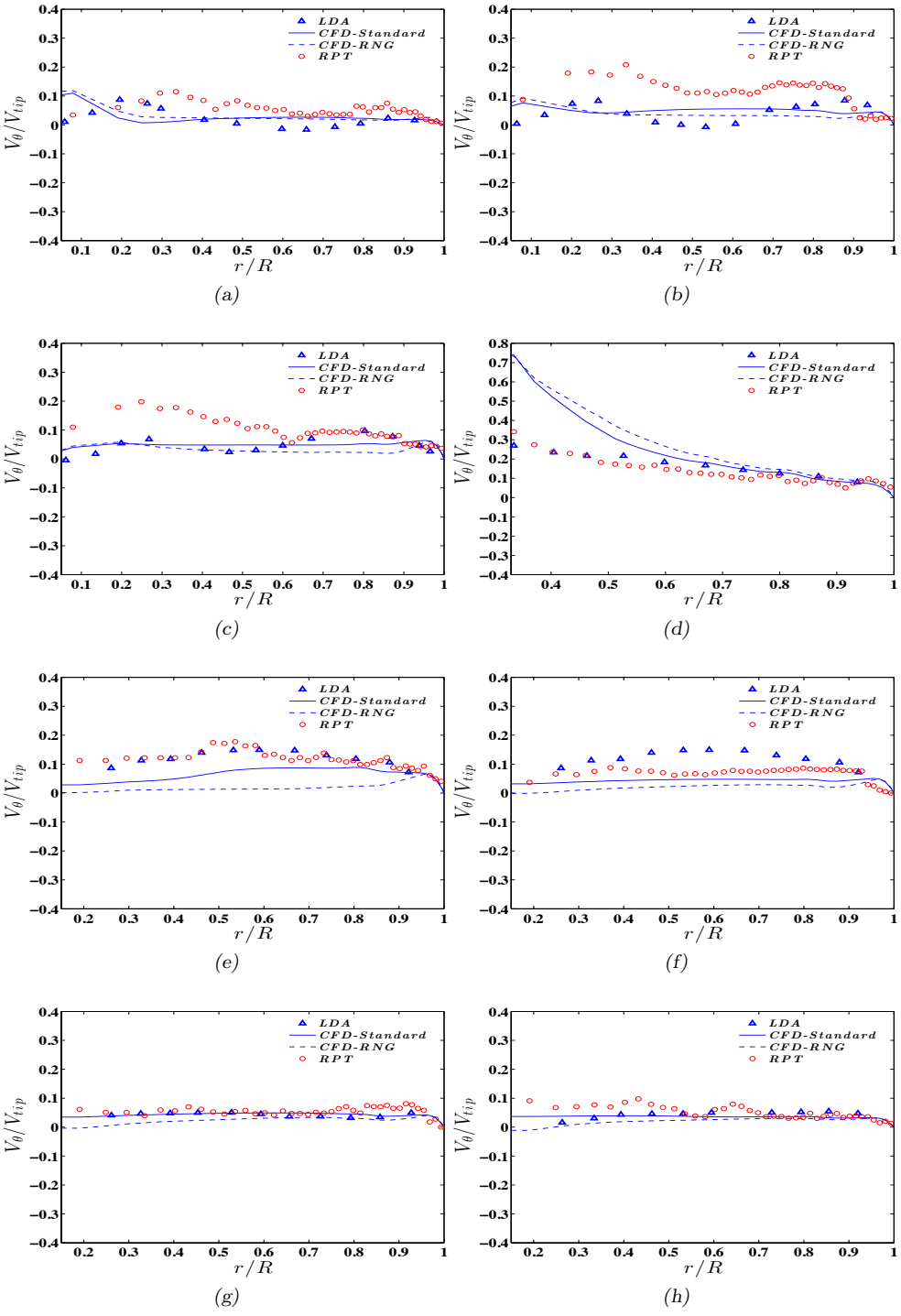

Figure 5.4: Comparison of the simulated and experimental radial profiles of the dimensionless mean tangential velocity for the RT impeller (case 1) at various heights : (a) z/H = 0.033, (b) z/H = 0.147, (c) z/H = 0.273, (d) z/H = 0.33, (e) z/H = 0.39, (f) z/H = 0.51, (g) z/H = 0.63, and (h) z/H = 0.81. The LDA data was reported by Murthy and Joshi (2008).

1989).

As can be seen in Figures 5.5a-d, the downward movement of the fluid flow reverses into an upward flow at $r/R \sim 0.7$. This can be attributed to the dead zone in the eye of the circulating loop in this system. Based on the mean axial velocity profiles in the upper part of the tank (Figures 5.5g and h), there is a clear transition to a fairly flat axial velocity profile between $z/H = 0.6$ and $z/H = 0.8$, indicating that the active volume where the main circulation occurs is in the bottom 60-80 % of the tank, which is similar to the value reported by Bittorf and Kresta (2000) ($\sim 70\%$).

Figures 5.6a-h show the radial profiles of the mean radial velocities at different heights. Generally, the radial velocities were small in whole tank, except in the region close to the bottom. In this region, as mentioned above, the axial jet generated by the turbine becomes a radial jet by changing its direction toward the tank wall (Figure 5.6a). The radial velocity decreased when z/H approached the impeller plane (Figures 5.6b-d). However, in the region just above the impeller plane (Figure 5.6e), where the fluid is sucked in by the PBT impeller, there was a higher mean radial velocity ($\sim 0.15V_{tip}$) toward the center of the tank.

The mean tangential velocity profiles at different heights are shown in Figures 5.7a-h. As with the RT impeller, the values of this velocity component are relatively high close to the impeller (Figures 5.7b-e) for radial positions $r/R \leq 0.5$. Figure 5.7a shows the small tangential velocity (~ 0.05-$0.15V_{tip}$) close to the bottom of the tank, where the base of the circulation loop changes direction from axial to radial.

Wall jet self-similarities

As discussed in the previous subsection, the discharge stream of the RT impeller impinges on the tank wall and is divided into upward and downward wall jets. On the other hand, the discharge stream of the PBT impeller impinges on the bottom of the tank close to the wall owing to its off-bottom clearance, and only generates upward wall jets. Turbulent flows in the bulk of the tank can be modeled using self-similar wall jets (Bittorf and Kresta, 2001;

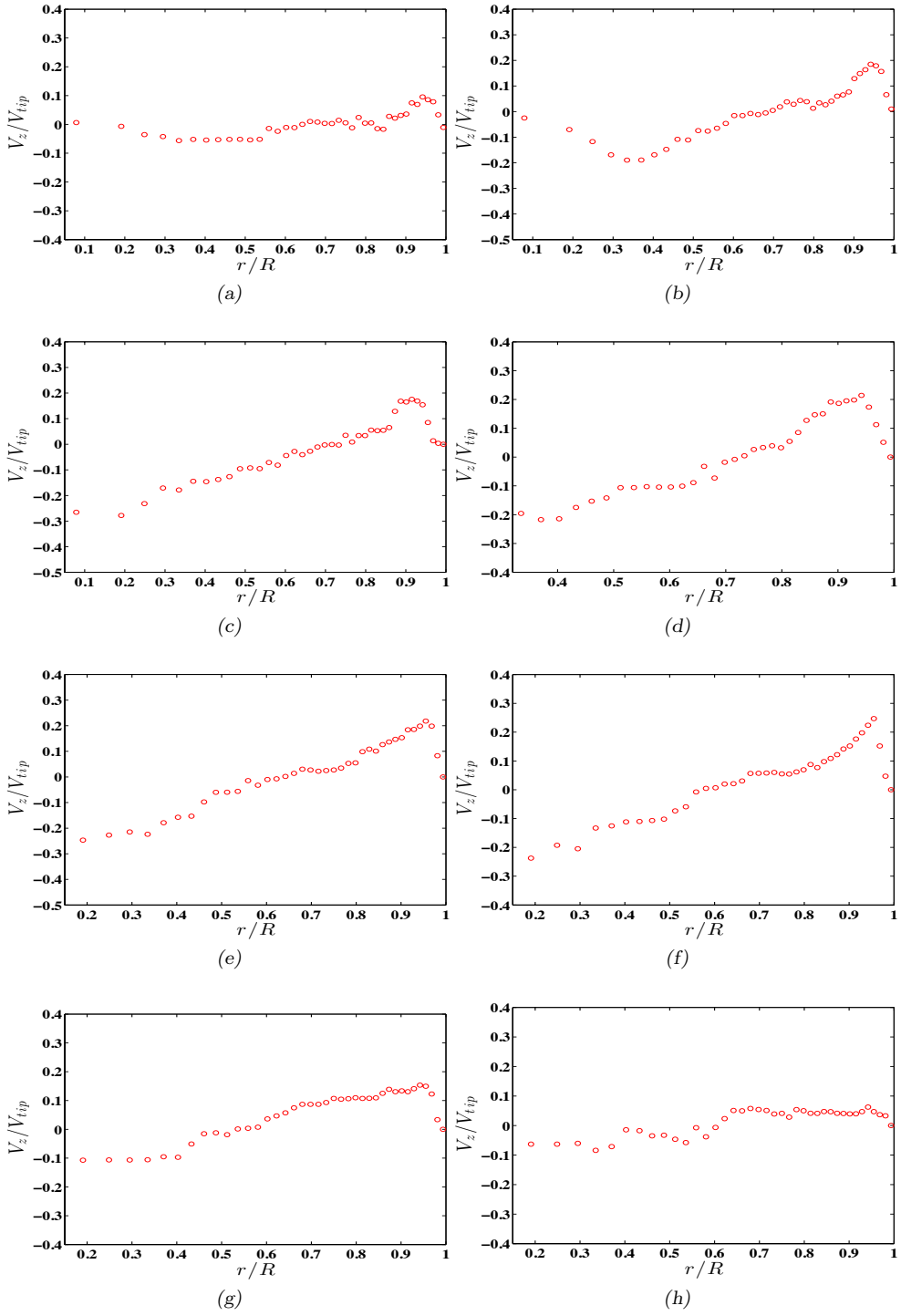

Figure 5.5: Experimental radial profiles of the dimensionless mean axial velocity for the PBT impeller (case 4) at various heights : (a) z/H = 0.033, (b) z/H = 0.147, (c) z/H = 0.273, (d) z/H = 0.33, (e) z/H = 0.39, (f) z/H = 0.51, (g) z/H = 0.63, and (h) z/H = 0.81.

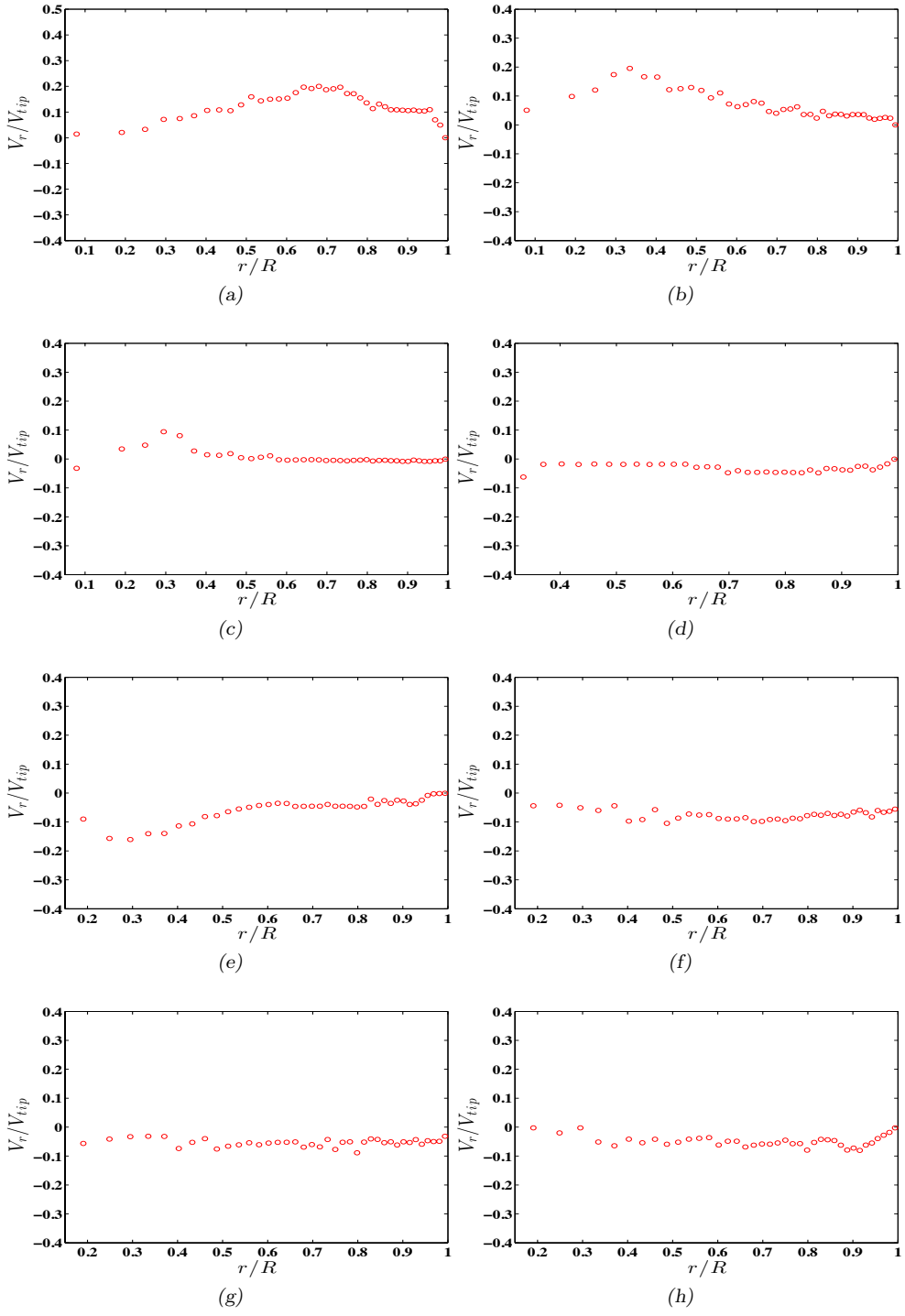

Figure 5.6: Experimental radial profiles of the dimensionless mean radial velocity for the PBT impeller (case 4) at various heights : (a) z/H = 0.033, (b) z/H = 0.147, (c) z/H = 0.273, (d) z/H = 0.33, (e) z/H = 0.39, (f) z/H = 0.51, (g) z/H = 0.63, and (h) z/H = 0.81.

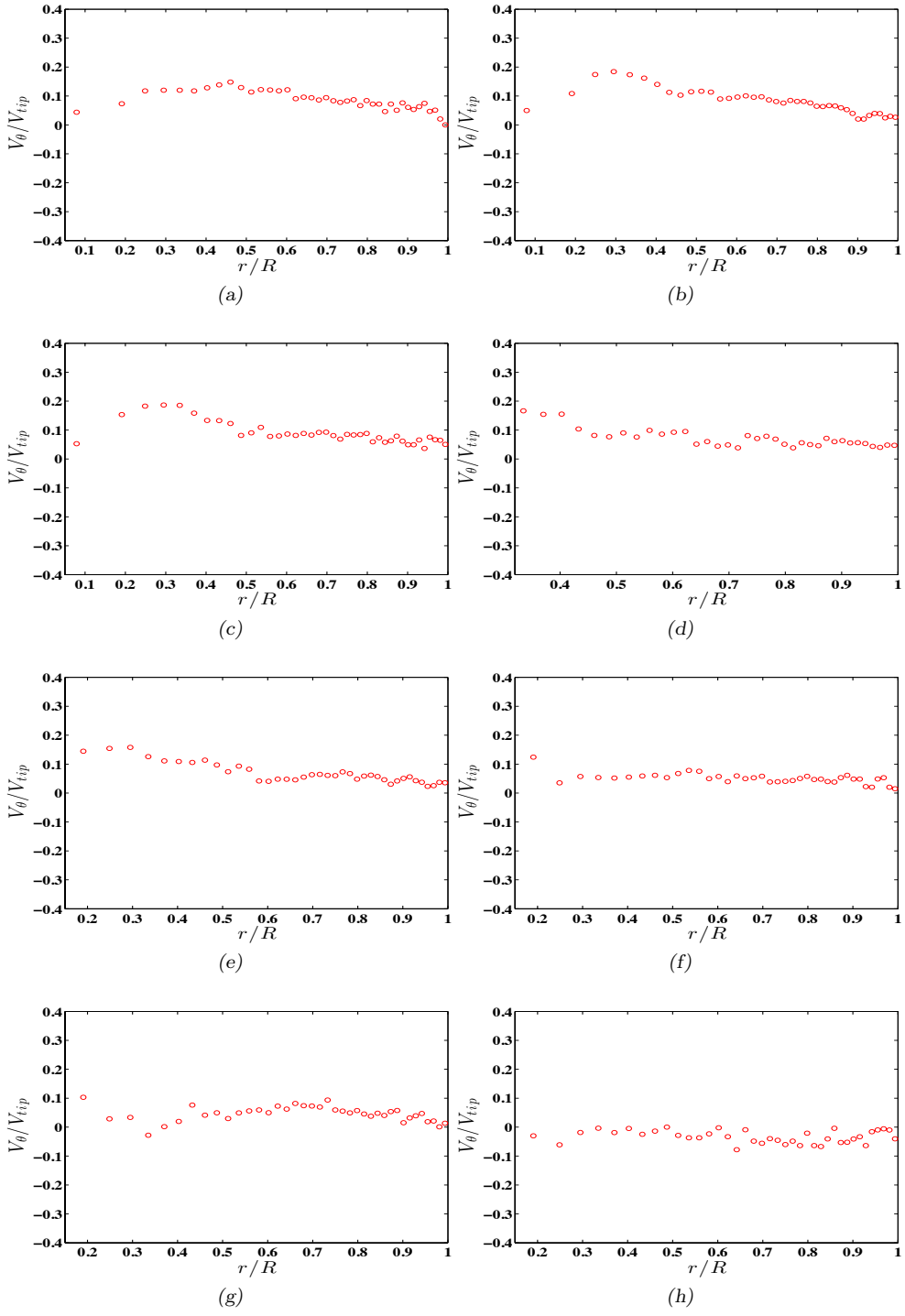

Figure 5.7: Experimental radial profiles of the dimensionless mean tangential velocity for the PBT impeller (case 4) at various heights : (a) z/H = 0.033, (b) z/H = 0.147, (c) z/H = 0.273, (d) z/H = 0.33, (e) z/H = 0.39, (f) z/H = 0.51, (g) z/H = 0.63, and (h) z/H = 0.81.

Kresta et al., 2001). These models can be used, for instance, to investigate solid concentration profiles in the bulk of the tank, determine cloud height, determine spacing between multiple impellers, understand the role of draft tubes, and optimize the feed position (Bittorf and Kresta, 2001).

One of the key features of wall jets is the similarity in their velocity profiles. More precisely, jets maintain a self-similar profile as z varies. To construct the similarity profiles, the streamwise axial velocities (V_z) measured using RPT and radial distances from the wall ($y = R - r$) should be made dimensionless, with respect to the local maximum velocity at height z (U_m) and half-width of the jet (b), respectively : $\frac{V_z}{U_m}$ and $\eta = \frac{y}{b}$. It should be noted that the half-width of the jet corresponds to the radial distance from the wall where $\frac{V_z}{U_m} = \frac{1}{2}$. Kresta et al. (2001) developed a model for similarity profiles using the following general form :

$$\frac{V_z}{U_m} = 1 - \psi tanh^2 \left[\zeta \left(\eta - 0.15\right)\right] \tag{5.5}$$

where ψ and ζ are constants in this model. The proposed values for these constants in the literature, which are based on experimental measurements, are summarized in Table 5.3 for the RT and PBT impellers (Bhattacharya and Kresta, 2002; Kresta et al., 2001). The ability of the RPT technique to capture self-similarity profiles can be assessed for both types of impeller (RT and PBT) by comparison with the proposed model.

Table 5.3: Constants for the wall jet similarity model (Bhattacharya and Kresta, 2002; Kresta et al., 2001).

Impeller type	**Constants**	
	ψ	ζ
Radial flow	1.75	0.70
Axial flow	1.58	0.78

To investigate the self-similarity of the wall jets, the impeller was located at height 0.75D (cases 2 and 5 in Table 5.1), and 1.35D (cases 3 and 6 in Table 5.1). The axial velocities were

measured by RPT at various axial locations. These locations were dependent on the impeller off-bottom clearance : $z/T = 0.1$, 0.2, and 0.3 for the low clearance cases and $z/T = -0.1$, -0.2, and -0.3 for the high clearance cases, where here $z = 0$ is the impeller plane.

Figures 5.8 and 5.9 show the similarities of the dimensionless axial velocity profiles for the RT and PBT impellers, respectively. There is very good agreement between the RPT measurements and the predictions of the semi-empirical model (equation (5.5)) for all locations in the case of the RT impeller (Figure 5.8), and for locations close to the tank wall ($\eta < 2$) of the PBT impeller. Indeed, in the latter case, the agreement in similarities starts to break down at locations far from the wall due to recirculation generated by the impeller. As can be seen in Figures 5.8 and 5.9, the dimensionless velocity is equal to approximately ± 0.5 at $\eta = 1$ and changes its sign when the η values are between 1 and 2, in all cases. Overall, these results are another indication that the RPT technique can be used to study the main features of turbulent flows in STs.

5.3.2 Lagrangian measurements of turbulent fluid flow

Eulerian-based measurements of fluid flow in a tank cannot directly provide information on mixing, which is intrinsically a Lagrangian process. Lagrangian tracking of a tracer in

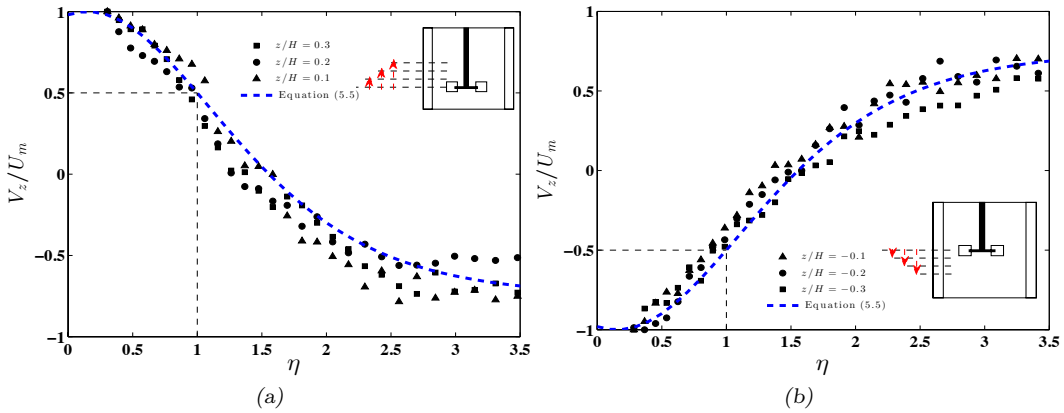

Figure 5.8: Dimensionless velocity profiles for the RT impeller at (a) C/D = 0.75 (case 2) and (b) C/D = 1.35 (case 3).

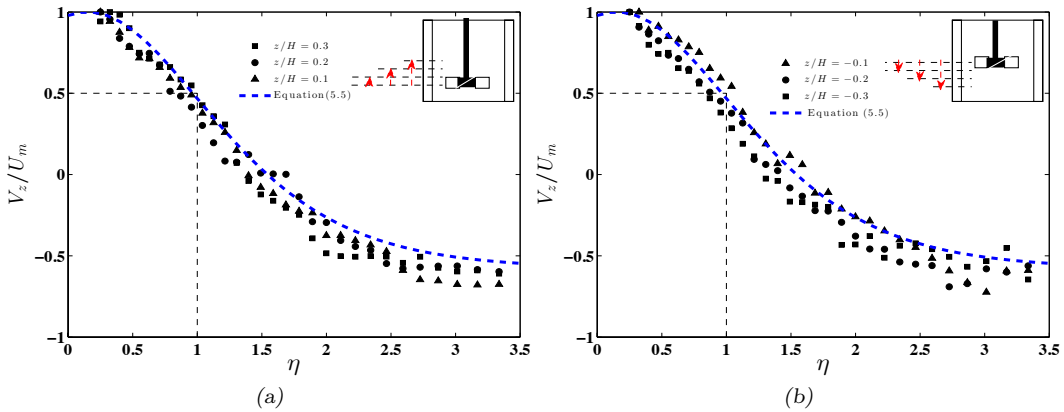

Figure 5.9: Dimensionless velocity profiles for the PBT impeller at (a) C/D = 0.75 (case 5) and (b) C/D = 1.35 (case 6).

the fluid provides information that can be used to visualize the flow structure and gain insight into its characteristics. In this subsection, the flow structures generated by the RT and PBT impellers are illustrated using RPT data and Poincaré maps. The Lagrangian velocity distributions in the ST and the measurements of mixing times using these RPT data are also described.

Poincaré maps for the RT and PBT impellers

Poincaré maps or sections can be used to study the behavior of dynamical systems. They consist of presenting an n-dimensional trajectory in an $(n-1)$-dimensional space in which the dynamical characteristics are maintained, which makes it easier to analyze. The use of dynamical system theory in fluid mechanics, especially in the context of laminar mixing, was first introduced by Aref (1984) and was later used by Kusch and Ottino (1992) to study chaotic mixing in the laminar flow regime of a 3D system. For a 3D Lagrangian particle trajectory, the occurrence of a tracer particle on the predefined 2D plane in the mixing system is recorded each time it passes through the plane. These plots are very useful for depicting the mixing behavior and flow structure of mixing systems.

In a Poincaré map, regions of chaotic motion appear as clouds of points that eventually

fill the entire domain. Regions of regular motion, also known as islands or isolated regions, appear either as empty regions (if no particles were initially placed in them) or as sets of closed curves. The boundaries between the regular and chaotic regions pose a significant barrier to transport because material exchanges can only occur across these boundaries by diffusive mechanisms (Paul et al., 2004).

For tanks agitated by an RT (case 1 of Table 5.1) or a PBT (case 4 of Table 5.1) impeller, several horizontal and vertical-azimuthal planes were used to construct the Poincaré maps. Figures 5.10a-d show the horizontal Poincaré maps for the RT impeller. In these figures, the blue dots represent a particle that crossed the plane toward the bottom of the tank, while the red stars indicate a particle that crossed the plane toward the top of the tank. Circulation patterns can be readily deduced in these figures. More specifically, when the horizontal plane was below the impeller plane (Figures 5.10a and b), the blue dots were mainly located around the external wall while the upward intersections (red stars) were located in the inner part of the tank. This trend was reversed for the planes above the impeller.

The Poincaré maps for different radii on $\theta - z$ planes are shown in Figures 5.11a-d for the same mixing system, where the blue dots represent a particle that crossed the plane toward the center of the tank and the red stars represent a particle that crossed the plane toward the wall of the tank. The strong radial flow generated by the RT impeller can be clearly seen as the red strip surrounding this impeller. This radial jet impinges on the wall and the return flow then forms, generating upper and lower circulating loops (blue dots) in the tank.

The effect of the baffles on the turbulent fluid flow inside the tank can also be observed, especially when the Poincaré plane moves toward the tank wall (Figures 5.11c-d). The alterations caused by the baffles to the boundaries of the red strip (impeller discharge flow) and the blue points region (return flow of the lower and upper circulating loops). Such information could be used, for instance, to find the best location for the boundary between the inner and outer regions of the MRF approach.

The horizontal Poincaré maps for the PBT impeller (case 4) are shown in Figure 5.12 for

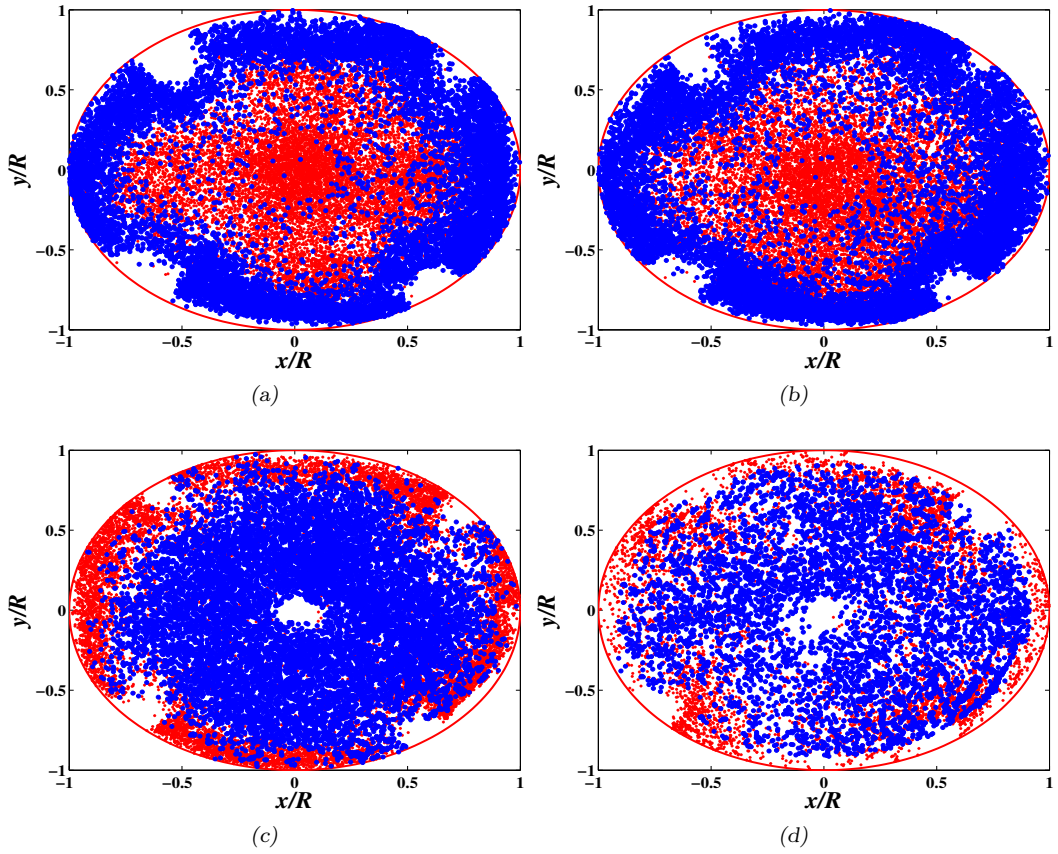

Figure 5.10: Poincaré maps for the RT impeller (case 1) at different heights on x-y planes : (a) z/H = 0.143, (b) z/H = 0.24, (c) z/H = 0.52, and (d) z/H = 0.81.

the same heights as those used for the RT impeller. As expected, there was just one circulating loop as the trajectory followed the same trend above and below the impeller (Figures 5.12b and c). This was opposite to the flow structure generated by the RT impeller, where there are two circulating loops above and below the impeller. Figures 5.12c and d show that the tangential movement of the fluid along the tank wall compresses the fluid toward the baffles and creates 3D upward wall jets. These jets are three-dimensional as they shrink when the top of the tank is approached. The corresponding flow structure can be readily deduced by comparing the sizes of the red regions behind the baffles at different axial locations in Figure 5.12. Figures 5.13a-d show the Poincaré maps on $\theta - z$ planes for the PBT impeller. The structure of one circulating loop can be observed in these maps as all four planes divide into outward (red stars) and inward flow regions (blue dots). They also show that the bottom

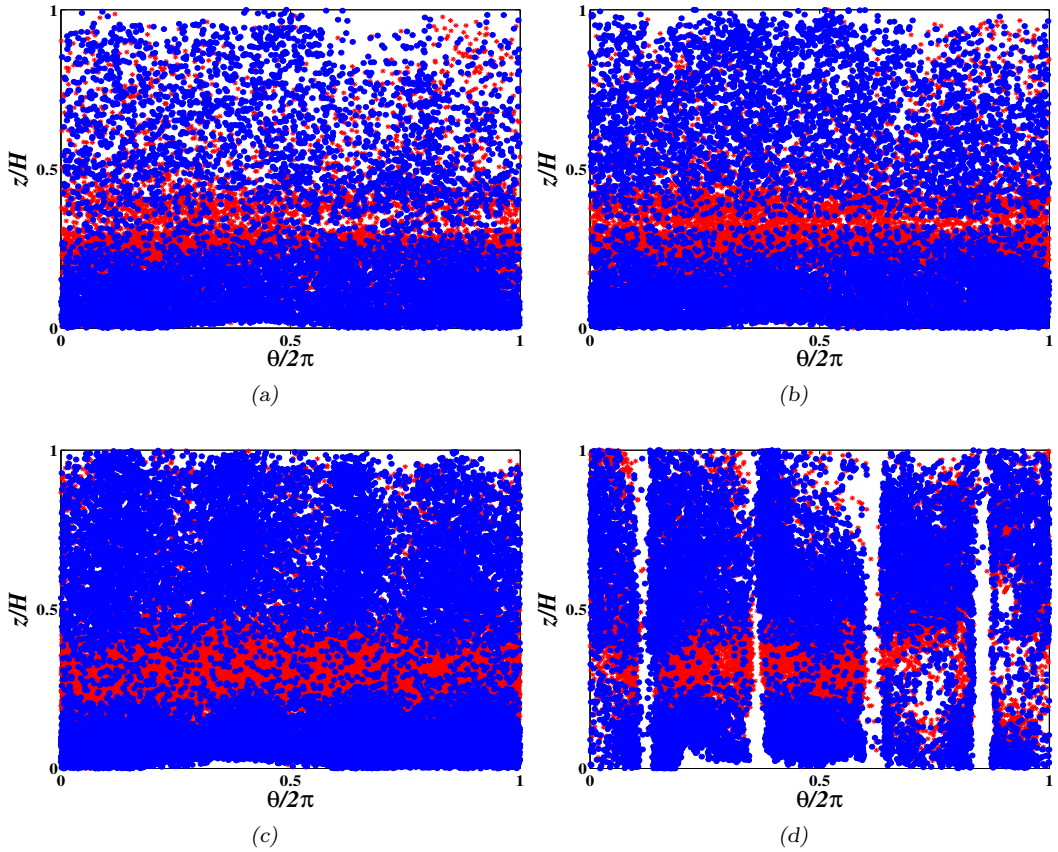

Figure 5.11: Poincaré maps for the RT impeller (case 1) at different radii on θ-z planes : (a) r/R = 0.25, (b) r/R = 0.33, (c) r/R = 0.6, and (h) r/R = 0.9.

two-thirds of the tank is more active in terms of mean circulation as there are more points in this region.

Lagrangian velocity distributions for the RT and PBT impellers

The distributions of the dimensionless Lagrangian velocity magnitudes (V/V_{tip}) inside the tank measured by the RPT technique are shown in Figure 5.14a for the RT impeller (case 1 of Table 5.1) and in Figure 5.14b for the PBT impeller (case 4 of Table 5.1). These distributions are nearly identical owing to the similarity of their statistical parameters, namely the calculated mean, standard deviation, and skewness given in Table 5.4. The values of these parameters for the RT that were calculated by Chiti et al. (2011) based on PEPT measurements are also included in this table. The means and standard deviations of the

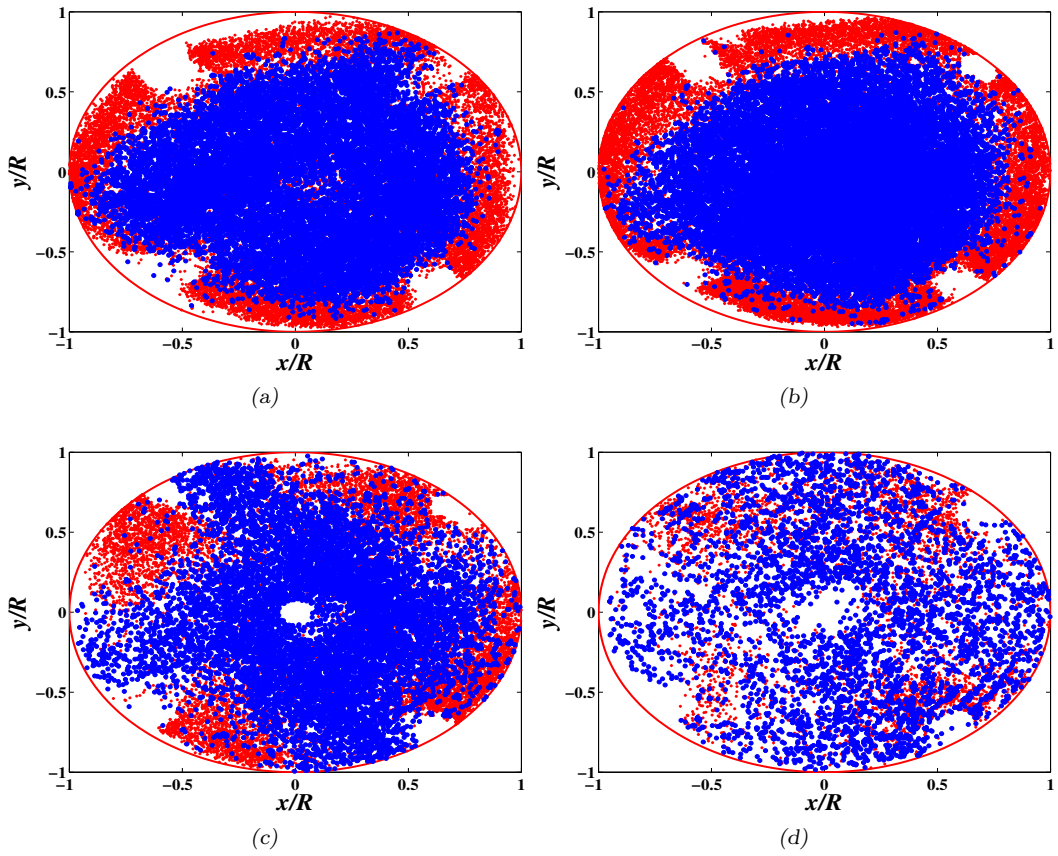

Figure 5.12: Poincaré maps for the PBT impeller (case 4) at different heights on x-y planes : (a) z/H = 0.143, (b) z/H = 0.24, (c) z/H = 0.52, and (d) z/H = 0.81.

distributions are indeed similar for the RT and PBT impellers. The skewness value for the PBT is slightly higher than for the RT, without reaching significance. The comparison of these statistical terms measured by the RPT and PEPT techniques shows that they are in fair agreement. These data can be well fitted into a log-normal distribution, with a correlation coefficient $> 98\%$:

$$\psi(x) = \frac{1}{x\sigma_x\sqrt{2\pi}} exp[-\frac{1}{2}(\frac{ln(x) - \bar{x}}{\sigma_x})^2] \tag{5.6}$$

where σ_x is the logarithmic standard deviation and $\bar{x}$ is the logarithmic mean of the distribution. It might be drawn from these results that, for a given Reynolds number in the fully turbulent flow regime, the distribution of Lagrangian velocity magnitudes scaled with the impeller tip speed is no longer dependent on the type of impeller. However, additional

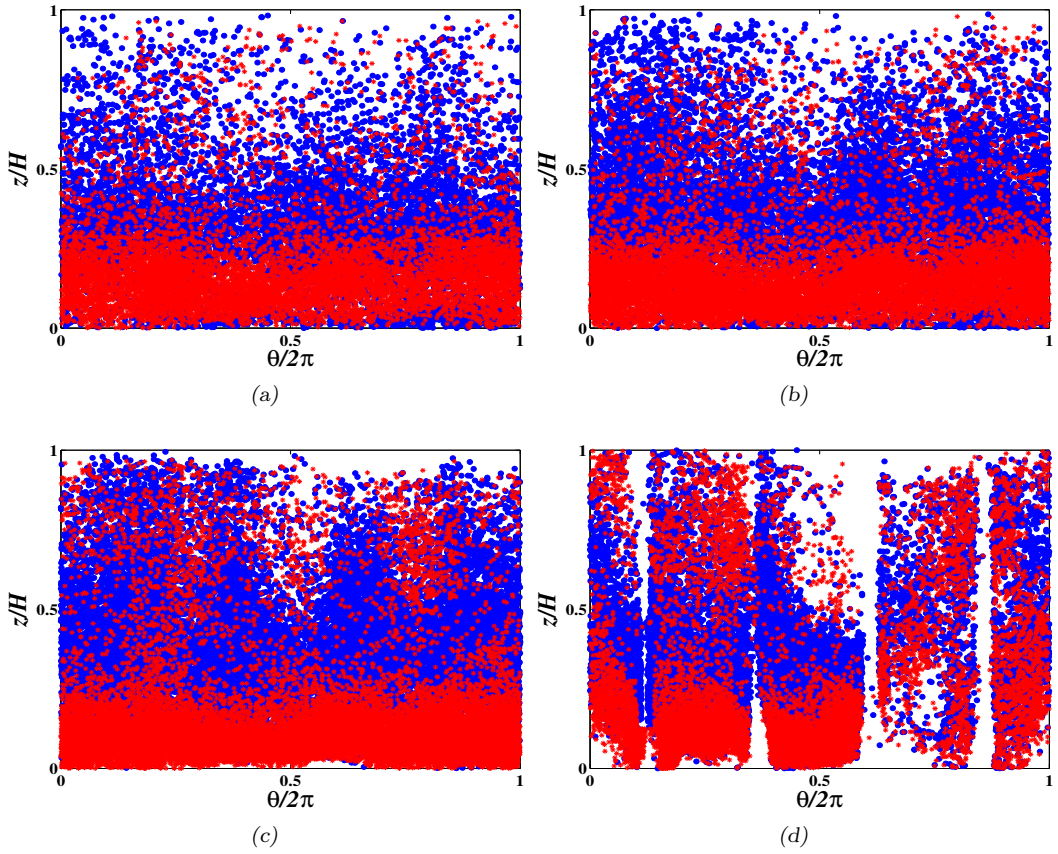

Figure 5.13: Poincaré maps for the PBT impeller (case 4) at different radii on θ-z planes : (a) r/R = 0.25, (b) r/R = 0.33, (c) r/R = 0.6, and (d) r/R = 0.9.

experiments are required to support this. In addition, the form of these distributions reveals that the high velocity zones in the impeller region are small compared to the lower velocity zones, which confirms our previous numerical observations (Bashiri et al., 2014).

Mixing measurements

The mixing time in STs is often correlated based on design characteristics (*e.g.* tank to impeller diameter ratio, T/D, power number, N_p) and operating conditions (impeller rotational speed, N) :

$$\theta_m = A(T/D)^B N_p^{-1/3} N^{-1} \tag{5.7}$$

Table 5.4: Mean, standard deviation, and skewness values for the dimensionless Lagrangian velocity distributions in the ST.

Mixing system	**Re**	**Mean**	**standard deviation**	**Skewness**
RT (Case 1)	2.2×10^4	0.17	0.12	2.39
PBT (Case 4)	2.2×10^4	0.17	0.12	2.52
RT (using PEPT) (Chiti et al., 2011)	2.1×10^4	0.18	0.12	1.8

where A and B are constants. Values proposed in the literature for these constants are summarized in Table 5.5 (Grenville et al., 1995; Groen, 1994; Ruszkowski, 1994; Van't Riet and Tramper, 1991). In this subsection, non-intrusive RPT measurements of the mixing times for the RT and PBT impellers (cases 1 and 4 of Table 5.1) are discussed.

Table 5.5: Parameters for mixing time correlations (equation (5.7)).

Reference	**A**	**B**
Grenville et al. (1995); Ruszkowski (1994)	5.3	2
Van't Riet and Tramper (1991)	3	3
Groen (1994)	3.5	3

Wittmer et al. (1998) showed that the concept of correlations in trajectory data can be used to assess mixing efficiency. Doucet et al. (2008b) then proposed two mixing indices that bridge the global mixing properties and local viewpoints of chaotic theory using Lagrangian trajectory data. They showed that these mixing indices can be used to measure mixing efficiency in both granular (*e.g.* cylindrical drum) and fluid (*e.g.* static mixer) mixing systems (Doucet et al., 2008b). The definition of mixing in the weak sense proposed by Doucet et al. (2008b) and based on the concept of stochastic independence, was used in the present study. It is briefly recalled here.

Let us consider M particles and denote the position of particle i at time t by R_i^t. This particle follows a trajectory $R_{i,t\geq 0}^t$, which can be obtained using the RPT technique. Given a probability measure $\mathcal{P}$, the system is said to be mixed in the weak sense if, for each particle

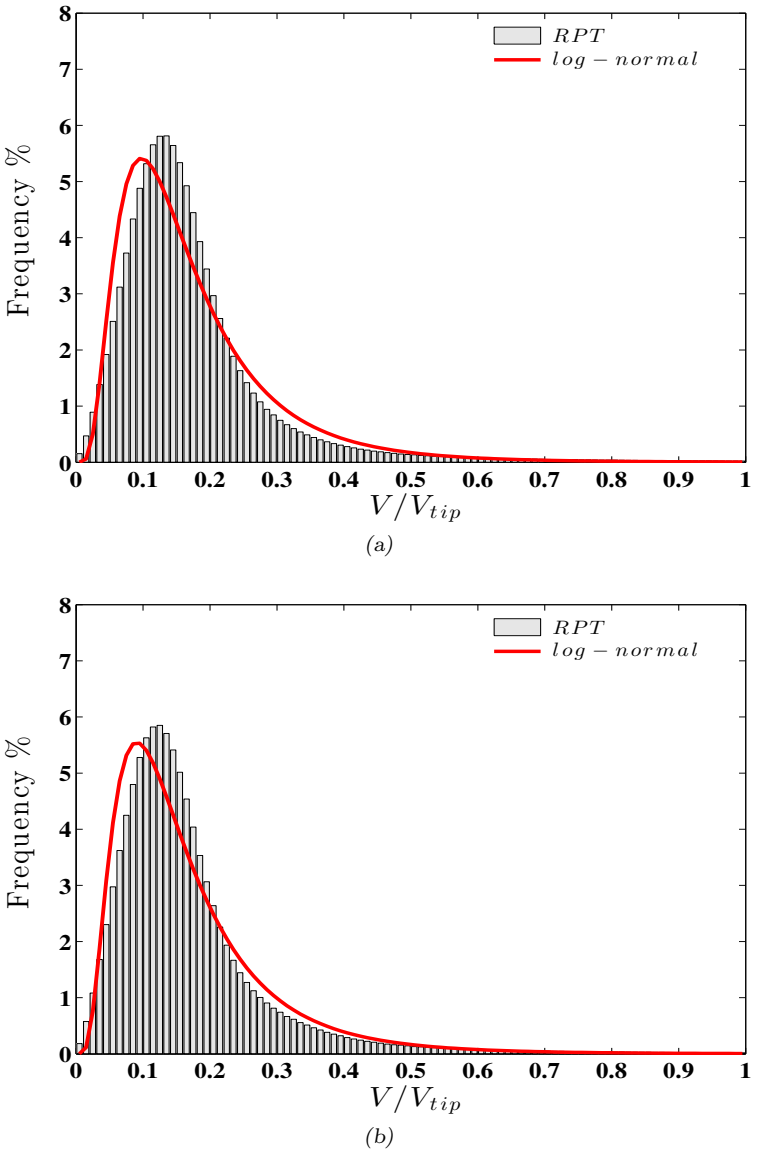

Figure 5.14: Dimensionless Lagrangian velocity magnitude distributions in the ST compared to log-normal distributions for (a) the RT impeller (case 1) and (b) the PBT impeller (case 4).

$i = 1, 2, ..., M$:

$$\mathcal{P}\{R_i^t | R_i^0\} = \mathcal{P}\{R_i^t\} \tag{5.8}$$

This definition states that, to be mixed in the weak sense, the distribution of particles at time t has to be independent of the initial distribution. In other words, the positions of the particles at time t must not correlate with their initial positions. Using this definition, Doucet

et al. (2008b) developed the weak sense mixing index (β_{ws}) based on a principal component analysis (PCA) and the construction of a correlation matrix that brings the particle positions at time t and their initial positions into play. Suffice it to say here that β_{ws} takes on the value of 0 when the system is perfectly mixed and 1 when it is completely segregated. While quite general, this definition is based solely on the spatial coordinates of the particles without taking their properties (e.g., size and density in the case of solids mixing) into consideration. When a single property defines the state of mixedness in the system (e.g., particle color), this definition of mixing is satisfactory. However, it does not completely characterize the state of mixing when more than one property (e.g., size, density, and shape) define the state of mixedness. In this case, Doucet et al. (2008b) showed how the weak sense mixing index can be generalized, and proposed a strong sense mixing index. More details on the mathematical formulation of these indices can be found in that paper (Doucet et al., 2008b).

In the present study, as the single-phase flow field was investigated using the RPT technique, the weak sense of mixing was sufficient to describe the state of mixedness. Assuming that the system was ergodic, it was possible to extrapolate the behavior of a cluster of tracer particles from the trajectory of a single tracer particle. Accordingly, in order to calculate index β_{ws}, the whole trajectory was divided into 1000 trajectories of length Δ. This resulted in a cluster of 1000 independent particle trajectories of length Δ, which could be used to compute the time evolution of β_{ws}.

Figures 5.15a and b show the evolution of β_{ws} for the RT (case 1 of Table 5.1) and PBT (case 4 of Table 5.1) impellers, respectively. The red dashed vertical lines correspond to predictions by equation (5.7) of the mixing time using the various constants listed in Table 5.5. As can be seen in these figures, the values of the mixing index level off to asymptotic values between 0 and 0.1 after approximately 5 s in both cases. These values are in good agreement with the values predicted by equation (5.7). However, as there are no solid guidelines for deciding when the values of β_{ws} are insignificant from zero, determining the mixing time based on the time evolution of β_{ws} is subjective. In the present study, a similar method for

measuring mixing time was developed to address this issue.

As mentioned previously, if the ergodic hypothesis holds, the information contained in a single long trajectory is the same as the information contained in several shorter trajectories of particles tracked simultaneously. In this case, the correlation coefficients used to develop the weak sense mixing index by Doucet et al. (2008b) can be replaced by an autocorrelation

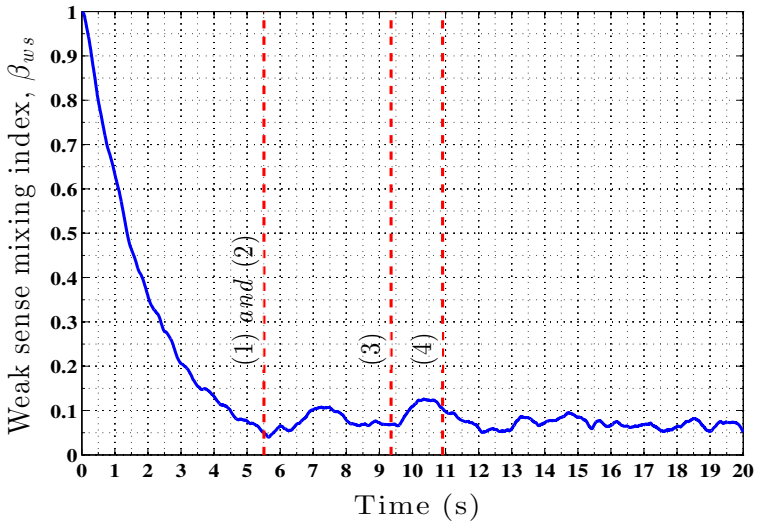

(a)

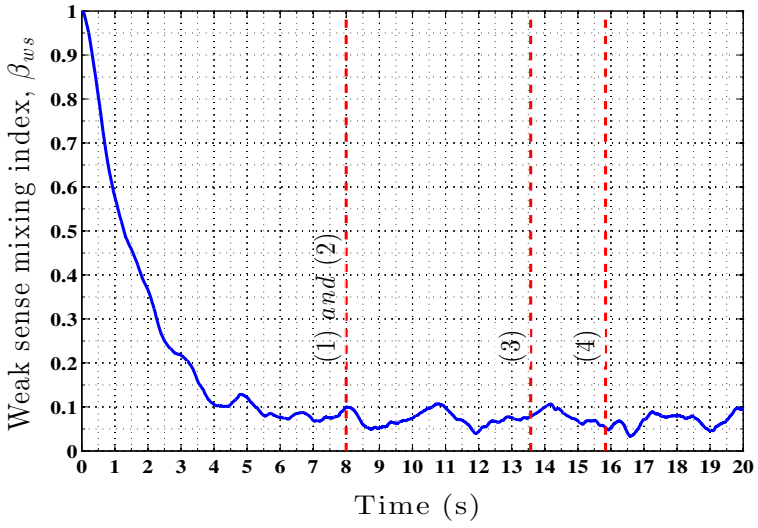

(b)

Figure 5.15: Evolution of the weak sense mixing index for (a) the RT impeller (case 1) and (b) the PBT impeller (case 4). The red dashed lines are the predictions of mixing times by (1) Grenville et al. (1995), (2) Ruszkowski (1994), (3) Van't Riet and Tramper (1991), and (4) Groen (1994).

function. Of course, these two mathematical concepts are closely related. If a blob of fluid goes through an efficient mixing process, two spatially close points in the blob should get dispersed more or less rapidly (Kresta and Brodkey, 2004). Accordingly, the correlation between their positions should decrease from 1 (non-mixed) to 0 (mixed) over time. However, if the blob of fluid is subjected to poor mixing, then the location of these points might remain correlated over time. This phenomenon can be monitored by looking at the evolution in the autocorrelation of particle trajectories. The autocorrelation function of the particle position vector, R^t, is defined as follows :

$$\Lambda^k = \frac{\sum_{t=1}^{n-k}(R^t - \overline{R}).(R^{t+k} - \overline{R})}{\sum_{t=1}^{n}(R^t - \overline{R}).(R^t - \overline{R})} \tag{5.9}$$

where k, n, and, $\overline{R}$ are the time lag, the total number of trajectory values, and the mean of the position vectors, respectively. By definition, Λ has a value of 1 at $k = 0$ and tends asymptotically toward 0 when k increases and mixing takes place. The decay of the autocorrelation of the position vector shows how fast the process loses its memory (i.e., the particle becomes independent of its initial position). It is thus important to determine a threshold that specifies when the autocorrelation of the position vector is insignificant from zero. This would provide a more precise and less subjective way to determine mixing time. Barlett's formula for calculating the standard error of the autocorrelation function (SE_{Λ^k}) can be used for this purpose. More specifically, when the autocorrelation function remains outside the boundaries defined by this formula, it has not been reduced to 0 (i.e., there is still a correlation with the initial position). This formula is defined as follows (for $k \geq 2$) (Box et al., 2013) :

$$SE_{\Lambda^k} = \pm\sqrt{\frac{1}{n}\left(1 + 2\sum_{k=1}^{k-1}(\Lambda^k)^2\right)} \tag{5.10}$$

It should be noted that, for $k = 1$, SE_{Λ^k} is equal to $\pm\sqrt{\frac{1}{n}}$.

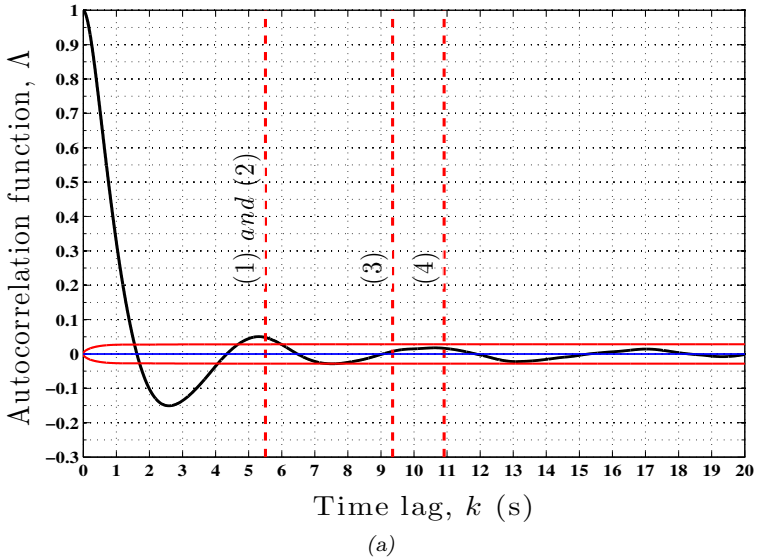

(a)

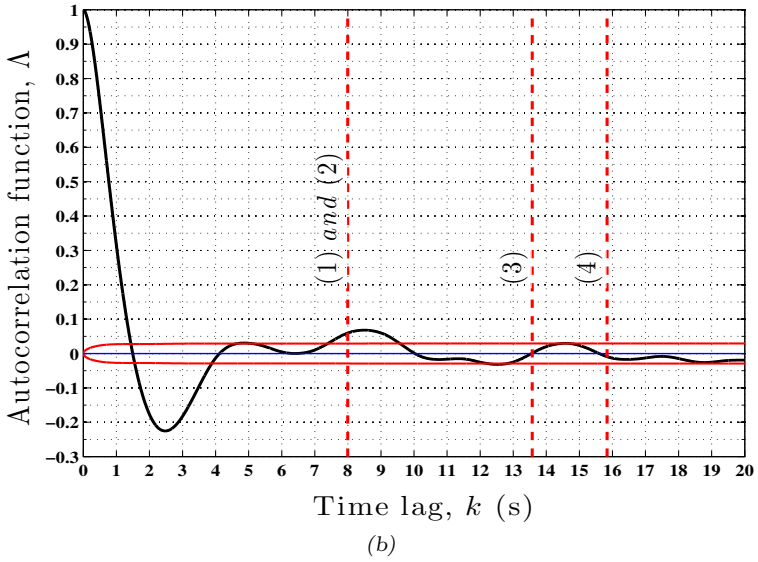

(b)

Figure 5.16: Evolution of the autocorrelation function of tracer positions for (a) the RT impeller (case 1) and (b) the PBT impeller (case 4). The red dashed lines are the predictions of mixing times by (1) Grenville et al. (1995), (2) Ruszkowski (1994), (3) Van't Riet and Tramper (1991), and (4) Groen (1994).

Figures 5.16a and b show the evolution of the autocorrelation function of the particle trajectories for the RT (case 1 of Table 5.1) and the PBT (case 4 of Table 5.1) impellers, respectively. The red envelope curves were obtained from Barlett's formula (equation (5.10)). As can be seen, the autocorrelation function of the tracer trajectories begins to stay inside the boundaries defined by equation (5.10) at time 6 s for the RT impeller (case 1). This

value is in close agreement with the mixing time predicted by equation (5.7) (5.5 s) using the constants proposed by Grenville et al. (1995) and Ruszkowski (1994). Using the same procedure, the autocorrelation function of the tracer trajectories for the PBT impeller (case 4) at time 9.5 s becomes insignificant from 0 and is also in good agreement with the value predicted by equation (5.7) using the constants proposed by the same authors (8 s) (Grenville et al., 1995; Ruszkowski, 1994).

5.4 Conclusion

The purpose of the present study was to assess the adequacy of the RPT technique to characterize fully turbulent fluid flows in a tank agitated by an RT or a PBT impeller. The Eulerian turbulent flow field measured using the RPT technique for the RT impeller was first benchmarked with CFD simulations using RANS-based models as well as laser-based measurements obtained by Murthy and Joshi (2008). Despite the inherent uncertainties of each method, good agreement between the methods was obtained. The RPT technique was also used to measure 3D velocity profiles in the case of the PBT impeller. The results obtained for studying the turbulent flow behavior of wall jets generated by both types of impeller (RT and PBT) were in agreement with previous studies (Bittorf and Kresta, 2001; Kresta et al., 2001).

Three Lagrangian measurements of the fluid dynamics, including Poincaré maps, the distribution of dimensionless velocity magnitudes in the ST, and mixing time were presented. We showed that the RPT technique can be used to generate Poincaré maps to visualize flow structures in STs. Similar distributions of dimensionless velocity magnitudes were observed for the RT and PBT impellers operating at the same Reynolds number. The mixing times were investigated using two closely related mixing indices, one based on the concept of stochastic independence and the other on the statistical concept of memory loss. The latter one was shown to lead to a less subjective determination of the mixing time by resorting to an autocorrelation function together with Barlett's formula. Our results showed that the

RPT technique holds great promise for measuring mixing times when traditional methods are insufficient (e.g., in opaque systems).

All the findings reported here showed the adequacy of the RPT technique to study turbulent fluid flows and mixing in STs. Given the vast amount of information generated by the RPT technique, it could be used to build an extensive database that could in turn serve to support the development of phenomenological models and to assess the adequacy of CFD models. For instance, it could be used to shed light on the mechanisms of solid suspension and dispersion, or to measure fluid circulation time distributions (CTD) in STs. This information is critical for analyzing the performance of mixing systems (Amanullah et al., 2004).

Acknowledgments

Our work was made possible by financial support from the Natural Sciences and Engineering Council of Canada (NSERC). We thank Dr. Rouzbeh Jafari for his help in preparing the tracer used in the RPT technique.

5.5 References

Alizadeh, E., Dubé, O., Bertrand, F., and Chaouki, J. (2013). Characterization of mixing and size segregation in a rotating drum by a particle tracking method. *AIChE Journal*.

Amanullah, A., Buckland, B. C., and Nienow, A. W. (2004). Mixing in the fermentation and cell culture industries. *Handbook of Industrial Mixing : Science and Practice*, pages 1071–1170.

Aref, H. (1984). Stirring by chaotic advection. *Journal of fluid mechanics*, 143(1) :1–21.

Aubin, J., Fletcher, D. F., and Xuereb, C. (2004a). Modeling turbulent flow in stirred tanks with CFD : the influence of the modeling approach, turbulence model and numerical scheme. *Experimental thermal and fluid science*, 28(5) :431–445.

Aubin, J., Le Sauze, N., Bertrand, J., Fletcher, D. F., and Xuereb, C. (2004b). PIV measurements of flow in an aerated tank stirred by a down-and an up-pumping axial flow impeller. *Experimental Thermal and Fluid Science*, 28(5) :447–456.

Aubin, J., Mavros, P., Fletcher, D. F., Bertrand, J., and Xuereb, C. (2001). Effect of axial agitator configuration (up-pumping, down-pumping, reverse rotation) on flow patterns generated in stirred vessels. *Chemical Engineering Research and Design*, 79(8) :845–856.

Baldi, S. and Yianneskis, M. (2003). On the direct measurement of turbulence energy dissipation in stirred vessels with PIV. *Industrial & engineering chemistry research*, 42(26) :7006–7016.

Baldi, S. and Yianneskis, M. (2004). On the quantification of energy dissipation in the impeller stream of a stirred vessel from fluctuating velocity gradient measurements. *Chemical engineering science*, 59(13) :2659–2671.

Bashiri, H., Heniche, M., Bertrand, F., and Chaouki, J. (2014). Compartmental modelling of turbulent fluid flow for the scale-up of stirred tanks. *The Canadian Journal of Chemical Engineering*, 92(6) :1070–1081.

Bashiri, H., Mostoufi, N., Radmanesh, R., Sotudeh-Gharebagh, R., and Chaouki, J. (2010). Effect of bed diameter on the hydrodynamics of gas-solid fluidized beds. *Iran. J. Chem. Chem. Eng. Vol*, 29(3).

Benedict, L. and Gould, R. (1999). Understanding biases in the near-field region of LDA two-point correlation measurements. *Experiments in fluids*, 26(5) :381–388.

Bhattacharya, S. and Kresta, S. M. (2002). CFD simulations of three-dimensional wall jets in a stirred tank. *The Canadian Journal of Chemical Engineering*, 80(4) :1–15.

Bittorf, K. J. and Kresta, S. M. (2000). Active volume of mean circulation for stirred tanks agitated with axial impellers. *Chemical engineering science*, 55(7) :1325–1335.

Bittorf, K. J. and Kresta, S. M. (2001). Three-dimensional wall jets : Axial flow in a stirred tank. *AIChE journal*, 47(6) :1277–1284.

Box, G. E., Jenkins, G. M., and Reinsel, G. C. (2013). *Time series analysis : forecasting and control*. John Wiley & Sons.

Boyer, C., Duquenne, A.-M., and Wild, G. (2002). Measuring techniques in gas-liquid and gas-liquid-solid reactors. *Chemical Engineering Science*, 57(16) :3185 – 3215.

Brucato, A., Ciofalo, M., Grisafi, F., and Micale, G. (1998). Numerical prediction of flow fields in baffled stirred vessels : a comparison of alternative modelling approaches. *Chemical Engineering Science*, 53(21) :3653–3684.

Butcher, M. and Eagles, W. (2002). Fluid mixing re-engineered. *Chemical engineer*, (733) :28–29.

Cabaret, F., Bonnot, S., Fradette, L., and Tanguy, P. A. (2007). Mixing time analysis using colorimetric methods and image processing. *Industrial & engineering chemistry research*, 46(14) :5032–5042.

Cassanello, M., Larachi, F., Legros, R., and Chaouki, J. (1999). Solids dynamics from experimental trajectory time-series of a single particle motion in gas-spouted beds. *Chemical engineering science*, 54(13) :2545–2554.

Chaouki, J., Larachi, F., and Dudukovic, M. P. (1997). *Non-invasive monitoring of multiphase flows*. Access Online via Elsevier.

Chiti, F., Bakalis, S., Bujalski, W., Barigou, M., Eaglesham, A., and Nienow, A. W. (2011). Using positron emission particle tracking (PEPT) to study the turbulent flow in a baffled vessel agitated by a Rushton turbine : Improving data treatment and validation. *Chemical Engineering Research and Design*, 89(10) :1947–1960.

Cooper, R. G. and Wolf, D. (1968). Velocity profiles and pumping capacities for turbine type impellers. *The Canadian Journal of Chemical Engineering*, 46(2) :94–100.

Coroneo, M., Montante, G., Paglianti, A., and Magelli, F. (2011). CFD prediction of fluid flow and mixing in stirred tanks : Numerical issues about the RANS simulations. *Computers & Chemical Engineering*, 35(10) :1959–1968.

Deglon, D. and Meyer, C. (2006). CFD modelling of stirred tanks : Numerical considerations. *Minerals Engineering*, 19(10) :1059–1068.

Delafosse, A., Collignon, M.-L., Crine, M., and Toye, D. (2011). Estimation of the turbulent kinetic energy dissipation rate from 2D-PIV measurements in a vessel stirred by an axial Mixel TTP impeller. *Chemical Engineering Science*, 66(8) :1728–1737.

Distelhoff, M., Marquis, A., Nouri, J., and Whitelaw, J. (1997). Scalar mixing measurements in batch operated stirred tanks. *The Canadian Journal of Chemical Engineering*, 75(4) :641–652.

Djeridane, T., Larachi, F., Roy, D., Chaovki, J., and Legros, R. (1998). Investigation of the mean and turbulent particle velocity fields in a spouted bed using radioactive particle tracking. *The Canadian Journal of Chemical Engineering*, 76(2) :190–195.

Doucet, J., Bertrand, F., and Chaouki, J. (2008a). An extended radioactive particle tracking method for systems with irregular moving boundaries. *Powder Technology*, 181(2) :195–204.

Doucet, J., Bertrand, F., and Chaouki, J. (2008b). A measure of mixing from lagrangian tracking and its application to granular and fluid flow systems. *Chemical Engineering Research and Design*, 86(12) :1313–1321.

Dubé, O., Dubé, D., Chaouki, J., and Bertrand, F. (2014). Optimization of detector positioning in the radioactive particle tracking technique. *Applied Radiation and Isotopes*, 89 :109–124.

Ducci, A. and Yianneskis, M. (2005). Direct determination of energy dissipation in stirred vessels with two-point LDA. *AIChE journal*, 51(8) :2133–2149.

Escudie, R. and Line, A. (2003). Experimental analysis of hydrodynamics in a radially agitated tank. *AIChE journal*, 49(3) :585–603.

Fishwick, R., Winterbottom, M., Parker, D., Fan, X., and Stitt, H. (2005). The use of positron emission particle tracking in the study of multiphase stirred tank reactor hydrodynamics. *The Canadian Journal of Chemical Engineering*, 83(1) :97–103.

Fluent (2010). ANSYS FLUENT theory guide : Version 13.0. *Ansys Inc, Canonsburg (2010)*.

Fontaine, A., Guntzburger, Y., Bertrand, F., Fradette, L., and Heuzey, M.-C. (2012). Experimental investigation of the flow dynamics of rheologically complex fluids in a Maxblend impeller system using PIV. *Chemical Engineering Research and Design*.

Gabriele, A., Nienow, A., and Simmons, M. (2009). Use of angle resolved PIV to estimate local specific energy dissipation rates for up-and down-pumping pitched blade agitators in a stirred tank. *Chemical Engineering Science*, 64(1) :126–143.

Grenville, R., Ruszkowski, S., and Garred, E. (1995). Blending of miscible liquids in the turbulent and transitional regimes. In *15th NAMF mixing conference*.

Groen, D. J. (1994). *Macro Mixing in bioreactors*. PhD thesis, T. U. Delft.

Guha, D., Ramachandran, P., and Dudukovic, M. (2007). Flow field of suspended solids in a stirred tank reactor by lagrangian tracking. *Chemical Engineering Science*, 62(22) :6143–6154.

Guida, A., Nienow, A. W., and Barigou, M. (2012). Lagrangian tools for the analysis of mixing in single-phase and multiphase flow systems. *AIChE Journal*, 58(1) :31–45.

Guillard, F., Trägårdh, C., and Fuchs, L. (2000). A study on the instability of coherent mixing structures in a continuously stirred tank. *Chemical Engineering Science*, 55(23) :5657–5670.

Hartmann, H., Derksen, J., Montavon, C., Pearson, J., Hamill, I., and Van den Akker, H. (2004). Assessment of large eddy and rans stirred tank simulations by means of lda. *Chemical Engineering Science*, 59(12) :2419–2432.

Heniche, M. and Tanguy, P. A. (2006). A new element-by-element method for trajectory calculations with tetrahedral finite element meshes. *International journal for numerical methods in engineering*, 67(9) :1290–1317.

Joshi, J. B. and Ranade, V. V. (2003). Computational fluid dynamics for designing process equipment : expectations, current status, and path forward. *Industrial & engineering chemistry research*, 42(6) :1115–1128.

Kemoun, A., Lusseyran, F., Mallet, J., and Mahouast, M. (1998). Experimental scanning for simplifying the model of a stirred-tank flow. *Experiments in fluids*, 25(1) :23–36.

Khopkar, A., Rammohan, A., Ranade, V., and Dudukovic, M. (2005). Gas–liquid flow generated by a Rushton turbine in stirred vessel : CARPT/CT measurements and CFD simulations. *Chemical Engineering Science*, 60(8) :2215–2229.

Kiared, K., Larachi, F., Chaouki, J., and Guy, C. (1999). Mean and turbulent particle velocity in the fully developed region of a three-phase fluidized bed. *Chemical engineering & technology*, 22(8) :683–689.

Kresta, S. M., Bittorf, K. J., and Wilson, D. J. (2001). Internal annular wall jets : radial flow in a stirred tank. *AIChE journal*, 47(11) :2390–2401.

Kresta, S. M. and Brodkey, R. S. (2004). Turbulence in mixing applications. *Handbook of Industrial Mixing : Science and Practice*, pages 43–45.

Kresta, S. M. and Wood, P. E. (1993a). The flow field produced by a pitched blade turbine : characterization of the turbulence and estimation of the dissipation rate. *Chemical engineering science*, 48(10) :1761–1774.

Kresta, S. M. and Wood, P. E. (1993b). The mean flow field produced by a 45 pitched blade turbine : changes in the circulation pattern due to off bottom clearance. *The Canadian Journal of Chemical Engineering*, 71(1) :42–53.

Kumaresan, T. and Joshi, J. B. (2006). Effect of impeller design on the flow pattern and mixing in stirred tanks. *Chemical engineering journal*, 115(3) :173–193.

Kusch, H. and Ottino, J. (1992). Experiments on mixing in continuous chaotic flows. *Journal of Fluid Mechanics*, 236(1) :319–348.

Lee, K. and Yianneskis, M. (1998). Turbulence properties of the impeller stream of a Rushton turbine. *AIChE journal*, 44(1) :13–24.

Lin, J., Chen, M., and Chao, B. (1985). A novel radioactive particle tracking facility for measurement of solids motion in gas fluidized beds. *AIChE Journal*, 31(3) :465–473.

Machado, M. B., Bittorf, K. J., Roussinova, V. T., and Kresta, S. M. (2013). Transition from turbulent to transitional flow in the top half of a stirred tank. *Chemical Engineering Science*, 98 :218–230.

Mavros, P. (2001). Flow visualization in stirred vessels : A review of experimental techniques. *Chemical Engineering Research and Design*, 79(2) :113 – 127.

Melton, L. A., Lipp, C., Spradling, R., and Paulson, K. (2002). DISMT-determination of mixing time through color changes. *Chemical Engineering Communications*, 189(3) :322–338.

Mostoufi, N. and Chaouki, J. (2001). Local solid mixing in gas–solid fluidized beds. *Powder Technology*, 114(1) :23–31.

Mostoufi, N. and Chaouki, J. (2004). Flow structure of the solids in gas–solid fluidized beds. *Chemical Engineering Science*, 59(20) :4217–4227.

Murthy, B. and Joshi, J. (2008). Assessment of standard k–ε, RSM and LES turbulence models in a baffled stirred vessel agitated by various impeller designs. *Chemical Engineering Science*, 63(22) :5468–5495.

Ng, K., Fentiman, N., Lee, K., and Yianneskis, M. (1998). Assessment of sliding mesh CFD predictions and LDA measurements of the flow in a tank stirred by a Rushton impeller. *Chemical Engineering Research and Design*, 76(6) :737–747.

Nienow, A. (1997). On impeller circulation and mixing effectiveness in the turbulent flow regime. *Chemical Engineering Science*, 52(15) :2557–2565.

Norton, T. and Sun, D.-W. (2008). Recent advances in the use of high pressure as an effective processing technique in the food industry. *Food and Bioprocess Technology*, 1(1) :2–34.

Panitz, T. and Wasan, D. (1972). Flow attachment to solid surfaces : The coanda effect. *AIChE Journal*, 18(1) :51–57.

Paul, E. L., Atiemo-Obeng, V., and Kresta, S. M. (2004). *Handbook of industrial mixing : science and practice*. John Wiley & Sons.

Pianko-Oprych, P., Nienow, A., and Barigou, M. (2009). Positron emission particle tracking (PEPT) compared to particle image velocimetry (PIV) for studying the flow generated by a pitched-blade turbine in single phase and multi-phase systems. *Chemical Engineering Science*, 64(23) :4955–4968.

Rammohan, A., Kemoun, A., Al-Dahhan, M., and Dudukovic, M. (2001a). Characterization of single phase flows in stirred tanks via computer automated radioactive particle tracking (CARPT). *Chemical engineering research and design*, 79(8) :831–844.

Rammohan, A., Kemoun, A., Al-Dahhan, M., and Dudukovic, M. (2001b). A lagrangian description of flows in stirred tanks via computer-automated radioactive particle tracking (CARPT). *Chemical engineering science*, 56(8) :2629–2639.

Ranade, V. and Joshi, J. (1989). Flow generated by pitched blade turbines I : measurements using laser doppler anemometer. *Chemical Engineering Communications*, 81(1) :197–224.

Rewatkar, V. and Joshi, J. (1991). Effect of impeller design on liquid phase mixing in mechanically agitated reactors. *Chemical engineering communications*, 102(1) :1–33.

Roy, D., Larachi, F., Legros, R., and Chaouki, J. (1994). A study of solid behavior in spouted beds using 3-D particle tracking. *The Canadian Journal of Chemical Engineering*, 72(6) :945–952.

Roy, S., Acharya, S., and Cloeter, M. D. (2010). Flow structure and the effect of macro-instabilities in a pitched-blade stirred tank. *Chemical Engineering Science*, 65(10) :3009–3024.

Ruszkowski, S. (1994). A rational method for measuring blending performance, and comparison of different impeller types. In *Institution of chemical engineers symposium series*, volume 136, pages 283–283. Hemsphere publishing corporation.

Rutherford, K., Lee, K., Mahmoudi, S., and Yianneskis, M. (1996a). Hydrodynamic characteristics of dual Rushton impeller stirred vessels. *AIChE Journal*, 42(2) :332–346.

Rutherford, K., Mahmoudi, S., Lee, K., and Yianneskis, M. (1996b). The influence of Rushton impeller blade and disk thickness on the mixing characteristics of stirred vessels. *Chemical engineering research & design*, 74(3) :369–378.

Sharp, K. and Adrian, R. (2001). PIV study of small-scale flow structure around a Rushton turbine. *AIChE journal*, 47(4) :766–778.

Sheng, J., Meng, H., and Fox, R. (2000). A large eddy PIV method for turbulence dissipation rate estimation. *Chemical Engineering Science*, 55(20) :4423–4434.

Sommerfeld, M. and Decker, S. (2004). State of the art and future trends in CFD simulation of stirred vessel hydrodynamics. *Chemical engineering & technology*, 27(3) :215–224.

Van't Riet, K. and Tramper, J. (1991). *Basic bioreactor design*. CRC Press.

Wittmer, S., Falk, L., Pitiot, P., and Vivier, H. (1998). Characterization of stirred vessel hydrodynamics by three dimensional trajectography. *The Canadian Journal of Chemical Engineering*, 76(3) :600–610.

Wolf, D. and Manning, F. (1966). Impact tube measurement of flow patterns, velocity profiles and pumping capacities in mixing vessels. *The Canadian Journal of Chemical Engineering*, 44(3) :137–142.

Wu, H. and Patterson, G. (1989). Laser-Doppler measurements of turbulent-flow parameters in a stirred mixer. *Chemical Engineering Science*, 44(10) :2207–2221.

Yapici, K., Karasozen, B., Schäfer, M., and Uludag, Y. (2008). Numerical investigation of the effect of the Rushton type turbine design factors on agitated tank flow characteristics. *Chemical Engineering and Processing : Process Intensification*, 47(8) :1340–1349.

Zhang, Q., Yong, Y., Mao, Z.-S., Yang, C., and Zhao, C. (2009). Experimental determination and numerical simulation of mixing time in a gas–liquid stirred tank. *Chemical Engineering Science*, 64(12) :2926–2933.

Zhou, G. and Kresta, S. M. (1996). Impact of tank geometry on the maximum turbulence energy dissipation rate for impellers. *AIChE journal*, 42(9) :2476–2490.

CHAPTER 6

ARTICLE 3 : DEVELOPMENT OF A MULTISCALE MODEL FOR THE DESIGN AND SCALE-UP OF GAS/LIQUID STIRRED TANK REACTORS

Hamed Bashiri, François Bertrand, Jamal Chaouki

Department of Chemical Engineering, École Polytechnique de Montréal, C.P. 6079 succ. Centre-Ville, Montréal, Québec, Canada, H3C 3A7

(Submitted to *Chemical Engineering Journal.*)

Presentation of the article : The development of a multiscale gas/liquid flow model will be discussed in a great detail. The adequacy of the model at each step will be carefully assessed using experimental data drawn from the literature. Next, the proposed model will be used to investigate the impact of various operating conditions and scale-up on local values of the volumetric mass transfer coefficient in STRs agitated with a Rushton turbine.

Abstract : A multiscale gas/liquid flow model was developed as a tool for the design and scale-up of stirred tank reactors (STRs). The model is based on the compartmentalization of the STR into zones and the use of simplified less computationally intensive gas/liquid flow simulations. It predicts the mean value of the local volumetric mass transfer coefficient (k_La) in each compartment based on the local hydrodynamic parameters therein (i.e., gas hold-up and liquid turbulent energy dissipation rate). The adequacy of the model at each step was carefully assessed using experimental data drawn from the literature. The proposed model was able to predict the overall volumetric mass transfer coefficient in STRs agitated with a Rushton turbine with good adequacy. The effects of operating conditions and scale-up on the distribution of k_La were also studied. The contributions of each compartment to the overall mass transfer inside the STR could be changed considerably by altering the operating conditions and scale-up. It was estimated that by increasing the STR size, the overall volumetric mass transfer coefficient decreased by at least 20% following a conventional scale-up rule. This was explored by combining the concepts of the local residence time distribution (RTD) of the liquid phase and the local k_La values inside the STR. These findings revealed the challenges involved in scaling up multiphase stirred tanks. Lastly, some alternative approaches are suggested for the design and scale-up of multiphase reactors that may mitigate the inherent limitations of conventional rules.

Keyword : gas/liquid, multiscale model, volumetric mass transfer coefficient, stirred tank, scale-up

6.1 Introduction

Gas/liquid stirred tank reactors (STRs) are widely used in the petroleum, chemical, petrochemical, mineral, and metallurgical industries to carry out reactions between gases and liquids. Over the last few decades, the increasing volumes of products manufactured in industrial processes have led to the use of larger and larger reactors. As a result, finding adequate rules for scaling up such processes from the lab to industrial scale has become a crucial task for process engineers.

The design and scale-up of gas/liquid STRs are not straightforward tasks, mainly because chemical reactions are generally related to mass and momentum transfer mechanisms in a complex manner. The current state of the art regarding the scale-up and design of large STRs is based on empirical correlations, best practices (know-how routines), and rules of thumb, even with existing research tools and advances in engineering design. With conventional scale-up procedures, the values of hydrodynamic parameters are assumed to be constant in the entire reactor ("well-mixed" assumption). However, in real cases, especially at the production level, the values of such parameters (the mass transfer coefficient, for example) may vary significantly.

The productivity of many processes is limited by mass transfer between phases, especially in the case of low soluble species in the gas phase that transfer to the liquid phase. This includes many bioprocesses such as those for the production of expensive specialty chemicals, including proteins, and bulk chemicals such as biofuels, lactic acid, and citric acid, where oxygen transfer is vital for the success of the process (Garcia-Ochoa et al., 2010; Lara et al., 2006). Understanding gas/liquid mass transfer is thus essential for the adequate design of mixing systems. The mass transfer rate can be quantitatively defined as the product of the volumetric mass transfer coefficient (k_La) and the driving force, which is the difference between the saturation concentration of gas and its actual concentration in the liquid phase ($C^* - C(t)$). Accordingly, k_La can affect operations by limiting productivity in various ways, including by changing the rate and, possibly, the selectivity.

The volumetric mass transfer coefficient is very sensitive to the hydrodynamics in the reactor, and predicting the coefficient is extremely difficult due to the complexity of the gas/liquid flows in STRs. Ideally, a uniform k_La and driving force inside STRs are desirable during scale-up. While there is a distribution of k_La due to variations in the hydrodynamics governing laboratory-scale STRs, the driving force can still be uniform when the mixing time is much shorter than the mass transfer time scale (Barigou and Greaves, 1996). However, this is not always true for large STRs, which leads to apparent changes in conversion to lower values, resulting in longer batch or residence times (cyanidation processes, for example) (Jafari, 2010) and higher production costs. Moreover, variations in the configuration of the reactor and the physiochemical and rheological properties of the flow may also hinder the transfer capacity of larger-scale STRs.

Numerous correlations have been proposed in the literature that express k_La as a function of the operating conditions of the STR, including power input per liquid volume (P_g/V_l) and superficial gas velocity (v_{sg}). They were often developed based on experimental data obtained using dynamic methods in laboratory-scale reactors. With this measurement technique, the concentration of dissolved gas over time is measured by a probe, which is calibrated beforehand, and the volumetric mass transfer coefficient is determined from the slope of the natural logarithm of these measured dissolved gas concentrations versus time, employing the least square method and assuming that the STR is "well mixed" (Kapic and Heindel, 2006; Linek et al., 1987; Van't Riet, 1979; Zhu et al., 2001). The empirical correlations of k_La are often expressed using the following form :

$$k_La = C(\frac{P_g}{V_l})^a(v_{sg})^b \tag{6.1}$$

The values of the constants inherent to this correlation that have been proposed by several authors for air/water flows inside an STR agitated by a single Rushton turbine are summarized in Table 6.1. The table also includes the range of operating conditions in which these parameters were determined. Since the power consumption per liquid volume is a function

of the superficial gas velocity, predictions of the k_La value using these correlations are even more complicated.

The discrepancies in the values of the exponents proposed by various authors can be attributed to differences in the geometries of the systems, the range of operating conditions, and the measurement techniques used. Xie et al. (2014) showed that predictions of these correlations can vary, with standard deviations ranging from 10 to 55%, even without a large difference in the scale of the STR. This means that these correlations are scale-dependent and that their application is limited for the design of large-scale reactors (Gabelle et al., 2011; Smith, 2006).

Understanding gas/liquid flow behavior in terms of operating regimes is vital and should be taken into account for successful STR scale-ups. Yawalkar et al. (2002) used experimental k_La values drawn from the literature for different sizes of STRs (T = 0.39 to 2.7 m) to take the effect of the flow regime into account and proposed the following correlation for k_La as a function of relative dispersion (N/N_{cd}) (with ±22% accuracy) :

$$k_La = 3.35(N/N_{cd})^{1.464}(v_{sg}) \tag{6.2}$$

where N and N_{cd} are the impeller rotational speed and the minimum rotational speed of the impeller for complete dispersion of the gas inside the STR, respectively. Nienow et al. (1977) proposed the following correlation for N_{cd} in STRs equipped with a Rushton turbine :

$$N_{cd} = \frac{4(Q_g)^{0.5}(T)^{0.25}}{D^2} \tag{6.3}$$

where Q_g, T, and D are the gas flow rate, the tank diameter and the impeller diameter, respectively. Kapic and Heindel (2006) used the same approach and developed the following correlation to predict k_La of STRs that operate in the effective flow regime :

$$k_La = 1.59(N/N_{cd})^{1.342}(v_{sg})^{0.93}(T/D)^{0.415} \tag{6.4}$$

Table 6.1: Constants of k_La correlations (Equation (6.1)) for air/water flows inside an STR agitated by a single Rushton turbine.

References	$v_{sg} * 10^3$ (m/s)	P_g/V_l (W/m^3)	$T(m)$	C	a	b
Smith et al. (1977)	4 - 46	20 - 5000	0.61 - 1.83	0.010	0.48	0.40
Van't Riet (1979)	5-40	300-3500	0.5	0.026	0.4	0.5
Linek et al. (1987)	2.12 - 2.42	100 - 3500	0.29	0.005	0.59	0.4
Hickman (1988)	2 - 17	50 - 3500	0.6	0.043	0.4	0.57
			2	0.027	0.59	0.68
Gagnon et al. (1998)	0 - 1.2	0.001 - 30	0.23	0.5	0.01	0.86
		30 - 10000		12.2	0.57	0.47
Gezork et al. (2001)	0 - 130	0 - 100000	0.29	0.005	0.59	0.27
Zhu et al. (2001)	1-7.5	100-1500	0.39	0.031	0.4	0.5
Kapic and Heindel (2006)	0.5-7.2	-	0.21	0.04	0.47	0.6

While these correlations may provide a better prediction for the k_La, at least up to the pilot-scale STRs, they do not provide any information on the local values of this parameter, which brings the concept of imperfect mixing into play.

The effects of imperfect mixing on the performance of reactors have been well characterized by the concept of residence time distribution (RTD) based on the pioneering work by Danckwerts (1953). Models based on combinations of well-mixed reactors (compartments) are often used to simulate observed RTD data (Kiared et al., 1997; Ranade, 2002; Utgikar, 2009). Relating reactor design, scale, and operating conditions to performance requires many experiments to fit the parameters of the models. Moreover, some concerns still need to be addressed, including the cost of the experimental methods and their scale limitations. Many processes involve high temperatures, high pressures and hazardous conditions for which the acquisition of detailed experimental data is not practical (Bashiri et al., 2015).

Thanks to the availability of powerful computers, CFD is being increasingly used to study the effects of hydrodynamics on the performance of reactors. Since it is important to take the local volumetric mass transfer coefficient into account, several studies have recently been carried out to predict local values of this parameter inside STRs using a coupled Eulerian-Eulerian approach and a population balance model (PBM) to describe their spa-

tial and temporal evolution (Gelves et al., 2014; Gimbun et al., 2009; Kerdouss et al., 2006, 2008; Laakkonen et al., 2006b; Moilanen et al., 2008; Petitti et al., 2013; Ranganathan and Sivaraman, 2011).

While full multiphase CFD simulations that take the evolution of bubble sizes and turbulent eddies into account can help to shed light on the mechanisms governing gas/liquid mixing operations, they suffer from several shortcomings. The enormous computational requirements for multiphase models coupled with population balance models (PBMs) make it difficult to use meshes that are fine enough for adequate simulations. This generally leads to an under-prediction of the turbulent energy dissipation rate (Coroneo et al., 2011; Deglon and Meyer, 2006). Since bubble breakage and coalescence kernels are functions of the liquid turbulent energy dissipation rate (Sajjadi et al., 2012), the accuracy of the predicted bubble size distributions and their mean values are significantly reduced by under-predictions of this parameter (Laborde-Boutet et al., 2009).

To mitigate the computational time issue of the coupled CFD-PBM approach, Laakkonen et al. (2006a, 2007a,b) developed a multiscale model to predict the local gas hold-up, bubble size distribution and mass transfer coefficient of two STRs. In their model, the tanks were divided into a limited number of ideally mixed compartments or zones that were connected to each other. The liquid flow rates between the compartments and the average values of the liquid turbulent dissipation rates inside each compartment were passed along to a meso-scale PBM. These quantities were obtained by single-phase CFD simulations and, when the gas flow rates were high, they were further modified to take the change in flow fields due to presence of the gas phase into account (Laakkonen et al., 2007b). However, several parameters of the bubble coalescence and breakage models were tuned to fit the experimental measurements. Moreover, different sets of parameters were used for various ranges of operating conditions. Wang et al. (2005) also showed that predictions of bubble size distributions by PBMs are totally dissimilar when different bubble breakup and coalescence models are used, revealing the uncertainty in their application due to the present state of understanding of breakage

and coalescence phenomena. These issues limit the use of this modeling approach for design purposes and have given rise to many on-going research endeavors (Ramkrishna and Singh, 2014).

Some effort has gone into developing theoretical predictions of k_La by tailoring the operating conditions to mass transfer theories. These methods successfully predict the values of the overall k_La for bubble columns (Kawase et al., 1987, 1992; Sánchez Mirón et al., 2000), airlifts (Sánchez Mirón et al., 2000; Tobajas et al., 1999), and STRs (Garcia-Ochoa and Gomez, 2004; Kawase et al., 1992) of different sizes and under various operating conditions. For instance, Garcia-Ochoa and Gomez (2004) used Higbie's penetration theory of mass transfer (Higbie, 1935) and Kolmogorov's theory of turbulence to predict k_L. Impeller power consumption was used to estimate the average value of the turbulent energy dissipation rate inside the system and thus predict the average value for k_L. The values of the global interfacial areas were calculated from a theoretical equation for gas hold-up and the mean size of the gas bubbles. While the predictions of the model were in reasonable agreement with experimental data and other empirical correlations for both Newtonian and non-Newtonian fluids, they were limited to the overall value of k_La in STRs and could not provide any information regarding local values.

The goal of the current study was to introduce a new approach that combines the concepts of multiscale modeling, mass transfer and turbulent theories to predict the local values of the volumetric mass transfer coefficient. In this model, the STR is divided into a limited number of characteristic zones, or compartments, based on their gas/liquid flow structures. The variables of the theoretical mass transfer and specific interfacial area models in each compartment are determined based on simplified and less computationally intensive CFD simulations for different operating conditions and scales of the STR. The simulations were performed using a uniform, mono-dispersed bubble size throughout the STR. Many studies have shown that this approach can satisfactorily predict the turbulent flow field and gas hold-up compared to experimental data (Deen et al., 2002; Khopkar et al., 2006, 2005; Khopkar

and Ranade, 2006; Morud and Hjertager, 1996; Scargiali et al., 2007).

The first part of this paper is devoted to introducing the main steps for building this model in detail. The adequacy of model predictions at each level is then assessed by comparing them with experimental data in the literature that were obtained using various measurement techniques. Following the validation step, the effects of operating conditions and scale-up on the local volumetric mass transfer coefficient inside the STRs are analyzed. Lastly, the possible implications of this model for scale-up studies are discussed.

6.2 Development of multiscale model

In this section, the models involved in different scales are discussed in detail. First, Subsection 6.2.1 explains the compartmentalization of the STR into five characteristic zones based on already published experimental and numerical findings. Subsection 6.2.2 introduces the methods based on mass transfer and isotropic turbulence theories that link the local hydrodynamics to the volumetric mass transfer coefficient. Subsection 6.2.3 presents the methodology for CFD modeling of the gas/liquid flow inside the STR, including the governing equations and numerical strategies. Lastly, Subsection 6.2.4 describes the algorithm that combines all this information to provide the volumetric mass transfer coefficient values in each meso-scale compartment and the overall value for the whole STR.

6.2.1 Compartmentalization

Radial flow impellers are often used for gas dispersion purposes (Bakker et al., 1994). The spatial variations of local hydrodynamics of turbulent gas/liquid flows generated by them inside the STR can be described by five characteristic compartments (Figure 6.1) in order to establish the flow structure.

In compartment I, the bubbles are small (Alves et al., 2002; Barigou and Greaves, 1992; Takahashi et al., 1992; Takahashi and Nienow, 1993) due to the high turbulent energy dissipation rate (Bashiri et al., 2014). In this compartment, gas hold-up is relatively high due

to the continuous flow of the gas toward the wall of the STR through the discharge of the impeller and gas cavities behind the impeller blades. This compartment is axially extended to 1.5-times the blade height above and below the impeller plane, and to the edges of baffles in the radial direction (Bashiri et al., 2014; Lee and Yianneskis, 1994).

In compartment II, where most of the bubble coalescence is completed (Alves et al., 2002) and the turbulent energy dissipation rate is lower (Bashiri et al., 2014; Vakili and Esfahany, 2009), the mean bubble size increases toward its equilibrium value in the bulk of the STR (Alves et al., 2002; Barigou and Greaves, 1992; Parthasarathy et al., 1991). In this compartment, gas hold-up is also high due to gas accumulation near the baffles, and above and below the impeller plane (Khopkar et al., 2005; Mueller and Dudukovic, 2010). The boundaries of this compartment are defined as ranging from the edges of baffles radially to the wall of the STR and axially to the planes where the value of the liquid turbulent energy dissipation rate reaches its average value in the bulk of the STR.

Compartment III is the part of the STR located above the gas sparger. The bubble formation process at the orifice of the sparger controls the mean bubble size in this compartment, which is characterized by a relatively larger mean bubble size and higher gas hold-up. It is radially extended to the radius of the ring sparger and axially extended from the sparger plane up to the lower horizontal boundary of compartment I.

The two remaining zones (compartments IV and V) are those inside the STR with the lowest liquid turbulent energy dissipation rate (Bashiri et al., 2014) and where the bubbles reach their stable size (Alves et al., 2002; Barigou and Greaves, 1992; Parthasarathy et al., 1991). It should be noted that when the gas/liquid STR is not operating at the complete dispersion flow regime, compartment V will make an insignificant contribution to the overall gas/liquid mass transfer inside the system (Middleton, 1992). In the next subsection, the models that establish a relation between k_La and the local hydrodynamics of the turbulent gas/liquid flow are discussed in detail.

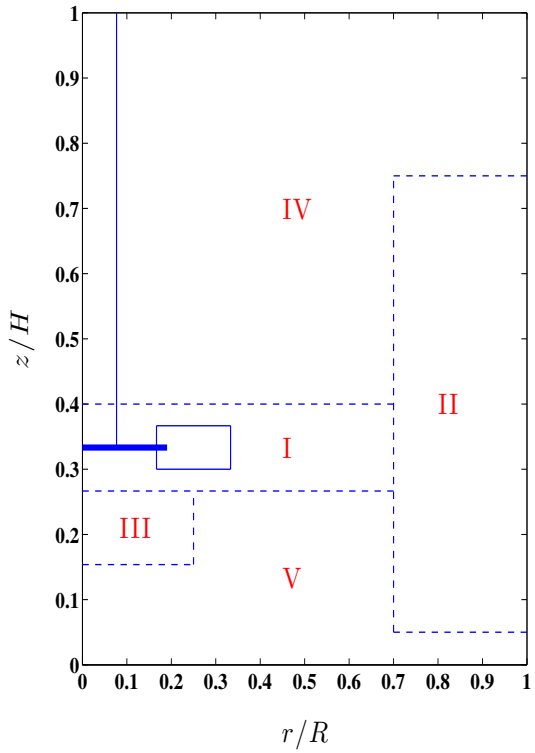

Figure 6.1: Characteristic compartments inside an STR agitated by a radial flow impeller.

6.2.2 Mass transfer models

The volumetric mass transfer coefficient ($k_L a$) is often measured experimentally as one coefficient, while it actually consists of two parts, namely the liquid-side mass transfer coefficient, k_L (transfer rate per unit area), and the specific interfacial area, a, which is defined as the transfer area per unit volume. Theoretical models that have been developed to bridge the gap between local hydrodynamics, k_L and a are discussed next.

Mass transfer coefficient (k_L) models

The two-film theory of Whitman (1923) is commonly used to illustrate the concept of mass transfer coefficient. This theory states that diffusion is a steady-state process, and it assumes that mass transfer from a gas phase into a liquid phase can be described by molecular diffusion through two stagnant films of gas and liquid on both sides of the gas/liquid interface. By applying Fick's first law, which assumes a constant concentration gradient through the

films, the following formula can be obtained for the liquid-side mass transfer coefficient :

$$k_L = \frac{D_A}{\delta_f} \tag{6.5}$$

where D_A and δ_f are the molecular diffusivity and the liquid film thickness, respectively. Despite the fact that this formula provides a simple relation between the physical properties of the liquid (i.e., molecular diffusivity (D_A)) and k_L, it is of limited use for STRs for two main reasons. First, the film thickness is not known and, second, there is no stagnant film surrounding the bubbles in turbulent flows (Clift et al., 2005).

To overcome these shortcomings, Higbie (1935) proposed the so-called penetration theory in which surface renewal occurs due to the continuous displacement of liquid turbulent eddies at the gas/liquid interface. The main assumption of this theory is that all liquid eddies that reach the gas/liquid interface have a constant exposure time. Unlike the two-film theory of mass transfer, with the penetration theory, the exposure time of liquid eddies to mass transfer is very short in order for a steady-state concentration gradient to develop. Fick's second law thus represents this unsteady-state diffusion of a solute in an eddy. Applying proper boundary conditions and solving a differential equation of transient diffusion, the average mass transfer coefficient is derived as follows :

$$k_L = 2\sqrt{\frac{D_A}{\pi\theta}} \tag{6.6}$$

where θ is the exposure time of the liquid eddies at the gas/liquid interface. While this exposure time is unknown, it can be estimated based on the ratio of the eddy length scale, η, and the velocity scale, u_η. These two parameters are functions of the liquid turbulent energy dissipation rate (ε) and the liquid kinematic viscosity (ν) following Kolmogorov's theory of isotropic turbulence :

$$\eta = (\frac{\nu^3}{\varepsilon})^{1/4} \tag{6.7}$$

and

$$u_\eta = (\nu\varepsilon)^{1/4} \tag{6.8}$$

Consequently, θ is estimated as follows :

$$\theta = \frac{\eta}{u_\eta} = (\frac{\nu}{\varepsilon})^{1/2} \tag{6.9}$$

By substituting equation (6.9) into equation (6.6), the following formula is obtained :

$$k_L = 2\sqrt{\frac{D_A}{\pi}}(\frac{\varepsilon}{\nu})^{1/4} \tag{6.10}$$

The penetration model was further refined by Danckwerts (1951) in order to take variations of the exposure time of the liquid eddies at the gas/liquid interface into account. Two types of model exist based on this refinement. For the first model, the mean velocity of the liquid relative to the bubble (i.e., the slip velocity) and the rigidity of the bubble surface are assumed to control surface renewal. For rigid bubbles ($d_b < 1\ mm$), Frössling (1938) proposed the following equation for k_L (Alves et al., 2004) :

$$k_L = C'\sqrt{\frac{v_{sl}}{d_b}}D_A^{2/3}\nu^{-1/6} \tag{6.11}$$

where C', v_{sl}, and d_b are the model constant, the slip velocity, and the bubble diameter, respectively. Alves et al. (2004) proposed a model that is an extension of Higbie's penetration theory for bubbles with mobile surfaces (large bubbles), by replacing θ with d_b/v_{sl} in equation (6.6) as follows :

$$k_L = 1.13\sqrt{\frac{v_{sl}D_A}{d_b}} \tag{6.12}$$

The second model is called the eddy cell model. It assumes that surface renewal is dictated by the small-scale eddies of the turbulent flow field rather than the slip velocity. Lamont and

Scott (1970) proposed an eddy cell model based on this assumption and used Kolmogorov's theory of isotropic turbulence as follows :

$$k_L = C_1 \sqrt{D_A} (\frac{\varepsilon}{\nu})^{1/4} \tag{6.13}$$

where C_1 is the model constant. Various authors have reported different values for C_1 (0.50 (Laakkonen et al., 2006a), 0.301 (Kawase et al., 1992), 0.4 (Lamont and Scott, 1970), 0.592 (Prasher and Wills, 1973) and 0.523 (Linek et al., 2004)).

Linek et al. (2004) thoroughly reviewed these two models of the mass transfer coefficient and concluded that the equation based on the eddy cell model (equation (6.13)) is more reliable for predicting k_L for both coalescent and non-coalescent media inside STRs. Laakkonen et al. (2007b) suggested that C_1 equals 0.46 for air/water flow in an STR agitated by a Rushton turbine.

Specific interfacial area (a)

The specific interfacial area (a) is based on the total interfacial area in the gas/liquid dispersion (A) and the volume of dispersion (V_d) :

$$a = \frac{A}{V_d} \tag{6.14}$$

The specific area is a function of the bubble mean Sauter diameter (d_{32}) and the gas hold-up (α_g). Assuming spherical bubbles, it is obtained by :

$$a = \frac{6\alpha_g}{d_{32}} \tag{6.15}$$

When gas bubbles move through a turbulent flow field inside an STR, there is a maximum or equilibrium size bubble diameter ($d_{b,max}$) that can be determined by applying a force balance to the bubble. These forces include (1) shear or disruptive forces that make the bubble shape unstable, possibly leading to the break up of the bubble into smaller bubbles,

(2) the surface tension force, which acts on the bubble and forces it to stabilize in a spherical shape, and (3) the viscous resistance in the gas phase to bubble deformations. The last force is negligible compared to the surface tension and shear forces. Hinze (1955) developed a theory that was originally intended for liquid/liquid dispersions, in which the turbulent fluctuations generate a disruptive shear force that is balanced by a stabilizing surface tension force. When the ratio of these two forces exceeds the critical value, the so-called critical Weber number, bubbles go through the breakage process. The Weber number (We) can be assumed to have a constant value in the equilibrium state :

$$We = \frac{\tau d_{b,max}}{\sigma} \tag{6.16}$$

where τ and σ are the turbulent shear stress and surface tension, respectively. By considering Kolmogorov's theory of isotropic turbulence, the liquid turbulent shear stress can be expressed as a function of the turbulent fluctuation velocity (u') as follows :

$$\tau = \rho_l u'^2 \tag{6.17}$$

where ρ_l is liquid density. The turbulent fluctuation velocity is a function of the turbulent eddy length scale at equilibrium (l) and the liquid turbulent energy dissipation rate :

$$u' = (\varepsilon l)^{1/3} \tag{6.18}$$

where l can be assumed to have the same order of magnitude as $d_{b,max}$ (Garcia-Ochoa and Gomez, 2004). By replacing l by $d_{b,max}$ in equation (6.18) and by combining equations (6.16), (6.17), and (6.18), the maximum stable bubble size can be expressed as a function of the physical properties of the flow and the turbulent energy dissipation rate :

$$d_{b,max} = C'' \frac{\sigma^{3/5}}{\rho_l^{3/5} \varepsilon^{2/5}} \tag{6.19}$$

The mean Sauter diameter (d_{32}) can be assumed to be proportional to $d_{b,max}$ (Alves et al., 2002; Takahashi and Nienow, 1993). Thus, d_{32} can be predicted by the following equation :

$$d_{32} = C_2 \frac{\sigma^{3/5}}{\rho_l^{3/5} \varepsilon^{2/5}} \tag{6.20}$$

Wang et al. (2006) and Zhang et al. (2008) proposed that the value of C_2 is equal to 0.493 for air/water dispersions.

Coalescence can be promoted in some regions inside STRs by high gas hold-up values. In the case of air/water mixing systems agitated by a single Rushton turbine, experimental results have shown that most bubble coalescence is complete by the time the impeller discharge stream reaches the baffles and wall of the STR (Alves et al., 2002; Barigou and Greaves, 1992; Takahashi and Nienow, 1993) where the gas hold-up is relatively high. To include the effect of gas hold-up on the mean Sauter diameter in these regions, equation (6.20) can be further modified on empirical grounds (Alves et al., 2002; Calderbank, 1958) :

$$d_{32} = C_2 \left(\frac{\sigma^{3/5}}{\rho_l^{3/5} \varepsilon^{2/5}} \right) \alpha_g^{1/2} \tag{6.21}$$

Takahashi et al. (1992) and Alves et al. (2002) showed experimentally that the value of the exponent of ε in equation (6.21) for the region close to the impeller is between 2/5 and 1/5.

For low gas inputs, the size of bubbles above the gas sparger (d_s) is dictated by the orifice diameter (d_o) and the surface tension. More precisely, the mean bubble diameter in this region can be determined by a force balance at the orifice of the sparger :

$$\pi d_o \sigma = \frac{\pi}{6} d_s^3 g (\rho_l - \rho_g) \tag{6.22}$$

where ρ_g and g are the gas density and the gravitational acceleration, respectively. In fact, bubbles are formed at the orifice of the sparger when the buoyancy force on the bubbles is greater than the surface tension force acting at the periphery of the orifice. By re-arranging

equation (6.22), the average bubble size in this region can be derived as follows (Kerdouss et al., 2008) :

$$d_s = [\frac{6\sigma d_o}{g(\rho_l - \rho_g)}]^{1/3} \tag{6.23}$$

This equation holds for very low gas flow rates (Green et al., 2008). Bhavaraju et al. (1978) proposed the following correlation for high gas flow rates :

$$d_s = 3.23 d_o Re_o^{-0.1} Fr_o^{0.21} \tag{6.24}$$

where Re_o and Fr_o are the modified orifice Reynolds number and the orifice Froude number, respectively :

$$Re_o = \frac{4\rho_l Q_{g,o}}{\pi d_o \mu_l} \tag{6.25}$$

$$Fr_o = \frac{Q_{g,o}^2}{g d_o^5} \tag{6.26}$$

and where $Q_{g,o}$ and μ_l are the gas flow rate at the orifice and the liquid dynamic viscosity, respectively. Figure 6.2 shows the experimental data of bubble size at the sparger reported by Laakkonen et al. (2007a) compared to the predictions of equation (6.24) for two scales of STR (14 and 200 liters). The predictions of the proposed model for the bubble size at the sparger are in excellent agreement with the experimental data ($R^2 = 0.98$).

It comes from above that if the average value of the liquid turbulent energy dissipation rate and the average value of the gas hold-up are known in all the zones of the STR (these have been discussed in Subsection 6.2.1 and shown in Figure 6.1), the values of $k_L a$ can be determined in these regions. This will be discussed in greater detail in Subsection 6.2.4. CFD simulations of the mixing system can provide these data. The CFD modeling approach used in the current study is discussed in detail in the following subsection.

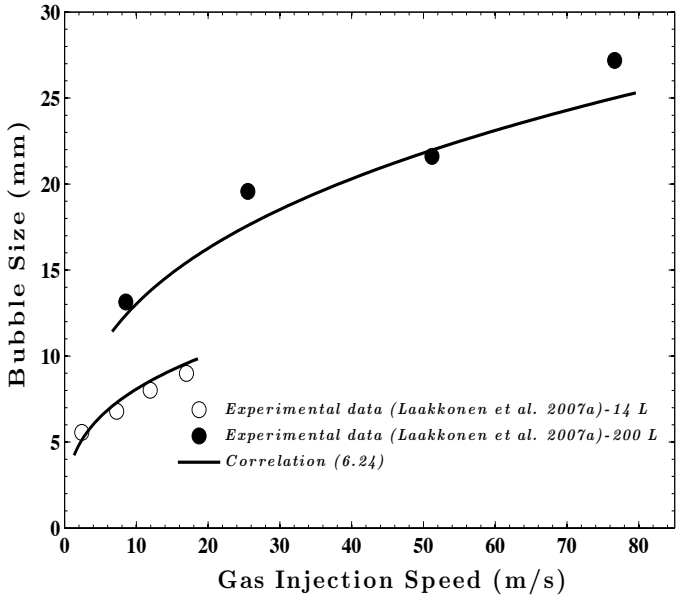

Figure 6.2: Measured and predicted mean bubble diameters in the sparger zone.

6.2.3 Modeling of the gas/liquid flow

The two-fluid Eulerian-Eulerian model was used in the current study to simulate turbulent gas/liquid flow. This model is commonly used to simulate the gas/liquid flow in STRs because it allows for calculations of a wide range of dispersed phase volume fractions (Gosman et al., 1992; Morud and Hjertager, 1996). In this approach, both the continuous and dispersed phases are modeled in the Eulerian frame of reference as interpenetrating continua identified by their local average volume fractions. The mass and momentum balance equations are solved for each phase separately. The momentum equations of the phases interact with each other through the inter-phase momentum exchange terms.

Governing equations

The continuity and momentum equations for each phase ($i = l$ or g) can be written as :

$$\frac{\partial}{\partial t}\left(\rho_i \alpha_i\right) + \nabla.\left(\rho_i \alpha_i \bar{u}_i\right) = 0 \tag{6.27}$$

$$\frac{\partial}{\partial t}\left(\rho_i \alpha_i \bar{u}_i\right) + \nabla.\left(\rho_i \alpha_i \bar{u}_i \bar{u}_i\right) = -\alpha_i \nabla p + \nabla.\overline{\tau}_{eff,i} + \rho_i \alpha_i g \pm F_D + F_i \tag{6.28}$$

where $\overline{u_i}$ and $\overline{\tau}_{eff,i}$ are the average velocity and the Reynolds stress tensor, respectively. The pressure (p) is shared by both phases and the volume fraction of the phases add up to unity in each control volume :

$$\alpha_l + \alpha_g = 1 \tag{6.29}$$

The Reynolds stress tensor based on the Boussinesq hypothesis is given by :

$$\overline{\tau}_{eff,i} = \alpha_i \mu_{eff,i}(\nabla \bar{u}_i + \nabla \bar{u}_i^T) - \frac{2}{3}\alpha_i(\rho_i k_i + \mu_{eff,i}\nabla.\bar{u}_i)\overline{\overline{I}} \tag{6.30}$$

The effective viscosity of the continuous (liquid) phase is comprised of three contributions, namely the dynamic viscosity, the turbulent viscosity (μ_{tl}) and an extra term for the bubble-induced turbulence ($\mu_{BI,l}$) :

$$\mu_{eff,l} = \mu_l + \mu_{tl} + \mu_{BI,l} \tag{6.31}$$

The dispersed turbulent model is used for turbulence modeling. More precisely, the turbulent viscosity of the liquid phase is calculated using the $k-\varepsilon$ turbulence model and by solving the following transport equations for the turbulent kinetic energy (k) and the turbulent energy dissipation rate (ε) :

$$\frac{\partial}{\partial t}\left(\alpha_l \rho_l k\right) + \nabla.\left(\alpha_l\left(\rho_l \bar{u}_l k - \left(\mu_l + \frac{\mu_{tl}}{\sigma_k}\right)\nabla k\right)\right) = \alpha_l\left(G - \rho_l \varepsilon\right) \tag{6.32}$$

$$\frac{\partial}{\partial t}\left(\alpha_l \rho_l \varepsilon\right) + \nabla.\left(\alpha_l\left(\rho_l \bar{u}_l \varepsilon - \left(\mu_l + \frac{\mu_{tl}}{\sigma_\varepsilon}\right)\nabla k\right)\right) = \alpha_l \frac{\varepsilon}{k}\left(C_{\varepsilon 1} G - C_{\varepsilon 2}\rho_l \varepsilon\right) \tag{6.33}$$

where G corresponds to the production of the turbulent kinetic energy. The turbulent viscosity of the liquid phase is then calculated using the values of k and ε as follows :

$$\mu_{tl} = c_\mu \rho_l \frac{k^2}{\varepsilon} \tag{6.34}$$

The turbulent viscosity induced by the gas bubbles ($\mu_{BI,l}$) can be determined using the Sato model (Sato and Sekoguchi, 1975) :

$$\mu_{BI,l} = c_{\mu p} \rho_l \alpha_g d_b |\bar{u_g} - \bar{u_l}| \tag{6.35}$$

where $c_{\mu p}$ is a constant of the model.

The effective viscosity of the dispersed phase is calculated as a combination of the gas dynamic and turbulent viscosities :

$$\mu_{eff,g} = \mu_g + \mu_{tg} \tag{6.36}$$

The turbulent viscosity of the gas phase is related to the turbulent viscosity of the liquid phase according to the following equation (Sato and Sekoguchi, 1975) :

$$\mu_{tg} = \frac{\rho_g}{\rho_l} \mu_{tl} \tag{6.37}$$

No extra model is used for the dispersed phase. The values of the constants inherent to all these models that are commonly used in the literature for simulations of gas/liquid STRs are summarized in Table 6.2 (Ansys, 2013).

Table 6.2: Values of the constants of the turbulence model.

Parameters	$C_{\epsilon 1}$	$C_{\epsilon 2}$	σ_k	σ_ϵ	C_μ	$C_{\mu p}$
values	1.44	1.92	1.0	1.3	0.09	0.6

The effects of lift, virtual mass, Basset history and turbulent dispersion forces are negli-

gible compared to the drag force (Khopkar et al., 2005; Scargiali et al., 2007; Zhang et al., 2013). Their effects were thus not considered in the current study, and only the drag force was included in the momentum equations, as in previous studies (Bakker and Akker, 1994; Gimbun et al., 2009; Kerdouss et al., 2006; Lane et al., 2005; Morud and Hjertager, 1996). The term F_i in equation (6.28) represents the centrifugal and Coriolis forces that are applied in the rotating reference frame. The drag force is given by (Ansys, 2013) :

$$F_D = -\frac{3\alpha_l \alpha_g C_D \mid \bar{u}_g - \bar{u}_l \mid (\bar{u}_g - \bar{u}_l)}{4d_b} \tag{6.38}$$

It was found experimentally that the value of the drag coefficient (C_D) is significantly affected by the prevailing turbulence (Brucato et al., 1998; Poorte and Biesheuvel, 2002). In the current study, the modified Brucato drag model for turbulent gas/liquid flow was used, which considers the effect of micro-scale turbulence on the inter-phase drag as follows (Khopkar and Ranade, 2006) :

$$\frac{C_D - C_{D0}}{C_{D0}} = 6.5 \times 10^{-6} (\frac{d_b}{\eta})^3 \tag{6.39}$$

where C_{D0} is the drag coefficient in a stagnant fluid. The Schiller and Naumann drag model has been commonly used to determine this drag coefficient (Gelves et al., 2014; Laborde-Boutet et al., 2009). However, this model was developed for rigid spherical particles and, as such, can be just as valid for small bubbles ($\approx 1\ mm$ or less) (Montante et al., 2008). Nevertheless, larger bubbles are distorted and become ellipsoidal or cap-shaped. In the distorted regime, the drag coefficient depends on both the bubble Reynolds number, Re_b, and its shape, which can be represented by the Eötvös number (E_o) (Clift et al., 2005). The correlation of Tomiyama et al. (1998) was used in the current study to take the bubble shape into account :

$$C_{D0} = max[min(\frac{24}{Re_b}(1 + 0.15 Re_b^{0.687}), \frac{72}{Re_b}), \frac{8}{3}\frac{E_o}{E_o + 4}] \tag{6.40}$$

where

$$E_o = \frac{g(\rho_l - \rho_g){d_b}^2}{\sigma} \tag{6.41}$$

$$Re_b = \frac{\rho_l u_{slip} d_b}{\mu_l} \tag{6.42}$$

and where u_{slip} is the slip velocity :

$$u_{slip} = |\bar{u}_l - \bar{u}_g| \tag{6.43}$$

Numerical strategy

In this subsection, the numerical strategy used in this work to solve the equations that were introduced in Subsection 6.2.3 is provided.

GAMBIT software was used to model and discretize the mixing systems into structured hexahedral cells. Hexahedral cells rather than tetrahedral cells were used in order to provide more accurate predictions of 3D turbulent gas/liquid flows with minimum numerical diffusion. The impeller rotation was modeled using the multiple reference frame (MRF) technique. Water and air were used as continuous and dispersed phases, respectively. The properties used in the simulations were as follows : $\rho_l = 998.2\ kg/m^3$, $\mu_l = 1 \times 10^{-3}$ Pa s, $\rho_g = 1.225\ kg/m^3$, μ_g =1.79$\times\ 10^{-5}$ Pa s and σ=73 mN/m.

Simulations were carried out in two stages. In the first stage, the solution of the steady-state turbulent liquid phase flow was obtained without gas sparging. The adequacy of the numerical models to predict the turbulent single phase flow was thoroughly assessed in our previous publication using the radioactive particle tracking (RPT) technique (Bashiri et al., 2015). In the second stage, the results of the first stage were used as an initial condition to obtain a solution for the unsteady-state turbulent gas/liquid flow inside the STR.

It should be noted that the geometries and meshes were prepared with a headspace in order to provide sufficient room for liquid expansion. More precisely, the liquid initially filled

the STR up to 65% of the total height (gas hold-up= 0) and was topped with the liquid-free headspace (gas hold-up= 1). The liquid surface could then freely expand and move while the gas was continuously sparged into the system. The top boundary of the headspace was set as a pressure outlet. A no-slip condition and standard wall function were used to specify the wall boundary conditions. The part of the sparger where the gas was introduced into the STR was defined as a velocity inlet. Since the volumetric flow rate of the gas was known for each case, the inlet velocity of the gas could be determined easily. The liquid velocity was set to zero at this boundary.

ANSYS FLUENT version 15.0 code based on the finite volume method was used to numerically solve the equations that were introduced in Subsection 6.2.3. Pressure-velocity coupling was performed with the SIMPLE algorithm. For all simulations, a second-order implicit transient solver was used with the QUICK scheme for the volume fraction and the second-order spatial upwind scheme for all the other variables. The use of a high-order numerical scheme is important for numerical simulations of turbulent multiphase flows in order to minimize the amount of numerical diffusion (Laborde-Boutet et al., 2009).

All the iteration residuals were set to fall below at least 1×10^{-4} at each time step to achieve good convergence. Additional criteria were set to be satisfied in order to ensure that the steady-state condition was established. These criteria included reaching the stabilized value of the volume averaged gas hold-up inside various predefined zones in the system and obtaining the perfect balance between the mass flow rate of gas entering and leaving the STR. The time to reach all these conditions was typically about the time needed for 100 rotations of the impeller. The simulations were subsequently run for the same time period in order to ensure that the volume averaged gas hold-up and the liquid turbulent energy dissipation rate inside the predefined zones did not change.

6.2.4 Framework of the multiscale model

Figure 6.3 shows the various steps of the multiscale model for finding the average values of the volumetric mass transfer coefficient (k_La) in the different zones of STRs. In the first step, the distributions of the gas hold-up and the liquid phase turbulent energy dissipation rate are obtained using gas/liquid CFD simulations based on a mono-dispersed bubble size. The mean bubble size for each simulation case is estimated based on the correlations developed by Alves et al. (2002) (for small-diameter STRs) and Calderbank (1958) (for large-diameter STRs ($T \geq 1\ m$)).

In the second step, the adequacy of the physical models (*e.g.* turbulent and drag models) and the numerical strategy (*e.g.* grid size) for the simulations of the turbulent gas/liquid flow inside STRs are assessed by benchmarking their predictions with available experimental data. As Coroneo et al. (2011) stated, RANS-based turbulent models slightly under-predict the average value of ε in mixing systems, even when millions of cells are used. The local values of ε can be scaled by the total power input of the mixing system, which is equal to the sum of the specific impeller power consumption and gas expansion power.

In the third step, the average values of ε and α_g are calculated in each compartment. These average values are then passed along to correlations in order to predict the bubble mean Sauter diameter (d_{32}). More precisely, equation (6.21) is used to predict the mean d_{32} in compartments I-II due to the relatively high gas hold-up in these compartments, while equation (6.20) is used to predict the mean d_{32} in compartments IV-V. The mean bubble size in compartment III is estimated using equation (6.24).

In the fourth step, the values of the average specific interfacial area in each compartment are predicted based on the values of α_g and d_{32} using equation (6.15). The average values of k_L in each compartment are predicted using equation (6.13) with local values of ε. The average value of k_La in each compartment is obtained by multiplying the values of k_L and a.

In the fifth and final step, the overall value of k_La inside the STR is obtained by averaging

the values of all the compartments as follows :

$$\overline{k_L a} = \frac{\sum_{j=I}^{V} V_j (k_L a)_j}{\sum_{j=I}^{V} V_j} \tag{6.44}$$

where V_j and $(k_L a)_j$ are the volume and the average volumetric mass transfer coefficient in compartment j, respectively.

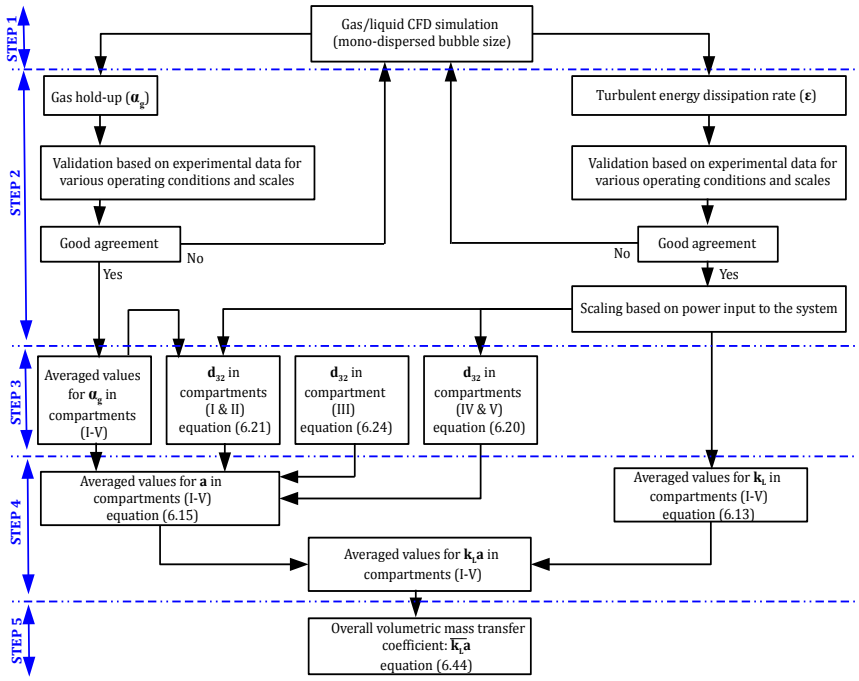

Figure 6.3: Multiscale model.

6.3 Results and discussion

In this section, the adequacy of the proposed multiscale model at different levels is assessed by benchmarking with available experimental data drawn from the literature. The specifications of all the simulations are summarized in Table 6.3. The experimental data were obtained using various techniques, including X-ray tomography (case 1 in Table 6.3) (Ford

et al., 2008), torque measurements (TM) (cases 2-6 in Table 6.3) (Laakkonen et al., 2007a), visual observations (VO) (cases 3-5 in Table 6.3) (Laakkonen et al., 2007a), digital photography (DP) (cases 2 and 4 in Table 6.3) (Laakkonen et al., 2007a), a capillary suction probe (CSP) (case 4 in Table 6.3) (Laakkonen et al., 2007a), and a dissolved oxygen probe (DOP) (cases 3-6 in Table 6.3) (Laakkonen et al., 2007b).

Ford et al. (2008) used X-ray tomography to measure local and global gas hold-up in a 7-liter gas/liquid STR agitated by a flat blade turbine (case 1 in Table 6.3). Since the profiles of the local gas hold-up and the maximum uncertainty of this technique in the prediction of local and global gas hold-ups were reported (i.e., ±15%) (Ford et al., 2008), the effects of grid size can be better analyzed. The rest of the experimental data were obtained by Laakkonen et al. (2007a,b) in two geometrically similar gas/liquid STRs (14 and 200 liters) agitated by a Rushton turbine (cases 2-6 in Table 6.3). More details on the geometries of the systems that the experimental data were obtained from can be found in the cited references. Moreover, a 1500-liter STR (case 7 in Table 6.3) that is geometrically similar to those in cases 2-6 was simulated in order to study the effects of scale-up.

6.3.1 Assessment of the CFD model

In this subsection, the adequacy of the CFD model for predicting local and global gas hold-ups and the average value of the liquid turbulent energy dissipation rate inside the STR are assessed. Good predictions of these quantities are required since the models used to predict the volumetric mass transfer coefficient are defined based on them, as discussed in Subsections 6.2.2 and 6.2.4.

Gas Hold-up

Gas hold-up is defined as the volumetric gas fraction in the STR. Adequate measurements or predictions of gas hold-up are required to reliably design and scale-up STRs. Global (or total) gas hold-up ($\overline{\alpha_g}$) can be determined visually by measuring the increase in liquid height

Table 6.3: Case studies for model validation and scale-up.

Case	**T (m)**	**N (RPM)**	**v_{sg} (cm/s)**	**d_b (mm) used in CFD simulations**	**Measurement technique** (Ford et al., 2008; Laakkonen et al., 2007a,b)	**Objective**	**Parameter**
1	0.21	350	0.43	3.5	X-ray tomography	validation and mesh sensitivity analysis	global and local gas hold-ups
2	0.26	700	0.3	2.8	DP,TM	validation and scale-up	bubble size and power consumption
3	0.63	300	0.74	3.1	VO, DOP, TM	validation and effects of operating conditions	global gas hold-up and mass transfer, power consumption
4	0.63	390	0.74	2.8	VO, DP, CSP, DOP, TM	validation and effects of operating conditions	global gas hold-up, bubble size, mass transfer and power consumption
5	0.63	390	0.32	2.6	VO, DOP, TM	validation and effects of operating conditions	global gas hold-up, mass transfer and power consumption
6	0.63	362	0.3	2.8	DOP, TM	validation and scale-up	mass transfer and power consumption
7	1.24	219	0.3	4	-	scale-up	mass transfer

due to gas sparging inside the STR :

$$\overline{\alpha_g} = \frac{H_D - H}{H_D} \tag{6.45}$$

where H and H_D are the heights of the liquid with no gas sparging and with gas sparging inside the STR, respectively. This method is subjective due to fluctuations of the liquid surface. To reduce measurement subjectivity, visual observations should be repeated for different locations. For instance, H_D can be measured at two diametrically opposite locations on the mid-planes between two adjacent baffles (Saravanan and Joshi, 1996). Several invasive and non-invasive methods have been developed in recent years to measure local gas hold-up. These methods all have inherent advantages and disadvantages that have been reviewed by Chaouki et al. (1997).

Effect of grid size on CFD predictions of gas hold-up

The experimental data obtained by Ford et al. (2008) was used to analyze the effects of grid size on the prediction of local gas hold-up. Three grid sizes, coarse ($0.5 * 10^6$ cells), medium ($0.7 * 10^6$ cells) and fine ($1.2 * 10^6$ cells), were considered to simulate case 1.

Figure 6.4 shows the predicted axial profiles of radially and azimuthally averaged gas hold-ups for all three grid sizes and values determined by X-ray tomography (Ford et al., 2008). In this figure, the dashed lines represent relative errors defined as follows :

$$\frac{predicted\ value - experimental\ value}{experimental\ value}(\%) \tag{6.46}$$

While the coarse grid predicted the shape of the gas hold-up profile qualitatively, it under-predicted the gas hold-up values in the impeller region and over-predicted it in the area above the impeller, compared with the experimental values. The prediction of the axial profile of the gas hold-up by the medium grid was significantly better than that of the coarse grid. However, the fine grid only provided a relatively small improvement compared to the medium grid.

All the grids provided reasonable predictions of global gas hold-up compared to the experimental value (3.5%). More precisely, the predicted gas hold-up for the coarse, medium, and fine grids were 3.21%, 3.32%, and 3.45%, respectively. The experimental value of the global gas hold-up also contained uncertainties as it was obtained by averaging local values (Ford et al., 2008). While the prediction of the global gas hold-up improved with the increase in the number of cells, the effect was less pronounced than the effect of the number of cells on local gas hold-up values. In fact, the over-predictions of local gas hold-up in some zones could be cancelled out by the under-predictions of local gas hold-up in other zones when calculating the global gas hold-up, which could mask an inadequate grid size.

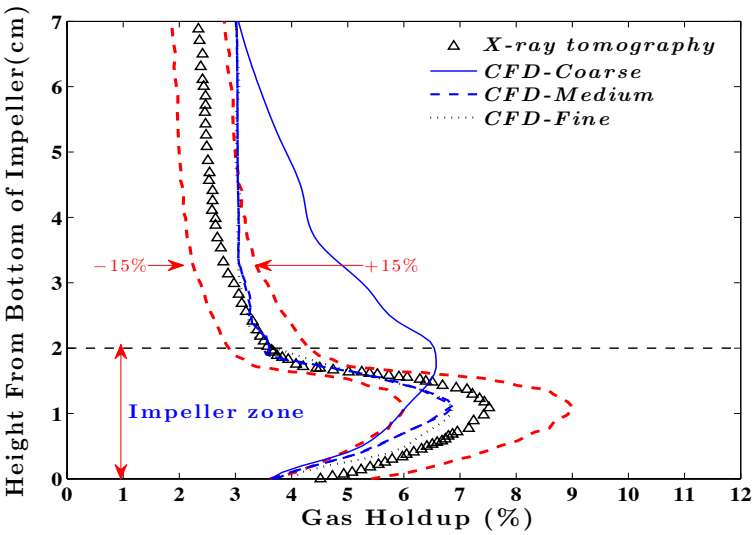

Figure 6.4: Effects of grid size on the predictions of the axial profiles of radially and azimuthally averaged gas hold-ups for three grid sizes (case 1). The X-ray tomography data was reported by Ford et al. (2008).

As discussed in Subsection 6.2.3, the level of turbulence affects the drag coefficient and, ultimately, the gas hold-up profile. Hence, accurate predictions of turbulent quantities that are quite sensitive to the number of cells in the solution domain are critical for the adequate calculation of the drag coefficient. As shown in this subsection, the medium and fine grids provided almost identical predictions for the local gas hold-up profile. All subsequent simulations (cases 2-7) were thus performed with $0.83 * 10^6$ cells (i.e., finer size than the medium

grid but coarser size than the fine grid) based on this mesh sensitivity analysis.

CFD predictions of global gas hold-up

The predicted global gas hold-ups for different STR sizes and operating conditions are compared to the experimental values measured by X-ray tomography (case 1) (Ford et al., 2008) and by visual observation (cases 3-5) (Laakkonen et al., 2007a) in Figure 6.5.

The CFD predictions of global gas hold-up are in good agreement (within less than 15%) with the experimental values, except for case 5 where there is a 25% over-prediction by the CFD model. Since the global gas hold-up is low in this case, the increase in the height of the liquid due to gas sparging is small based on equation (6.45). This can increase the uncertainty of the measurement of the global gas hold-up based on visual observations. This uncertainty can be magnified even more with a high impeller rotational speed (such as case 5) due to more intense fluctuations of the liquid surface. Saravanan and Joshi (1996) showed that the reproducibility of the visual determinations of global gas hold-up becomes significantly low at lower gas hold-ups ($\leq 3\%$).

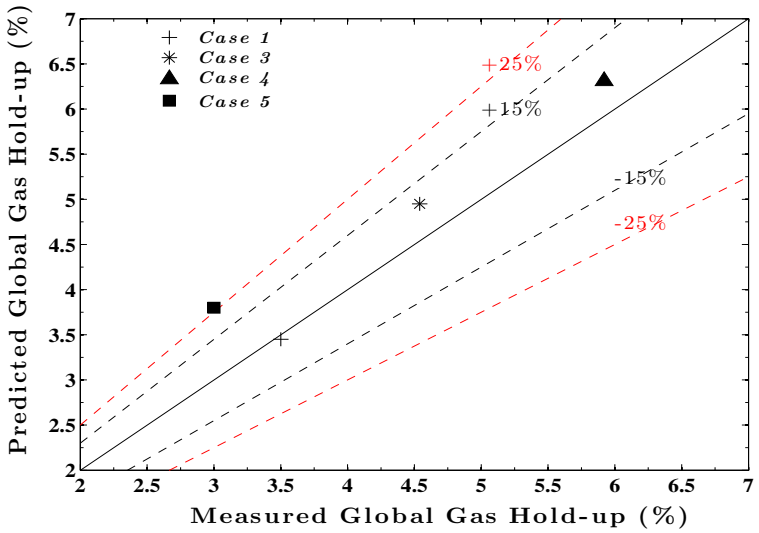

Figure 6.5: CFD predictions of global gas hold-up *vs.* experimental measurements of Ford et al. (2008) for case 1 and Laakkonen et al. (2007a) for cases 3-5.

CFD prediction of relative power demand

Relative power demand (RPD) is defined as the ratio of the gassed to the ungassed power consumption of the mixing system. It depends on the gas flow rate (Q_g) and on the impeller shape, diameter and rotational speed. It generally decreases in parallel with higher values of the gas flow number,

$$Fl_g = \frac{Q_g}{ND^3} \tag{6.47}$$

RPD can be determined based on the turbulent energy dissipation rate (ε) predicted by CFD as follows :

$$RPD = \frac{(\int_{V_d} \alpha_l \varepsilon dv)_{gassed}}{(\int_V \varepsilon dv)_{ungassed}} \tag{6.48}$$

where V_d is the total volume of the gas/liquid dispersion. As the calculated RPD is based on local values of (ε) predicted by CFD, it can show the adequacy of a computational model for predicting the level of turbulence (i.e., turbulent energy dissipation rate) inside the mixing system.

Figure 6.6 shows the comparison of the predicted RPD with the experimental values measured by Laakkonen et al. (2007a). As depicted in this figure, there is close agreement (discrepancy<10%) between the CFD predictions and the experimental measurements of RPD due to the use of fine grids and higher-order discretization schemes. This further justifies the adequacy of the grid size and numerical strategy in order to simulate the mixing system that was used by Laakkonen et al. (2007a).

It is worth pointing out that the total energy dissipated in the mixing system under gassed conditions can be obtained from the sum of the specific impeller power consumption, which is determined by the torque measurement, and the power input due to gas sparging estimated by gv_{sg} (Linek et al., 2012; Moucha et al., 2012). The small over-predictions of RPD by CFD could be due to over-predictions of the contribution of gas-induced pseudo-turbulence in the

liquid phase by the Sato model (equation (6.35)) compared to the values used to estimate the gas input power (i.e. from gv_{sg}).

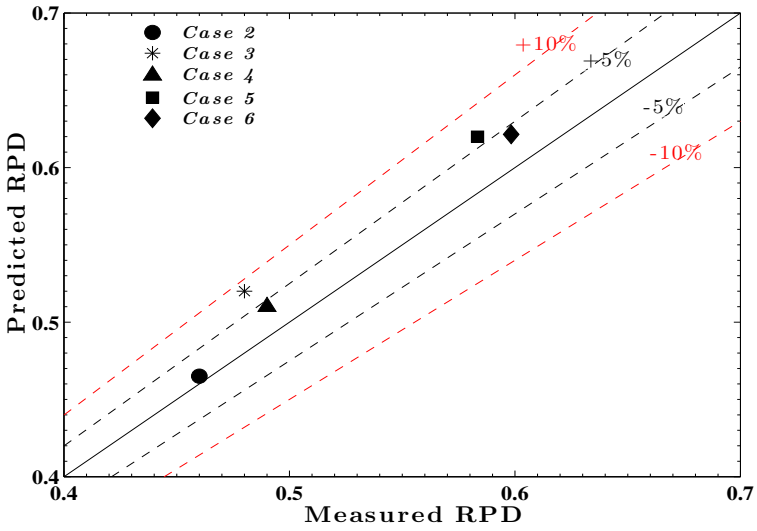

Figure 6.6: CFD predictions of relative power demand (RPD) *vs.* experimental measurements of Laakkonen et al. (2007a).

Overall, the parameters required for the multiscale model (i.e., gas hold-up and the turbulent energy dissipation rate) were predicted fairly well by the computational model despite the use of a mono-dispersed bubble size. In the next subsection, the ability of the multiscale model to predict the bubble size and the volumetric mass transfer coefficient is analyzed.

6.3.2 Assessment of the multiscale model

In this subsection, the mean bubble sizes predicted by the multiscale model for the compartments of the STR are compared to the experimental DP and CSP values measured by Laakkonen et al. (2007a). The predictions of the overall volumetric mass transfer coefficient by the multiscale model are then compared with the values measured by Laakkonen et al. (2007b) with a DO probe and several empirical correlations.

Bubble size

Figure 6.7 shows the predictions of the bubble mean Sauter diameter by the multiscale model compared to the values measured by Laakkonen et al. (2007a) for cases 2 (14 liters) and 4 (200 liters). Laakkonen et al. (2007a) used DP for locations close to the wall of the STR (compartment II) and CSP for a location in the bulk (compartment IV) of the larger STR (case 4). The experimental mean bubble size value in compartment I was measured in a location where the impeller discharge flow reached the STR wall. No experimental data are available for compartments III and V.

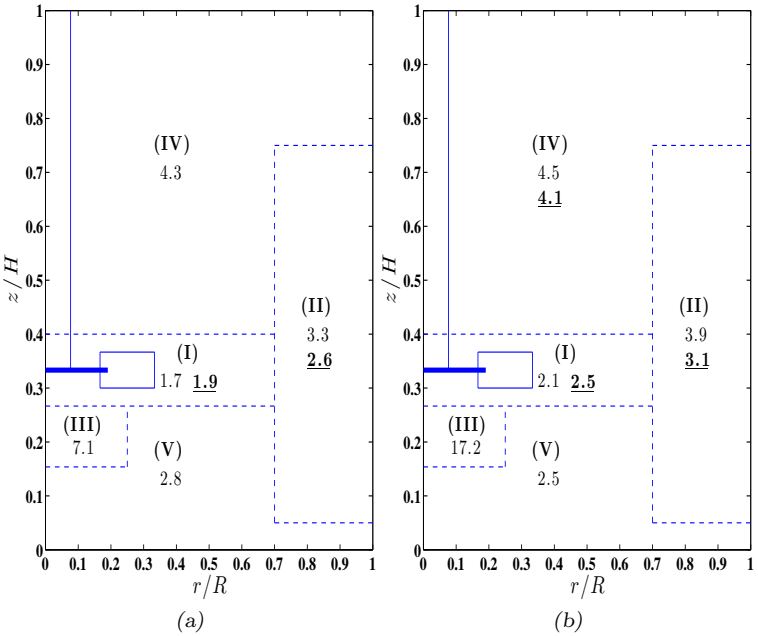

Figure 6.7: Predicted and experimental values of the bubble mean Sauter diameter (mm) inside the STR : (a) case 2, (b) case 4. The normal fonts are the predictions of the multiscale model, and underlined bold fonts are experimental values reported by Laakkonen et al. (2007a).

In general, the multiscale model predicts the values of mean bubble size in both STRs fairly well compared to the experimental data. Moreover, the experimental values of the mean bubble size in compartment II correspond to arithmetic means of all the experimental values reported by Laakkonen et al. (2007a) for this compartment.

In both cases, the smallest mean bubble size is in compartment I due to the high level of turbulence generated by the impeller rotation in this zone. The largest mean bubble size is in compartment III, where the mean size of the bubbles is controlled by the gas flow rate at the orifice of the sparger and the diameter of the orifice (equation (6.24)). It can be observed that the mean bubble size increases from the impeller discharge flow to the STR wall and then to the bulk of the STR. This structure of the mean bubble size inside STRs predicted by the multiscale model is in total agreement with the trend of local bubble size variations observed by Barigou and Greaves (1992), based on experimental measurements of bubble size distributions using CSP in an air/water mixing system agitated by a single Rushton turbine.

Overall volumetric mass transfer coefficient (k_La)

The overall volumetric mass transfer coefficient (k_La) was measured by Laakkonen et al. (2007b) using the dynamic gassing-in/gassing-out method with a polarographic DO probe. It should be noted that the values of k_La were not reported explicitly. However, the authors mentioned that the measured values of k_La were well fitted ($\pm 20\%$) with the correlations proposed by Yawalkar et al. (2002) and Kapic and Heindel (2006) (equations (6.2) and (6.4)).

The method described in Subsection 6.2.4 was used to determine the overall k_La inside the STR using equation (6.44). Figure 6.8a and b show the overall volumetric mass transfer coefficient values predicted by the multiscale model compared to the predictions of the empirical correlations (equation 6.1 and Table 6.1) and the experimental measurements of Laakkonen et al. (2007b), respectively. As can be seen in Figure 6.8a, there is a wide discrepancy (up to $\simeq 50\%$) between the values predicted by various correlations that are defined based on the specific gassed power consumption, P_g/V_l, and the superficial gas velocity, v_{sg} (equation (6.1)). In particular, the well-known correlation by Van't Riet (1979) markedly under-predicts the k_La compared to the other correlations. The predictions of the overall k_La by the mutltiscale model are in fairly close agreement with the values predicted by the correlations proposed by Linek et al. (1987) and Kapic and Heindel (2006).

Figure 6.8b shows that there is good correspondence between the predictions of the multiscale model and the experimentally measured values considering the range of uncertainties in the experimental data (±20%) (Laakkonen et al., 2007b) and the simulation results as well as the assumptions of the multiscale model (*e.g.*, assuming spherical bubbles to calculate the specific interfacial area). In the next two subsections, the effects of operating conditions and scale-up on the local values of k_La are discussed.

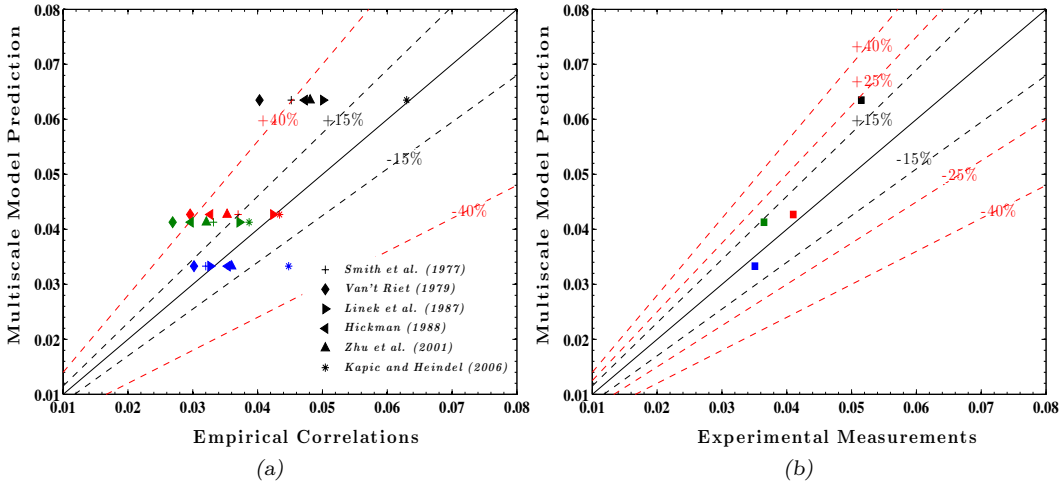

Figure 6.8: Predicted values of the overall mass transfer coefficient by the multiscale model for cases 3-6 : (a) *vs.* empirical correlations based on P_g/V_l and v_{sg} (equation 6.1 and Table 6.1) , and (b) *vs.* experimental measurements of Laakkonen et al. (2007b). Marker colors ; case 3 : blue, case 4 : black, case 5 : red, case 6 : green.

6.3.3 Effects of operating conditions on the local values of k_La

Figures 6.9 (a-c) show the contributions of the local volumetric mass transfer coefficient (in %) to its overall value in the whole STR as predicted by the multiscale model in cases 3, 4, and 5, respectively. These contributions were calculated using the following equation :

$$\frac{V_j(k_La)_j}{V_{tot}\overline{k_La}} \times 100 \tag{6.49}$$

In general, the gas/liquid STR is extremely heterogeneous in terms of mass transfer. The largest contributions are in the impeller compartment (compartment I) and near the

wall of the STR (compartment II), where the turbulent dissipation rate and gas hold-up are high. The relatively larger mean bubble diameter in the sparger compartment (compartment III) results in small values of a (based on equation (6.15)) and k_La. Compartments IV and V make the smallest contributions to the overall mass transfer ($\simeq$ 20%) even though they involve $\simeq$ 60% of the total volume of the STR.

Figures 6.9a and b show the effects of increases in the impeller rotational speed at a constant gas flow rate on the contributions of each zone to the overall k_La. In Figure 6.9a (case 3), the gas hold-up is low in the zone below the impeller (compartment V) due to the relatively low impeller rotational speed (300 rpm). Hence, the contribution of this compartment to the overall mass transfer inside the STR is low. However, by increasing the impeller rotational speed to 390 rpm at a constant gas flow rate (v_{sg}=0.74 cm/s) (case 4 in Figure 6.9b), more gas is pushed to the bottom of the STR by the liquid flow (compartment V and the lower part of compartment II). The increase in gas hold-up in these compartments thus enhance their

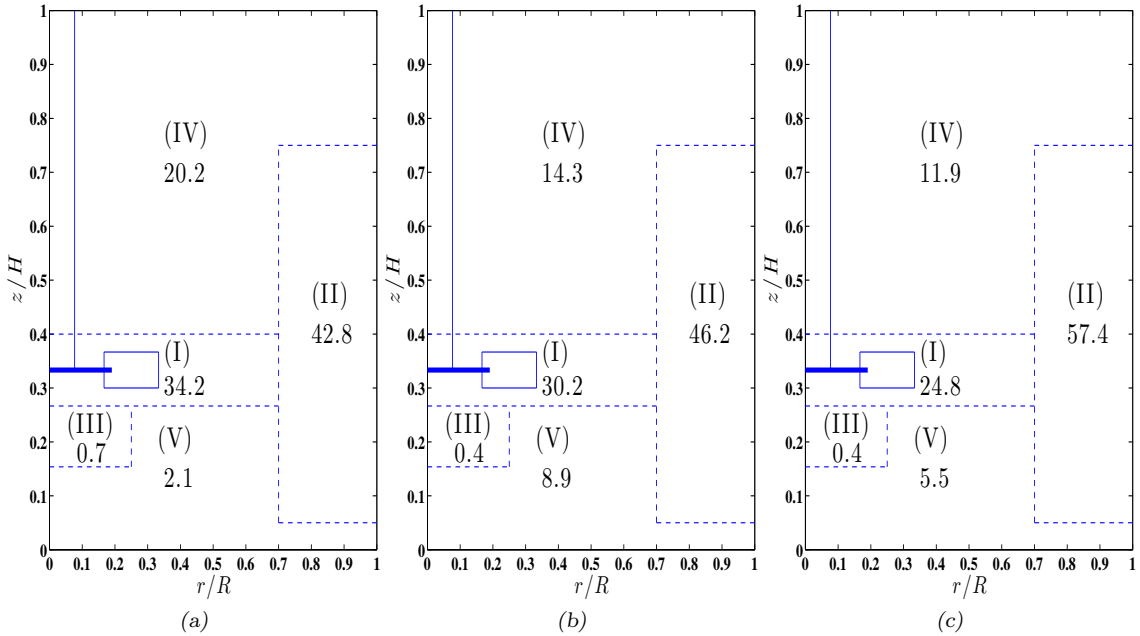

Figure 6.9: Effects of operating conditions on the contributions of the local volumetric mass transfer coefficient to the overall value inside the STR (in %) : (a) case 3, (b) case 4, and (c) case 5.

contributions to the overall mass transfer coefficient from 2.1% to 8.9% and from 42.8% to 46.2%, respectively. At a constant impeller rotational speed, decreasing the gas flow rate from v_{sg}=0.74 cm/s to v_{sg}=0.32 cm/s decreases the gas hold-up in the middle part of the STR, namely compartments I, IV, and V, which leads to a decrease in their contributions to the overall k_La from 30.2% to 24.8%, from 14.3% to 11.9%, and from 8.9% to 5.5%, respectively (Figures 6.9b and c), resulting in an increase from 46.2% to 57.4% in compartment II.

As can be seen, the local mass transfer coefficients are changed significantly by altering the operating conditions. This situation can lead to the occurrence of a dissolved gas gradient when the characteristic time for mass transfer ($1/k_La$) is higher than the characteristic time for the gas uptake rate (Lara et al., 2006). This can have a marked effect on the performance of industrial-scale STRs for bacterial cell cultures, for instance, where the well-mixed assumption for the liquid phase inside the STR is likely to be wrong (Amanullah et al., 2004).

6.3.4 Effects of scale-up on the local values of k_La

Scale-ups of gas/liquid mixing systems are often carried out based on empirical correlations for k_La (Amanullah et al., 2004), as described in Section 6.1 (equation (6.1)). The scale-up rule that follows this approach keeps the specific power consumption (P_g/V_l) and the superficial gas velocity (v_{sg}) values constant during scale-up. Conservative guidelines suggest maintaining the volumetric flow of gas per liquid volume per minute (VVM) constant rather than the superficial gas velocity during scale-up (Amanullah et al., 2004; Nauha et al., 2014). However, this can lead to a completely different flow regime at the industrial scale than at the lab scale. In fact, by following this approach (constant VVM), the flow structure inside industrial-scale STRs would be governed by the gas flow rate (heterogeneous regime) instead of by the impeller (homogeneous regime) (Gezork et al., 2000, 2001), making foaming and liquid entrainment more likely.

In the current study, the scale-up approach based on constant (P_g/V_l) and v_{sg} was applied in 14-, 200-, and 1500-liter STRs (cases 2, 6, and 7). Figures 6.10 (a-c) show the effects of

the scale-up on the contributions of the local k_La to its overall value inside the system as predicted by the multiscale model. The contribution of compartment I, a zone with a high volumetric mass transfer coefficient value, is decreased by the scale-up. As reported in our previous publication (Bashiri et al., 2014), the ratio of the average turbulent energy dissipation rate in the impeller zone (compartment I) to its average value in the bulk of the STR is decreased following the scale-up criterion based on constant power consumption per liquid volume. This can explain, using equation (6.13) for k_l and equations (6.15) and (6.21) for a, the decrease in the contribution of compartment I to the overall k_La. The variation in gas hold-up distributions inside the STR due to scale-up may also explain these changes. As can be readily seen in Figures 6.10 (a-c), this scale-up criterion does not ensure a similar distribution of k_La during the scale-up, even with a marginal scale factor on T (2.4 and 4.8).

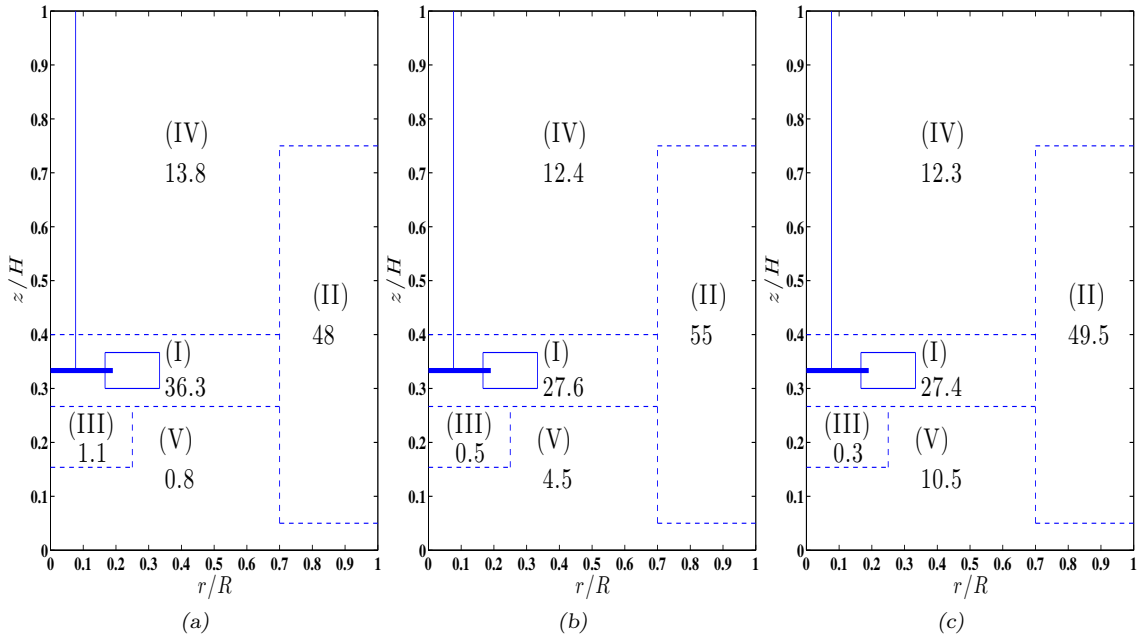

Figure 6.10: Effects of scale-up on the contributions of the local volumetric mass transfer coefficient to the overall value inside the STR (in %) : (a) case 2 (14 liters), (b) case 6 (200 liters), and (c) case 7 (1500 liters).

6.3.5 Possible implications for scale-up

The simple volume averaging of the k_La values obtained from the multiscale model for all the compartments (equation (6.44)) in order to estimate the overall volumetric mass transfer coefficient ($\overline{k_La}$) is of practical use when the mixing time of a system is smaller than the characteristic time for mass transfer ($= 1/k_La$) (Paul et al., 2004). In this case, the volume averaging of the local volumetric mass transfer coefficients gives values similar to those measured experimentally, as shown in Subsection 6.3.2. However, when the mixing in the STR becomes the limiting factor (as in industrial-scale STRs), this averaging will not give an accurate estimation of the overall volumetric mass transfer coefficient.

To maintain constant the overall value of k_La based on empirical correlations, the values of P_g/V_l and v_{sg} should remain constant. Since $P_g \propto N^3D^5$ in the turbulent regime and assuming geometrical similarity during scale-up ($H/T, D/T = constant$), then $V \propto D^3$ and :

$$\frac{P_g}{V_l} \propto N^3D^2 \tag{6.50}$$

Since N^3D^2 should remain constant, it follows that :

$$N \propto D^{-2/3} \tag{6.51}$$

The impeller rotational speed must thus be decreased for scale-up of geometrically similar STRs based on a constant P_g/V_l. Since mixing time (t_m) is inversely proportional to impeller rotational speed ($t_m \propto N^{-1}$), then :

$$t_m \propto D^{2/3} \tag{6.52}$$

This inherent increase in mixing time is one of the major challenges facing scale-up when using this approach. In fact, as the mixing time increases with the scale-up, its value gradually becomes equal to the characteristic time for mass transfer. As such, one can conclude that the assumption of a well-mixed system would only be valid for not too large STRs.

The effects of imperfect mixing on the estimation of the overall mass transfer coefficient can be elaborated based on the weighting of the local values of $k_L a$ by the local residence time of the liquid in the different zones of the STR, which can be non-dimensionalized by the mean circulation time of the mixing system (Paul et al., 2004) :

$$\bar{t}_c = \frac{V_l}{KND^3} \tag{6.53}$$

where K is the pumping capacity of the impeller.

The radioactive particle tracking (RPT) technique can provide Lagrangian information that can give insights into circulation patterns and mixing in STRs (Bashiri et al., 2015). RPT tracks the position of a single radioactive tracer, which emits gamma rays, over time using an array of scintillation detectors located around the STR. This technique was used to determine the residence time distribution (RTD) of liquid (water) inside the compartments of our laboratory-scale baffled STR ($T = 20\ cm$) agitated by an standard Rushton turbine at 300 RPM, by assuming ergodic motion for the tracer in the mixing system. Ergodicity means that, on average, the time behavior of a large number of distinct tracers released at the same time from a given position inside the mixing system can be statistically reproduced from the time behavior of a single tracer injected many times from the same position.

To find the RTD of each compartment, the tracer was followed until it crossed the boundaries of the compartment to be inside it. The elapsed time was recorded until the tracer again crossed the boundaries of the compartment to be outside it. The RTD in each compartment was constructed by repeating this procedure iteratively each time the tracer crossed the boundaries of the compartment.

Figures 6.11 (a-e) show the RTDs in the different compartments of the STR. In these figures, the red dashed lines indicate the mean values of the RTDs. As it can be readily seen, the liquid spends more time inside the compartments with lower local mass transfer coefficient values (compartments IV and V). The long tail of the RTD in these compartments (see Figures 6.11d and e) illustrates the presence of very low velocity zones. On an industrial

scale, the mean residence time of the liquid phase in these compartments would increase significantly due to the increase in the volume of low velocity zones and the reduction of the impeller rotational speed following equation (6.51). It is interesting to note that the sum of the mean residence times in the different zones is equal to the mean circulation time inside the STR using equation (6.53) and a pumping capacity (K) equals to 1.6. This value is exactly the same as that reported by Bertrand et al. (1980), which shows the adequacy of the RPT technique for investigating the mixing pattern in the system. The values of the mean residence time in each compartment can be non-dimensionalized by the mean circulation time of the mixing system. This represents the time that the liquid spends in each compartment as a fraction of the overall circulation time ($\frac{\overline{t_j}}{\overline{t}_c}$). This in turn can be used as a weighting factor to estimate the overall mass transfer coefficient based on the local values of k_La, as is discussed next.

We showed in Figure 6.10 that the local volumetric mass transfer coefficients do not remain constant during the scale-up. Moreover, the residence time of the liquid in the zones with low mass transfer coefficient values is expected to increase by enlarging the STR size as the mixing time would then increase (equation (6.52)). However, to have a crude estimate of the reduction in the value of the overall mass transfer coefficient in industrial-scale STRs due to imperfect mixing, we could simply assume that both ($\frac{\overline{t_i}}{\overline{t}_c}$) and $(k_La)_j$ remain constant. The overall mass transfer coefficient of a large vessel (*e.g.*, $T > 2\ m$) could then be roughly estimated using the predicted local values of k_La for case 7 in Table 6.3, and the weighting factor calculated based on the local residence time of the liquid in the different zones ($\frac{\overline{t_j}}{\overline{t}_c}$) as follows :

$$\overline{k_La} = \frac{\sum_{j=I}^{V} \overline{t}_j (k_La)_j}{\overline{t}_c} \tag{6.54}$$

where $\overline{t}_j$ is the mean value of the liquid residence time in the j^{th} compartment. The predicted local values of k_La for case 7 is chosen for this calculation as it is believed to be more

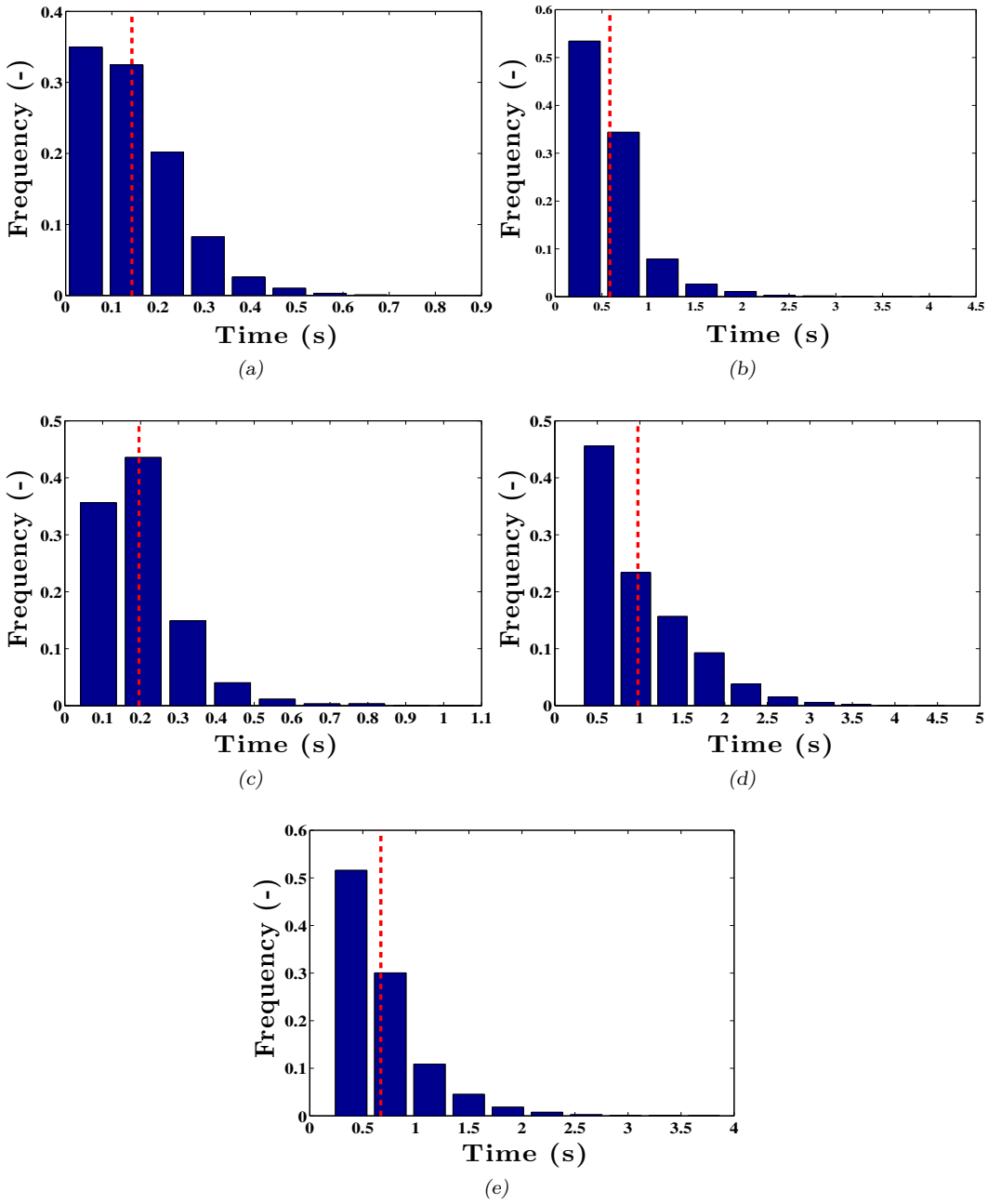

Figure 6.11: Local residence time distribution (RTD) inside the STR : (a) compartment I, (b) compartment II, (c) compartment III, (d) compartment IV, (e) compartment V.

representative for the $k_L a$ distribution of an industrial-scale STR. By applying this averaging, we found that the overall volumetric mass transfer coefficient decreases at least by 20% when imperfect mixing is considered. It has been shown experimentally that this level of reduction in the overall mass transfer coefficient can be observed even with a very low scaling factor

(Jafari, 2010).

Another possibility would be of course to resort to our multiscale model to predict the local values of the mass transfer coefficient in this industrial-scale STR. Keeping the same grid size would be difficult to achieve in practice as the number of cells scales as T^3. On the other hand, keeping constant the number of cells, which entails an increase of the grid size, might at first sight lead to inaccurate results. In order to assess the impact of a coarse grid on the accuracy of the contributions of the local values of k_La to its overall value, an additional simulation was performed for case 7 ($T = 1.24\ m$) and a rather coarse grid of $0.05 * 10^6$ cells, which corresponds to the grid size that would be used for a $T = 5.74\ m$ STR (when one sixth of the geometry and periodic boundary conditions are considered) and a number of cells equal to that of the fine grid of this study ($0.83 * 10^6$). We observed (not shown here) that, while the radial component of the velocity profile predicted with the coarse grid is sizably smaller near the impeller than that obtained with the fine grid, and the values of ε are smaller everywhere in the tank, the impact on the contributions of the local values of k_La to its overall value are insignificant : below 10% for the compartments with the largest contributions (I, II, and IV), 1% for compartment III and around 15% for compartment V. This is due to the use of compartment-averaged values of hydrodynamic quantities in the model that are not sensitive to local hydrodynamic variations resulting from a coarsening of the grid. It also indicates that the proposed multiscale model, even when combined with a coarse grid, can be adequate for design and scale-up purposes.

The inherent limitations of scale-up due to changes in the local values of hydrodynamic parameters provide some innovative ideas for commercializing new processes. One path for scale-up could be to increase the size of the STR up to the scale where the mass transfer is about to become limited by mixing. Then, instead of increasing the STR size even further (scale-up), many parallel STRs (scale-out) could be used to meet production requirements. The challenge here would be the potential increase in total production costs of many parallel reactors compared to a single large reactor. However, these costs could be compensated for

by improving the yields, especially for the production of fine chemicals. Another path would be a retrofit design of an industrial-scale STR by altering the geometrical similarities in order to improve mixing and enhance the local volumetric mass transfer coefficient inside the deficient zones. This would be achieved, for instance, by adding more impellers or by changing the design of the sparger for larger STRs. It should be kept in mind that monitoring local variations of hydrodynamic parameters is essential for successful process scale-ups, and the proposed multiscale model in the present study could be an adequate design tool in this regard.

6.4 Conclusion

A multiscale gas/liquid flow model was developed to predict the mean local values of the volumetric mass transfer coefficient (k_La) inside STRs. In this model, data from simplified and less computationally intensive gas/liquid flow simulations were used. It was shown that mono-dispersed bubble sizes, adequate drag models and sufficiently refined grids in CFD simulations can provide satisfactory information on the hydrodynamics of turbulent gas/liquid flows. It was also shown that the number of cells has a significant effect on the prediction of the local hold-up profile by CFD. However, the effect on the prediction of global gas hold-up was marginal. The predictions of the suggested numerical strategy with respect to the characteristics of turbulent gas/liquid flow inside STRs, including gas hold-up and relative power demand (RPD), were in good agreement with experimental data.

The multiscale model provided good predictions of the overall mass transfer coefficient inside the STR compared to experimental values. This model revealed that approximately 80% of the total mass transfer occurs in about 40% of the total volume of the STRs. We also determined whether variations in operating conditions and the scale of the STRs had a significant effect on the distribution of the local values of the volumetric mass transfer coefficient. Based on the analysis of the local liquid RTDs using the radioactive particle tracking technique and the local values of volumetric mass transfer coefficient, we showed

that conventional scale-up approaches are not effective at maintaining similar values for the overall volumetric mass transfer coefficient inside industrial-scale and laboratory-scale STRs.

Our results suggested that the size of the STR be scaled up to the point where the mass transfer rate is about to become limited by the liquid mixing inside the STR, and then the STR be scaled out to meet production requirements. When this approach is not economically viable, a retrofit design of the STR should be considered. The multiscale model proposed in the present study could be a very efficient design tool in this regard.

Acknowledgement

The authors would like to thank the Natural Sciences and Engineering Research Council of Canada for financial support. The authors are grateful to Habibollah Hajhashemi for helpful discussions on how to generate structured meshes for mixing systems.

6.5 References

Alves, S., Maia, C., and Vasconcelos, J. (2004). Gas-liquid mass transfer coefficient in stirred tanks interpreted through bubble contamination kinetics. *Chemical Engineering and Processing : Process Intensification*, 43(7) :823–830.

Alves, S., Maia, C., Vasconcelos, J., and Serralheiro, A. (2002). Bubble size in aerated stirred tanks. *Chemical Engineering Journal*, 89(1) :109–117.

Amanullah, A., Buckland, B. C., and Nienow, A. W. (2004). Mixing in the fermentation and cell culture industries. *Handbook of Industrial Mixing : Science and Practice*, pages 1071–1170.

Ansys, A. F. (2013). 15.0 theory guide. *ANSYS inc.*

Bakker, A. and Akker, H. A. (1994). A computational model for the gas-liquid flow in stirred reactors. *Chemical Engineering Research and Design*, 72 :594–606.

Bakker, A., Smith, J., and Myers, K. (1994). How to disperse gases in liquids. *Chemical engineering*, 101(12) :98–104.

Barigou, M. and Greaves, M. (1992). Bubble-size distributions in a mechanically agitated gas-liquid contactor. *Chemical Engineering Science*, 47(8) :2009–2025.

Barigou, M. and Greaves, M. (1996). Gas holdup and interfacial area distributions in a mechanically agitated gas-liquid contactor. *Chemical engineering research & design*, 74(3) :397–405.

Bashiri, H., Alizadeh, E., Chaouki, J., and Bertrand, F. (2015). Investigation of turbulent fluid flows in stirred tanks using a non-intrusive particle tracking technique. *Manuscript submitted for publication.*

Bashiri, H., Heniche, M., Bertrand, F., and Chaouki, J. (2014). Compartmental modelling of turbulent fluid flow for the scale-up of stirred tanks. *The Canadian Journal of Chemical Engineering*, 92(6) :1070–1081.

Bertrand, J., Couderc, J., and Angelino, H. (1980). Power consumption, pumping capacity and turbulence intensity in baffled stirred tanks : comparison between several turbines. *Chemical Engineering Science*, 35(10) :2157–2163.

Bhavaraju, S., Russell, T., and Blanch, H. (1978). The design of gas sparged devices for viscous liquid systems. *AIChE Journal*, 24(3) :454–466.

Brucato, A., Grisafi, F., and Montante, G. (1998). Particle drag coefficients in turbulent fluids. *Chemical Engineering Science*, 53(18) :3295–3314.

Calderbank, P. (1958). Physical rate processes in industrial fermentation. part I : The interfacial area in gas-liquid contacting with mechanical agitation. *Trans. Inst. Chem. Eng*, 36 :443–463.

Chaouki, J., Larachi, F., and Dudukovic, M. P. (1997). *Non-invasive monitoring of multiphase flows.* Access Online via Elsevier.

Clift, R., Grace, J. R., and Weber, M. E. (2005). *Bubbles, drops, and particles*. Courier Dover Publications.

Coroneo, M., Montante, G., Paglianti, A., and Magelli, F. (2011). CFD prediction of fluid flow and mixing in stirred tanks : Numerical issues about the rans simulations. *Computers & Chemical Engineering*, 35(10) :1959–1968.

Danckwerts, P. (1951). Significance of liquid-film coefficients in gas absorption. *Industrial & Engineering Chemistry*, 43(6) :1460–1467.

Danckwerts, P. (1953). Continuous flow systems : distribution of residence times. *Chemical Engineering Science*, 2(1) :1–13.

Deen, N. G., Solberg, T., and Hjertager, B. H. (2002). Flow generated by an aerated Rushton impeller : Two-phase PIV experiments and numerical simulations. *The Canadian Journal of Chemical Engineering*, 80(4) :1–15.

Deglon, D. and Meyer, C. (2006). CFD modelling of stirred tanks : Numerical considerations. *Minerals Engineering*, 19(10) :1059–1068.

Ford, J. J., Heindel, T. J., Jensen, T. C., and Drake, J. B. (2008). X-ray computed tomography of a gas-sparged stirred-tank reactor. *Chemical Engineering Science*, 63(8) :2075–2085.

Gabelle, J.-C., Augier, F., Carvalho, A., Rousset, R., and Morchain, J. (2011). Effect of tank size on $k_l a$ and mixing time in aerated stirred reactors with non-newtonian fluids. *The Canadian Journal of Chemical Engineering*, 89(5) :1139–1153.

Gagnon, H., Lounes, M., and Thibault, J. (1998). Power consumption and mass transfer in agitated gas-liquid columns : A comparative study. *The Canadian Journal of Chemical Engineering*, 76(3) :379–389.

Garcia-Ochoa, F. and Gomez, E. (2004). Theoretical prediction of gas–liquid mass transfer coefficient, specific area and hold-up in sparged stirred tanks. *Chemical Engineering Science*, 59(12) :2489–2501.

Garcia-Ochoa, F., Gomez, E., Santos, V. E., and Merchuk, J. C. (2010). Oxygen uptake rate in microbial processes : an overview. *Biochemical Engineering Journal*, 49(3) :289–307.

Gelves, R., Dietrich, A., and Takors, R. (2014). Modeling of gas–liquid mass transfer in a stirred tank bioreactor agitated by a Rushton turbine or a new pitched blade impeller. *Bioprocess and biosystems engineering*, 37(3) :365–375.

Gezork, K., Bujalski, W., Cooke, M., and Nienow, A. (2000). The transition from homogeneous to heterogeneous flow in a gassed, stirred vessel. *Chemical Engineering Research and Design*, 78(3) :363–370.

Gezork, K., Bujalski, W., Cooke, M., and Nienow, A. (2001). Mass transfer and hold-up characteristics in a gassed, stirred vessel at intensified operating conditions. *Chemical Engineering Research and Design*, 79(8) :965–972.

Gimbun, J., Rielly, C. D., and Nagy, Z. K. (2009). Modelling of mass transfer in gas–liquid stirred tanks agitated by Rushton turbine and CD-6 impeller : a scale-up study. *Chemical Engineering Research and Design*, 87(4) :437–451.

Gosman, A., Lekakou, C., Politis, S., Issa, R., and Looney, M. (1992). Multidimensional modeling of turbulent two-phase flows in stirred vessels. *AIChE Journal*, 38(12) :1946–1956.

Green, D. W. et al. (2008). *Perry's chemical engineers' handbook*, volume 796. McGraw-hill New York.

Hickman, A. (1988). Gas-liquid oxygen transfer and scale-up. a novel experimental technique with results for mass transfer in aerated agitated vessels. In *Proc.* 6^{th} *European Conf. on Mixing, Pavia, Italy, 1988*.

Higbie, R. (1935). *The rate of absorption of a pure gas into still liquid during short periods of exposure*.

Hinze, J. (1955). Fundamentals of the hydrodynamic mechanism of splitting in dispersion processes. *AIChE Journal*, 1(3) :289–295.

Jafari, R. (2010). *Solid Suspension and Gas Dispersion in Mechanically Agitated Vessels*. PhD thesis, École Polytechnique de Montréal.

Kapic, A. and Heindel, T. (2006). Correlating gas-liquid mass transfer in a stirred-tank reactor. *Chemical Engineering Research and Design*, 84(3) :239–245.

Kawase, Y., Halard, B., and Moo-Young, M. (1987). Theoretical prediction of volumetric mass transfer coefficients in bubble columns for newtonian and non-newtonian fluids. *chemical Engineering science*, 42(7) :1609–1617.

Kawase, Y., Halard, B., and Moo-Young, M. (1992). Liquid-phase mass transfer coefficients in bioreactors. *Biotechnology and bioengineering*, 39(11) :1133–1140.

Kerdouss, F., Bannari, A., and Proulx, P. (2006). CFD modeling of gas dispersion and bubble size in a double turbine stirred tank. *Chemical Engineering Science*, 61(10) :3313–3322.

Kerdouss, F., Bannari, A., Proulx, P., Bannari, R., Skrga, M., and Labrecque, Y. (2008). Two-phase mass transfer coefficient prediction in stirred vessel with a CFD model. *Computers & Chemical Engineering*, 32(8) :1943–1955.

Khopkar, A., Kasat, G., Pandit, A., and Ranade, V. (2006). CFD simulation of mixing in tall gas–liquid stirred vessel : role of local flow patterns. *Chemical Engineering Science*, 61(9) :2921–2929.

Khopkar, A., Rammohan, A., Ranade, V., and Dudukovic, M. (2005). Gas–liquid flow generated by a Rushton turbine in stirred vessel : CARPT/CT measurements and CFD simulations. *Chemical Engineering Science*, 60(8) :2215–2229.

Khopkar, A. R. and Ranade, V. V. (2006). CFD simulation of gas–liquid stirred vessel : VC, S33, and L33 flow regimes. *AIChE journal*, 52(5) :1654–1672.

Kiared, K., Larachi, F., Guy, C., and Chaouki, J. (1997). Trajectory length and residence-time distributions of the solids in three-phase fluidized beds. *Chemical engineering science*, 52(21) :3931–3939.

Laakkonen, M., Alopaeus, V., and Aittamaa, J. (2006a). Validation of bubble breakage, coalescence and mass transfer models for gas–liquid dispersion in agitated vessel. *Chemical engineering science*, 61(1) :218–228.

Laakkonen, M., Moilanen, P., Alopaeus, V., and Aittamaa, J. (2006b). Dynamic modeling of local reaction conditions in an agitated aerobic fermenter. *AIChE journal*, 52(5) :1673–1689.

Laakkonen, M., Moilanen, P., Alopaeus, V., and Aittamaa, J. (2007a). Modelling local bubble size distributions in agitated vessels. *Chemical Engineering Science*, 62(3) :721–740.

Laakkonen, M., Moilanen, P., Alopaeus, V., and Aittamaa, J. (2007b). Modelling local gas–liquid mass transfer in agitated vessels. *Chemical Engineering Research and Design*, 85(5) :665–675.

Laborde-Boutet, C., Larachi, F., Dromard, N., Delsart, O., and Schweich, D. (2009). CFD simulation of bubble column flows : Investigations on turbulence models in rans approach. *Chemical Engineering Science*, 64(21) :4399–4413.

Lamont, J. C. and Scott, D. (1970). An eddy cell model of mass transfer into the surface of a turbulent liquid. *AIChE Journal*, 16(4) :513–519.

Lane, G., Schwarz, M., and Evans, G. (2005). Numerical modelling of gas–liquid flow in stirred tanks. *Chemical Engineering Science*, 60(8) :2203–2214.

Lara, A. R., Galindo, E., Ramírez, O. T., and Palomares, L. A. (2006). Living with heterogeneities in bioreactors. *Molecular biotechnology*, 34(3) :355–381.

Lee, K. and Yianneskis, M. (1994). The extent of periodicity of the flow in vessels stirred by Rushton impellers. In *AIChE Symposium series*, volume 90, pages 5–18. New York, NY : American Institute of Chemical Engineers, 1971-c2002.

Linek, V., Kordač, M., Fujasová, M., and Moucha, T. (2004). Gas–liquid mass transfer coefficient in stirred tanks interpreted through models of idealized eddy structure of turbulence in the bubble vicinity. *Chemical Engineering and Processing : Process Intensification*, 43(12) :1511–1517.

Linek, V., Moucha, T., Rejl, F., Kordač, M., Hovorka, F., Opletal, M., and Haidl, J. (2012). Power and mass transfer correlations for the design of multi-impeller gas–liquid contactors for non-coalescent electrolyte solutions. *Chemical Engineering Journal*, 209 :263–272.

Linek, V., Vacek, V., and Beneš, P. (1987). A critical review and experimental verification of the correct use of the dynamic method for the determination of oxygen transfer in aerated agitated vessels to water, electrolyte solutions and viscous liquids. *The Chemical Engineering Journal*, 34(1) :11–34.

Middleton, J. (1992). Gas-liquid dispersion and mixing. *Mixing in the process industries*, 2 :349–352.

Moilanen, P., Laakkonen, M., Visuri, O., Alopaeus, V., and Aittamaa, J. (2008). Modelling mass transfer in an aerated 0.2 m^3 vessel agitated by Rushton, phasejet and combijet impellers. *Chemical Engineering Journal*, 142(1) :95–108.

Montante, G., Horn, D., and Paglianti, A. (2008). Gas–liquid flow and bubble size distribution in stirred tanks. *Chemical engineering science*, 63(8) :2107–2118.

Morud, K. and Hjertager, B. (1996). LDA measurements and CFD modelling of gas-liquid flow in a stirred vessel. *Chemical Engineering Science*, 51(2) :233–249.

Moucha, T., Rejl, F., Kordač, M., and Labík, L. (2012). Mass transfer characteristics of multiple-impeller fermenters for their design and scale-up. *Biochemical Engineering Journal*, 69 :17–27.

Mueller, S. G. and Dudukovic, M. P. (2010). Gas holdup in gas-liquid stirred tanks. *Industrial & Engineering Chemistry Research*, 49(21) :10744–10750.

Nauha, E. K., Visuri, O., Vermasvuori, R., and Alopaeus, V. (2014). A new simple approach for the scale-up of aerated stirred tanks. *Chemical Engineering Research and Design*.

Nienow, A., Wisdom, D., and Middleton, J. (1977). The effect of scale and geometry on flooding, recirculation and power in gassed stirred vessels. In *Proceedings of the* 2^{nd} *European Conference on Mixing*, page 1.

Parthasarathy, R., Jameson, G., and Ahmed, N. (1991). Bubble breakup in stirred vessels : Predicting the sauter mean diameter. *Chemical engineering research & design*, 69(A4) :295–301.

Paul, E. L., Atiemo-Obeng, V., and Kresta, S. M. (2004). *Handbook of industrial mixing : science and practice*. John Wiley & Sons.

Petitti, M., Vanni, M., Marchisio, D. L., Buffo, A., and Podenzani, F. (2013). Simulation of coalescence, break-up and mass transfer in a gas–liquid stirred tank with CQMOM. *Chemical Engineering Journal*, 228 :1182–1194.

Poorte, R. and Biesheuvel, A. (2002). Experiments on the motion of gas bubbles in turbulence generated by an active grid. *Journal of Fluid Mechanics*, 461 :127–154.

Prasher, B. D. and Wills, G. B. (1973). Mass transfer in an agitated vessel. *Industrial & Engineering Chemistry Process Design and Development*, 12(3) :351–354.

Ramkrishna, D. and Singh, M. R. (2014). Population balance modeling : Current status and future prospects. *Annual review of chemical and biomolecular engineering*, 5 :123–146.

Ranade, V. V. (2002). *Computational flow modeling for chemical reactor engineering*. Process systems engineering series. Academic Press, San Diego.

Ranganathan, P. and Sivaraman, S. (2011). Investigations on hydrodynamics and mass transfer in gas–liquid stirred reactor using computational fluid dynamics. *Chemical Engineering Science*, 66(14) :3108–3124.

Sajjadi, B., Raman, A., Ibrahim, S., and Shah, R. (2012). Review on gas-liquid mixing analysis in multiscale stirred vessel using CFD. *Reviews in Chemical Engineering*, 28(2-3) :171–189.

Sánchez Mirón, A., Garcia Camacho, F., Contreras Gomez, A., Grima, E. M., and Chisti, Y. (2000). Bubble-column and airlift photobioreactors for algal culture. *AIChE Journal*, 46(9) :1872–1887.

Saravanan, K. and Joshi, J. (1996). Fractional gas hold-up in gas inducing type of mechanically agitated contactors. *The Canadian Journal of Chemical Engineering*, 74(1) :16–30.

Sato, Y. and Sekoguchi, K. (1975). Liquid velocity distribution in two-phase bubble flow. *International Journal of Multiphase Flow*, 2(1) :79–95.

Scargiali, F., Doorazio, A., Grisafi, F., and Brucato, A. (2007). Modelling and simulation of gas–liquid hydrodynamics in mechanically stirred tanks. *Chemical Engineering Research and Design*, 85(5) :637–646.

Smith, J. (2006). Large multiphase reactors : some open questions. *Chemical Engineering Research and Design*, 84(4) :265–271.

Smith, J., Van't Riet, K., and Middleton, J. (1977). Scale up of agitated gas–liquid reactors for mass transfer. In *Proceedings of* 2^{nd} *European conference on mixing. F*, volume 4, pages 51–66.

Takahashi, K., McManamey, W. J., and Nienow, A. W. (1992). Bubble size distributions in impeller region in a gas-sparged vessel agitated by a Rushton turbine. *Journal of chemical engineering of Japan*, 25(4) :427–432.

Takahashi, K. and Nienow, A. W. (1993). Bubble sizes and coalescence rates in an aerated vessel agitated by a Rushton turbine. *Journal of chemical engineering of Japan*, 26(5) :536–542.

Tobajas, M., Garcıa-Calvo, E., Siegel, M., and Apitz, S. (1999). Hydrodynamics and mass transfer prediction in a three-phase airlift reactor for marine sediment biotreatment. *Chemical Engineering Science*, 54(21) :5347–5354.

Tomiyama, A., Kataoka, I., Zun, I., and Sakaguchi, T. (1998). Drag coefficients of single bubbles under normal and micro gravity conditions. *JSME international journal. Series B, fluids and thermal engineering*, 41(2) :472–479.

Utgikar, V. P. (2009). Modeling in multiphase reactor design : Solid phase residence time distribution in three-phase sparged reactors. *Industrial & Engineering Chemistry Research*, 48(17) :7910–7914.

Vakili, M. and Esfahany, M. N. (2009). CFD analysis of turbulence in a baffled stirred tank, a three-compartment model. *Chemical Engineering Science*, 64(2) :351–362.

Van't Riet, K. (1979). Review of measuring methods and results in nonviscous gas-liquid mass transfer in stirred vessels. *Industrial & Engineering Chemistry Process Design and Development*, 18(3) :357–364.

Wang, T., Wang, J., and Jin, Y. (2005). Population balance model for gas-liquid flows : influence of bubble coalescence and breakup models. *Industrial & engineering chemistry research*, 44(19) :7540–7549.

Wang, W., Mao, Z.-S., and Yang, C. (2006). Experimental and numerical investigation on gas holdup and flooding in an aerated stirred tank with Rushton impeller. *Industrial & engineering chemistry research*, 45(3) :1141–1151.

Whitman, W. G. (1923). A preliminary experimental confirmation of the two-film theory of gas absorption. *Chemical and Metallurgical Engineering*, 29 :146–148.

Xie, M., Xia, J., Zhou, Z., Chu, J., Zhuang, Y., and Zhang, S. (2014). Flow pattern, mixing, gas hold-up and mass transfer coefficient of triple-impeller configurations in stirred tank bioreactors. *Industrial & Engineering Chemistry Research*, 53(14) :5941–5953.

Yawalkar, A. A., Heesink, A., Versteeg, G. F., and Pangarkar, V. G. (2002). Gas–liquid mass transfer coefficient in stirred tank reactors. *The Canadian Journal of Chemical Engineering*, 80(5) :840–848.

Zhang, Y., Bai, Y., and Wang, H. (2013). CFD analysis of inter-phase forces in a bubble stirred vessel. *Chemical Engineering Research and Design*, 91(1) :29–35.

Zhang, Y., Yang, C., and Mao, Z.-S. (2008). Large eddy simulation of the gas–liquid flow in a stirred tank. *AIChE journal*, 54(8) :1963–1974.

Zhu, Y., Bandopadhayay, P. C., and Wu, J. (2001). Measurement of gas-liquid mass transfer in an agitated vessel. a comparison between different impellers. *Journal of chemical engineering of Japan*, 34(5) :579–584.

CHAPTER 7

GENERAL DISCUSSION

With conventional scale-up procedures, the values of hydrodynamic parameters are assumed to be constant in the entire STR ("well-mixed" assumption). However, in real cases, especially at the production level, the values of such parameters (*e.g.* the mass transfer rate) may vary significantly. It is well known that the design and scale-up of process equipment can barely be successful without taking local hydrodynamics into account. The productivity of many processes is limited by the mass transfer between phases, especially in the case of low soluble species in the gas phase that transfer to the liquid phase. Accordingly, the volumetric mass transfer coefficient (k_La) can affect operations by limiting productivity in various ways, including by changing the rate and, possibly, the selectivity. Understanding gas/liquid mass transfer is thus essential for the adequate design of STRs. The overall objective of this study was to gain insight into the hydrodynamics prevailing in STRs and help improve their design and scale-up by using a strategic combination of different tools including compartmental modeling, computational fluid dynamics (CFD) and experimental fluid dynamics (EFD).

The turbulent energy dissipation rate significantly affects the local volumetric mass transfer coefficients (Figure 2.7). A few studies used CFD to investigate non-homogeneities of turbulent dissipation rate in STRs. However, they are limited to mixing systems provided with simple impellers (two-blade paddle impellers) that are inefficient for gas/liquid STRs. In addition, the impact of operating conditions and common scale-up approaches on the extent of turbulent non-homogeneities has not been addressed in the literature.

While CFD can help to gain insight into the flow patterns and local hydrodynamics in stirred tanks, the closure rules inherent to CFD models (*e.g.* for turbulence and phase interactions) often lead to uncertainties and further justify the need to assess the adequacy of these models using experimental data obtained through reliable validation techniques. However,

quantitative assessments of the accuracy of CFD analyses rely mainly on a comparison of flows close to the impeller. Very little attention has been paid to the accuracy of predictions near the walls, baffles and in the bulk of STR. Accurate predictions of flow characteristics in these regions are essential for predicting the mixing characteristics of the STR.

The methodologies that have been developed to predict the local volumetric mass transfer coefficient are based on coupling a population balance model with the Eulerian multi-fluid approach. This approach suffers from two main limitations : (1) it greatly increases the computational demands, and (2) the inherent complexities involved in this approach and the present state of understanding of breakage and coalescence phenomena imply that the final results depend on a considerable number of parameters that should be tuned to fit the experimental measurements. These issues limit the applicability of this approach for design and scale-up purposes. In this thesis, the following three specific objectives were defined to address the above-mentioned gaps in the body of knowledge :

1. To assess the impact of operating conditions and scale-up criteria on turbulent non-homogeneities in STRs ;
2. To characterize turbulent fluid flows in STRs using RPT ;
3. To develop a multiscale model for predicting the local volumetric mass transfer coefficient in gas/liquid STRs.

The main findings corresponding to these objectives are described next.

First specific objective

The results of single-phase CFD simulations of STRs with four baffles agitated by a Rushton turbine are used to determine the parameters of a two-compartment model that describes the turbulent non-homogeneities therein. These STRs were three geometrically similar cylindrical vessels. The simplest configuration was used to describe turbulent non-homogeneities in an STR consisting of two compartments, a small one around the impeller and characterized by a large energy dissipation rate and turbulence intensities, as well as

a larger circulating region, far from the impeller, where the turbulent flow field is nearly homogeneous and the energy dissipation rate is small. The cut-off energy dissipation rate, ε_{cut}, can serve to identify this boundary so that the cells with a turbulent energy dissipation rate higher and lower than ε_{cut} belong to the impeller region and the circulating region, respectively. The adequate determination of these two regions depends on the selection of ε_{cut}. Previous studies suggested that this parameter can be found by determining the break in the cumulative weighted sums of the energy dissipation rate curve. However, finding the exact location of this break is not straightforward and rather subjective. One contribution of the first part of this thesis was to introduce a more precise method of finding the ε_{cut}.

A new method was introduced to determine the boundary between these two regions based on the use of the volume fraction curves. It was shown that this method can server as a more precise and straightforward way to find ε_{cut}. The compartmental model defined by two parameters, the ratio of the energy dissipation rates in each compartment ($\lambda = \frac{\bar{\varepsilon}_{imp}}{\bar{\varepsilon}_{cir}}$) and the compartment volume ratio ($\beta = \frac{V_{imp}}{V_{cir}}$). It was observed that an increase of the impeller rotational speed leads to an increase in the cut-off energy dissipation rate for both scales (58.2 and 465.5 L). This is in fact associated with a shift of the energy dissipation rate distributions to higher values with an increase in the impeller rotational speed, thus leading to greater homogeneity in the vessel. It was found that an increase in impeller rotational speed causes a decrease of β while λ remains almost constant. On the one hand, the values of ε in both regions are increased, which means that they change in the same proportions because λ does not change significantly. On the other hand, a decrease in β, which is less considerable in the larger vessel due to the detrimental effect of the tank wall on the radial jet flow, means that the relative size of the impeller region decreases. In other words, an increase in rotational speed does improve mixing in the impeller region owing to a higher turbulent energy dissipation rate in a smaller volume. For the circulating region, the increase in volume is compensated by a larger increase in the turbulent energy dissipation rate, which explains why mixing is improved in this region as well. It was revealed that the exchange flow rate

between the two compartments increases with an increase of impeller rotational speed, more importantly in the case of the larger vessel.

Moreover, the impacts of three scale-up approaches, including constant impeller speed (rule 1), constant tip speed (rule 2), and constant power consumption per liquid volume (rule 3), on the parameters of the two-compartment model were also investigated. The value of the cut-off energy dissipation rate, ε_{cut}, slightly decreased during the scale-up with rules 2 and 3, and increased with rule 1. It was shown that the value of ε_{cut} depends on both the impeller rotational speed and the impeller diameter. With rules 2 and 3, the impeller rotational speed decreased considerably during the scale up, causing a decrease in ε_{cut}. However in the case of rule 1, an increase in impeller diameter resulted in an increase of the impeller tip speed and ε_{cut}. The compartment volume ratio (β) increased during the scale-up with all these rules, thus leading to a higher degree of compartmentalization and more non-homogeneities in the larger STRs. The energy dissipation rate ratio (λ) decreased considerably during the scale-up with all rules. This indicates that the energy dissipation rate distributions change during the scale-up, which can affect the process characteristics. The ratio of volumetric exchange flow rate between the two compartments increased during the scale-up in all cases, implying that the effect of the impeller diameter on this quantity is greater than that of the impeller rotational speed. The concept of general maps for predicting of the compartmental model parameters was finally discussed. These maps could be used to monitor changes in turbulent non-homogeneities by predicting the value of compartmental model parameters in an STR during scale-up based on the Reynolds number.

Second specific objective

In the second part of this thesis, fully turbulent fluid flows in a laboratory-scale STR (6.3 L) equipped with an RT or a PBT were analyzed using the radioactive particle tracking (RPT) technique. The present study covered both Eulerian and Lagrangian descriptions of fluid motions. The RPT measurement of the turbulent flow field in a tank agitated by an RT

was benchmarked with CFD simulations of RANS-based turbulence models (standard and RNG k-ε) and laser-based measurements (LDA).

Generally, there was good agreement between all the methods for the measured and predicted 3D mean velocity profiles at all locations in the STR. The wall jet, which was predicted by both turbulent models, had a tendency to attach to the wall of the tank. The radial velocity at the impeller plane close to the impeller tip measured by the RPT technique was lower than the LDA value ($\sim 30\%$). However, the difference was less marked at locations close to the wall of the tank ($< 5\%$). It was shown that the RNG model predicted the same maximum radial velocity at the plane of the impeller disc as that measured by the LDA. However, the standard turbulent model under-predicted this value by $\sim 10\%$. Both of these models over-predicted the radial velocity values compared to those measured by the LDA and RPT techniques away from the impeller towards the wall of the tank. The RPT results showed the swirling flow structure that forms just below the impeller and dissipates progressively toward the bottom of the tank. While this 3D flow structure was captured to some extent by the LDA technique, it was not captured by the turbulent models. The mean tangential velocity was over-predicted by both turbulent models compared to values measured by the LDA and RPT techniques ($\sim$ 30-40%) at the impeller plane close to the impeller tip ($0.33 \leq r/R \leq 0.5$). It was shown that the swirling effect of the impeller was lower in regions far from it towards the surface of the tank.

It was also found that the largest differences between the measured and predicted mean velocities occurred close to the impeller tip, for which there is also a significant discrepancy in the literature. Several sources for this dissimilarity were discussed, such as the presence of the extremely complex flow structure in this region, bias in the velocity measurement by LDA, and uncertainty in the reconstruction of tracer particle positions due to the statistical nature of the emission and counting processes in the RPT technique. Discrepancies between the numerical and experimental results were attributed to the CFD models themselves, which are based on simplifying assumptions such as isotropic turbulent eddies, the wall function

used, and a flat surface at the top.

The measurement of turbulent flow fields generated by the PBT impeller was also presented in this thesis using the RPT technique. It was found that the downward axial jet generated by the PBT reaches its maximum axial velocity in the $0.2 \leq r/R \leq 0.35$ range. The axial jet died down when it reached the bottom of the tank, being transformed into a radial jet toward the side wall. The downward movement of the fluid flow reversed into an upward flow at $r/R \sim 0.7$. This was attributed to the dead zone in the eye of the circulating loop in the STR. There was a clear transition to a fairly flat axial velocity profile between $z/H = 0.6$ and $z/H = 0.8$, indicating that the active volume where the main circulation occurs is in the bottom 60-80% of the tank. The radial velocities were small in the whole tank, except in the region close to the bottom of the STR. In this region, the axial jet generated by the turbine becomes a radial jet by changing its direction toward the tank wall. The radial velocity decreased when z/H approached the impeller plane. However, in the region just above the impeller plane, where the fluid is sucked in by the PBT impeller, there was a higher mean radial velocity ($\sim 0.15V_{tip}$) toward the center of the tank. The values of the mean tangential velocity are relatively high close to the impeller for radial positions $r/R \leq 0.5$. Also, a small tangential velocity ($\sim$ 0.05-$0.15V_{tip}$) was observed close to the bottom of the tank, where the base of the circulation loop changes direction from axial to radial.

The behaviour of the wall jet was investigated for both impellers. One of the key features of wall jets is the similarity in their velocity profiles. There was very good agreement between the RPT measurements and the predictions of the semi-empirical model for the similarities of the dimensionless axial velocity profiles in all locations in the case of the RT impeller, and for locations close to the tank wall of the PBT impeller. Indeed, in the latter case, the agreement in similarities starts to break down at locations far from the wall due to the recirculation generated by the impeller.

It was shown that particle trajectories can be used to generate Poincaré maps, which in turn can be used as a tool to visualize the 3D flow structure inside mixing systems. This tool

was used to depict the circulation patterns, locations of internals, the effect of the baffles on the turbulent fluid flow, and the wall jets. Similar distributions of the dimensionless Lagrangian velocity magnitudes (V/V_{tip}) inside the STR were observed for both RT and PBT operating at the same Reynolds number. A definition of mixing based on the concept of stochastic independence was used to investigate mixing time using Lagrangian trajectory data. The mixing index based on this definition takes on the value of 0 when the system is perfectly mixed and 1 when it is completely segregated. This mixing index levelled off to asymptotic values between 0 and 0.1 after approximately 5 seconds in both STRs equipped with RT and PBT. These values were in good agreement with the values predicted by existing correlations in the literature. However, as there were no solid guidelines for deciding when the values of this mixing index were insignificant from zero, determining the mixing time based on the time evolution of this mixing index is subjective.

In this thesis, a novel method for a less subjective determination of the mixing time was developed based on the statistical concept of memory loss by resorting to an autocorrelation function together with Barlett's formula. It was shown that the mixing time measured by this novel method is in very good agreement with the value predicted by existing correlations in the literature and better reflects the mixing effectiveness of the impellers. Our results showed that the RPT technique holds great promise for measuring mixing times when traditional methods are insufficient (*e.g.*, in opaque systems). RPT also was used to validate a CFD model for simulating single-phase turbulent flow. The results of this model were used as an initial condition for more complex CFD simulations of gas/liquid turbulent flow in the STRs presented in the final part of this thesis.

Third specific objective

In the last part of this thesis, a multiscale gas/liquid flow model was developed as a tool for the design and scale-up of STRs. The model was based on the compartmentalization of the STR into zones and the use of simplified less computationally intensive gas/liquid flow

simulations. It was shown that the use of a mono-dispersed bubble size, an adequate drag model, and sufficiently refined grids in CFD simulations can provide satisfactory information on the local hydrodynamics of turbulent gas/liquid flows in STRs. Also, mesh sensitivity analysis revealed that the effects of grid size on the global gas hold-up were less pronounced than on local gas hold-up values. It was shown that the CFD model and proposed numerical strategy can predict with a good adequacy the global gas hold-up (discrepancy<15%) and relative power demand (discrepancy<10%) of STRs in various operating conditions compared to experimental values.

The spatial variations of the local hydrodynamics of turbulent gas/liquid flows generated by RT inside an STR were described by five characteristic compartments in order to establish the flow structure. The mean local values of the gas hold-up and liquid turbulent energy dissipation rate were passed along to models for predicting the bubble mean Sauter diameter and the liquid-side mass transfer coefficient, which were based on Kolmogorov's theory of isotropic turbulence and the eddy cell model. The proposed multiscale model could predict fairly well the bubble mean Sauter diameter compared to the experimental data drawn from the literature for two geometrically similar STRs of 14 and 200 L. A good correspondence was also found between the predictions of the multiscale model and the experimentally measured values of the overall mass transfer coefficients (discrepancy<25%).

Based on the predicted local values of the volumetric mass transfer coefficient (k_La) by the multiscale model, it was found that the gas/liquid STR is extremely heterogeneous in terms of mass transfer. The largest contributions were near the impeller and wall of the STR, where the turbulent dissipation rate and gas hold-up are high. The relatively larger mean bubble diameter in the sparger compartment compensated for the increase in the value of k_La due to the high gas hold-up value. The bulk of the STR made the smallest contributions to the overall mass transfer ($\simeq 20\%$) even though it involved $\simeq 60\%$ of the total volume.

The local mass transfer coefficients were changed significantly by altering the operating conditions. This situation can lead to the occurrence of a dissolved gas gradient when the

characteristic time for mass transfer ($1/k_La$) is higher than the characteristic time for the gas uptake rate. It was shown that by increasing the impeller rotational speed at a constant gas flow rate, more gas was pushed to the bottom of the STR by the liquid flow. The increase in gas hold-up in theses compartments enhanced their contribution to the overall k_La. At a constant impeller rotational speed, decreasing the gas flow rate resulted in a decrease in the gas hold-up in the middle part of the STR, which led to a decrease in their contribution to the overall k_La.

The scale-up approach based on a constant (P_g/V_l) and v_{sg} was applied in 14-, 200-, and 1500-L STRs. The contribution of the zone with the higher volumetric mass transfer coefficient value (the region close to the impeller) was decreased by the scale-up. As reported in the first part of this thesis, the ratio of the average turbulent energy dissipation rate in this zone to its average value in the bulk of the STR is decreased following the scale-up criteria based on constant power consumption per liquid volume, which can explain the decrease in the contribution of this region to the overall k_La. The variation in gas hold-up distributions inside the STR due to scale-up may also explain these changes. It was found that this scale-up criterion does not ensure a similar distribution of k_La during the scale-up, even with a marginal scale factor on T (2.4 and 4.8).

The effect of imperfect mixing on the overall mass transfer coefficient was elaborated based on the weighting of the local values of k_La by the local residence time of the liquid in different zones of the STR, which was non-dimensionalized by the mean circulation time of the mixing system. The RPT technique was used to determine the residence time distribution (RTD) of the liquid inside these zones, and it was found that the liquid spent more time inside the compartments with lower local volumetric mass transfer coefficient values. We found that the overall volumetric mass transfer coefficient decreases at least by 20% when imperfect mixing is considered.

As monitoring variations of the hydrodynamic parameters is essential for successful process scale-up, the developed multiscale model in the present study could be an adequate

design tool in this regard. For instance, it can either be used to determine the deficient zones for gas/liquid mass transfer and help retrofit design of STRs, or find the maximum permissible scale of STRs at which mass transfer is not limited by mixing.

CHAPTER 8

CONCLUSION AND RECOMMENDATIONS

In this dissertation, liquid and gas/liquid flows in STRs were investigated numerically and experimentally. In this regard, some light has been shed on hydrodynamic parameters, which are of great importance in terms of the design and scale-up of STRs.

8.1 Summary of the thesis

In the first part of this thesis a compartmental model was proposed, the calibration of which was based on CFD simulation results, to investigate the turbulent fluid flow in STRs. Two compartments were defined to characterize turbulent flows in an STR equipped with an RT : a small region near the impeller with a high value of the average turbulent energy dissipation rate, and a larger zone with significantly lower value of this quantity. A new method, relying on the use of volume fraction curves, was introduced for finding the location of the boundary between these compartments, which is more straightforward and precise than existing methods in the literature. Volume and energy dissipation rate ratios between these regions were used to determine the parameter values of the compartmental model. It was shown that the compartmental model parameters depend on both operating conditions and the STR size. The concept of general maps for the prediction of the compartmental model parameters was finally discussed. These maps can be used to monitor changes in turbulent non-homogeneities in an STR during scale-up.

Next, the adequacy of the RPT technique to characterize fully turbulent fluid flows in an STR equipped with an RT or a PBT impeller was studied. The Eulerian turbulent flow field measured using the RPT technique for the RT impeller was first benchmarked with CFD simulations using RANS-based models, as well as laser-based measurements. Despite the

inherent uncertainties of each method, good agreement between the methods was obtained. The RPT technique was also used to measure 3D velocity profiles in the case of the PBT impeller. The results obtained for studying the turbulent flow behaviour of wall jets generated by both types of impeller (RT and PBT) were in agreement with previous studies. We showed that the RPT technique can be used to generate Poincaré maps to visualize flow structures in STRs. The mixing times were investigated using two closely related mixing indices, one based on the concept of stochastic independence, and the other on the statistical concept of memory loss. The latter was shown to lead to a less subjective determination of the mixing time by resorting to an autocorrelation function together with Barlett's formula. Our results showed that the RPT technique holds great promise for measuring mixing times and offering insight into circulation patterns when traditional methods are insufficient (*e.g.*, in opaque systems).

A multiscale gas/liquid flow model was developed to predict the mean local values of the volumetric mass transfer coefficient ($k_L a$) inside STRs. In this model, data from simplified and less computationally intensive gas/liquid flow simulations were used. It was shown that mono-dispersed bubble sizes, adequate drag models, and sufficiently refined grids in CFD simulations can provide satisfactory information on the hydrodynamics of turbulent gas/liquid flows. The multiscale model provided good predictions of the overall mass transfer coefficient inside the STR compared to experimental values. This model revealed that approximately 80% of the total mass transfer occurs in about 40% of the total volume of the STRs. We also determined whether variations in operating conditions and the scale of the STRs had a significant effect on the distribution of the volumetric mass transfer coefficient. Based on the analysis of the local liquid RTDs using the RPT technique and the local values of volumetric mass transfer coefficient, we showed that conventional scale-up approaches are not effective at maintaining similar values for the overall volumetric mass transfer coefficient inside industrial-scale and laboratory-scale STRs. We believe that the multiscale model proposed in the present study can be a very efficient tool for design and scale-up of gas/liquid STRs.

8.2 Contributions of the thesis

The scientific findings and novel aspects of the current study are as follows :

1. the introduction of a new method for finding the location of the boundary between the two characteristic compartments of STRs that describes the turbulent non-homogeneities therein ;
2. the systematic investigation of the effects of operating conditions and different scale-up approaches on the extent of turbulent non-homogeneities in STRs equipped with an RT ;
3. the comprehensive experimental investigations of the turbulent fluid flows in STRs using RPT for both RT and PBT impellers ;
4. the introduction of a novel method for non-invasive measurement of mixing time in STRs based on the statistical concept of memory loss ;
5. the development of a multiscale gas/liquid flow model to serve as a tool for the design and scale-up of STRs ;
6. the scrutinization of operating conditions and scale-up impacts on the local volumetric mass transfer coefficient values.

8.3 Future work and recommendations

1. The proposed methodology for the investigation of the turbulent non-homogeneities in STRs was used for the Rushton turbine mixing systems. It would be of interest to use this method to study the turbulent non-homogeneities in tanks agitated by other types of impellers, such as PBT and hydrofoils.
2. As the adequacy of RPT to measure the turbulent fluid flow in STRs was established in this work, this technique can be extended to characterize multiphase (gas-liquid, solid-liquid and gas-solid-liquid) flows in STRs. The careful preparation of tracer particles is an important aspect in this regard.

3. RPT also can be used to assess the mixing performances of STRs with new geometries other than the standard design.
4. Experimental measurements of gas/liquid flows in STRs and empirical correlations are often only available for a limited range of vessel geometries and operating conditions, old-fashioned impellers, and mainly air/water mixing systems. More experimental work is necessary to asses the adequacy of numerical models and to help in the development of multiscale models such as the one proposed in this study.
5. The proposed multiscale model in this work may be employed with limited changes for other gas/liquid reactors, such as airlift or bubble column reactors, in order to assess their performance.
6. The proposed multiscale model can be used to predict the local volumetric mass transfer coefficient for gas/liquid reactors involving non-Newtonian fluids.
7. The proposed multiscale model can be further extended to determine the dissolved oxygen concentration profiles in STRs at different scales. It can be obtained by solving the oxygen balance equations for both gas and liquid phases, which include an oxygen sink term to take the reaction rate into account. The proposed multiscale model can provide the required information for these equations, including the local volumetric mass transfer coefficient, as well as liquid and gas flow rate between the compartments.